Light Generation, Transport, Mixing and Extraction in Luminescent Solar Collectors

Jim Franklin
BSc (Hons) ANU

A dissertation submitted for the requirements for the degree of
Doctor of Philosophy

Faculty of Science
University of Technology, Sydney

2012

CERTIFICATE OF AUTHORSHIP/ORIGINALITY

I certify that the work in this thesis has not previously been submitted for a degree nor has it been submitted as part of requirements for a degree except as fully acknowledged within the text.

I also certify that the thesis has been written by me. Any help that I have received in my research work and the preparation of the thesis itself has been acknowledged. In addition, I certify that all information sources and literature used are indicated in the thesis.

_____

Jim Franklin

February 2013

ACKNOWLEDGEMENTS

Professor Geoff Smith was my supervisor for the whole of this project and I am grateful for his guidance during the lengthy experimental and development phases, and his patient editing assistance during the writing of this thesis. I would also like to thank my co-supervisor, Professor Peter Ralph, for his support and encouragement during the writing phase of this thesis.

I developed all of the mathematical theory of the thesis except for section 7.2, which was developed jointly with Dr Paul Swift and Prof Geoff Smith, with the largest contribution being made by Dr Paul Swift.

I designed all of the experiments described in this thesis except those of section 5.4.1 (jointly designed with Chris Deller) and chapter 10 (jointly designed with Dr Alan Earp).

Tristan Rawling suggested the possible useful contribution of antioxidants to photostability of light transport in LSC sheets described in section 10.3.1.

I would also like to thank doctoral students, Allan Earp and Chris Deller for their assistance with many of the measurements in this work. After his graduation, Dr Earp continued this collaboration while working on the commercialization phase of this project at Fluorosolar Systems Ltd.

Russell Collier at Fluorosolar Systems Ltd provided expert assistance with *SolidWorks*® models for curled-sheet flat-to-round couplers and other optical components.

Eddy Joseph at Poly Optics Australia Pty Ltd contributed very generously with his time and access to invaluable facilities.

BASF, especially Dr Arno Böhm in Germany and David Bleasby in Melbourne, gave considerable in-kind support over a lengthy period.

Special thanks are due to Michael Bonello and Steve Lynch of Skydome Skylight Systems Pty Ltd who supported the project over the long term. Skydome Skylight Systems Pty Ltd contributed considerable funding and in-kind assistance to this project.

The early phase of this project was partially supported by a NSW SERDF grant. The commercialization phase was partially supported by an AusIndustry Commercial Ready grant.

AUTHOR'S PUBLICATIONS

Parts of this thesis have been published in the journal articles, peer reviewed conference proceedings, granted patents and patent applications listed below. This thesis is unusual in that a substantial portion of the work was first published as patents. There are a number of problems in how to cite these patents. See Appendix 2 for a discussion of the problem and the conventions adopted.

Granted Patents and Published Patent Applications

Franklin, J.B. 2001, *Lighting system for transmitting and releasing luminescent radiation* Patent US 6272265.

Franklin, J.B., Joseph, E.K. & Smith, G.B. 2004, *Improvements in side-scattering light guides* Patent AU 2003/258363 B2.

Franklin, J.B. & Smith, G.B. 2004a, *A light collector* Patent AU 2003/277982 B2.

Franklin, J.B. & Smith, G.B. 2004b, *A light transfer component* Patent AU 2003/273627 B2.

Franklin, J.B. & Smith, G.B. 2007, *A Method of Coupling Light Collector sheets to a Light Transfer Component* WO 2007/048181 A1.

Franklin, J.B., Smith, G.B. & Joseph, E.K. 2003, *Side scattering polymer light guide and method of manufacture* Patent AU 2002/308415 B2.

Franklin, J.B., Smith, G.B. & Joseph, E.K. 2007, *Light emitting device* Patent US 7218824 B2.

Franklin, J.B. & Swift, P.D. 1997, *Improvements in fluorescent materials* Patent AU 717665 B2.

Henderson, M., Franklin, J.B. & Smith, G.B. 2005, *An Optically Traceable Transmission Cable for Transmitting Data or Electricity and a Traceable Conduit* WO 2005/106899 A1.

Joseph, E.K., Franklin, J.B. & Smith, G.B. 2008, *Side-scattering light guides* Patent US 7433565 B2.

Smith, G.B. & Franklin, J.B. 1996, *Sunlight collecting and transmitting system* Patent US 5548490.

Smith, G.B. & Franklin, J.B. 1998, *Sunlight collecting and transmitting system* Patent US 5709456.

Smith, G.B. & Franklin, J.B. 2000, *Sunlight collecting and transmitting system* Patent US 6059438.

Smith, G.B. & Franklin, J.B. 2004, *A hybrid lighting system* Patent AU 2003/275796 B2.

Smith, G.B. & Franklin, J.B. 2007, *A lighting system* AU 2006/101069 A4.

Peer Reviewed Articles

Journals

Deller, C.A., Franklin, J. & Smith, G.B. 2006, 'Monte Carlo ray-tracing in particle-doped light guides', *Lighting Research and Technology*, vol. 38, no. 2, pp. 95-108.

Deller, C.A., Smith, G. & Franklin, J. 2004, 'Colour mixing LEDs with short microsphere doped acrylic rods', *Optics Express*, vol. 12, no. 15, pp. 3327-33.

Earp, A., Franklin, J. & Smith, G.B. 2011, 'Absorption tails and extinction in luminescent solar concentrators', *Solar Energy Materials and Solar Cells*, vol. 95, pp. 1157–62.

Earp, A., Smith, G. & Franklin, J. 2007, 'Simplified BRDF of a Non-Lambertian Diffuse Surface', *Lighting Research and Technology*, vol. 39, no. 3, pp. 265-81.

Earp, A.A., Rawling, T., Franklin, J.B. & Smith, G.B. 2010, 'Perylene dye photodegradation due to ketones and singlet oxygen', *Dyes and Pigments*, vol. 84, no. 1, pp. 59-61.

Earp, A.A., Smith, G.B., Franklin, J.B. & Swift, P. 2004a, 'Optimisation of a three-colour luminescent solar concentrator daylighting system', *Solar Energy Materials and Solar Cells*, vol. 84, no. 1-4, pp. 411-26.

Earp, A.A., Smith, G.B., Swift, P.D. & Franklin, J. 2004b, 'Maximising the light output of a Luminescent Solar Concentrator', *Solar Energy*, vol. 76, no. 6, pp. 655-67.

Smith, G.B., Jonsson, J.C. & Franklin, J. 2003, 'Spectral and Global Diffuse Properties of High-Performance Translucent Polymer Sheets for Energy Efficient Lighting and Skylights', *Applied Optics*, vol. 42, no. 19, pp. 3981-91.

Swift, P.D., Smith, G.B. & Franklin, J. 2006, 'Hotspots in cylindrical mirror light pipes: description and removal', *Lighting Research and Technology*, vol. 38, no. 1, pp. 19-31.

Peer Reviewed Conference Proceedings

Deller, C.A. & Franklin, J.B. 2005, 'Optimising the Length of Doped Polymer Light Mixers', *Proceedings of the Australian Institute of Physics 16th Biennial Congress*, ANU, pp. 85-8.

Deller, C.A., Franklin, J.B. & Smith, G.B. 2006, 'Lighting simulations using smoothed LED profiles compared with measured profiles', *Proceedings of SPIE 6337. Sixth International Conference on Solid State Lighting)*, vol. 6337, San Diego.

Deller, C.A., Smith, G.B. & Franklin, J.B. 2004, 'Uniform white light distribution with low loss from colored LEDs using polymer-doped polymer mixing rods', *Proceedings of SPIE Vol 5530: Fourth International Conference on Solid State Lighting*, vol. 5530, pp. 231-40.

Deller, C.A., Smith, G.B., Franklin, J.B. & Joseph, E. K. 2002, 'The integration of forward light transport and lateral illumination of polymer optical fibre', *Proceedings of the Australian Institute of Physics 15th Biennial Congress* pp. 307-9.

Earp, A.A., Franklin, J.B. & Smith, G.B. 2005, 'Extraction of Trapped Light From Luminescent Solar Concentrators', *Proceedings of the Australian Institute of Physics 16th Biennial Congress*, AIP, ANU, pp. 104-7.

Earp, A.A., Smith, G.B., Swift, P. & Franklin, J. 2003, 'Optimisation of a three-colour luminescent solar concentrator daylighting system', paper presented to the *International Solar Energy Society World Congress 2003*, Gothenburg, Sweden.

Smith, G.B., Earp, A., Franklin, J. & McCredie, G. 2001, 'Novel high-performance scattering materials for use in energy-saving light fittings and skylights based on polymer pigmented with polymer', *Proceedings of the SPIE 4458 (Solar Materials)*, vol. 4458, San Diego, pp. 8-18.

Smith, G.B., Earp, A.A., Stevens, J. Swift, P. D., McCredie, G. &Franklin, J. 2000, 'Materials Properties for Advanced Daylighting in Buildings', *World Renewable Energy Congress VI*, Elsevier, Brighton, pp. 201-6.

Swift, P.D., Smith, G.B. & Franklin, J.B. 1999, 'Light-to-light efficiencies in luminescent solar concentrators', *SPIE 3789 Conference on Solar Optical Materials XVI*, vol. SPIE 3789, Denver, pp. 21-8.

TABLE OF CONTENTS

GLOSSARY OF SYMBOLS AND ACRONYMS

(x, y, z)	Cartesian coordinate system with an origin at the centre of the entry face of a flat-to-round converter
(θ,ϕ,l)	Spherical coordinates

Roman Symbols and Acronyms

a	Aspect ratio of a sheet [m]
a	Axial particle number (the number of particles intercepted by a straight line drawn through a TRIMM-doped system parallel to the optic axis) [m^{-1}]
A	Cross sectional area of the optical system [m^2]
A	Absorbance of an optical system
A	Area of a source [m^2]
$\overline{A}$	Mean absorption fraction of light entering an LSC
dA	An infinitesimal area [m^2]
$\boldsymbol{dA}$	Vector associated with an infinitesimal area, dA [m^2]
$A(\lambda)$	Absorption spectrum
A_{eff}	Effective collection area of an LSC [m^2]
$A_{extractor}$	Area of the exit face of a hybrid LSC-LED light extractor [m^2]
A_{LED}	Area of individual LED chips in hybrid LSC-LED light extractor [m^2]
B	Fraction of total lumens from hybrid LSC-LED light extractor provide by the LED's
$BRDF$	Bidirectional Reflectance Distribution Function [sr^{-1}]
$c_o(z)$	Transverse curvature of the outer surface of a flat-to-round converter at distance z from the entry face [m^{-1}]
C	Contrast ratio between specular and diffuse light
$\boldsymbol{C'}_o(z)$	Position of the centre of the transverse curvature of the outer surface of a flat-to-round converter which has been adjusted so that the intersection of the outer surface with the y-z plane is a straight line [m]
$\boldsymbol{C}_i(z)$	Position of the centre of the transverse curvature of the inner surface of a flat-to-round converter at distance z from the entry face [m]
$\boldsymbol{C}_o(z)$	Position of the centre of the transverse curvature of the outer surface of a flat-to-round converter at distance z from the entry face [m]
d	Diameter of an inflated tube [m]
$D(\delta)$	Divergence of a TRIMM microsphere i.e. the ratio of the intensity of light scattered by a TRIMM particle at angle δ to the illuminating beam with the intensity of light scattered in the same direction as the illuminating beam
DABCO	1,4-diazabicyclo-[2.2.2] octane, a useful antioxidant
$E_C(\lambda)$	Measured spectrometer signal from the end surface of a clear sheet [counts]
$E_D(\lambda)$	Measured spectrometer signal from the end surface of a dyed sheet [counts]
E_e	Total power emitted by dye molecules [W]
EPO	European Patent Office
$E_x(\lambda)$	Spectral intensity at the side of an LSC at lateral distance x [$counts.sec^{-1}$]
f	Matrix loss factor (the fraction of the light lost in the clear reference sheet due to matrix extinction and Fresnel reflection at the far end).
$f(\delta)$	Probability density distribution of the ray's angular deviation [rad^{-1}]

f_{cone} Fraction of fluorescently emitted light in each escape cone

$f_{diffuse}$ Fraction of light in a hybrid LSC-LED light extractor that is diffuse rather than specular

f_{edge} Fractional loss of light in a flat-to-round converter due to scattering from rounded sidewall edges

f_{end} Fraction of fluorescently emitted light that is endlight (includes the correction for reflection at a LSC sheet's end mirror)

f_{escape} Fraction of fluorescently emitted light in combined escape cones

f_{geom} Fraction of rays striking a TRIMM microsphere that are within the geometric limit i.e. the fraction of rays that are well approximated by geometric optics

f_{scat} Fractional loss of light in a flat-to-round converter due to scattering off rough sidewalls

$f_{trapped}$ Fraction of fluorescent emission that reaches the a LSC's exit surface in the form of

F Output luminous flux from an LSC [lm]

F Output luminous flux from an LSC [lm]

F_{all} The ratio of the total amount of light reaching a LSC's exit surface (i.e. the sum of endlight and trapped light) to the endlight

F_{in} Flux of a collimated light beam illuminating an annulus on a TRIMM microsphere [W]

F_l Luminous flux at the collection edge when LSC is illuminated at a plane of constant distance, l, from the collection edge [lm]

F_L Luminous flux at collection edge when LSC of length L is illuminated uniformly [lm]

F_o Luminous flux of the fluorescent test lamp [lm]

FSL Fluorosolar Systems Ltd

g_{max} Maximum possible étendue per unit area [sr.m^2]

G Étendue [sr.m^2]

G_{gap} Étendue of light at an air gap [sr.m^2]

G_{limit} Smallest value of the limiting étendue in an optical system [sr.m^2]

$G_x^{\max}$ Maximum possible étendue at cross section x [sr.m^2]

h Impact ratio, $h = h/r$. h is independent of the microsphere's radius, r

h_{geom} Impact ratio for the geometric limit, i.e. the impact ratio beyond which Mie theory is required to calculate the scattering pattern

H Perpendicular separation distance of a ray impacting on a microsphere from the parallel ray passing through a sphere's centre. [m]

HDPE High Density Polyethylene

$i(\delta,l)$ Intensity of the light scattered by a single TRIMM microsphere measured at distance l from the sphere and a deviation angle of δ from the illuminating light beam [W.m^{-2}]

I Average number of interactions of light with the sidewalls of a flat-to-round converter

$\boldsymbol{I}$ The point on the inner sidewall edge of a flat-to-round converter corresponding to point P on the outer surface [m]

$I(\delta)$ The intensity light scattered by a TRIMM microparticle at a deviation angle of δ to the illuminating beam, measured inside the host material [W.m^{-2}]

I_{in} Intensity of a collimated light beam illuminating a TRIMM microsphere [W.m^{-2}]

I_0 The intensity light scattered by a TRIMM microparticle in the direction of the illuminating beam, measured inside the host material [W.m^{-2}]

INPADOC International Patent Documentation Center

I_{sol}	Solar luminous intensity incident on the top surface of the collector [lux]
k	A proportionality constant for the fitted variation of the mean half-cone angular spread, $\overline{\Sigma}$, with the axial particle number, a
l	Length of a sheet [m]
l	Linear distance between point of illumination and collection edge [m]
l	Path length of a ray inside a light guide [m]
L	Length of a light guide [m]
L	Length of a clear reference sheet or collector sheet [m]
L	Radiance of a source [$W.m^{-2}.sr^{-1}$]
$L_{½}$	Half-length i.e. the path length over which 50% of the fluorescently emitted light is lost due to extinction [m]
L_{crit}	Critical length of a TRIMM doped mixer rod i.e. the length where the mean half-cone angular spread of the light is equal to the material's critical angle [m]
$L_{d½}$	Half-length contribution from the collector sheet's dye [m]
$L_{diffuse}$	Diffuse radiance of a skylight or LED-hybrid luminaire interpolated to the angle of maximum radiance [$W.m^{-2}.sr^{-1}$]
LDPE	Low Density Polyethylene
LED	Light Emitting Diode
$\overline{L}_{extractor}$	Mean radiance from a hybrid LSC-LED light extractor [$W.m^{-2}.sr^{-1}$]
$L_{g½}$	Half-length contribution from collector sheet's geometry [m]
L_{LED}	Radiance of the LED's in a hybrid LSC-LED light extractor [$W.m^{-2}.sr^{-1}$]
L_{local}	Radiance of the diffuse component of a system's output measured near the specular component [$W.m^{-2}.sr^{-1}$]
$L_{m½}$	Half-length contribution from collector sheet's matrix [m]
L_{max}	Maximum radiance of the specular component of a system's output [$W.m^{-2}.sr^{-1}$]
$L_{proj\ image}$	Radiance of the a mixer in a LED projector near the specular beam [$W.m^{-2}.sr^{-1}$]
$L_{proj\ specular}$	Radiance of the specular beam from a mixer in a LED projector [$W.m^{-2}.sr^{-1}$]
LSC	Luminescent Solar Collector
$L_{specular}$	Maximum specular radiance of a skylight or LED-hybrid luminaire [$W.m^{-2}.sr^{-1}$]
$L_{v\ image}$	Luminance of the image from a LED projector near the specular spot [$lm.m^{-2}.sr^{-1}$]
$L_{v\ specular}$	Luminance of the specular spot from a LED [$lm.m^{-2}.sr^{-1}$]
m	Ratio of the refractive index of a fibre's core to its cladding
m	Relative refractive index (usually the ratio of the ratio of the particle's refractive index to the matrix containing it)
n	Refractive index
n_{host}	Refractive index of the host matrix containing a TRIMM microsphere
n_i	Refractive index of component i, such as a TRIMM microsphere or a light guide matrix
$n_{particle}$	Refractive index of a TRIMM microsphere
n_{pix}	Number of pixels that specular transmission is focused onto
N	Number of measurement positions along a the side of a LSC
N_{LED}	Number of LED chips in hybrid LSC-LED light extractor
N_{pix}	Number of pixels in a display
p	A power index for the fitted variation of the mean half-cone angular spread, $\overline{\Sigma}$, with the axial particle number, a
p	Pressure of an inflated tube [Pa]
$p(\theta_i)$.	Path length inside a LSC for light with an angle of incidence of θ_i [m]

$\boldsymbol{P}$	A chosen point at the intersection of the outer surface of a flat-to-round converter a the sidewall [m]
$P(h)$	The cumulative probability density distribution at impact ratio h
$P_a(x)$	Probability of a ray encountering exactly x microparticles in a light guide with an axial particle number of a
PCT	Patent Cooperation Treaty
PMMA	Poly methyl methacrylate, colloquially called "acrylic plastic" or Perspex®
$P_o(\lambda)$	Spectral power of light immediately inside the entry surface of the clear reference sample [counts.sec^{-1}.nm^{-1}]
$P_s(\lambda)$	Total spectral power scattered from the top, bottom and sides of a sheet [counts.sec^{-1}.nm^{-1}]
$P_T(\lambda)$	Spectral power transmitted by a LSC [counts.sec^{-1}.nm^{-1}]
Q	Heat [J]
$\boldsymbol{Q_1}$, $\boldsymbol{Q_3}$	Auxiliary points at the intersection of the outer surface of a flat-to-round converter with a sidewall, chosen to be on either side of $\boldsymbol{P}$ [m]
$\boldsymbol{Q_2}$	Auxiliary point on the outer surface of a flat-to-round converter with the same z value as $\boldsymbol{P}$ [m]
QD	Quantum Dot
r	Particle radius (e.g. of a TRIMM microsphere)
r	Reflectivity of an end mirror
r_i	Radius of the inner surface of the exit ring of a flat-to-round converter [m]
$r_i(z)$	Radius of transverse curvature of the inner surface of a flat-to-round converter at distance z from the entry face [m]
r_n	Radius of the neutral surface of the exit ring of a flat-to-round converter [m]
r_o	Radius of the outer surface of the exit ring of a flat-to-round converter [m]
$r_o(z)$	Radius of transverse curvature of the outer surface of a flat-to-round converter at distance z from the entry face [m]
r_{side}	Nominal radius of the sidewalls' edges in a flat-to-round converter [m]
R	Fresnel reflectance of a surface
R	Reflectance of an optical system
R_1	Reflectance from a single TRIMM microsphere
$\overline{R}_1$	Mean reflectance from a single TRIMM microsphere
$R_{1\,TE}$	Reflectance coefficient from a TRIMM microsphere for light with transverse electric polarisation
$R_{1\,TM}$	Reflectance coefficient from a TRIMM microsphere for light with transverse magnetic polarisation
R_c	Reflectivity of one surface of the collector
R_{end}	Fresnel reflection loss at the far end surface of the LSC
RI	Refractive Index
$R_{particles}$	Mean total back reflectance from a mixer with a microparticles
R_{TE}	Reflectance coefficient for light with transverse electric polarisation
R_{TM}	Reflectance coefficient for light with transverse magnetic polarisation
s	Circumferential stress of an inflated tube [N.m^{-2}]
$\overline{S}$	Mean scattered fraction of light entering an LSC
$\boldsymbol{S}$	The vector normal to the surface of a flat-to-round converter at point $\boldsymbol{P}$ and having a magnitude equal to the sheet thickness, t [m]
$S(\lambda)$	Scattering spectrum [W.m^{-2}.nm^{-1}]

$S(\lambda)$	Spectral intensity of sunlight of wavelength λ [W.m^{-2}.nm^{-1}]
$S(\Psi)$	Spectral intensity of sunlight of wavelength Ψ [W.m^{-2}.nm^{-1}]
SCATS	Sunlight Collecting And Transmission System
S_T	Side-loss of an optical system i.e. the fraction of light that is transported laterally for a sufficient distance so that it does not enter the entry port of the detector
t	Thickness of a sheet measured perpendicular to the surface [m]
t	Wall thickness of an inflated tube [m]
T	Transmittance of an optical system
$\overline{T}$	Mean tails transmission for light entering an LSC
$T(\lambda)$	Transmission spectrum a LSC sheet
$T(z)$	Distance between the inner and outer surfaces of a flat-to-round converter in the y-z plane at distance z from the entry face [m]
$T_{diffuse}$	Hemispheric forward transmittance diffuse transmittance of a skylight or other diffuser sheet
TIR	Total Internal Reflection
TRIMM	Transparent Refractive Index Matched Microparticle
$T_{specular}$	Specular transmittance; for a TRIMM system the fraction of rays completely undeviated scattering
U	Symbol for étendue used by some workers. This thesis uses G [sr.m^2]
UTS	University of Technology, Sydney
w	Width of the collector sheet [m]
w_C	Width of clear reference sheet [m]
w_D	Width of a dyed LSC [m]
w_{det}	Width of detector port on integrating sphere [m]
$w_i(z)$	Arc length of the inner surface of a transverse cross section of a flat-to-round converter at distance z from the entry face [m]
$w_o(z)$	Arc length of the outer surface of a transverse cross section of a flat-to-round converter at distance z from the entry face [m]
W	Work [J]
x	Lateral distance on an LSC measured from the entry surface [m]
x	Number of microparticles encountered by a ray
$\overline{x}$	Mean number of microparticles encountered by a ray over a specified distance
dx	Length interval represented by each measurement [m]
$y(\lambda)$	Standard photopic response of human eye
$y_o(z)$	y value of the exterior surface of a flat-to-round converter in the y-z plane [m]
z_i	z coordinate of the bottom of the exit ring in a flat-to-round converter [m]
z_o	z coordinate of a sidewall at the exit ring in a flat-to-round converter [m]

Greek Symbols

α	Linear particle density i.e. the number of particles per metre intercepted by a straight line drawn through a TRIMM-doped light guide [m^{-1}]
$\alpha(\lambda)$	Attenuation coefficient at wavelength λ [m^{-1}]
$\alpha_d(\lambda)$	Dye-related attenuation coefficient (including the effects of dye photodegradation, if applicable) [m^{-1}]
$\alpha_g(\theta,\phi, l)$	Attenuation coefficient for losses due to light guide geometry [m^{-1}]
α_m	Matrix attenuation coefficient, assumed independent of wavelength [m^{-1}]
γ	Exponential loss coefficient averaged over all rays [m^{-1}]
δ	Semi-cone angular component of a ray's deviation, relative to the previous direction of the ray [rad]
$\bar{\delta}$	Mean deviation angle of the rays interacting with a single TRIMM microsphere [rad]
$\delta(h)$	General expression for deviation angle of a ray impacting a TRIMM sphere, in terms of the impact ratio h [rad]
δ_{geom}	Deviation angle at the geometric limit [rad]
δ_{median}	Median deviation angle of the probability density distribution of the deviation $f(\delta)$ [rad]
δ_{median}	Median deviation angle of the rays interacting with a single TRIMM microsphere [rad]
$\varepsilon(\lambda,L)$	Spectral intensity at the collection edge of an illuminated LSC sheet [$W.m^{-2}.nm^{-1}$]
$\varepsilon_o(\lambda)$	Emission power spectrum of fluorescent dye [$W.m^{-2}.nm^{-1}$]
η_{abs}	Fraction of light incident on an LSC collector stack that is absorbed by the dye molecules
$\eta_{conduit}$	Transport efficiency of an LSC system's optical conduit(s)
$\eta_{coupler}$	Fraction of the light reaching a LSC sheet's collection edge that is coupled into the optical conduit(s)
η_{cover}	Fraction of light transmitted by the protective cover
η_{direct}	Fraction of light from a light extractor that is directed to usefully illuminate a room
$\eta_e(\lambda)$	Energy-to-energy conversion efficiency of fluorescent dye (average emitted photon energy/incident photon energy)
$\eta_{extract}$	Extraction efficiency of a light extractor
η_{geom}	Geometric efficiency of a LSC sheet (i.e. losses due to the sheet not being a perfect rectangular prism)
$\eta_{l\text{-}l}$	Lumens-to-lumens efficiency of a LSC system (output lumens/input lumens)
$\eta_{lum\text{-}lum}$	Ratio of the luminous efficacy for a dye molecule of the emitted light to that of the absorbed light. Note that $\eta_{lum\text{-}lum}$ can exceed 100%
$\eta_{material}$	Efficiency of a LSC sheet due to material properties including: dye self-absorption, absorption by the matrix, scattering by dye particles, scattering by the matrix and absorption at the sheet's end mirror
η_{quant}	Photon-to-photon quantum efficiency (photons out/photons in)
η_{sheet}	Fraction of the fluorescently emitted light that reaches a LSC sheet's collection edge
η_{TIR}	Fraction of the fluorescent emission is trapped inside a LSC sheet by total internal reflection at the top and side surfaces
θ	Altitude angle between ray and normal to collector surface [rad]
θ_{crit}	Critical angle [rad]
$\theta_{diffuse}$	Half-width of diffuse radiation form a skylight or other diffuser [rad]

θ_i	Angle of incidence of external light entering a collector sheet [rad]
θ_{sun}	Half-width of specular solar radiation [rad]
κ	Lumens per watt conversion factor (683 lm W^{-1}) [lm W^{-1}]
λ	Wavelength of light [nm]
$\langle\lambda\rangle$	The average wavelength of photons emitted by the dye molecule [nm]
$\Delta\lambda$	Wavelength interval [nm]
Ψ	Wavelength of light incident on a LSC [nm]
μ	Difference of the relative refractive index, m, from 1
τ	Spectrometer integration time [s]
ϕ	Azimuthal angle on x-y plane between ray and positive x-axis (long axis) [rad]
ϕ	Angle between the geometric cross section surface and the effective cross section surface [rad]
ϕ	Inclination of the end surface of a light guide [rad]
ϕ	Misalignment angle between two components [rad]
Φ	Radiant flux of a source [W]
χ	Critical angle at the collector-air interface (chapter 7 only – the rest of the thesis uses θ_{crit}) [rad]
$\bar{\Sigma}$	Mean half-cone angular spread of light in the cross-sectional plane of a light guide [rad]
Ω	Emission solid angle of a source [sr]
Ω	Solid angle [sr]
Ω	Solid angle of a light field at a given point [sr]
Ω	Solid angle subtended by a source [sr]
$\boldsymbol{\Omega}$	Vector of magnitude Ω in the central direction of a light field that has a solid angle of Ω [sr]
Ω_{escape}	Solid angle of the escape cone [sr]
$\Omega_{extractor}$	Solid angle subtended by the LSC component of light from hybrid LSC-LED light extractor [sr]
Ω_{LED}	Solid angle subtended by light from an LED [sr]
Ω_{max}	Maximum possible solid angle of light confined in the system at a specified cross section [sr]
$\Omega_{max\ mer}$	Maximum solid angle of meridional light trapped inside an optical fibre [sr]
$\Omega_{max\ rect}$	Maximum solid angle of light trapped inside a rectangular light guide [sr]
$\Omega_{max\ sheet}$	Maximum solid angle of light trapped inside a sheet [sr]

LIST OF FIGURES

CHAPTER 1 INTRODUCTION

CHAPTER 2 FUNDAMENTAL CONCEPTS

CHAPTER 3 ÉTENDUE ANALYSISI OF LSC'S

CHAPTER 4 FLAT-TO-ROUND CONVERTERS FOR OPTICAL FIBRES

CHAPTER 5 TRIMM DOPED SHEETS AND LIGHT GUIDES

CHAPTER 6 LIGHT EXTRACTION FROM SOLID OPTICAL SYSTEMS

CHAPTER 7 LIGHT TRANSPORT IN LSC SHEETS

CHAPTER 8 MAKING LSC SHEETS

CHAPTER 9 EXTINCTION MECHANISMS IN LSC'S

LIST OF TABLES

Abstract

The difficulty of directing daylight deep into the heart of buildings means that much artificial lighting is required during the day, which substantially increases energy costs for lighting and air conditioning. This thesis explores the feasibility of daylighting with luminescent solar collectors.

An LSC is a stack of thin sheets of polymer doped with fluorescent dyes. Sunlight entering the sheets is absorbed and emitted isotropically at longer wavelengths. 75% of this emission is trapped by total internal reflection and propagates towards the sheets' edges. A special coupler channels some of this light into a flexible optical fibre that guides it to a remote luminaire. High quality white light with zero excess heat is produced by appropriate dye use. LSC's collect both diffuse and specular sunlight, so their luminous output is only weakly affected by light clouds.

The best previous LSC's for daylighting gave an outdoor-to-indoor lumens-to-lumens efficiency of only 0.2%. This project achieved an efficiency of 5%.

The basic tool for optical design was étendue analysis. Key results are: i) the system's cross sectional area must not decrease along the optical path, ii) the collector sheets need a high aspect ratio, and iii) an often neglected requirement for a solid optical system with no air gaps. Other optical design problems solved include high-efficiency flat-collector-sheet to cylindrical-optical-fibre couplers and high-efficiency light extractors (which boost output by approximately 50%).

Major advances in mechanical design resulted in several new practical solutions including: strong, enduring optical joints; mass produced collector-sheet to optical-fibre couplers using injection moulding with demonstrated efficiencies of 96%; affordable flexible light guides; high-performance cover materials; roof and façade mounting; and reduced mass.

Required system performance is impossible without high quality LSC sheets. Maximising fluorescence yield involves detailed understanding of the roles of: dye quantum efficiency, Stokes shift, long wavelength absorption "tails", dye dispersion, light transport inside a sheet and long term sheet stability. A substantial improvement in the performance of collector sheets was achieved.

Solutions to all the key problems for daylighting with practical LSC systems have been demonstrated using outdoor mounted collectors channeling light to indoor spaces, with one key exception: the increase in absorption tails over the long term. Techniques were developed for measuring this weak tails absorption, which significantly reduces light output from the required long collector sheets. Suggestions are made as to its cause, and possible methods of its reduction.

1 INTRODUCTION

1.1 MOTIVATION FOR THIS WORK

Daylight is an underused resource that has the potential to improve the quality of indoor lighting, as well as substantially reducing energy costs. Artificial lighting is one of the major sources of electrical energy costs in office buildings, both directly through lighting energy consumption and indirectly by production of significant heat gain, which increases cooling loads (Lam & Li 1999). A number of studies have shown that effective use of daylighting in conjunction with artificial lighting can produce significant energy savings in office buildings (Balaras et al. 2002; Ne'eman 1984; Rutten 1994). The excellent colour rendering properties of daylight and its close match to the photopic response of the human eye make it an ergonomic light source that is generally preferred for pleasant working conditions (Robbins 1986). Thus the use of daylight to supplement artificial lighting has proven beneficial for minimizing energy usage and improving lighting quality.

Daylighting in perimeter zones of buildings is readily achievable through careful window design (Inoue 2003; Li & Lam 2001), although relatively little work has been done investigating mechanisms to transport daylight to remote rooms. For regions further away from the window façade reasonable daylighting is possible with light shelves (Compagnon, Scartezzini & Paule 1993; Page, Kaempf & Scartezzini 2003), or laser-cut light deflecting panels (Edmonds 1993). However, these systems are only capable of transporting daylight over relatively small distances and can be very difficult to retrofit to existing buildings.

Various mirror light pipe systems have been proposed for daylighting of deeper interior spaces with light pipes (Chirarattananon, Chedsiri & Renshen 2000; Pohl & Anslem 2002; Rosemann & Kaase 2005; Zastrow & Wittwer 1986a), but these systems can be fairly complex, and to date they are all still at a prototype stage. There are a number of fundamental problems. First, attenuation per metre is high unless the light pipes have a large diameter or use ultra-high reflectivity materials (such as multi-layer polymeric films similar to 3M® VM2000®), which are very expensive. Second, it is difficult to bend the light pipes so installations require an unobstructed path from the roof to the luminaire, which is often impractical in existing buildings. Third, the reflection off the cylindrical mirror surfaces leads to the formation of caustics and very uneven illumination (Swift, Smith & Franklin 2006) that many consumers find objectionable (Bonello 2003; Lynch 2000). Our experiments show that this can be overcome with negligible losses (Swift, Smith & Franklin 2006) by using a diffuser doped with

special materials such as Transparent Refractive Index Matched Microparticles, also called TRIMM (this material is the subject of chapter 5).

An alternative approach is to use a computer controlled sun-tracker with a Fresnel lens or parabolic mirror that focuses concentrated sunlight onto a bundle of optical fibres, such as those shown in Figure 1.1. The flexibility and low attenuation of the optical fibres means that the sunlight collector can be retrofitted to existing buildings on a roof or wall a considerable distance from the luminaire. The first stage of this daylighting project investigated computer controlled sun-trackers that focus light into a solid cored optical fibres. However, focusing systems inherently can only concentrate the specular portion of sunlight. Even thin clouds can reduce the specular component of sunlight to almost zero, despite the fact that their effect on total lux levels is small. Measurements made as part of this project showed that for Sydney the specular component of sunlight frequently dropped to almost zero within a few seconds as light clouds moved across the sun. Further, even in summer there were relatively few long periods of cloudless sky. This problem is inherent to any focusing system. Luminescent solar collectors promised superior performance with their ability to fully utilise diffuse light. Accordingly, the focusing sun-tracking approach was discontinued without building any prototypes.

This appears to have been the correct decision. It is noteworthy that despite a considerable drop in the cost of computer controls, there is still no commercially successful sun tracking system that focuses light onto an optical fibre. Available systems, such the Parans® SP3 (Parans Solar Lighting AB) shown in Figure 1.1(b), remain expensive niche products with negligible market penetration.

(a) (b)

Figure 1.1 (a) A two axis sun tracker that uses a single large Fresnel lens to focus the specular component of sunlight onto an optical fibre for remote illumination (Solar Magazine 2002). (b) A Parans® two-axis sun tracking system that uses multiple small lenses to focus sunlight onto individual small optical fibres (Parans 2011).

Another possible approach is to use photovoltaic panels on the roof or façade of a building to generate electricity and to deliver the power via wires to a remote lamp. Electrical wiring is cheap and would permit optimal locations of the PV panels and lamp. The high cost and low efficiency of existing photovoltaic panels and the relatively low luminous efficiency of current electric lights (including LEDs) mean that this option is not currently viable. However, PV cost and efficiency is constantly improving and the luminous efficacy of lamps is rising. So this method may become cost competitive.

1.2 Luminescent Solar Collectors

What is needed is a way of collecting the diffuse component of sunlight as well as the specular component as the sum of these components is much more stable than the specular light. This light then needs to be coupled into optical fibres so that it can be easily distributed deep inside existing buildings as shown in Figure 1.2 after (DayRay 2009). This thesis explores the scientific and commercial feasibility of using a luminescent solar collector to collect solar radiation and ways of coupling that light into large diameter solid core optical fibres to illuminate rooms throughout an existing building.

Figure 1.2 Schematic of a luminescent solar collector capturing sunlight and coupling the light into optical fibres that distribute the light throughout a building.

A luminescent solar collector is a thin sheet of a transparent matrix doped with a fluorescent luminophore. Sunlight entering the sheet is absorbed and emitted isotropically at a longer wavelength. Total internal reflection traps most of the emission inside the light guide. This thesis will concentrate on LSC's made from a polymer doped uniformly with a fluorescent dye, as illustrated in Figure 1.3. Alternative designs are considered in section 8.1.

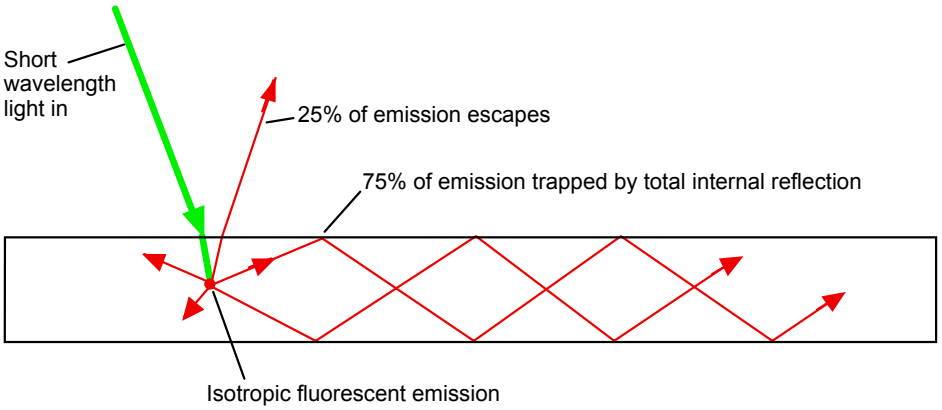

Figure 1.3 Schematic cross section of a luminescent solar collector sheet.

Approximately 75% of the fluorescently emitted light is trapped inside the sheet by total internal reflection and propagates towards the sheet's edges. The Stokes shift between the absorbed and emitted light means that the tendency for re-absorption is minimized and a considerable fraction of the fluorescently emitted light reaches the sheets edges, as shown in Figure 1.4 from (Acrylite 2012). Since the surface area of the edges is much smaller than the surface area of the entry surface, the light at the edges is highly concentrated compared to the received light. It is important to note that this concentration works equally well for diffuse light and specular light. Another important feature is that the edge light has no infrared component. Thus a LSC can potentially provide light without excess heat.

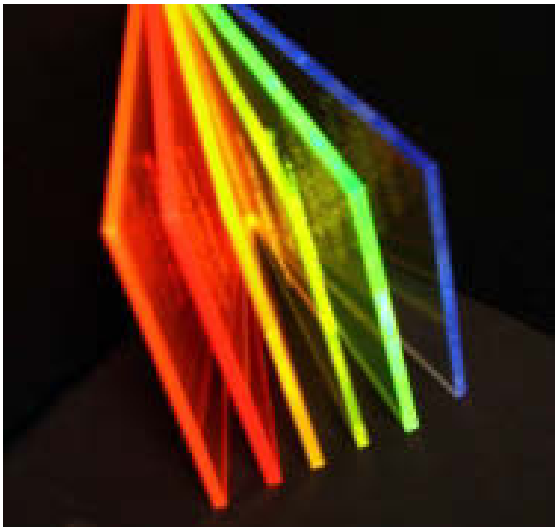

Figure 1.4 The edges of fluorescent sheets are bright because light is collected over the large flat surfaces and transported by total internal reflection to the much smaller edges.

LSC's have been extensively studied since the mid-1970's, primarily as concentrators for photovoltaic applications with solar cells bonded to the edges of LSC collector sheets (Debije & Verbunt 2012; Hermann 1982; Reisfeld & Jorgensen 1982; Soti et al. 1996; Weber & Lambe

1976). Another key application of LSC's is outdoor signage with particular benefits for maintaining contrast ratios in daylight due to increased luminescent output at high solar illuminance (Element Displays Dr Wiemer GmbH 2012). This contrasts to conventional electronic signage that is often unreadable in bright sunlight. There is also intriguing recent experimental work on a LSC based "smart window" that uses a fluorescent dye-doped liquid-crystal solution between electrically conductive plates for adjustable window opacity and solar cells around the window's periphery for power generation (Debije 2010).

The small amount of experimental work done prior to this project's beginnings on daylighting with LSC's by workers such as (Zastrow & Wittwer 1986b) showed considerable potential, and provided some of the motivation for this study.

A single collector sheet gives light of one colour. As shown in Figure 1.5 after (Earp et al. 2004b; Smith & Franklin 1996; Smith & Franklin 2000), the output from a three-layer stack of violet, green and pink collector sheets can be coupled to thin flexible light guides and combined to make white light for useful remote illumination.

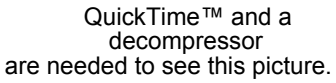

[Production Note: This figure is not included in this digital copy.
The print copy of the thesis is available for consultation at UTS Library.]

Figure 1.5 Schematic of a three colour LSC stack connected to light guides and a luminare.

In this design each coloured LSC sheet consists of a clear poly(methyl methacrylate) (PMMA) matrix that is as thin as possible, and much longer than it is wide. Typical collector sheet dimensions are 1200 mm x 250 mm x 2.0 mm. Each LSC sheet is doped with a coloured fluorescent dye with the sheet absorbing the shortest wavelengths on the top of the stack and the longest wavelength absorber on the bottom. For the purpose of light transport, these collectors are coupled with optically clear glue to thin clear PMMA light guides up to 5m in length. Thus daylight can be transported to underground rooms or windowless rooms in the centre of a building. By appropriate selection of dyes, white light output can be produced, giving a good match with the colour of daylight.

Ideally the topmost sheet of the collector stack would emit blue light. However, there are no known stable high quantum efficiency dyes emitting only blue light and there are good

theoretical reasons for believing that there are unlikely to be any available in the foreseeable future (Böhm 1997, 2004). Accordingly, this project used a violet dye (BASF *Lumogen*® 570), although this is sometimes referred to as a blue dye.

Optical transport of daylight using an LSC stack operates by the following process. Solar energy enters the stack where it may be absorbed and randomly re-emitted by the violet dye in the top sheet. If the emitted photon travels below the critical angle with respect to the top or side surface of the sheet (42^{o} for PMMA), it will leave the collector. Otherwise it will be totally internally reflected to the end of the collector, then through the light guide to the luminaire. Photons that are not absorbed by the violet dye may be transmitted through to the next sheet, where they may be absorbed and re-emitted by a fluorescent green dye. Highly reflective mirrors are fixed to the back edge of each sheet to reflect photons that are originally directed away from the light guides. Some emitted photons may also leave each sheet at its base, and enter the pink sheet at the bottom of the stack, where they may be subsequently re-absorbed and re-emitted. A white base plate is placed underneath the pink sheet to reflect any light reaching the base of the stack, thus increasing the absorption efficiency of the stack.

Although total internal reflection effectively transports light to the end of the light guides, a large quantity of this may be trapped, as shown in Figure 1.6. Assuming the dye molecules emit isotropically, approximately 1/8 of the emitted light will be lost at each of the six surfaces of the sheet. In an ideal system with no self-absorption or matrix scattering, the remaining $1 - 6 \times 1/8 = 2/8$ of the total emitted light falls within an angular range such that it is totally internally reflected at every surface and is totally trapped within the system. A mirror at the back edge reflects light that would ordinarily leave through the back edge, and most of this light is transported through the light guides to the luminaire. In summary, with no losses 2/8 of the total emitted light will leave the system at the collection edge, 2/8 is lost through the sides, 2/8 is lost through the top and bottom surfaces and the remaining 2/8 is trapped, and will at some stage reach the collection edge. Provided no air gaps exist between the collector and the light guides, 4/8 of the light can travel to the collection edge. That is to say that approximately half of the light reaching the collection edge will naturally leave through this edge and the other half is trapped inside the light guide.

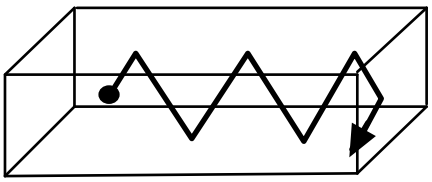

Figure 1.6 Trapped light is totally internally reflected at all surfaces.

Most of the trapped light can be extracted by installation of an appropriate light extractor in the luminaire. Light extractors are (patented) devices added to the end of a light guide that convert otherwise useless trapped light into useful end light (Franklin 2001a). Chapter 6 discusses the theory of light extractors and designs for practical high-efficiency light extractors.

This thesis will explore the problems in designing and manufacturing a practical LSC. To assist the discussion, it is useful to consider the fundamental components of a luminescent solar collector system, as illustrated in Figure 1.7.

It is obvious that a LSC has at a minimum a collector stack (usually made from flat sheets doped with a fluorescent dye, but other shapes are possible), an optical conduit (made from various types of light guide) and a luminaire (to direct the light in a useful direction). In addition, there must be some way of coupling the collector stack to the light guide that we will call the *sheet coupler*. For some designs, this is just the region where the collector sheets butt up against the light conduit with a thin air gap in between, but many workers have designed elaborate optical devices for sheet coupling. The design in Figure 1.5 uses thin rectangular strips of polymer as light guides. However, there is considerable interest in using round optical fibres as these are much more flexible and so much easier to install. In order to achieve this, the sheet coupler must somehow bridge the different form factors of the collector sheets and round light guides while leaking a minimum of light. This difficult problem will be discussed briefly in section 2.3.5 and at length in chapter 4.

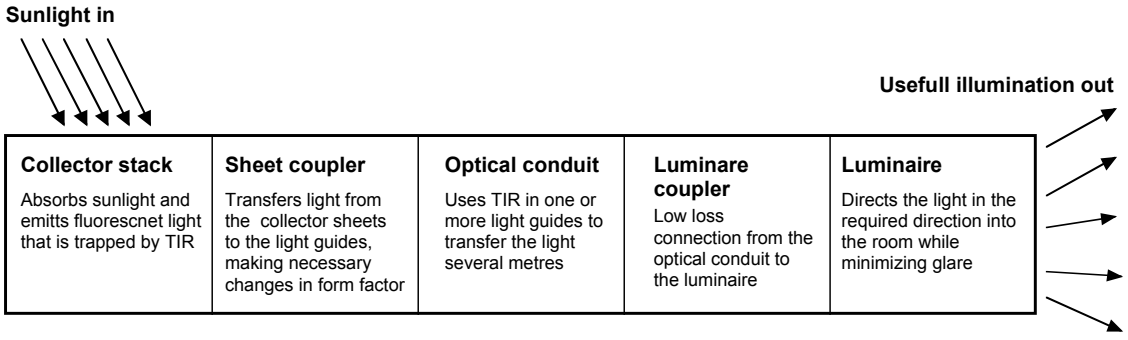

Figure 1.7 Schematic of a generic LSC system.

There must also be some kind of coupling from the light conduits to the luminaire. Again, the luminaire coupler may be just an air gap or it may be an elaborate optical component. It is noteworthy that most workers do not explicitly consider the sheet coupler or the luminaire coupler, which usually has profoundly deleterious consequences for system performance.

It is also useful to bear in mind some fundamental dimensions. First, there is no point in installing a LSC where a cheap window or skylight can do the same job: LSC's only make sense where they can get light into a room where conventional means cannot. This means that the light guides will have to be several metres long. In practice, as discussed in section 4.4, this

means that the cost of the light guides dominates the cost of the LSC system. Second, it is obvious that the thinner the collector sheets the smaller the required cross section of the light guides (and hence the lower the cost of this very expensive component). Thus there are great incentives to make the collector sheets as thin as possible.

The problem of making good LSC sheets is of such critical importance to the question of mass-producing LSC's that the whole of chapter 8 and Appendix A will be devoted to this topic. We have had extensive discussions and on-site visits to manufacturers of fluorescent sheets in Spain, Germany, Japan and Australia, about the minimum practical thickness for collector sheets. There was a unanimous view that the minimum practical thickness of an individual sheet is 2.0 mm. See section 8.4 for details.

Trials with LSC's can only be conducted by using full-sized collector sheets. This sheet size is far beyond the production capabilities of any Australian laboratory or factory (Australia has closed down all cell-casting factories). Accordingly, custom manufactured fluorescent sheets were commissioned from manufactures using extrusion in Australia and Germany and cell casting in Spain, Germany, Japan, China and Indonesia. The optical quality of the extruded sheets was not acceptable because of problems with dye dissolution and the molecular weight of the masterbatch granules (see section 8.4.1 and appendix A.1 for details). Every cast sheet manufacturer experienced great difficulty in reliably meeting a thickness specification of 2.0 mm. There are no obvious prospects for decreasing collector sheet thickness below this value.

1.3 THESIS STRUCTURE

Creating a practical LSC system for daylighting is a difficult task that requires the simultaneous solution of many complex problems including: optical design (a lack of understanding of the key role of étendue has reduced the efficiency of many prior LSC systems), mechanical design suitable for mass production and, most important of all, the mass production of high performance collector sheets. The first half of the thesis explores the physics of LSC's from light generation, to light transport, to light extraction. We then consider the practicalities of making high performance collector sheets, with a particular emphasis on the key issues of extinction mechanisms and photodegradation.

- Chapter 2 introduces the fundamental concepts for practical LSC's and describes the advantages and problems of LSC's as light collection systems. This chapter summarizes key concepts from later chapters, so there is some overlap with later sections.

- Chapter 3 explores the basic physics of LSC's in more depth with particular reference to the role of étendue and trapped light. It will be shown that in many designs most of the fluorescent emission is trapped inside the system and cannot be used for illumination.
- Chapter 4 examines ways of coupling light from the rectangular edge of collector sheets to round optical fibres.
- Chapter 5 discusses light propagation in systems doped with microparticles that have a refractive index close to their host matrix.
- Chapter 6 describes the nature of trapped light and how it may be extracted as useful illumination.
- Chapter 7 examines the physics of light transport in LSC sheets including the problems of self-absorption.
- Chapter 8 describes ways of making and testing high performance LSC sheets by mass production.
- Chapter 9 examines extinction mechanisms in LSC sheets. This is a key issue as system performance is dominated by sheet extinction.
- Chapter 10 describes experimental studies of the photodegradation of LSC sheets.
- Chapter 11 contains the study's conclusions and suggestions for further work.

2 FUNDAMENTAL CONCEPTS

2.1 INTRODUCTION

The purpose of a luminescent solar collector system is to capture and transport sunlight to illuminate an interior room. A key parameter for characterizing an LSC system in daylighting is the light-to-light efficiency, $\eta_{l\text{-}l}$. This is defined as the ratio of the output luminous flux, F_L, to the incident luminous flux (i.e. lumens out/lumens in). From an LSC that has an effective area of, A_{eff}, illuminated by sunlight with an illuminance, I_{sol}, the light-to-light efficiency is (Earp et al. 2004c)

$$\eta_{l-l} = \frac{F_L}{I_{sol} A_{eff}} \tag{2.1}$$

LSC lighting systems built prior to this project had an efficiency of at most 0.2% (Zastrow & Wittwer 1986a) while this project achieved light-to-light efficiencies of better than 5%. Achieving a useful output of say, 1,200 lumens at a solar illuminance of 100 Klux requires that the collectors have an effective area of 0.24 m^2. It will be shown in section 3.1.5 that there are fundamental reasons for making the collectors sheets long and narrow. For a sheet length of 1.2 m, the required width is 0.20 m.

Equation (2.1) is deceptively simple and conceals a great deal of physics and some very challenging engineering. For a more detailed analysis we need to consider the action and interaction of every component of a LSC system shown in figures 1.5 and 1.7.

The luminous flux incident on the collector stack is $I_{sol}A_{eff}$. The LSC collector sheets need to be protected by a suitable weatherproof cover so only some fraction, η_{cover}, of the luminous flux will reach the collector sheets. The cover sheet is doped with a UV absorbing compound to protect the collector sheets (the violet dyes being particularly prone to UV bleaching). Significant work was done in this project to find a material that completely blocked short wavelength UV (which damages violet dyes) while letting though a maximum amount of long wavelength UV (which that dye converts into violet/blue light). For these cover sheets the main loss is Fresnel reflection and η_{cover} = 90%.

The dye molecules then absorb fraction η_{abs} of the light reaching the collector sheets. The dye molecules emit with a quantum efficiency of η_{quant} (for the dyes used in this project dissolved by the techniques described in section 8.3, $\eta_{quant} > 0.95$). The emitted light has a longer wavelength than the absorbed light. Because of this Stokes shift, the ratio of the luminous efficacy of the emitted light to that of the absorbed light, $\eta_{lum\text{-}lum}$, can exceed 100% (in other words, if the spectrum of the emitted light is a better match to the sensitivity of the human

eye than that of the absorbed light, the lumens emitted can exceed lumens absorbed) (Swift & Smith 2003).

We then have to calculate the fraction of the fluorescently emitted light that reaches the sheets' collection edges, η_{sheet}. There are several factors to consider. Only fraction, η_{TIR}, of the fluorescent emission is trapped by total internal reflection at the top and side surfaces. (For PMMA η_{TIR} = 48.4%, see section 3.1.8 for details). An ideal LSC sheet is a rectangular prism with constant thickness and perfectly smooth top and bottom surfaces that meet perfectly smooth side surfaces at infinitely sharp right angle edges. Deviations from this geometric ideal (e.g. surface roughness, thin spots in the sheet, rounded edges, etc) mean the geometric efficiency is, η_{geom}. Finally, there are losses due to material properties including: self-absorption by the dye, absorption by the matrix, scattering by dye particles, scattering by the matrix and absorption at the sheets' end mirrors. These factors mean that in the absence of geometric losses, only fraction $\eta_{material}$ of the trapped fluorescent radiation would reach the sheet's collection edge.

The sheet's efficiency parameters are related by

$$\eta_{sheet} = \eta_{TIR}\eta_{geom}\eta_{material} \tag{2.2}$$

Referring to Figure 1.7, we see that fraction $\eta_{coupler}$ of the light reaching the collection edges is then coupled into the optical conduits that transport the light to the luminaire with an efficiency of, $\eta_{conduit}$. The luminaire extracts the light reaching the end of the conduit with an efficiency of, $\eta_{extract}$. Some fraction, η_{direct}, is then directed to usefully illuminate the room (note that many luminaires for electric lamps have η_{direct}, < 50%).

So we may rewrite equation (2.1) as

$$F_L = I_{sol}A_{eff}\left(\eta_{cover}\eta_{abs}\eta_{quant}\eta_{lum-lum}\eta_{TIR}\eta_{geom}\eta_{material}\eta_{coupler}\eta_{conduit}\eta_{extract}\eta_{direct}\right) \tag{2.3}$$

where the term in brackets is equal to the light-to-light efficiency , $\eta_{l\text{-}l}$.

Equation (2.3) is something of a simplification because, as shown in Figure 1.5, a real LSC system uses a multilayer stack of collector sheets (at least one for each colour) and there is substantial coupling between the sheets in the collector stack (Earp et al. 2004b; Earp et al. 2004c; Smith & Franklin 1996; Smith & Franklin 1998; Swift & Smith 2003). However, this expression does capture the chain-like nature of the overall efficiency and makes it clear that the chain will be no stronger than the weakest link. The poor light-to-light efficiencies of prior work are due largely to the neglect of (and indeed lack of knowledge of the existence of) some of these efficiency factors.

Note that equation (2.3) is the product of 11 efficiency factors. The protective cover developed for this project has a transmission of approximately 90%. The dyes have an average

quantum efficiency of about 93% and a lumens-to-lumens efficiency of approximately 100%. The PMMA matrix has a TIR capture efficiency of 48.4%. This means that in order to achieve a light-to-light efficiency of 5%, the (geometric) mean efficiency of the other seven terms must exceed 74%, which is quite challenging.

One problem with equation (2.3) is that it implies that the various efficiency factors are all independent parameters. However, it is important to realize that this is *not* so and there can be a high degree of linkage between the various efficiency parameters. The principle mode of interaction is through changes in the amount of high-angle light i.e. rays that make a large angle to the system's local optic axis. This topic will be explored in more detail in chapters 3, 4 and 6. Another problem with equation (2.3) is that it also implies that each individual efficiency factor is constant. However, this is definitely not so and has a profound impact on the commercial feasibility of LSC systems for daylighting. The key problem is photodegradation of the collector sheets which causes $\eta_{material}$ to decrease with time. This topic is briefly explored in section 2.4 and some length in chapters 9 and 10.

2.2 Spectra of Fluorescent Emission

The collector sheets are the heart of any LSC and the system's luminous output is proportional to their efficiency. In an LSC sheet the fluorescent dyes absorb and re-emit light isotropically, and due to total internal reflection the re-emitted light is highly concentrated on the small edges of the collector. If the design parameters are optimised, this concentrated light can provide sufficient illumination for natural room lighting. LSC systems appear to be the most compatible solar collectors for use with flexible solid light guides since they collect and deliver sunlight very simply without requiring any tracking, and their output is easily and efficiently coupled to a flexible optical fibre by using a flat-to-round converter (Franklin & Smith 2004b). These essential components are described briefly in section 2.3.5 and in more depth in chapter 4.

Good transport efficiency of light within the collector sheets is essential because much of the fluorescent emission has to travel a considerable distance to the collection edge (the average path length inside the collector sheet is over a metre). Now transport efficiency always depends on sample dimensions. This means that the output of LSC system does not scale linearly with collection area (unlike most solar collector systems). In fact, it will be shown in chapter 7 that increasing the length of a collector sheet beyond a certain size gives very little extra luminous output (see Figure 7.9).

In order to model the performance of an LSC, it is important to know a number of key parameters. In photovoltaic applications of LSC's the most commonly used parameters for performance evaluation are collection efficiency or transport loss - the fraction of absorbed photons lost during transport; flux gain - increase in photon flux incident on solar cell produced

by using an LSC; and electrical efficiency - electrical energy output divided by solar energy input (Batchelder, Zewail & Cole 1979a). These performance parameters can be theoretically modelled using conventional mathematical techniques (Batchelder, Zewail & Cole 1981), or Monte Carlo simulations (Carrascosa, Unamuno & Agullo-Lopez 1983; Wittwer, Goetzberger & Heidler 1982). For lighting applications of LSC's the performance parameters are similar, but the final focus is on light-to-light efficiency rather than solar-to-electrical efficiency. Light-to-light efficiency is governed by the spectral sensitivity of the eye, while solar-to-electrical efficiency depends on the spectral sensitivity of solar cell output. In this thesis, LSC performance is described mainly in terms of light-to-light efficiency (lumens at collection edge divided by incident solar lumens) and total lumen transport loss within the LSC. Modelling that takes account of individual photon processes is presented in section 7.2, while the efficiency and transport parameters describing total visible spectral performance are discussed in section 7.4

If the light output of an LSC is to be successfully optimised it is important to distinguish between dye-related losses (scattering and absorption) and losses due to the material properties of the matrix. Ways of measuring the relative contributions of these various processes will be discussed in chapters 7, 8 and 9.

Discovering the optimum dye concentration plays a major part in the optimisation of the light output. Chapter 8 describes the patented procedure (Franklin & Smith 2004a) that was developed for finding the optimum dye concentration. The main influence of dye concentration on loss is due to self-absorption loss (see section 2.4 and chapter 9 for measurements of the relative contributions of dye related absorption and scattering). Self-absorption occurs when the dye's extinction and emission bands overlap. This is illustrated in Figure 2.1 which shows the absorption and emission spectra for the red fluorescent dye *Lumogen*® F300. If a photon is self-absorbed, the combined loss rate due to non-emission (the absorbed photon is degraded to heat) and immediate escape (the fluorescently emitted photon is not trapped by total internal reflection) is $(1-\eta_{quant}\eta_{TIR}) \approx (1-0.95\times 0.48) \approx 54\%$. This high loss rate, combined with the long path length for trapped light (averaging over a metre), means that very little of the light emitted in the overlap bands will reach the LSC's collection edge.

Figure 2.1 also shows the measured emission spectrum from a 1.2 m long LSC sheet doped with 40 ppm of *Lumogen*® F300 red dye. It is clear that almost no photons from the overlap region of the absorption and emission bands reach the LSC's exit surface. This wavelength selective loss causes a considerable shift in the colour of the LSC's output spectrum as compared to that of the dye. For the red collector sheet this spectral shift to longer wavelengths decreases the luminous efficacy of the light. However, in the cases of the violet and green sheets, the self-absorption leads to the spectrum being shifted toward the peak

sensitivity of the eye, so that there is an increase in the luminous efficacy of those spectra. In a LSC system the green sheet typically provides the bulk of the lumens with the relatively small amount of light from the violet and red light collector sheets being used for colour balance to achieve good colour rendering. This means that the increase in the luminous efficacy of the green and violet sheets significantly outweighs the decrease in the red sheet (Swift, Smith & Franklin 1999b).

Section 7.2 uses the measured spectral absorption and emission spectra of the dyes to construct a model of luminous output of an LSC. The theory and the experiments described in that section formed the basis for a patent on methods for optimising the dye concentration of an LSC sheet (Franklin & Smith 2004a). A theoretical output spectrum calculated using the methods of section 7.2 is also plotted in Figure 2.1. The agreement between the calculated and measured spectra for the LSC sheets is very close.

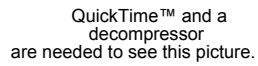

[Production Note: This figure is not included in this digital copy.
The print copy of the thesis is available for consultation at UTS Library.]

Figure 2.1 Measured spectra of dye absorption (**- - -**) and dye emission (⋯⋯) along with the associated measured (—) and calculated (**—**) emission spectra for a 1.2 m LSC doped with *Lumogen*® F300 (red).

2.3 LIGHT TRANSPORT AND EXTRACTION IN LSC'S

2.3.1 Light Distribution Inside a Rectangular Light Guide

For a material with a refractive index, n, the critical angle, θ_{crit} is

$$\theta_{crit} = \sin^{-1}\left(\frac{1}{n}\right) \tag{2.4}$$

A photon of sunlight enters the sheet where it may be absorbed and another photon is randomly re-emitted at a longer wavelength by the fluorescent dye with a quantum efficiency of

η_{quant}. For all effective purposes, the emitted light is completely isotropic. As shown in Figure 3.4, if the emitted photon travels below the critical angle with respect to the top or side surface of the sheet (42^o for PMMA), it will leave the collector. Otherwise, it will be totally internally reflected and will be confined inside the sheet by TIR until it reaches one of the sheets edges or is absorbed by an impurity or by a dye molecule (the great majority of known fluorescent dyes have significant self-absorption). Light reaching an edge will escape if the angle of incidence is less than the critical angle, or be totally internally reflected if the angle of incidence is greater than the critical angle. The precise pattern of the light field is explored in some detail in section 6.

The key point is that because the original fluorescent emission is isotropic, the light field inside the collector sheet has the largest possible solid angle for light confined within the sheet.

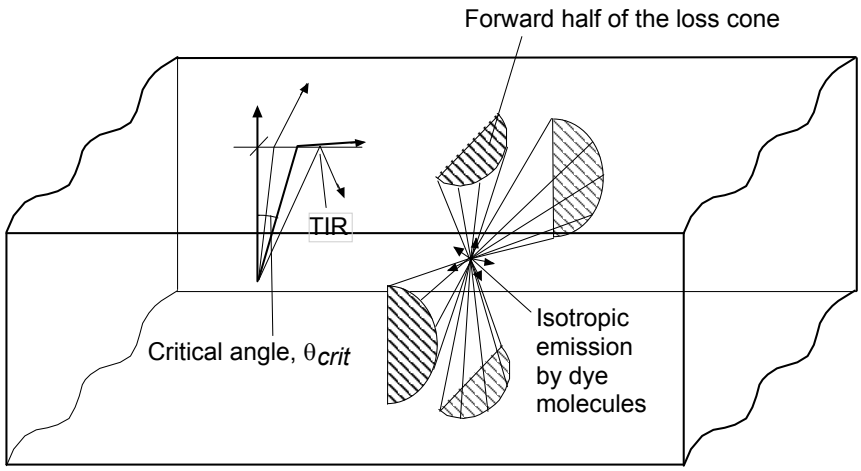

Figure 2.2 Emission inside a sheet of refractive index *n* showing TIR and the forward halves of the four side loss cones.

2.3.2 Étendue

The patent literature has a large number of LSC designs, many of them hopelessly impractical. The key problem is that very few inventors appear to understand the concept of étendue and the fundamental limitations it places on LSC performance.

Étendue is a key parameter in understanding the theoretical limits of linear non-imaging optical systems such as LSC's. It characterizes how "spread out" a light field is in terms of area and angle. Suppose we have a light field in a light guide of refractive index *n*, cross sectional area *A* as shown in Figure 2.3. The light crossing an infinitesimal area, dA, with associated area vector, **dA,** has a solid angle of Ω and we form a vector, **Ω,** of magnitude Ω in the central direction of the light.

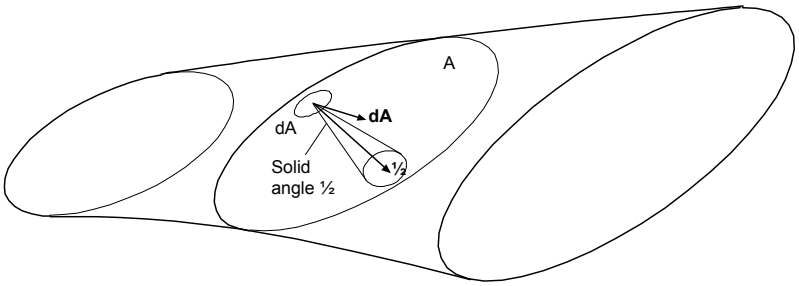

Figure 2.3 Definition of étendue in a light guide of cross sectional area A for light with a solid angle of Ω.

The étendue of the light guide, G, is defined by

$$G = \int_A n^2 \mathbf{\Omega} \bullet \mathbf{dA} \tag{2.5}$$

(Note that some authors use the symbol U for étendue.)

If the light field is uniform across the light guide and we measure the cross sectional area perpendicular to the central direction of the light (which is usually parallel to the light guide's axis of symmetry), then equation (3.1) can be simplified to

$$G = n^2 A\Omega \tag{2.6}$$

There are many proofs that étendue cannot decrease as light propagates through a linear optical system and this will be discussed at some length in section 3.1. There are formal analogies between étendue and Liouville's theorem in statistical mechanics which can be developed in some detail (Welford & Winston 1989, pp. 223-8). It follows from this linkage of étendue and entropy that it is not possible to decrease the étendue of a linear system, as doing so would violate the Second Law of Thermodynamics. This means that if étendue decreases along a linear optical system then some of the light entering the system must escape or be absorbed. If we calculate the étendue at various positions along an optical system then the smallest étendue will set the limit for the entire optical system. See section 3.1.2 and 3.1.5 for more details and a brief discussion of étendue in non-linear systems.

Figure 2.4 shows the effect of a thin section in a light guide that is confining light that has the maximum possible solid angle for that light guide (e.g. the inside of a LSC collector sheet). In the entry section the étendue of the light matches that of the light guide so there are no losses. In the thin section the étendue of the light guide decreases so that it is smaller than that of the light in the entry section. However, by the Second Law of Thermodynamics, the light's étendue cannot decrease. This means that some of the light must escape. (As the high-angle light is "squeezed" its angle increases to the point where it is no longer confined by total internal reflection). If the section beyond the narrow section is smooth then the light adiabatically

expands to fill the light guide. Individual rays that make it past the thin section end up with the same angle as before that section. The fraction of the light that is lost depends upon the angular distribution of the entering light. If that light is uniformly distributed then equation (3.2) shows that an x% decrease in the thickness of a light guide sheet will cause an x% decrease in cross sectional area and hence an x% decrease in the amount of light inside the light guide. For cell-cast fluorescent sheets thickness variations can reach 10%. For extruded or continuously cast sheet the thickness variation is typically <1% over the length of a LSC collector sheet.

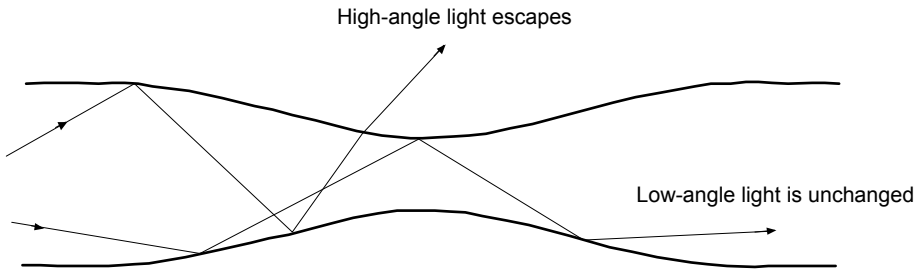

Figure 2.4 Effect of a thin section in a light guide. The thickness variation is exaggerated for clarity.

Almost all designs for LSC's have joints between components. These joints are typically either an air gap or an optical joint consisting of a thin layer of a polymer that has a similar refractive index to the components (care being taken to ensure that the polymer has no bubbles and is fully bonded to each component). It will be shown in section 3.2 that for prior art systems, the limiting étendue of the joints is considerably less than that of the other components in the optical train. This means that the joints can have large impacts on the theoretical maximum performance of the LSC system (Franklin 2001a) in ways that are not well understood by most workers "with ordinary skill in the art".

2.3.3 Trapped Light

Before going any further, it is important to make distinctions between the different categories of light within a LSC system (Earp, Franklin & Smith 2005). Consider a LSC consisting of a rectangular block of transparent dielectric with perfectly parallel sides, doped with a fluorescent dye. Light is emitted isotropically from the dye molecules, so that a small fraction (referred to as 'endlight') will strike the end surface inside the critical angle cone and escape, as shown in Figure 2.5(a). By connecting a clear light guide to this edge, the endlight can be used as a light source. It can be seen from Figure 3.4 that a considerably larger fraction (referred to as 'side loss') will escape through critical angle loss cones at the top, bottom and sides of the block. Some of the side loss cones can be converted to endlight using suitable reflectors (Franklin 2001a). The remainder of the light is 'trapped light', and does not escape at any of the surfaces of the LSC. When a clear light guide is attached to the end of the LSC sheet, without any air gap

(however small), both the endlight and the trapped light enter the light guide and will undergo total internal reflection and travel to the end of the light guide. Approximately 91% of the endlight will escape upon striking the light guide's end surface with the remaining 9% being trapped by Fresnel reflectance. It has been shown elsewhere that the light reaching the end of the light guide is approximately half endlight and half trapped light (Earp et al. 2004b; Franklin 2001a). Therefore approximately half of the available light remains trapped within the light guide (as illustrated in Figure 2.5(b)), unless the end surface of the light guide is given special treatment.

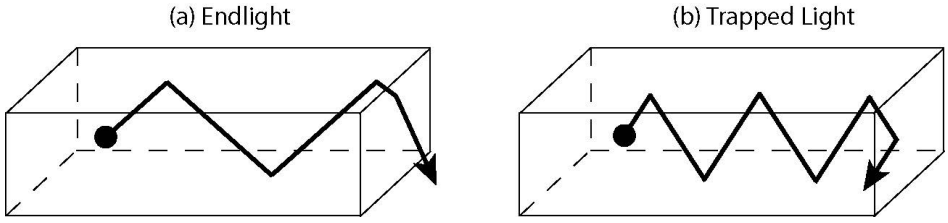

Figure 2.5 (a) Endlight can pass through an end surface of a light guide, whereas (b) trapped light is totally internally reflected at all surfaces.

It is a fundamental principle of linear optics that no optical system in which all the light enters from outside the system can ever have any trapped light. This is because light trapping requires that once light is generated within a system, it must be totally internally reflected off all surfaces. However, all linear optical systems are time reversible (Pedrotti & Pedrotti 1987). So in these systems, if light can pass in through a surface at a particular angle, then light traveling in the exact opposite direction will pass out through that surface.

If light enters a light guide system from the outside and is reflected from the far end, it will tend to reach the entry surface with an angle similar to that with which it started, and will thus be able to pass through that surface and so escape from the system. This means that any optical system in which the light enters from an external source can have no trapped light.

Only light sources that generate light inside a material can produce internally trapped light. Examples of internal light sources are fluorescent molecules and electron–hole pairs in semiconductor light emitting diodes. A substantial portion of the emission from such sources is often completely trapped within the system by total internal reflection (Saleh & Teich 2007, pp. 689 - 92). The key point is that some of this internally generated light can travel on a closed path that cannot be duplicated by light entering from the outside.

2.3.4 Light Extractors

Light extractors are devices added to a the end of a light guide that convert otherwise useless trapped light into useful end light (Franklin 2001a). They are required because the étendue of a light guide coupled to a LSC sheet can significantly exceed the étendue of free space (the

étendue of various parts of a LSC system are calculated in section 3.1). This means that as shown in Figure 2.5, a considerable fraction of light inside a light guide will be reflected by a perpendicular end surface as trapped light. Étendue is proportional to cross sectional area so one method of extracting the trapped light is to increase the light guide's cross sectional area in the terminal zone, as shown in Figure 2.6 from (Franklin 2001a). This design works but has the defect of requiring a large volume of plastic, which can be quite expensive.

QuickTime™ and a
decompressor
are needed to see this picture.

[Production Note: This figure is not included in this digital copy.
The print copy of the thesis is available for consultation at UTS Library.]

Figure 2.6 Expanded area light extractor (66) connected by an optical joint (67) to flexible thin rectangular light guides (58).

An alternative approach is shown in Figure 2.7(b) from (Earp et al. 2004b). Here the light extractor has a diffusely reflecting white coating on its rear and side surfaces. When trapped light enters the extractor it (by definition) undergoes total internal reflection at the exit face and is reflected back to the diffusely reflecting white rear surface. This reflects the light with a random orientation so that much to this light can now pass though the exit face. The fraction that does not escape is reflected by TIR back to the rear-diffusing reflector and the process continues until (i) the light enters free space via the exit face, (ii) the light is reflected back down the light guide, or (iii) the light is absorbed by the matrix or the white diffuser. For a well-made light extractor, the efficiency of converting trapped light into useful illumination is about 90%.

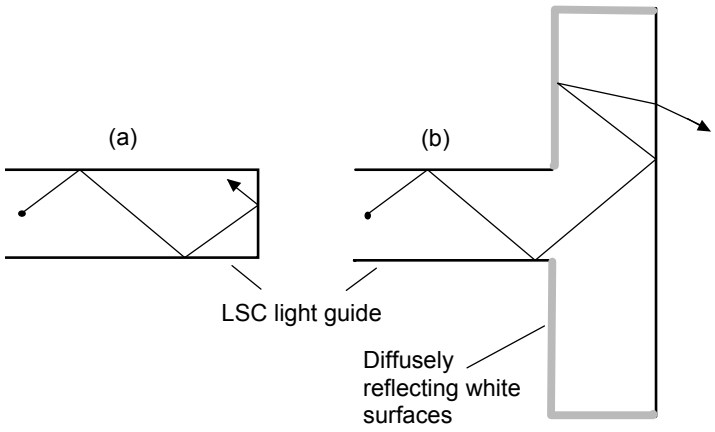

Figure 2.7 (a) A perpendicular end surface reflects almost half of the available light. (b) Extraction of trapped light by a luminare with expanded area and diffusely reflecting white surfaces.

2.3.5 Flat-to-Round Converters

The thin, flexible sheet type light guides described in section 1.2 were a considerable advance on the existing state of the art. However, they have somewhat limited flexibility and optical grade PMMA sheet is expensive. Solid core optical fibres have lower attenuation and are much more flexible. This means that it is highly desirable to somehow couple the light from a multicolour set of fluorescent collectors into a solid core optical fibre. At the start of this Daylighting project there was no known method of efficiently coupling fluorescent emission from (with its maximal solid angle) the rectangular side of a collector sheet to a cylindrical optical fibre. (The patent literature is full of attempts, but they all lack of consideration of étendue and have excessive fibre cost, as described in section 3.2).

It is clear from section 2.3.2 that the local maximum étendue must not decrease between the rectangular entry portion and the circular exit portion. In practice, since the light typically fills each component and everywhere has the largest possible solid angle, this means that the cross sectional area must not decrease. (If the cross section does decrease then this will cause large light losses, similar to those in Figure 2.4.)

The basic design is to "curl the sheet up" to a circular cross section and to then adiabatically collapse the hollow ring to a solid cylinder that is connected via an optical joint to a solid core optical fibre (Franklin & Smith 2004b). Section 4.6 describes how a version of this design was developed for injection moulding. The resulting flat-to-round converter, illustrated in Figure 2.8, has a measured transfer efficiency of 96%.

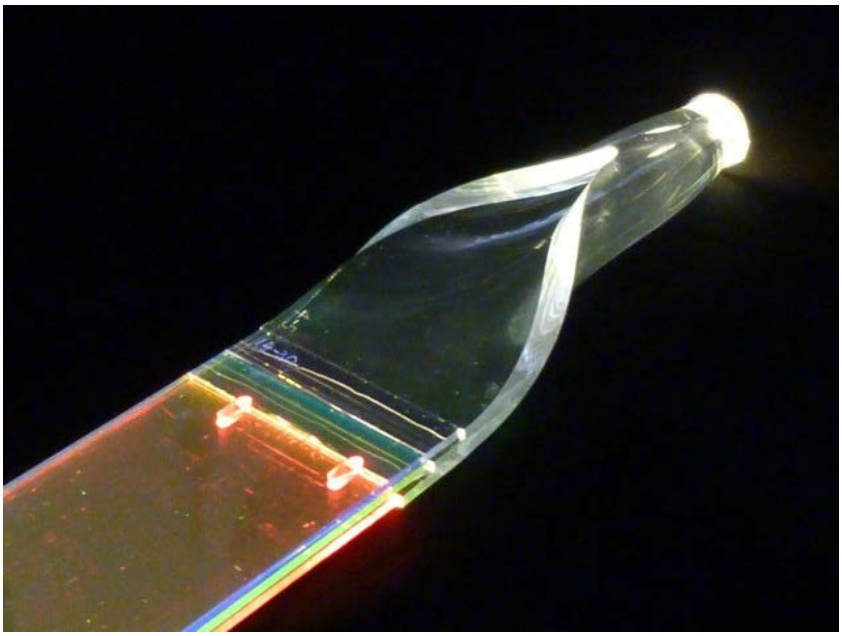

Figure 2.8 An injection-moulded flat-to-round coupler fed by a green LSC sheet feeding light to a solid core optical fibre.

2.4 EXTINCTION IN LSC SHEETS

One of the most significant remaining technical obstacles preventing widespread utilisation of LSC's is the limited photostability of the fluorescent species (Debije & Verbunt 2012; Deshpande & Namdas 2000; Earp et al. 2010; Mansour 1998a; Mansour 1998b). Light loss from an as-produced LSC sheet can be attributed to both scattering and absorption. In general, scattering arises from the matrix and absorption losses arise from the dye, but doping the matrix with dye may induce additional scattering, even if the dye appears to be fully dispersed. The reader should keep in mind that the normal reabsorption/reemission process of the dye molecules, even in the case of 100% quantum yield, behaves like an inelastic scattering process. Every re-emission redistributes the propagation angles of light nearly isotropically over the whole solid angle (assuming that the dye molecules have random orientation). A fraction of the light is not guided and leaves the collector (see section 3.1.2 for details). The remainder is trapped in the collector and may be re-absorbed and re-emitted, resulting in longer average path lengths.

Dye related losses are observed chiefly via self-absorption in the overlapping region between the dye attenuation and emission spectra (see Figure 2.1). Losses due to scattering and a wavelength independent absorption component are discussed below.

Scattering and self-absorption are greatly influenced by details of the processes used for manufacturing the LSC sheets. There are three methods of making dyed PMMA sheets of a size suitable for LSC's: extrusion, continuous casting and cell casting. Some of the advantages and disadvantages of each method are compared in section 8.4. Optical quality is highest for cell casting and lowest for extrusion. Minimum batch sizes are lowest for cell casting and highest for extrusion. For mass production the most important factors are performance and photostability (cost per sheet is a secondary factor because this is only a modest part of system cost). However, for a test programme, minimum batch size is also important since a test programme must explore many different possibilities.

In order to make ultra-high quality fluorescent sheets, it is essential that the dye is completely dissolved and dispersed at a monomolecular level. Unfortunately, most of the *Lumogen*® series of dyes have a tendency to form molecular complexes that absorb the light fluorescently emitted by single dye molecules (Bleasby 1995). Because of the long path lengths for florescent light in LSC collector sheets (typically more than 1000 mm), tiny quantities of these molecular complexes can greatly reduce the fluorescent emission from a large sheet of dyed PMMA. So an important part of the art in making fluorescent sheets for a LSC is to disperse the fluorescent dyes at a molecular level in a way that minimises the formation of molecular complexes.

A number of trials were undertaken in Australia and Germany to produce dyed collector sheets by extrusion using the standard method of mixing masterbatch granules dyed at a high concentration with clear granules and extruding the mixture on a commercial extrusion line. However, as described in section 8.4.1 and section A.1 of Appendix A, all such sheets had unacceptable scattering due to a mismatch between the molecular weight of the masterbatch granules and the clear granules. Extensive work has made it plain that the dye must be incorporated into the matrix at the time of polymerisation. This means that for this project the collector sheets had to be produced by cell casting.

The ordinary way of dissolving sparingly soluble materials, such as the *Lumogen*® series of dyes for casting, is to make up a masterbatch at high concentration in a good solvent. However, extensive trials by BASF in Germany and Australia have shown that this leads to poor optical quality sheets (Bleasby 1995; Böhm 2000). The only suitable solvent finally identified by UTS is MMA or "pre-pol" (partly polymerized MMA). An additional problem is that the laser scattering tests (see section 8.3) show that high dye concentrations rapidly lead to the creation of molecular complexes. These complexes are hard to remove once they have formed. This problem is most acute with the green F086 dye, less serious with the pink F285 dye and least serious with the violet 570 dye. It has been found experimentally that the formation of these molecular complexes can be avoided if the maximum dye concentration is always kept below 10x the final sheet concentrations. Note that because the photopic response of the human eye is peaked in the green, the green sheet supplies most of the lumens for the LSC with the principle roles of the violet and pink sheets being restricted to providing colour balance (Earp et al. 2004b; Smith & Franklin 2004; Swift & Smith 2003; Swift, Smith & Franklin 1999b). Thus any diminution of the output of the green sheet has a large adverse effect on both luminous output and colour balance.

The best way of dissolving *Lumogen*® dyes is to use ultrasonic agitation (Franklin & Swift 1997). Unfortunately few manufactures have this capability for mass production although following the success of our work at UTS, BASF GmbH have built multi-million euro plants with this capability (Böhm 2000). However, this project showed that good results can be achieved with traditional high-shear mechanical agitation. Section 8.2 and 8.3 describe ways of making and testing fluorescently dyed sheets that have the optical quality needed for LSC systems. Good optical quality collector sheets were custom manufactured for this project by these methods in factories in Spain, Germany, Japan, Indonesia and China (Australia no longer has a cell casting capacity).

As self-absorption is the major cause of dye-related losses, the emission region is the most important region for studying the absorption losses. For the green dye studied here, the emission region is approx. 470 nm < λ < 600 nm, and most of the dye absorption is observed

between 400 nm and 500 nm. In the 'tails' attenuation region above 550 nm the dye does not significantly absorb, and transmission is very close to unity. The very small, almost wavelength independent attenuation may be due to dye scattering, or to the slowly varying absorption tails. Because this region overlaps with the dye's emission peak, it has a large impact on output in the long LSC's needed for useful architectural illumination (it may be less important for short LSC's used for solar cells). This means that it must be carefully investigated.

Figure 2.9 shows the tails region of the green dye transmission spectrum in a 2.0 mm thick sample. The solid line represents the measured transmittance with the Fresnel reflectance removed. The dashed line is the same spectrum, except that the transmission in the 'tails region' beyond 550 nm has been artificially set to 100% as a reference. Chapter 9 further investigates dye related scattering and evaluates the extent to which it affects the attenuation in the tails region, and hence overall LSC performance.

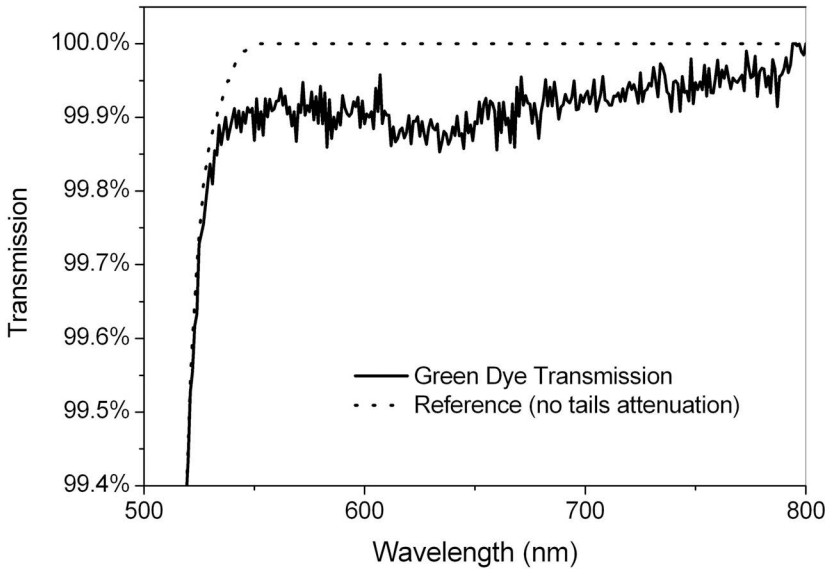

Figure 2.9 Transmission tails measured through a 2.00 mm thick LSC sheet doped with 60 ppm *Lumogen*® F083. The solid line represents the measured transmission of the green dye (excluding Fresnel reflectance), and the dashed line is the same spectrum, except that the transmission in the 'tails region' beyond 520 nm has been artificially set to 100% as a reference.

Section 9.2 describes a new technique developed to experimentally isolate and quantify the extinction losses due to scattering and absorption. The advantages of this technique are that: (i) it can non-destructively measure both absorption and scattering over very long path lengths, which greatly increases the sensitivity, (ii) all the measurements are made for the same sample whereas previous methods required different samples for absorption and scattering, and (iii) the technique is suitable for measuring the full-sized sheets used in production units.

Figure 2.10 shows the results for a 1200 mm long green LSC before and after exposure to sunlight. The luminous output of this sheet was greatly reduced by exposure and the diagram

shows that the loss was due almost entirely to increased tails absorption with no significant change in scattering.

The green sheet was under a cover sheet that had a UV transmission that was approximately 0.035% ± 0.01%, so any effect is not due to UV degradation. Chapter 10 explores the mechanism of this photodegradation, and what can be done to minimize it.

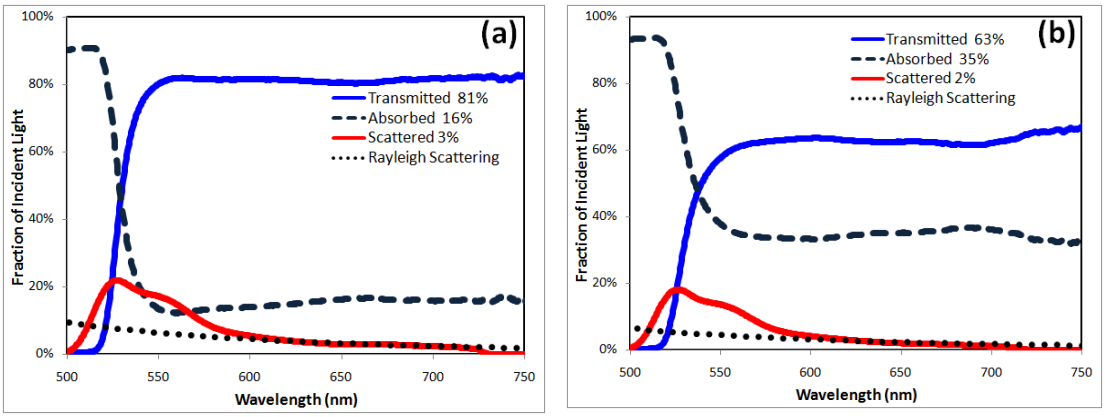

Figure 2.10 Tails extinction measurements for a **1200 mm long** green LSC (a) before exposure, (b) after exposure. A Rayleigh scattering function has been fitted for $\lambda > 600$ nm.

3 ÉTENDUE ANALYSIS OF LSC'S

Before we look at specific designs for luminescent solar collector systems for daylighting, we need to explore some of the basic physics of LSC systems. One of the most important parameters is étendue. The very poor performance of most prior LSC systems can be traced back to a lack of understanding of the role of étendue in LSC systems.

3.1 ÉTENDUE

3.1.1 What is Étendue?

Étendue characterizes how "spread out" a light field is in terms of area and angle. Because it is very closely linked to the entropy of the light field, étendue sets fundamental limits on system performance.

The definition of étendue was discussed in section 2.3.2 but is repeated here for the sake of convenience. Suppose we have a light field in a light guide cross sectional area A and of refractive index n, as shown in Figure 3.1. The light crossing an infinitesimal area, dA, with associated area vector, **dA** has a solid angle of Ω and we form a vector **Ω** of magnitude Ω in the central direction of the light.

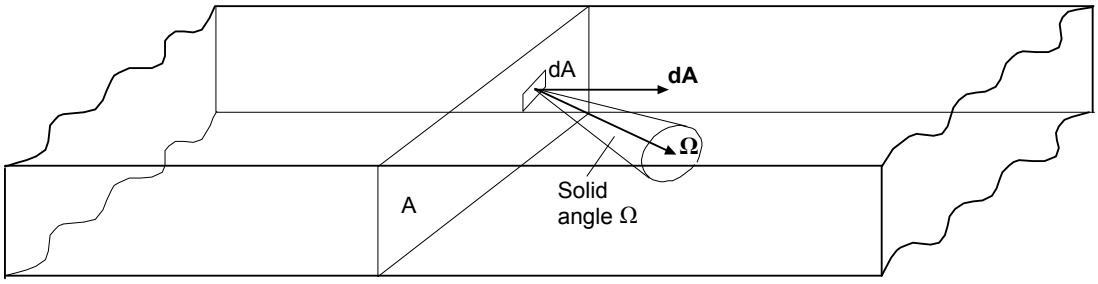

Figure 3.1 Definition of étendue in a light guide.

The étendue of the light guide, G, is defined as

$$G = \int_A n^2 \boldsymbol{\Omega} \bullet \mathbf{dA} \tag{3.1}$$

(Note that some authors use the symbol U for étendue.)

If the light field is uniform across the light guide and we measure the cross sectional area perpendicular to the central direction of the light (which is usually parallel to the light guide's axis of symmetry), then equation (3.1) can be simplified to

$$G = n^2 A \Omega \tag{3.2}$$

We noted in Chapter 2 that there have been many proofs that étendue cannot decrease if light propagation through an optical system is to be maintained without loss, including elegant and rigorous proofs using Hamiltonian mechanics and Liouville's theorem in statistical mechanics (Welford & Winston 1989, pp. 223-8). However, it is possible to show this more intuitively. Let us suppose that there existed some kind of optical system that decreased étendue. Then we could use this system to focus thermal radiation from one black body onto a smaller area on a target black body with the radiation subtending a smaller solid angle (Wilson, Minano & Benitez 2005). The higher radiation density at the target would mean that it was hotter than the source. However, as shown in Figure 3.2, this would permit a heat engine that accepted heat Q from the (hot) target and rejected a smaller amount, Q' to the (colder) source, turning the balance, $W = Q - Q'$, into work.

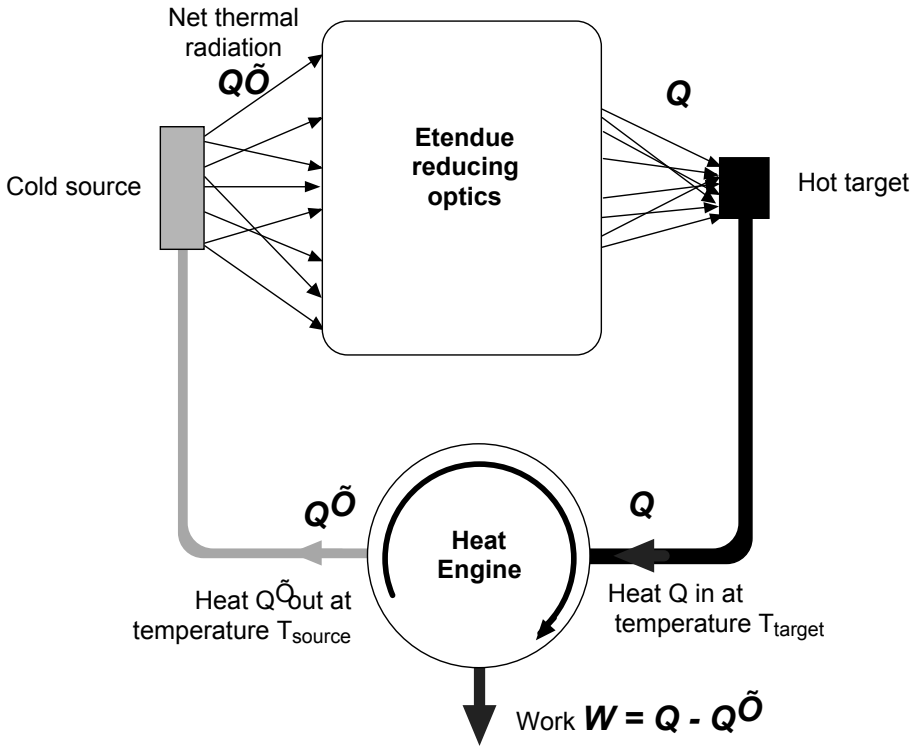

Figure 3.2 A linear optical system that decreased étendue could be combined with a heat engine to construct a perpetual motion machine of the second kind (turning heat spontaneously into work).

This system is a perpetual motion machine of the second type (turning heat spontaneously into work). As Sir Arthur Stanley Eddington observed, this is a fatal problem:

> *If someone points out to you that your pet theory of the universe is in disagreement with Maxwell's equations — then so much the worse for Maxwell's equations. If it is found to be contradicted by observation — well, these experimentalists do bungle things sometimes. But if your theory is found to be*

against the second law of thermodynamics I can give you no hope; there is nothing for it but to collapse in deepest humiliation. (Eddington 1928, p. 74).

(It will not have escaped the reader's attention that the above argument carefully refers only to *linear* optical systems and does not necessarily apply to *non-linear* optical systems, such as fluorescent sheets. In fact, it is possible to decrease the étendue in such systems, but they do not violate the Second Law (Yablonovitch 1980). The arguments are quite complex and not relevant to LSC design, so they will not be discussed here.)

Of course, as Figure 3.3 illustrates, it is very easy to *increase* étendue in a poorly designed system. That diagram shows three light guides with the same exit cross sectional area. Guide (a) contains a diffuser that increases the solid angle of the light (without increasing the area) and so increases the étendue. Guide (b) has an abrupt change in cross sectional area that increases the area without changing the light's solid angle. This also increases étendue.

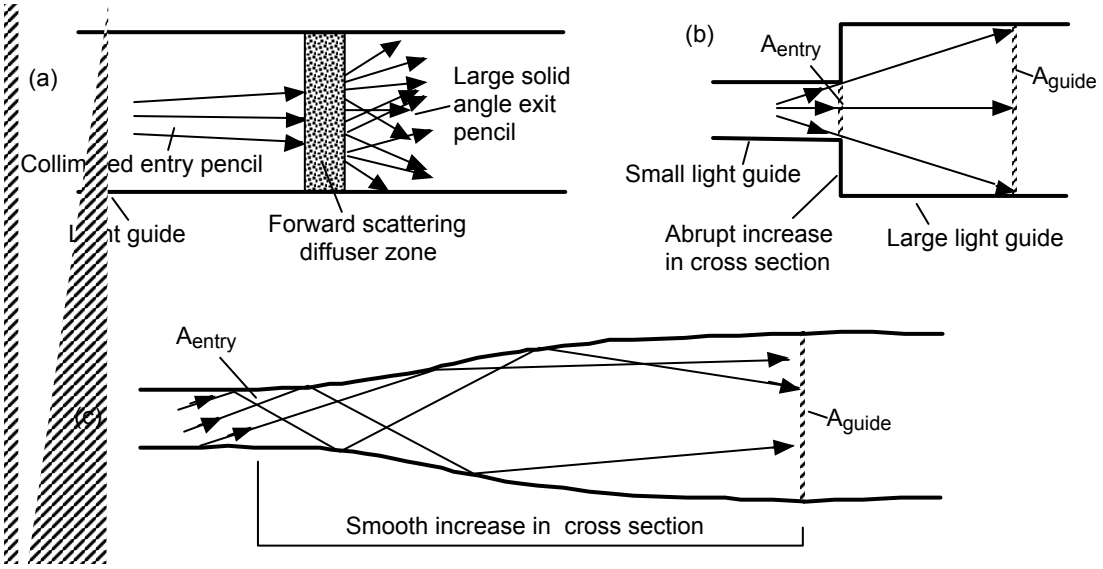

Figure 3.3 Light in various light guides. (a) Étendue increases due to diffusion. (b) Étendue increases due to excessively rapid increase in cross sectional area. (c) Étendue conserved by an adiabatic expansion area that trades more area for smaller solid angle.

It is noteworthy that both the diffusion and rapid area expansion are irreversible processes and the increase in étendue cannot be undone. However, as Figure 3.3(c) shows, a gradual, adiabatic expansion in cross sectional area can potentially preserve étendue provided there is sufficient length for the solid angle of the light to decrease proportionally as the cross sectional area increases. As Figure 3.3 (a)-(c) suggests, there is a very close link between étendue and entropy. For example, a gas flowing in systems (a) and (b) would increase its entropy and hence the process would be irreversible. On the other hand, a gas undergoing an adiabatic expansion such as guide (c) is a reversible process. The formal analogies between étendue and Liouville's

theorem in statistical mechanics can be developed in some detail (Welford & Winston 1989, pp. 223-8). A key result is that if the étendue increases then the process is irreversible,.

3.1.2 Limiting Étendue

Étendue as defined by equation (3.1) is a combined property of the light source and the light transmitting optical system. If the source's light distribution changes, then so does the étendue. For example, if a broad angle light source is replaced with a highly collimated laser beam then the system's étendue drops almost to zero.

When analyzing LSC's, it is useful to talk of the *limiting local étendue*, $G_x^{\max}$, the maximum possible étendue at cross section x. This parameter has the virtue of being determined purely by the physical properties of the local components at location x and is time independent. Let Ω_{max} be the maximum possible solid angle of light that could be confined in the system at the region of interest ("the maximum light angle"). Then $G_x^{\max}$ can be computed by using Ω_{max} rather than Ω in equations (3.1) or (3.2).

There are four cases of general interest for which we wish to know the value of Ω_{max} so that we can compute the limiting local étendue: free space, a wide sheet, a rectangular light guide and a cylindrical light guide. The results are summarized in

Table 3-1.

For free space, it clear by definition that for forward propagating light $\Omega_{max} = 2\pi$.

We define a wide sheet as a planar block of material of refractive index, n, where the light is so remote from the sides, so that it essentially interacts only with the top and bottom surfaces. In practice this means that the width of the sheet (measured perpendicular to the optic axis) is much greater than its length.

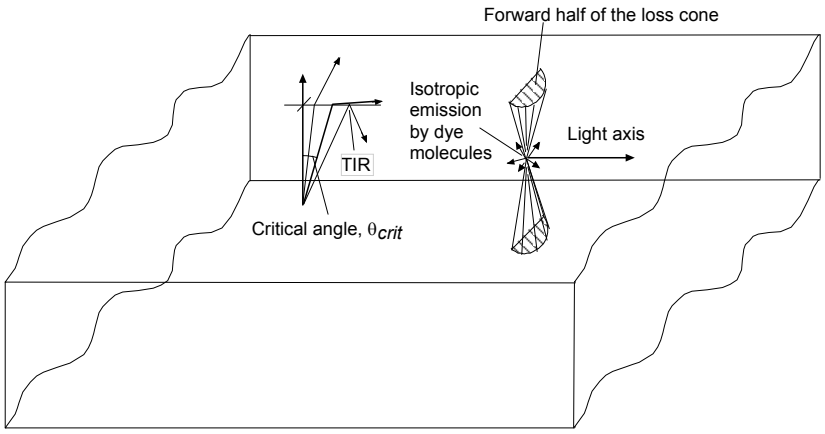

Figure 3.4 Emission inside a sheet of refractive index n showing TIR and the forward halves of the upper and lower loss cones.

As shown in Figure 3.4, all the light striking one of the top and bottom surfaces at less than the critical angle escapes. (Note that this escape may not be immediate since a ray can

initially be trapped by Fresnel reflection. However, the mean Fresnel reflection coefficient is 9% (Earp, Franklin & Smith 2005). So, after just three bounces (during which the light travels less than three sheet thicknesses transversely, i.e. typically less than 6 mm) escape efficiency is better than 99.9%. Thus for almost all purposes we can ignore trapping by Fresnel reflection[1].)

If the boundary layer surrounding the block is air then the critical angle, θ_{crit} is

$$\theta_{crit} = \sin^{-1}\left(\frac{1}{n}\right) \tag{3.3}$$

Now the solid angle of a cone with a semi-angle of θ is

$$\Omega = 2\pi(1-\cos\theta) \tag{3.4}$$

and we see from Figure 3.5, equation (3.3) and Pythagoras's theorem that

$$\cos\theta_{crit} = \sqrt{1-1/n^2} \tag{3.5}$$

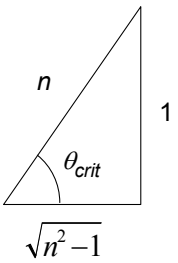

Figure 3.5 Calculation of the cosine of θ_{crit}.

Thus the solid angle of the escape cone, Ω_{escape}, is

$$\Omega_{escape} = 2\pi\left(1-\sqrt{1-1/n^2}\right) \tag{3.6}$$

In the wide sheet illustrated in Figure 3.4, the escaped forward traveling light fills two half-cones of semi-angle θ_{crit}. So from (3.6) the maximum solid angle of the forward traveling light confined within a sheet by TIR is $\Omega_{max\ sheet}$, where

[1] The reflection coefficient at a PMMA air interface increases from 2.7% at normal incidence to 100% at the critical angle. For uniformly distributed light the mean Fresnel reflection coefficient is 9% (assuming random polarization) (Earp, Franklin & Smith 2005). The reflection coefficient increases after each reflection as light close to normal incidence escapes preferentially. The small amount of initial light at just less than the critical angle can travel for several centimetres before it escapes. However, this is much less than the sheet length, so this complication can usually be ignored. Self-absorption also has a small effect on the fraction of emitted light that is lost in the escape cone (Goldschmidt et al. 2009).

$$\Omega_{max\ sheet} = 2\pi - 2 \times 0.5 \times \Omega_{escape} = 2\pi\sqrt{1 - 1/n^2} \tag{3.7}$$

In a rectangular light guide, the light interacts with the sidewalls so that there are four escape cones, as shown in Figure 3.6. In a high refractive index guide surrounded by air the loss cones do not overlap. However, for a low refractive index guide (or one with a low refractive index cladding) the cones overlap and the calculation becomes more difficult. The condition for the escape cones overlapping is that the critical angle is more than 45°, i.e. $n < \sqrt{2} = 1.414$. The refractive index of PMMA is 1.49 (MatWeb-Cast 2011; MatWeb-Extruded 2011) so there no overlap in the escape cones in PMMA rectangular light guides that have an air boundary layer.

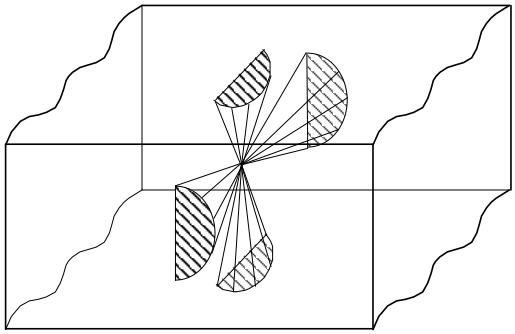

Figure 3.6 Light inside a rectangular light guide of refractive index *n* showing the forward halves of the four loss cones.

Using equations (3.3) and (3.4) we see that for a rectangular light guide, with $n > 1.414$ the maximum solid angle of forward traveling light confined by TIR, $\Omega_{max\ rect}$ is

$$\Omega_{max\ rect} = 2\pi\left(2\sqrt{1 - 1/n^2} - 1\right) \quad (n \geq \sqrt{2}) \tag{3.8}$$

We are also interested in cylindrical light guides, such as solid core optical fibres. The limiting solid angle for skew light in a cylindrical light guide is a complex function of transverse position. However, as Figure 3.7 shows, it is easy to calculate the axial case. We see by inspection that meridional rays of light will be confined by total internal refection provided they make an angle smaller than $\pi/2 - \theta_{crit}$ with the fibre's axis.

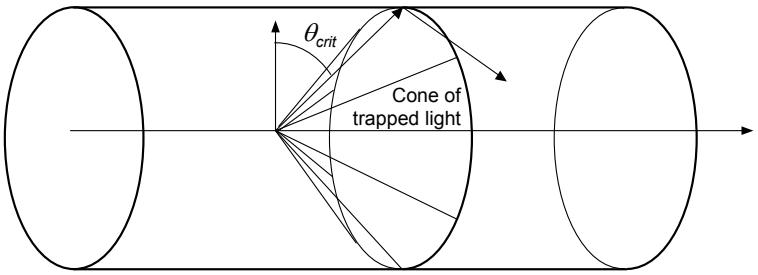

Figure 3.7 Trapping of meridional light in an optical fibre.

Let m be the ratio of the refractive index of the fibre's core to its cladding (for an air gap fibre $n = m$). Then from equations (3.3), (3.4) and Figure 3.5, we see that the maximum solid angle for meridional light is

$$\begin{aligned}\Omega_{max\,mer} &= 2\pi\left[1-\cos\left(\frac{\pi}{2}-\theta_{crit}\right)\right] \\ &= 2\pi\left(1-1/m\right)\end{aligned} \tag{3.9}$$

which is a good approximation for the average maximum solid angle for the whole fibre.

Table 3-1 Maximum solid angles for forward propagating light in various geometries.

Free space	Wide Sheet	Rectangular Light Pipe	Cylindrical Optical Fibre
2π	$2\pi\sqrt{1-1/n^2}$	$2\pi\left(2\sqrt{1-1/n^2}-1\right)$	$\approx 2\pi\left(1-1/m\right)$

3.1.3 The Light Field in a Fluorescent Sheet

A photon of sunlight enters the sheet where it may be absorbed and randomly re-emitted at a longer wavelength by the fluorescent dye. The resulting light distribution is quite complex (Patrick et al. 2011) and has to be modelled by Monte Carlo methods for detailed calculations. The absorption and emission patterns of an individual dye molecule are typically dipoles with the their axes at small angles to the long axis of the molecule. Molecules that happen to have their absorption dipole perpendicular to the incoming sunlight will preferentially absorb the incoming radiation. These molecules' emission dipoles will be at a small angle to the absorption dipole so the emission "donuts" will be preferentially aligned perpendicular to the incoming ray. This means that even if the dye molecules are randomly orientated, the preferential alignment of the absorption dipoles produces an anisotropy in the average emission with enhanced emission parallel and antiparallel to the direction of the incoming light. However, the effect is not very large and is counteracted by self-absorption that is essentially isotropic. For the sake of simplicity we will assume that bulk emission is isotropic unless otherwise stated.

As an aside, it is intriguing to note that the anisotropy of the emission pattern of individual dye molecules means that that if some method could be found to orientate the dye molecules with their axis perpendicular to the sheet's surface, then the light-to-light efficiency of a LSC system could be significantly increased (MacQueen et al. 2010; Mulder et al. 2010; Patrick et al. 2011). Note that dye absorption would be decreased which would require increased dye, although this can be alleviated by using an external diffuser (Mulder et al. 2010). The

increased dye would cause increased self-absorption, with possible adverse effects on the sheet's light transport properties.

Creating and maintaining the molecular orientation in a solid sheet is difficult. The thermal energy from the Stoke's Shift heats the immediate vicinity of dye molecules to several hundred degrees and so over time an unbound individual dye molecule may migrate several millimetres due to thermal diffusion. This means that it is necessary to anchor the dye molecules in a way that preserves their orientation. Demonstrated methods on a laboratory scale include: dissolving the dyes in a liquid crystal solution and applying an external voltage to align the liquid crystals and hence the dye molecules (Debije & Verbunt 2012); and using a suitable alignment layer to orientate liquid crystals containing the dye (Mulder et al. 2010) which may be fixed by crosslinking the liquid crystal (Verbunt et al. 2009). However, these are methods for the future and will not be considered further.

For our purposes, we can assume that the emitted light is completely isotropic. As shown in Figure 3.4, if the emitted photon travels below the critical angle with respect to the top or side surface of the sheet (42^o for PMMA), it will leave the collector. Otherwise, it will be totally internally reflected and will be confined inside the sheet by TIR until it reaches one of the sheets edges or is absorbed by an impurity or by a dye molecule (all known fluorescent dyes have significant self absorption.) Light reaching an edge will escape if the angle of incidence is less than the critical angle, or be totally internally reflected if the angle of incidence is greater than the critical angle. The precise pattern of the light field is explored in some detail in section 6.4.

However, we do not at this stage need to know the details of the light field. The key point is that because the original fluorescent emission is essentially isotropic, the light field inside the collector sheet has the largest possible solid angle for light confined within the sheet. If the light does not interact with the sheets edges (which it will not if the collector sheet is much shorter than its width) then the solid angle is given by equation (3.7). If the light interacts with the sheet's edges, as it will if the collector sheet is long and narrow, then the solid angle is given by equation (3.8).

3.1.4 Étendue of Air Gaps and Optical Joints

Almost all designs for LSC's have joints between components. These joints are typically either an air gap or an optical joint consisting of a thin layer of a polymer that has a similar refractive index to the components (care being taken to ensure that the polymer is fully bonded to each component with no bubbles at the interfaces or inside the polymer). It turns out that these joints can have large impacts on the theoretical maximum performance of the LSC system (Franklin 2001a) in ways that are not well understood by most workers. So it is useful to explicitly calculate the étendue of these elements.

Figure 3.8 shows the air gap at the end of a light guide that has its end inclined to the light guide axis by angle axis, ϕ. The diagram illustrates a rectangular light guide of cross sectional area *A*, but the argument is readily generalized to any shape of light guide. By the term "air gap" we mean any layer of air between optical components that is thick enough so that high angle rays inside one component could undergo total internal reflection. In practice this means a gap thickness of more than two wavelengths (say > 10^{-6} m). If the gap is thinner than this, the evanescent wave will bridge the gap, leading to frustrated total internal reflection (Hecht 2002, p. 126). The transport efficiency of the evanescent waves is an inverse exponential function of the gap's thickness and is close to unity for gaps less than a tenth of a wavelength (Klein 1970, p. 579).

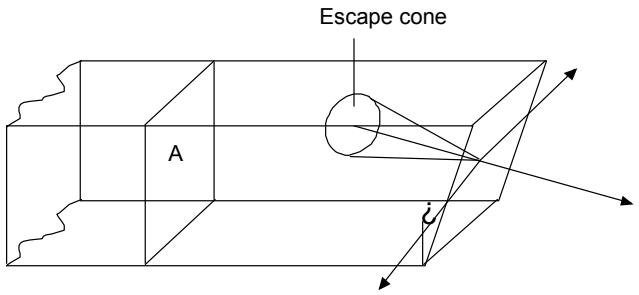

Figure 3.8 Calculation of the étendue of the end of a light guide inclined at angle ø.

Let us initially suppose that the light field is uniform across the exit plane for any angle of incidence up to the critical angle. Now only rays up to the critical angle can cross the surface: rays at higher angles are totally internally reflected and so are trapped inside the light guide (this topic is explored in some detail in chapter 6). Moreover, the process of refraction preserves étendue. Therefore, the étendue of the light in the air gap is equal to the étendue of the light in the exit cone. Thus, from equations (3.1) and (3.6), we see that the étendue in the air gap, G_{gap}, is

$$G_{gap} = \frac{2\pi n^2 A\left(1-\sqrt{1-1/n^2}\right)}{\cos\phi} \tag{3.10}$$

Equation (3.10) is in fact an upper bound on G_{gap}. This is because a key assumption in its derivation was that the light field is uniform across the exit plane for any angle of incidence up to the critical angle. However, high angle rays can escape through the light guide's surfaces and so may not be reach the exit surface which would reduce Ω and hence *G*. If, as illustrated in Figure 3.8, one of the exit surface's edges is perpendicular to the light guide axis, the restriction on ϕ is $\phi \le \pi/2 - 2\theta_{crit}$. For PMMA this is $\phi < 5.8^{o}$. Skew orientations for the exit surface have a slightly larger limit on ϕ before the étendue in the gap is reduced.

An optical joint has a considerably larger étendue than an air gap. In fact, if it is thin and has no bubbles it will be lossless. So the limiting étendue will be that of a block of polymer, $2\pi n^2 A$. However, the actual étendue of a good optical joint is the étendue of the optical conduit.

3.1.5 Étendue – The Implications

The conservation (at best) of étendue inside a light guide system is of fundamental importance to designing LSC systems. First, suppose that the étendue in one part of the system is G_1 and this is connected by various optically lossless components to a region two which has étendue G_2 and limiting étendue of $G_2^{\max}$. Now $G_2 \le G_2^{\max}$. So if $G_2^{\max} < G_1$ then $G_2 \le G_2^{\max} < G_1$, which we showed in section 3.1.1 is not possible as it would violate the Second Law of thermodynamics. This means that the connection between regions one and two cannot in fact be lossless. Enough light must leak from the system (or be back reflected) so that the étendue does not decrease. If we back propagate the light from region two to region one, we will find that the solid angle of these rays (and/or) the effective cross sectional area at region one is only a subset of the light present at position one. Everything else is lost along the way (or reflected back to region one – where so ever it goes, it does not get to region two).

This gives us the following minimum condition for a high efficiency LSC:

In a well-designed LSC system, the local maximum étendue, G^{max}, does not decrease. **R1**

This condition is rather like using the conservation of energy to analyze a complex mechanical system. The designer may have the most beautiful arguments to show that if you put one joule of work into his system you will get two joules out (a perpetual motion machine of the first kind). The conservation of energy tells us that he is wrong. It does not say where the mistake is, or why the machine does not work, it just proves beyond all doubt that it will not work as claimed. Of course, the fact that a design does not violate the conservation of energy does not mean that it will actually work (let alone be commercially viable). It just means that it *could* work and *might* be commercially interesting.

The second implication the conservation of étendue is that

In a well-designed LSC system, the local maximum étendue will remain as constant as possible throughout the system. **R2**

We can use results R1 and R2 to determine the optimum aspect ratio for the collector sheets (i.e. the ratio of a sheet's length to width). Now it follows from R1 and R2 that the light guides will have at least as large a cross sectional area as that of the collector sheets (measured

perpendicular to the mean direction of light transport). But the cost of the light guides, whether optical fibre or strips of polymer, is by far and away the most expensive component of a LSC used for daylighting, and this cost is proportionate to their cross sectional area (see section 4.4 for more details of the costs of optical fibre).

Now the cross sectional area of the collector sheets is their width times their thickness and we can assume that the sheets are as thin as possible. So to minimize system costs, we need to minimize the light guides' cross-section, and hence, by R1, the width of the collector sheets. This means that in order to collect adequate light the collector sheets must be as long as possible i.e. have the largest possible aspect ratio. The useful length of the sheets will be determined by their internal light transport properties. Ways of measuring this are discussed in chapter 7.4.

To summarize,

The aspect ratio of the collector sheets must be as large as possible **R3**

It is informative to calculate the limiting étendue at all the parts of a LSC system from the light collector sheets (where the fluorescently emitted light starts) through to the free space in the room being illuminated. Now étendue cannot decrease. So the smallest value of limiting étendue in the system will limit overall system performance. We call this parameter G_{limit}

$$G_{limit} = \min(G^{\max}) \tag{3.11}$$

If $G_{limit} < G_{sheet}^{max}$ then the conservation of étendue requires that there must be inherent light losses (or back reflections) somewhere between the collector sheet and the illuminated room. We will call this the G_{limit} test. Note that this is a very weak condition, since (3.11) uses the theoretical maximum value of the étendue at every point. It is quite possible that the achieved étendue will be smaller than this, so a system may inherently leak light even if it passes the G_{limit} test. This leads to the following result:

If $G_{\text{limit}} < G_{\text{sheet}}^{\max}$ then there are inherent light losses along the LSC system.
The converse is not true. **R4**

3.1.6 Étendue Inside a Generic LSC

In order to analyze the optical performance of different components of a LSC system, it is useful to compute the limiting étendue per unit area, g_{max}, for each component. From equation (3.1),

$$g_{\max} = \frac{1}{A}\int_A n^2 \boldsymbol{\Omega}_{\max} \bullet \mathbf{dA} \tag{3.12}$$

If the limiting solid angle is constant across a cross section measured perpendicular to the central direction of the light, we can simply equation (3.12) to

$$g_{\max} = n^2 \Omega_{\max} \tag{3.13}$$

We can use the results of equation (3.13), section 3.1.3 and

Table 3-1 to calculate the limiting étendue per unit area in a LSC of the generalized form described in Figure 1.7. The results are summarized in Table 3-2. For the sake of simplicity, we have assumed that all polymer components other than cylindrical light guides are made from PMMA with a refractive index of 1.491. The refractive index of large diameter solid core fibres is taken as 1.480 (Deller et al. 2002). If these fibres are air-clad then $m = n = 1.480$. If the fibres are in optical contact with a fluoropolymer jacket such as Teflon® (refractive index 1.35) then $m = 1.096$.

Table 3-2 Limiting étendue per unit area in various generic LSC components.

Component	Type	Limiting Étendue per Unit Area (sr)
Collector stack	Wide sheets	10.36
	Narrow rectangle	6.75
Sheet coupler	Air gap	3.61
	Optical joint	13.97
Light guides	Narrow rectangle	6.75
	Cylindrical (air gap)	4.46
	Cylindrical (Teflon® cladding)	1.21
Luminaire coupler	Air gap (normal)	3.61
	Air gap (30 deg)	≤ 4.17
	Optical joint	13.97
Luminaire	Free space	6.28

There are two key results from Table 3-2. The first is the very low étendue per unit area of an air gap in comparison to the values for other components. Thus, by the G_{limit} test, any air gaps in the optical train will greatly reduce system performance. This topic is explored in some detail in chapter 6.

The second result is the very low étendue per unit area for optical fibre where the core is in optical contact with a fluoropolymer jacket. This means that there is a considerable advantage of using a fibre in which the core is loose enough in its fluoropolymer tube so that there is an air jacket at the boundary of the cylindrical core.

3.1.7 Étendue and Light Squeezing

The conservation of étendue inside a light guide has profound consequences for the design of LSC systems. As mentioned in section 1.2, the cost of the light guides in the optical conduit tends to dominate the cost of the system. So the smaller the cross sectional area of the light guides, the cheaper the system. Thus there is a big incentive to find some way to "squeeze" the light from a big collector stack into a narrow optical conduit. Many, many, suggestions have been made and an inordinate number have been patented. The implicit designs are all similar to that shown in Figure 3.9. A large area collector stack is coupled to a small (cheap!) light guide by a sheet coupler that is promised to somehow funnel all the light from the collector stack into the light guide and hence turn it into useful remote intense illumination.

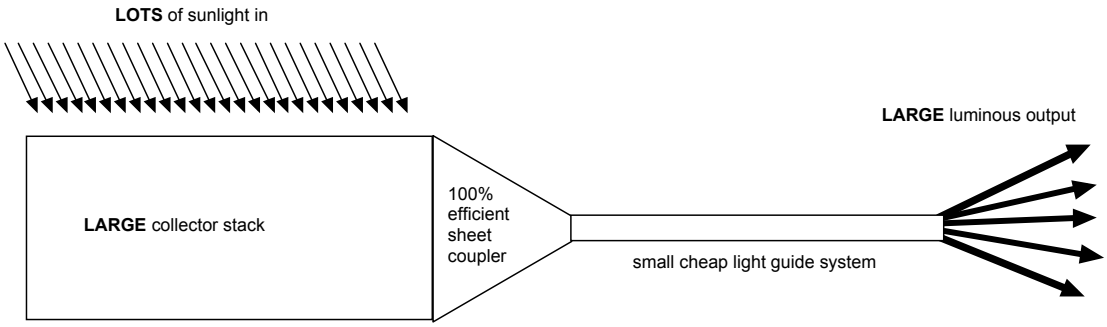

Figure 3.9 Claimed schematic of many (impractical) LSC designs.

Now equation (3.2) shows that the étendue is proportional to the product of cross sectional area and the solid angle of the light that passes through the system while we see from

Table 3-1 that the limiting solid angle for the light guide is at best equal to that of the collector sheets. However, the large cross sectional area of the collector stack means that its local étendue will be much greater than that of the small light guide system. But it was shown in section 3.1.1 that the Second Law of Thermodynamics requires that étendue cannot decrease. So only a small fraction of the light from the collector stack can in fact pass through the sheet coupler into the light guide. Depending on the details of the sheet coupler, it may be that only the very low angle rays are transmitted through it into the light guide. Alternatively, it might be that only light from a very small part of the collector stack can cross the sheet coupler into the light guide. But whatever the details, ***there is no possible design*** of sheet coupler that can transmit most of the light. The system really functions at *best* as shown in Figure 3.10, with the effective cross section of the collector stack being at most that of the light guides. (And in practice, few designs even reach this abysmal level of efficiency.)

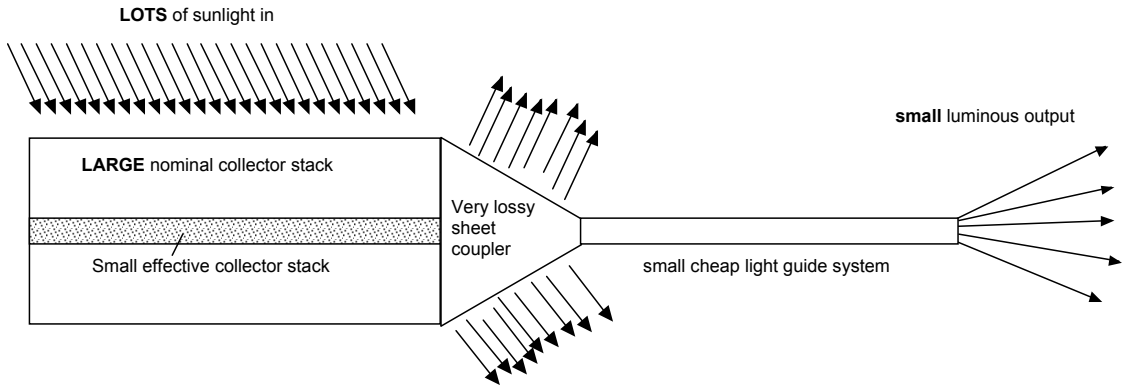

Figure 3.10 How the system in Figure 3.9 actually works *at best* (it may well actually have substantially lower performance).

3.1.8 Some Limitations of Étendue Analysis

In a flat collector sheet there are four escape cones. So from equation (3.6) the fraction of fluorescent emission trapped inside the collector sheet by total internal reflection, η_{TIR}, is

$$\eta_{TIR} = \frac{4\pi - 4\Omega_{escape}}{4\pi} = 2\sqrt{1 - 1/n^2} - 1 \quad (n \geq \sqrt{2}) \tag{3.14}$$

For PMMA η_{TIR} = 48.4% with 24.2% of the light travelling forward and an equal amount travelling to the opposite end of the collector sheet. By adding a suitable specular end reflector, the direction of the light that reaches the sheet's end can be reversed. This means that the forward travelling light can potentially approach 48%. (Attenuation in the sheet and absorption at the end reflector will restrict the attainable fraction to somewhat less than this limit.)

Note that while adding the specular end reflector nearly doubles the amount of forward travelling light, and hence output lumens, it does not change the angular distribution of that light and so the sheet's étendue is unchanged. Downstream étendue will also be unchanged. Thus adding the end reflector almost doubles system output while leaving the étendue everywhere unchanged.

This illustrates the fact that while étendue analysis is a good tool for understanding some aspects of system performance (particularly losses due to "light squeezing" and losses due to air gaps) it is not sufficient by itself to calculate output lumens, which is often *the* key performance parameter.

3.2 PRACTICAL LSC SYSTEMS

3.2.1 Bornstein and Friedman

By far the best LSC design prior to the work at UTS was that of Bornstein and Friedman described in their US 4,539,625 patent (Bornstein & Friedman 1985). As it happens, this work was unknown when the UTS SCATS design (Sunlight Collection And Transmission System) was developed and was only discovered during the literature search for the SCATS patent applications. It is instructive to compare and contrast the similarities and differences in approach in trying to solve common problems. Copies of Figs 1 and 2 in Bornstein and Friedman's patent are shown in Figure 3.11 with some labels added to Fig 1 and the numbers in Fig 2 replaced by labels.

Bornstein and Friedman's basic design has a three-layer stack of polymer sheets dyed with blue, green and red fluorescent dyes. There is a layer of air above and below each sheet. The low refractive index of the air layers confines an (unstated) portion of the fluorescently emitted light inside each sheet by total internal reflection. This light is transported by total internal reflection to one of the sheets' long edges that are butted against rectangular light guides. These light guides then transport the fluorescently emitted light to a remote luminaire. The collector sheets' edges opposite to the light guides have specular side reflectors to increase output by directing fluorescent light back towards the light guides. There is also a specular bottom reflector that boosts output by redirecting any daylight not absorbed during the downward path back up through the stack with an additional chance of absorption. Bornstein and Friedman's preference is that the light guide should consist of an array of flexible square optical fibres. If that is too expensive, they envisage using a single block of thick plastic that is as wide as the full length of the collector sheets.

While Bornstein and Friedman's design is a substantial improvement on prior work, it has a considerable number of fundamental problems including the very high cost of the light guides, the intrinsic difficulty of installation, and great difficulties of manufacture. Let us look first at the light guides. Bornstein and Friedman do not suggest any dimensions for the collector sheets, but a reasonable luminous output would require collectors with a width of about one metre and a length (measured along the optic axis) of perhaps 200 mm for an aspect ratio of about 0.2 or less. We showed briefly in section 1.2 that the minimum practical thickness for collector sheets is 2.0 mm and this topic will be addressed in more detail in section 8.4. The existence of this minimum sheet thickness means that the minimum height of the collector stack is at least 6.0 mm (and probably somewhat larger to allow for the all-important air gaps between the sheets). So with 6.0 mm square optical fibres, one would need 167 fibres. (Or fewer, but more expensive larger fibres if the thickness of the collector stack exceeds 6 mm). Joining these to the

collector sheets would present formidable production problems. More importantly, there is no known current manufacturer of high performance square optical fibres. At UTS we explored the feasibility of a different design of LSC that used square optical fibres. We worked with *Poly Optics Australia Pty Ltd*, one of the world's leading manufactures of round solid core optical fibres, to try to make high quality fibres that had a rectangular cross section. However, we were never able to achieve satisfactory results.

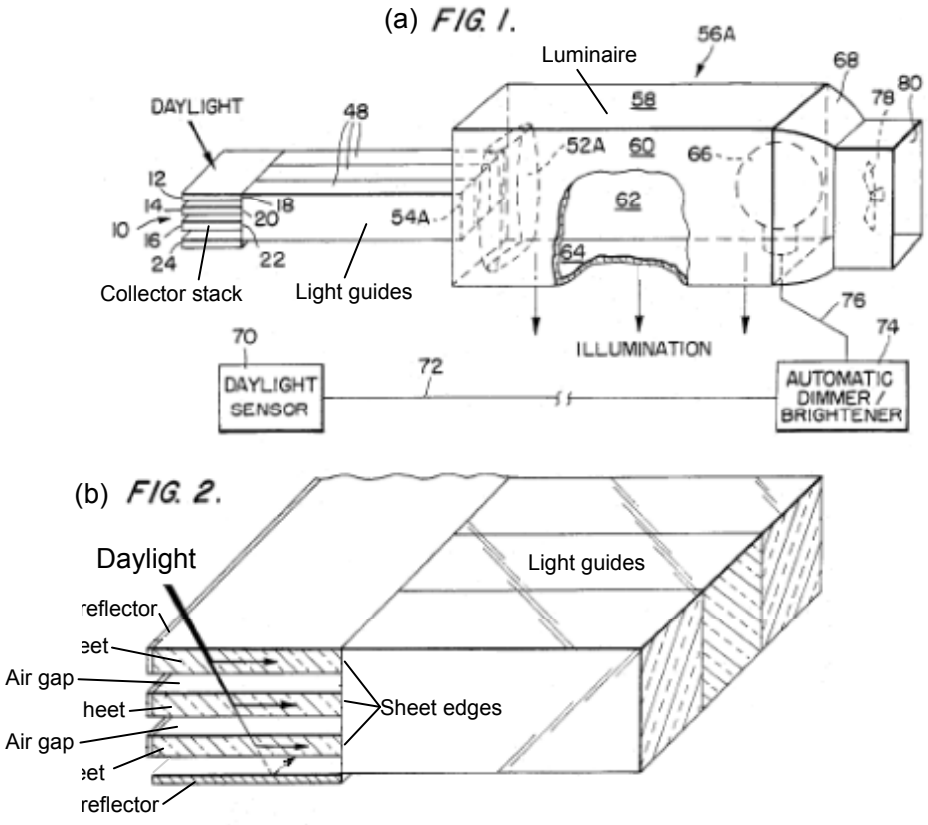

Figure 3.11 Key drawings from Bornstein and Friedman's patent US 4,539,625 with some numbers replaced by labels. (a) Overview of their system. (b) Details of the collector stack.

The best currently available optical fibre for a Bornstein and Friedman system would be solid core round optical fibres, such as those produced by *Poly Optics Australia Pty Ltd* (Poly Optics Australia Pty 2011) or Lumenyte International Corporation (Lumenyte Optical Fiber 2011). The geometric miss-match between the fibres' circular profile of the rectangular sheets would lead to a significant coupling loss. A much more important problem is the expense. Solid core fibre of this size costs about US$10 per metre in bulk (see section 4.4 for more details). So a one metre run of light guide would cost about US$1670.

Now there is no point in installing a LSC where a cheap window or skylight can do the same job: LSC's only make sense where they can get light into a room where conventional means cannot. This means that the light guides will have to be several metres long. Three

metres of optical fibres for the Borstein & Friedman system would cost US$5,000, which is unaffordable. Flexible PMMA optical fibres would not be an option as they are more expensive per unit area and transport a smaller fraction of the high angle light.

Borstein and Friedman implicitly recognized the impracticality and unrealistically high cost of using flexible optical fibres for the light guide and suggested the alternative of using a single thick sheet of polymer. This would have the at least the same thickness as the combined collector stack (i.e. at least 6 mm) and run the full width of the stack (about a metre). A PMMA sheet that is 1 meter wide, 6 mm thick and say three metres long would be completely rigid and extraordinarily hard to install. The building would have to be designed around it. I am not saying that it could not be done, but it would be horrendously expensive. The very high cost of the light guides, the great difficulties in system assembly and the severe installation problems probably explain why I have not been able to locate any published examples of a Bornstein and Friedman system ever having been built.

While the Bornstein and Friedman system may not be a practical LSC, it does serve as good example for using étendue to analyze a system. The étendue of the various components are examined in turn below and the results summarized in **Table 3-3**.

The collector stack is much wider than it is long, so the fluorescently emitted light will have only a little interaction with the sheet edges that are parallel to the light guide axis. This means that the étendue per unit area will be slightly smaller than that for perfect sheet. A limit of about 10 sr seems reasonable (compared to 10.36 sr if there was no interaction with the short edges).

The nature of the joints between the collector stack and the light guides is not clear in the specification. Optical joints would transmit a lot more light than an air gap. Note that although the limiting étendue per unit area for a lossless optical joint is 13.97 sr, in fact the actual étendue per unit area cannot be more than that of the collector stack, i.e. about 10 sr.

The inventors discuss both rectangular light guides and a massive sheet (here estimated at 3 m x 1 m x 6 mm). However, the sheet type light guide is long enough in relation to its width so that all high angle light will have multiple interactions with the sidewalls. Thus its limiting étendue is the same as that for a standard rectangular light guide.

The luminaire coupler is just the end surface of the light guide(s). In the basic design this is normal to the light guides' axis, so from section 3.1.4 the limiting étendue per unit area is 3.61 sr. Bornstein and Friedman also discuss an alternative design with an inclined end to the light guides. This is component 51 in Figure 3.12 that is taken from Fig 3 in their specification. It was shown in section 3.1.4 than an inclined end to the light guide can increase the limiting étendue of the exit surface. The increase can be at most equal to the secant of the inclination, but it will be limited by the absence of high-angle light.

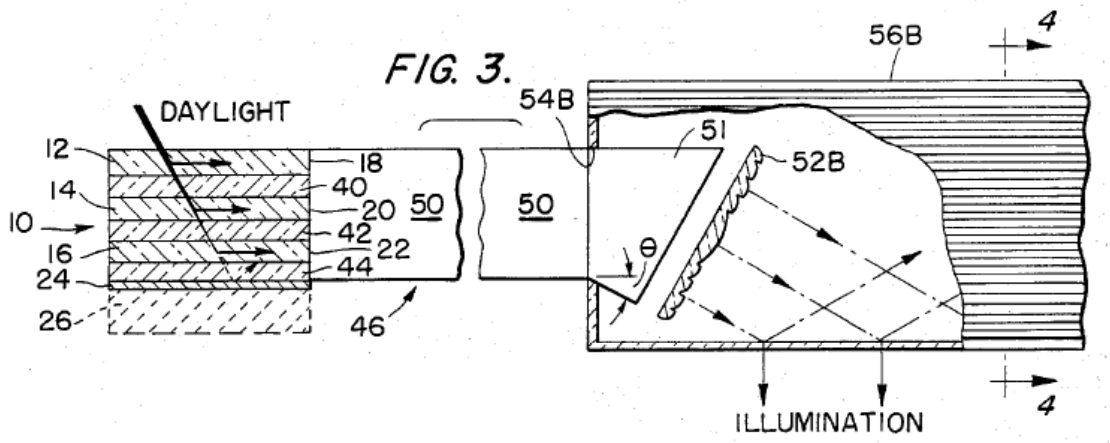

Figure 3.12 Bornstein and Friedman's design for a luminaire with an inclined end (51) to the light guide (50) feeding a Fresnel lens (52B) inside a prismatic light guide (56B) that disperses the light. Note the use of spacer sheets (40, 42, 44) between the collector sheets (12, 14, 16) that would significantly increase the size of the light guides.

We see from **Table 3-3** that the smallest limiting étendue per unit area for the system is either the air gap between the collector sheets and the light guide (3.6 sr), or the air gap at the end of the light guide (3.6 sr for their basic design, < 4.2 sr for an end inclined at 30^{o}). These figures are substantially less than the limits for the collector stack (≈10 sr) or the light guides (6.7 sr). Thus only about a third of the light reaching the exit surface of the collector stack can be converted into useful illumination beyond the end of the light guides. Étendue analysis does not tell us where this light goes: it just proves that the light cannot exit the luminaire.

Table 3-3 Limiting étendue per unit area of components in a Bornstein & Friedman LSC

Component	Type	Limiting Étendue per Unit Area (sr^{-})
Collector stack	Wide sheets	≈10
Sheet coupler	Air gap	3.61
	Optical joint	< 10
Light guides	Multiple rectangular	6.75
	Single sheet	6.75
Luminaire coupler	Air gap (normal)	3.61
	Air gap (30 deg)	< 4.17
Luminaire	Free space	6.28

The performance degradation at the joint between the collector stack and the light guides could be eliminated by using an optical joint to connect these components. However, the performance limitation set by the limited étendue of the air gap at the end of the light pipe is much more fundamental and is common to all LSC daylighting systems described before the start of this project. Ways of overcoming this generic problem form the basis for chapter 6.

3.2.2 Zastrow and Witter

One interesting LSC system that was built, and that influenced the UTS Daylighting Group, is the test unit constructed by Zastrow and Witter to illuminate one of the kitchens in the student accommodation at the Universität Hohenheim in Stuttgart (Zastrow & Wittwer 1986a, 1986b). As shown in Figure 3.13, an inverted hollow cone of PMMA doped with a greenish-yellow fluorescent dye (BASF *Lumogen*® 241 yellow) was used as a collector assembly. The distal end of the cone was sliced at an angle and the cut edge polished in an attempt to direct more fluorescent light downwards. At the small end of the cone there was a light guide consisting of a 300 mm diameter, 5.0 m long tube of PMMA with a wall thickness of 6.0 mm. Light emitted from the bottom of the light guide was directed into the kitchen by a mirror.

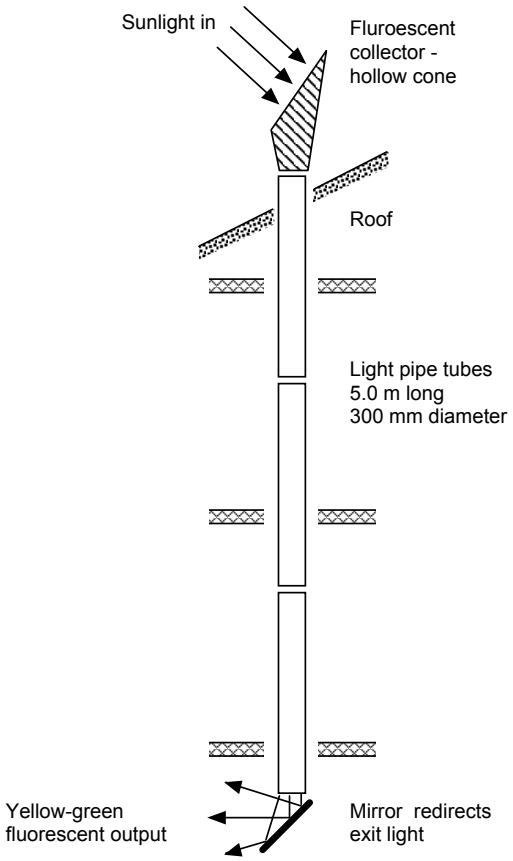

Figure 3.13 Single colour fluorescent collector system of (Zastrow & Wittwer 1986a) using a hollow cone of fluorescent PMMA as light collector, a 5.0 long assembly of hollow tube of PMMA as a light guides and an end mirror to illuminate a kitchen two floors below the roof.

The system was not a great success - it had a light-to-light efficiency of only 0.2% and the emitted semi-monochromatic light was yellow-green (*not* a pleasant colour for appreciating food!). Further, the 300 mm diameter hollow pipe light guide was expensive to buy, difficult to install (the building had to be designed around the light guide which was so heavy that it had to be installed in three sections) and visually very intrusive. In addition, the large diameter of the light emitting zone and the uncollimated nature of the emitted light made directional light control exceedingly difficult. Nevertheless, this installation did demonstrate that luminescent solar collectors can emit enough lumens to provide useful lighting.

An étendue analysis of the Zastrow and Witter system is instructive and the limiting étendue of the various components are summarized in Table 3-4. Let us examine the components in turn.

The first component was the collector made from a hollow cone with a constant wall thickness. Provided the wall thickness is substantially smaller than the radius, the only form of direct light escape is via the loss cones perpendicular to the surface. However, the cross sectional area of the light guiding portion of the collector cone decreases as one moves down the cone's axis towards the light tube. This is an attempt to "squeeze the light", and as shown in section 3.1.7, it cannot work. The "extra" light will in fact be reflected back up the cone. One would get just as much light out from a collector by using a simple hollow cylinder that had the same cross section as the small end of the cone. Zastrow and Witter observed the losses from the cone and suggested that a cylindrical light collector might be just as effective.

The final radius of the cone is approximately one half of the top radius. This means that the reduction in light guiding area along the cone axis a factor of two. The light everywhere has the largest possible solid angle for light confined by total internal reflection. So the conservation of étendue tells us that at least half of the fluorescently emitted light from the top of the collector cannot reach the bottom of the cone. As this light proceeds down the cone, reflection off the inclined walls causes it to move at a steeper and steeper angle to the cone's axis until it reverses direction and heads back up the cone. The back reflection of the majority of trapped fluorescent emission is one reason for the system's very poor light-to-light efficiency.

Note that in principle one could increase the light output by using a cone whose wall thickness was inversely proportional to the radius. This would keep the cross sectional area of the light guiding section constant, and so permit full contributions from the whole length of the cone. However, such a collector cone would have to be made by custom casting and would be very expensive.

Light guides in the form of thin walled hollow tubes act as infinite sheets (they have no side edges). This means that they have a very high limiting étendue per unit area of 10.4 sr. However, it needs to be remembered that the applicable area is just the light-carrying portion of

cross section, which is only a few percent of the total cross sectional area. So the light guides are actually exceedingly bulky for the amount of light they transport.

In fact, the light tubes were so bulky, heavy and awkward to handle that it was not possible to use a one-piece 5.0 m long tube (despite the building being designed around the LSC system). Instead three tubes had to be used. It was not possible to glue the tubes together (to form an optically continuous system) because the liquid acrylic resin would have leaked out and ruined the finish of the tubes. Instead, the tubes ends were given an optical polish and they were just placed in contact. Note that Fresnel reflection averages approximately 10% at each polymer/air interface in the tube assembly. So the six interfaces for the three tubes mean that even perfect tubes in perfect alignment would only transmit $(1 - 0.1)^6 = 53\%$ of the light that exits the collection cone.

Last, the end of the final light tube was a simple orthogonal surface. This surface has only one third of the limiting étendue of the rest of the system (unless there are air gaps along the way), which correspondingly reduces luminous output.

Table 3-4 Limiting étendue per unit area of various components in the Zastrow and Witter system. Note that the area of all components is just the light-carrying portion of the cross section.

Component	Type	Limiting Étendue per Unit Area (sr)
Collector	Hollow cone	10.36
	Hollow cylinder	10.36
Collector coupler	Air gap	3.61
	Optical joint	10.36
Tubular light guides	Hollow cylinder	10.36
Air gaps between tube sections	Air gap	3.61
Exit from light tubes	Air gap	3.61
Luminaire	Free space	6.28

One problem mentioned earlier with the Zastrow and Witter system was the large area of the emitting region (which has a nearly Lambertian beam pattern) and the consequent difficulty of directing the light in the desired direction. (The mirror they used was not very effective.) One solution would be to use the “hollow tube to solid cylinder converter” described in (Smith &

Franklin 1998) and discussed in section 3.3.3. This device adiabatically compresses the light from a hollow tubular light guide into a solid cylinder of the same light guiding cross sectional area. For example, light in a 300 mm diameter tube with a wall thickness of 6 mm can be losslessly compressed into a solid cylinder with a radius of 42 mm, which would be much easier to direct in the desired direction.

3.3 THE UTS DAYLIGHTING PROJECT

3.3.1 SCATS: A Sunlight Collection and Transmission System

A key problem for making a practical LSC is how to achieve affordable flexible light guides. The cost of the light guides is essentially proportional to their combined cross sectional area, so it is essential to minimize this key parameter. Prior art LSC's had used square collector sheets, or sheets that were short and wide (Bornstein & Friedman 1985). At the start of this project I suggested that instead the collector sheets should be long and thin, with an aspect ratio of at least five and preferably ten. This compares to the Bornstein and Friedman system discussed in section 3.2.1 where the aspect ratio was estimated at less than 0.2. The experiments described in section 8.5 showed that if the long edges of the collector sheets were diamond polished, the resulting surfaces were smooth enough so that there was very little light loss from scattering. The long thin sheets of PMMA doped with fluorescent dyes act as high quality light guides, with very low losses due to geometric defects. Ideally, one would like to somehow couple these rectangular sheets to cylindrical solid core light guides. However, at the time there was no known method of doing this. So we developed the idea of using light guides made from long strips of clear PMMA that had the same width and thickness as the collector sheets. Because the light guides are thin and narrow, they are surprisingly flexible. An in-plane bend radius of about 200 mm proved feasible while the sheets could be twisted through 90^{o} over a distance of about a metre. The result was the SCATS (Sunlight Collection and Transmission System) patent families (Franklin 2001a; Smith & Franklin 1996; Smith & Franklin 1998; Smith & Franklin 2000) illustrated in Figure 3.14. (This drawing is a composite of diagrams in (Smith & Franklin 1996) and (Franklin 2001a))

The initial name for the design was SCATS (Sunlight Collection and Transmission System). However, when the technology was commercialized by Fluorosolar Systems Ltd (a subsidiary of Skydome Skylight Systems Pty Ltd), a trademark search showed that in some European languages "scats" means "faeces". So the trademarks Fluorosolar® and DayRay® were registered internationally by Fluorosolar Systems Ltd and used commercially for the SCATS system. However, the term "SCATS" is used in most of the published scientific papers and patents, so it will be used in this thesis.

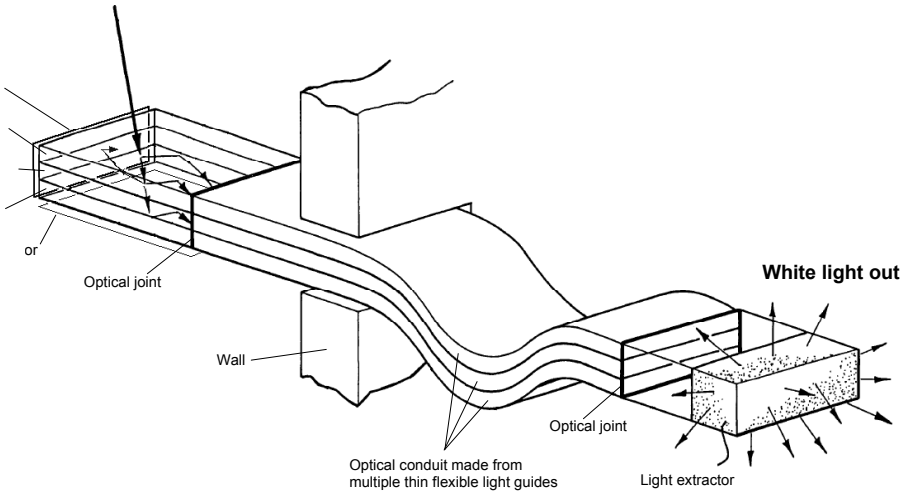

Figure 3.14 Schematic of a SCATS (Sunlight Collecting And Transmitting System) with a three-layer stack of fluorescent sheets optically coupled to thin, flexible light guides and a light extractor. A properly designed system emits white light. Using long, narrow collector sheets permits the light guides to be narrow enough to give good flexibility to the optical conduit – essential for practical installation.

The SCATS system has a three-layer stack of polymer sheets dyed with violet, green and red fluorescent dyes. There is a layer of air above and below each sheet. The low refractive index of the air layers confines most of the fluorescently emitted light inside each sheet by total internal reflection. The long, thin collector sheet acts as a light guide, confining most of the light by TIR off the top and bottom surfaces and the sidewalls. The confined light is transported by TIR to one of the sheet's short edges that is bonded by an optical joint to a flexible thin transparent rectangular light guide. The optical conduit made up of these light guides then transports the fluorescently emitted light via an optical joint to a remote luminaire. By appropriate selection of dyes, white light output can be produced, giving a good match with the colour of daylight (Earp 2006; Earp et al. 2004b; Earp et al. 2003; Swift & Smith 2003; Swift, Smith & Franklin 1999b).

The luminaire/light extractor can have such an impact on system performance that the whole of chapter 6 will be devoted to this poorly understood component. For the time being, we will just regard it as the end of the light guides where the light is emitted into the room we are illuminating.

The collector sheets' short edges opposite to the light guides have specular end reflectors to increase output by directing fluorescent light back towards the light guides. There is also a non-specular bottom reflector that boosts output by redirecting any daylight not absorbed during the downward path back up through the stack with an additional chance of absorption. Both experiment and calculations showed that a white diffuse reflector is slightly superior to even the best specular reflectors because on average the light reflected by the diffuse surface has a longer path length in the collector sheet and hence an increased probability of absorption. This more

than outweighs the slightly greater reflectivity of high performance reflective films. Further advantages are that the white plastic base is much cheaper and it can serve as a structural component.

Figure 3.15 illustrates the final form of the SCATS system with a roof mounted three colour collector stack and an optical conduit using flexible light guides made from thin PMMA strips connected to a ceiling mounted luminaire/light extractor.

The original version of the SCATS system used dyed PMMA collector sheets measuring 1200 mm × 135 mm × 2.0 mm with an aspect ratio of 8.9. These were individually glued with an optical epoxy to clear PMMA two metre long light guides made from 2.00 mm thick PMMA. Each light guide was enclosed in an individual protective tube of thin polymer film (not shown in Figure 3.14). Initial prototypes used low-density polyethylene film. However, experiments showed that under pressure the LDPE film scratched the PMMA sheets, despite the fact that PMMA is usually thought to be much harder than LDPE. This was very perplexing as one does not normally think of soft objects scratching harder materials. Microscopic examination suggested that under pressure, the soft LDPE film spot-welded to the PMMA and microscopic chunks of PMMA were ripped out the sheet when the film was moved. These fragments then acted as abrasive teeth when the LDPE film moved over the PMMA.

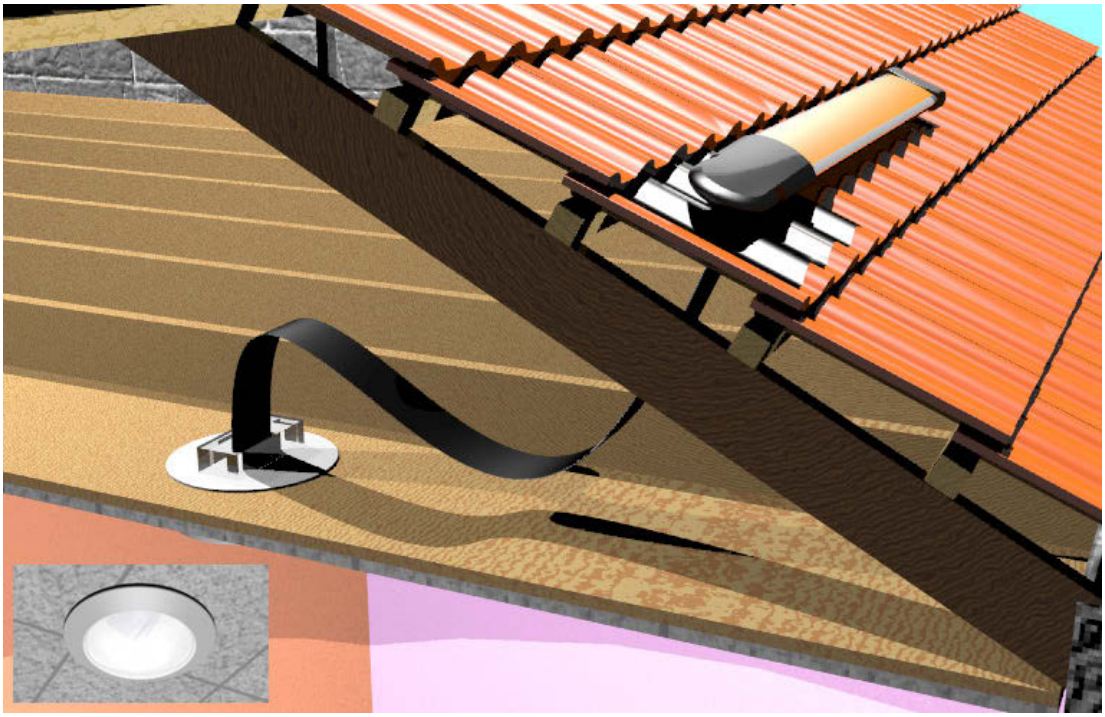

Figure 3.15 The final form of the SCATS LSC system with a three colour fluorescent stack on the roof connected by an optical conduit made from thin, flexible PMMA, connected to a luminare.

The solution, as suggested by Norm Booth, was to use a *harder* type of polymer film for the protective tube. Experiments showed that the right grade of high-density polyethylene did not scratch the PMMA, despite the HDPE film being significantly harder than the "abrasive" LDPE.

One potential drawback of the SCATS type design with its long, narrow light collector sheets is the long path length of fluorescently emitted light inside each collector sheet (over one meter) and the consequent sensitivity to absorption or scattering. As discussed in chapter 8 and Appendix A, a great deal of time, effort and money was spent in improving the manufacture of high performance collector sheets to reduce attenuation. This included extensive collaboration and multiple factory visits to manufacturers in Australia, Spain, Germany, Japan and Australia, Indonesia and China.

3.3.2 Improved Joints and Mixer/Couplers

It was shown in sections 3.1.4 to 3.1.6 that high quality optical joints are essential to good system performance. (In fact, it will be shown in chapter 6 that they are actually even more important than has been discussed so far.) However, the butt joints shown in Figure 3.14 are quite weak and, if one is not careful, the forces at the joints can easily be large enough to break them. A broken joint creates an air gap which, because of the effect on étendue outlined in section 3.1.4, will greatly decrease the transfer of the light from that sheet and hence will have a large effect on colour balance.

Figure 3.14 is oversimplified in that it shows the three clear light guides being in mutual contact for their full length. However, the path length for the upper light guide in the diagram (on the concave side of the bend) is shorter than the path length for the lower light guide (which follows the outer part to the bend). If all the guides have the same initial length, this difference in path length will place the upper guide under compression and it will buckle to minimize the stress. The central light guide will experience little force but the lower (outer) guide will be under considerable tension. In Figure 3.14 all of the optical joints are simple butt joints, which are very weak under tension (but good in compression). If the ends of the light guides are unrestrained, bending the optical conduit by more than a few degrees will impose tension forces on one of light guides that will break any feasible glued butt joint. Accordingly, there needs to be a clamp to remove the mechanical stress at each end of the light guide assembly, as shown in Figure 3.16 from (Smith & Franklin 2000).

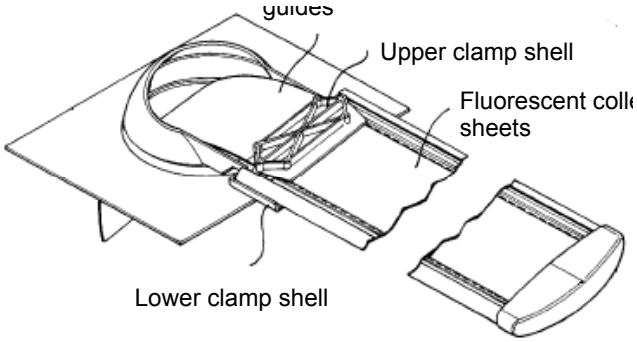

Figure 3.16 Light guide clamp in a SCATS system.

However, a much better solution is to use lap joints rather than butt joints when the light guides are connected to the collector sheets. This is actually a very difficult task because it is essential to make sure that the (top) violet sheet is optically isolated from the (middle) green sheet. If this isolation is not maintained then light from the violet sheet will be absorbed by the dye in the green sheet. This will cause both a drop in system output and a big change in colour balance. (Similarly, the green sheet must be optically isolated from the red sheet.) Thus, we need a system that mechanically couples the various collector sheets while keeping them optically isolated. The design developed is shown in Figure 3.17, redrawn from (Franklin & Smith 2007). It uses "offset T-joints", an innovative combination of butt joints (to couple the ends of the light guides) and lap joints (that transfer the mechanical stresses between sheets). By offsetting the butt joints, no light from the violet sheet can enter the green sheet and no light from the green sheet can enter the red collector sheet. A patent was applied for (Franklin & Smith 2007) and is at the PCT stage. Some light from the violet sheet will enter the central clear light guide, but it will not be lost from the system and will not affect colour balance. Note that all the joints are very strong except for the butt joint from the bottom red sheet to its light guide. However, the red sheet is at the bottom of the stack and receives no stress (all loads being taken by the T-joint to its right), so this butt joint is acceptable. It does, however mean that the red sheet must be supported at all times during the assembly process whereas the other sheets are very robust once glued.

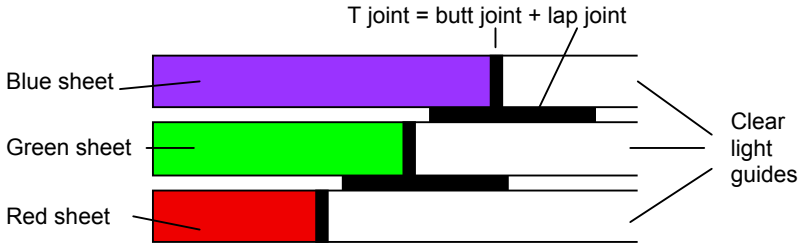

Figure 3.17 Glued "offset T-joints" provide mechanical strength but optical isolation.

In the basic SCATS design there is one light guide coupled to each (optically isolated) collector sheet. Thus each light guide in Figure 3.14 transports light of a single colour. These different colour lights are then combined in the light extractor/luminaire to make white light. However, this means that if there is a leakage in one light guide, the colour balance of the entire system will be degraded. This problem can be overcome by mixing the light before it enters the light guide so that each light guide transports white light as illustrated in Figure 3.18 (redrawn from (Franklin & Smith 2007)). In this system a three-layer stack of fluorescent sheets on the left that is mixed and fed as white light to two clear light guides. (Experience shows that dual light guides are more flexible and easier to make than the triple light guide system shown in Figure 3.14.) All the joints in the coupler are mechanically very strong, except for the butt joint to the red sheet. An additional advantage of this design is that the steps provide a mechanical alignment feature that greatly facilitates assembly. A drawback of using steps on the coupler is that assembly may be difficult (or even impossible) if some sheets are too thick. For example, if the thickness of the green sheet plus glue exceeds the height of its step then there will be interference with the violet sheet. Thus one either needs good control of sheet thickness (which is difficult with cell cast sheets) or excessive step heights on the coupler (to allow for the worst possible sheet thickness).

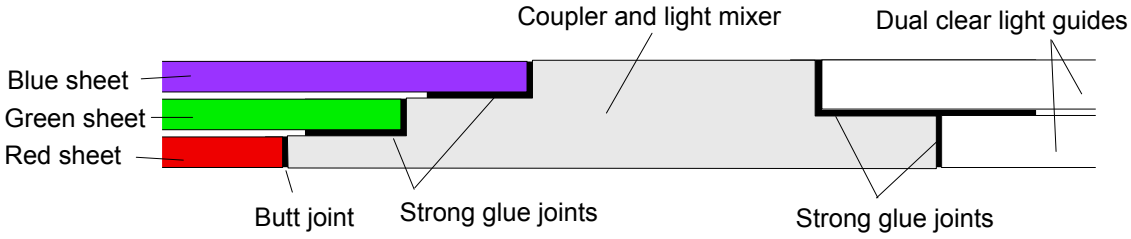

Figure 3.18 Coupler and light mixer from that combines the light from a three layer stack of fluorescent collector sheets and transfers it to dual light guides.

Light collectors need to be installed where they can capture sunlight for most of the day, typically on a roof. This means that, as shown in Figure 3.15 and Figure 3.16, the light conduit must bend through a right angle to pass though the roof surface. In order to pass between the roofing timbers, this bend must be as tight as possible. Bending twin light guides on such a tight a radius could cause problems in the long term with an increased risk of fatigue cracking, etc. However, the problem can be overcome by bending the coupler in Figure 3.18 to give the design illustrated in Figure 3.19 from (Franklin & Smith 2007). This monolithic component can be made by heat forming or injection molding, and hence has no internal stresses. Using a bend coupler/mixer greatly reduces the stresses on the light guides and facilitates the use of dual light guides. Provided the bend radius is more than 5 times the thickness, the optical losses are very

low and almost entirely restricted to light that would be lost elsewhere in the system. Ray tracing and measurements on heat formed components all gave net losses of less than 1%.

QuickTime™ and a
decompressor
are needed to see this picture.

[Production Note: This figure is not included in this digital copy.
The print copy of the thesis is available for consultation at UTS Library.]

Figure 3.19 Bent coupler/mixer (50) to mix light from a three-layer collector stack (glued on the left to surfaces 50a, 50b and 50c) and to transfer it as white light to twin light guides (glued on the right to surfaces 50d and 50e).

3.3.3 Coupling to Cylindrical Optical Fibres

The thin flexible light guides described above for the SCATS system were a considerable advance on the state of the art. However, they have somewhat limited flexibility and optical grade PMMA sheet is expensive. Solid core optical fibres have much lower attenuation and are much more flexible. Therefore, it would be highly desirable to somehow couple the light from a multicolour set of fluorescent collectors into a solid core optical fibre. At the start of the UTS Daylighting project there was no known method of efficiently coupling fluorescent emission (with its maximal solid angle) from a flat collector sheet to a cylindrical optical fibre.

The flat-to-round coupling problem is very hard and will be discussed in detail in the next chapter. Section 3.2.2 described the seminal work of Zastrow and Wittwer using a hollow conical fluorescent collector and a hollow tubular light guide to illuminate a kitchen (Zastrow & Wittwer 1986a). Their 300 mm tubular light guide was not a practical solution as it was very expensive and so bulky that the building had to be designed around it. However, their system did give useful amounts of light (despite an abysmal light-to-light efficiency of 0.2%). What was needed was a way to compress the tubular cross section down to a solid cylinder. Figure 3.3(c) suggests that this might be possible. The key is to change the cross section slowly enough so that the transition is adiabatic and étendue is preserved.

Figure 3.20 from (Smith & Franklin 1998) shows how this can be done. Light is captured by concentric cylindrical fluorescent cylinders (blue 40, green 41 and red 42) with the air

surrounding each cylinder acting as a low refractive index layer that traps most of the fluorescent emission inside its cylinder by total internal reflection. The cylinders are coupled by an optical joint (30) to a ring-to-solid circle converter (44) that adiabatically changes the cross section from a hollow ring to a solid circle while keeping the cross sectional area constant, or at most slightly increasing. The coupler is bonded by and optical joint (46) to a solid core optical fibre (46) that also uses air as its low refractive index The étendue of the combined collector cylinders and the final optical fibre are the same. End (47) and bottom (48) reflectors boost performance. As discussed in section 3.1.4, high quality optical joints are essential. An air gap would greatly increase étendue and hence cause very large losses.

Several ring-to-solid circle converters were constructed, measured and modelled (see section 4.6.1). It was found that as long as the transition sections near the optical joints were smooth and the coupler length was about five times the diameter of the optical fibre, there were very few light losses inside the coupler.

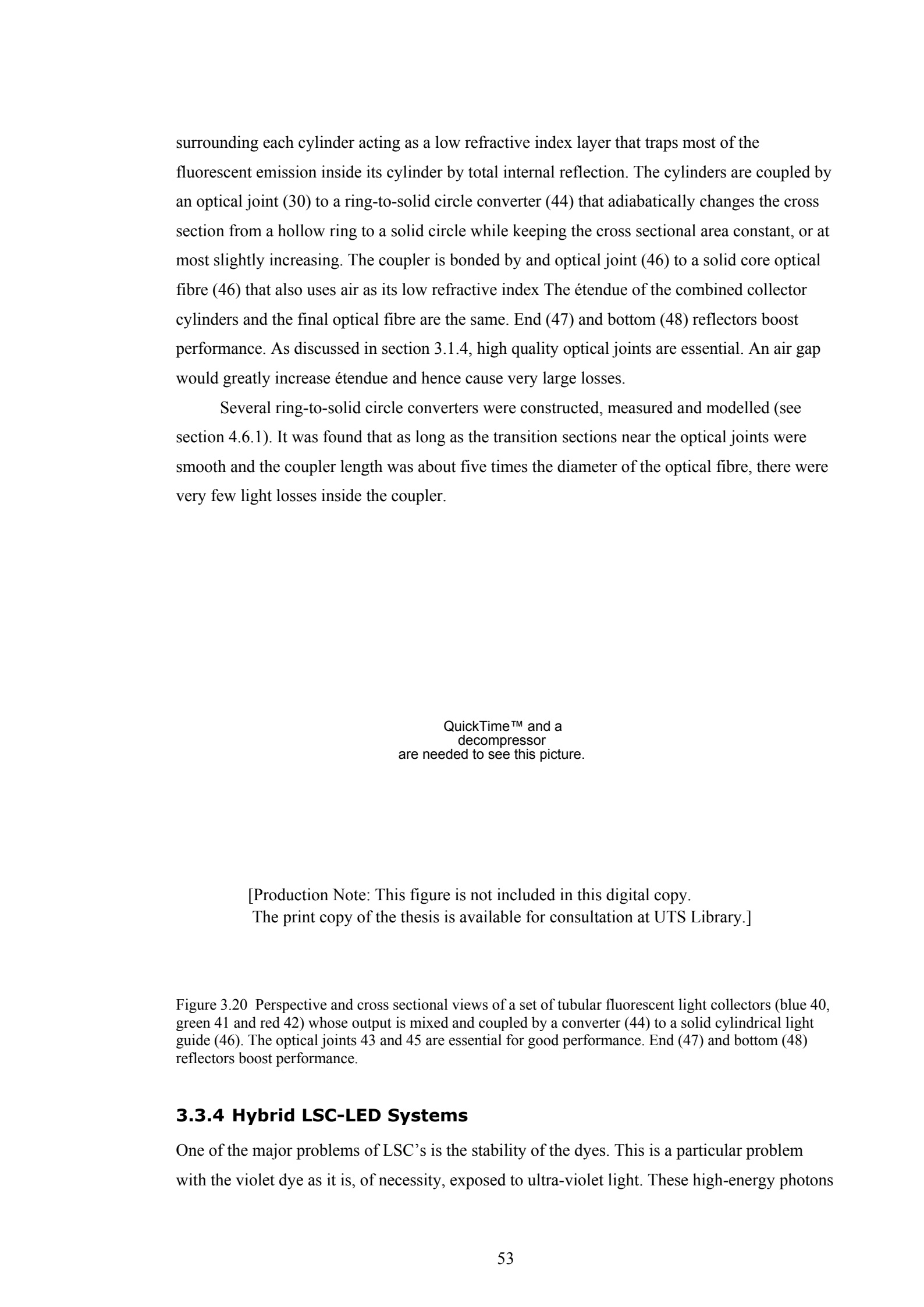

[Production Note: This figure is not included in this digital copy.
The print copy of the thesis is available for consultation at UTS Library.]

Figure 3.20 Perspective and cross sectional views of a set of tubular fluorescent light collectors (blue 40, green 41 and red 42) whose output is mixed and coupled by a converter (44) to a solid cylindrical light guide (46). The optical joints 43 and 45 are essential for good performance. End (47) and bottom (48) reflectors boost performance.

3.3.4 Hybrid LSC-LED Systems

One of the major problems of LSC's is the stability of the dyes. This is a particular problem with the violet dye as it is, of necessity, exposed to ultra-violet light. These high-energy photons

are much more likely to cause dye degradation than the light which reaches the green and red sheets. Accordingly, all known violet and blue-violet fluorescent dyes are somewhat fugitive.

Now the violet sheet, while essential for colour balance, supplies very few lumens (Earp et al. 2004b; Swift & Smith 2003). This raises the intriguing possibility of a hybrid LSC-LED system that uses green and red collector sheets to provide most of the lumens, supplemented for colour balancing with a small amount of blue light from solar powered blue LED's. Eliminating the violet sheet would cut down the cross sectional area of the collector stack by one third with a similar reduction in the required size of the light guides. Since the cost of the light guides dominates the system cost, and the light guides' cost is essentially proportional to their cross sectional area (see section 4.4), eliminating the blue sheet can potentially reduce the system cost by almost one third. The thinner light guides are also much more flexible which makes the unit easier to install.

Figure 3.21 illustrates a LSC-LED hybrid lighting system from the granted patent (Smith & Franklin 2004). A blue LED (44) powered by a solar cell (48) provides enough blue light to colour balance the fluorescent emission from a collector sheet stack (43). Note that both the electrical output of the solar cell and the fluorescent output of the collector stack respond in the same way to sunlight. Thus if the system is colour balanced for one solar condition, it will be colour balanced under almost any solar condition. The only exception is very close to sunset where red sunsets can somewhat shift the system's colour balance (although by a smaller amount than for the red sunlight).

[Production Note: This figure is not included in this digital copy.
The print copy of the thesis is available for consultation at UTS Library.]

Figure 3.21 A LSC- LED hybrid lighting system. A blue LED (44) powered by a solar cell (48) provides enough blue light to colour balance the fluorescent emission from a collector sheet stack (43).

In Figure 3.21 the blue LED (44) is directly coupled to the light guide (42). However, as Figure 3.22 from (Smith & Franklin 2004) shows, it is easier to add the blue LED's to the light extractor/luminaire at the end of the optical train. Here the dual light guides (64) are coupled by

an optical joint (65) to the luminaire/light extractor (66) that combines the fluorescent light with the light from the blue LED's (67). The big advantage of this approach is that it does not increase the size (and hence the cost) of the light guides. Étendue considerations mean that in Figure 3.21, either light from the collector sheets is lost where the LED is coupled into the light guides, or the area of the light guides must be increased. However, making the luminaire/light extractor large enough to incorporate the LED's requires only minimal extra cost.

One problem with hybrid light extractors is that the blue LED's are very intense sources while the LSC's light is diffuse. Using tradition methods mix the light to create a uniform white light with constant colour would involve unacceptable losses due to backscatter. Chapter 5 discusses TRIMM doped systems (Transparent Refractive Index Matched Microparticles) that combine excellent diffusion with very low backscatter.

QuickTime™ and a
decompressor
are needed to see this picture.

[Production Note: This figure is not included in this digital copy.
The print copy of the thesis is available for consultation at UTS Library.]

Figure 3.22 A hybrid LED-LSC system with the blue LED's (67) at the luminaire/light extractor (66) colour balancing the fluorescent emission from the light guides (64).

Figure 3.23(a) shows the assembly of a hybrid light extractor based on the designs discussed in section 6.5.3. Figure 3.23(b) shows the extractor in operation – the blue output from the LED's is combined with the fluorescent emission from green and red collector sheets to give a high-quality white light. A thin sheet of TRIMM doped polymer is bonded to the front of the extractor to eliminates glare from the high intensity LED's. See section 5.3.2 for details.

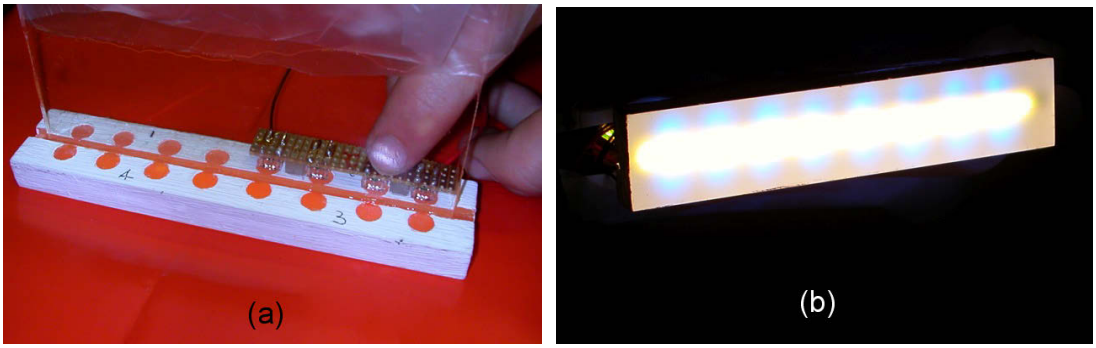

Figure 3.23 (a) Assembly of a hybrid light extractor. (b) The hybrid light extractor in operation.

A number of hybrid SCATS systems were constructed and tested. Figure 3.24 shows the final laboratory testing on one system prior to field trials. The collector stack on the left has small solar cell arrays at each end that power blue LED's in the luminaires. Twin flat light guides in an orange protective sheath connect the stack to the luminaire on the right. The luminaire has been inserted into an integrating sphere where the colour of the light output is being visually assessed.

Figure 3.24 Using an integrating sphere (on the right) for the visual colour assessment of the light output from a hybrid SCATS system. The collector stack on the left has two small solar cell arrays that power blue LED's in the luminaire. The twin light guides are protected by an orange plastic sheath.

For preliminary field trials, a pair of hybrids SCATS collectors were installed on the facade of a building at Skydome Skylight Systems Pty Ltd as shown in Figure 3.25.

Figure 3.25 Façade mounting of two hybrid SCATS collectors to illuminate an interior room.

The orientation of the site meant that the collector stacks were only in full sunlight for part of the afternoon. The awning above the collectors also created shadows that significantly reduced the output of the solar cell arrays. Despite these problems, as Figure 3.26 shows, when the collectors were in sunlight they gave excellent white light.

Figure 3.26 Installation of the hybrid SCATS system.

Despite the good performance of the hybrid SCATS system, our commercial partner decided to opt for a conventional three layer red, green and blue stack. There were several reasons for this decision. One was that their marketing department had reservations about using blue LED's to supplement the LSC's green and red light – they felt that the fluorescently emitted light from the collector sheets was "more natural" and the "electrical light" from the LED's would conflict psychologically with this "naturalness". Another factor was that solar cells were temporarily in short supply and costs were actually increasing with time due to market pressures. A final key factor was reservations about installation problems with flat light guides. As can be seen from Figure 3.26, these guides are fairly flexible. However, they are definitely less flexible and have higher losses than high-quality solid-core optical fibres.

The next chapter describes the development of flat-to-round converters that can efficiently couple flat LSC collector sheets to low loss, flexible solid-core light guides. Once this was achieved, our commercial partners decided to abandon the hybrid SCATS system, although is was an instructive exercise and with the rapid improvement in solar cells and LED's, the design may be worth revisiting.

4 FLAT-TO-ROUND CONVERTERS FOR OPTICAL FIBRES

4.1 INTRODUCTION

The SCATS system described in section 3.3 used optical conduits made from thin, flexible strips of PMMA. These light guides worked well and the design has significant commercial potential. However, the limited flexibility of this type of light guide makes them difficult to install in some existing buildings. Also, extinction losses in extruded PMMA sheet limit light guides made from this material to lengths of less than about 3 metres, which is too short for many applications. Continuous cast PMMA has lower attenuation but is not readily available in lengths of more than 2.4 m. Solid core optical fibres have low attenuation (runs of 20 metres are feasible) and are also very much more flexible. The desirability of somehow coupling LSC's to optical fibre was widely recognized prior to the start to the UTS Daylighting project, but at that time there was no known method of efficiently coupling the fluorescent emission from a collector sheet (with its maximal solid angle) to a cylindrical optical fibre. The main problem was that very few workers in the field understood the importance of étendue in the design of LSC daylighting systems.

This chapter will first explore some of the important practicalities of using optical fibres for daylighting including: fabrication problems, difficulties in using numerous small diameter fibres and the critical issue of fibre cost (which tends to dominate system cost). It will be shown that the key step is to use a small number of large diameter fibres, the bigger better. The theory of making a high efficiency coupling from a flat collector sheet to a large diameter optical fibre is developed, tested experimentally and demonstrated in a design suitable for mass production.

However, before we examine flat-to-round converters, it is useful to explore alternative designs. A typical multi-fibre approach is that of Bornstein and Friedman as discussed in section 3.2.1 and illustrated in figure 3.11. This LSC system uses multiple small optical fibres that are connected at one end to a collector stack and at the other end to a luminaire. It is simple to say, "connected at one end to a collector stack", but in practice, this is very challenging. It was shown in sections 3.1.4-6 that if the fibres are simply butted up against the end of the collector stack then the high étendue of the air gap means that most of the fluorescent emission inside the collector sheets is reflected at the gap and can not enter the light guides. However, it is very difficult to make good optical joints from the collector stack to the optical fibres. The problem is that in order to minimize cross sectional area (and hence the cost) of the light guides, the space between the collector sheets must be kept to an absolute minimum. But if the collector sheets are closely spaced, then even a small amount of glue can bridge the space between the blue sheet and the green sheet (or the green sheet and the red sheet). This would allow the short

wavelength to be absorbed by a dye in another sheet where most of it would be lost, upsetting the colour balance and decreasing total lumens. This problem is particularly serious when the space between the collector sheets is small (essential for low light guide cost) because in this situation capillary action tends to pull the glue into the space between the sheets where it may be impractical to remove. Even a tiny amount of glue between the collector sheets can ruin the colour balance and cause major reductions in system output. Using a precise amount of high viscosity glue can minimize this problem, but making large numbers of small optical joints directly onto collector sheets is a *very* challenging problem.

The glue joints have such a critical impact on the practicality, cost and durability of a LSC system that it is worth considering this subject in some detail.

4.2 Cutting and Gluing Solid Core Optical Fibre

In order to make a high quality optical joint with solid core optical, it is essential that the end of the optical fibre is smooth and flat. (It is usually also desirable that the end surface is at right angles to the fibre's axis as a sharp change in the direction of the optic axis at an inclined fibre joint can cause large losses). Proper cutting tools and procedures are more important for large diameter fibres (such as those used for this project) than for small diameter fibres. As discussed in section 4.4, the material used for large diameter fibres is much softer than that used for small diameter fibres. This makes it much more prone to distortion or damage during cutting. Solid core optical fibre must be cut with fibre shears such as a *Poly Cutter*™ (Poly Optics Australia Pty 2011). These are essentially secateurs with a highly polished chisel edged blade. In order to get a good quality cut surface, it essential that the blade is very sharp and that the blade's side surfaces are as smooth as possible. The cutting must be done with a single smooth motion, without any hesitation, jerks or second cuts. If there is any kind of interruption to the smooth cutting motion, it is very difficult to avoid a jump in the cut surface. It is simply not practical to get a good surface with a knife or scalpel.

As Figure 4.1 shows, the two surfaces of the cut are not of equal quality. The highly polished triangular blade moves at right angles to the anvil. The primary surface of the blade is parallel to this motion while the secondary surface is inclined by a few degrees. The inclination of the secondary surface forces the cut fibre away from the blade. Consequently, when the blade moves, the freshly cut fibre rubs with considerable force against the secondary surface with a somewhat discontinuous motion as it sticks and releases. This erratic motion gives a poor surface finish. On the other hand, the highly polished primary surface does not have to force the fibre sideways and so it tends to glide over the cut surface, giving a much better finish. *Poly Cutters*™ and similar fibre shears have a simple chisel edge blade with a flat primary surface. The Japanese are world leaders in cutting difficult materials. A literature search suggests that a

slightly concave primary cutting surface (what the Japanese call *urasuki*) would help to a reduce the drag during cutting and hence give a better quality cut surface (Jakhua 2011). However, no experiments have been conducted to test this idea.

Note that the chisel edge of the fibre shears means that they are a handed tool (usually right handed). This means that if it is necessary for the offcut to have a good finish, the fibre shears should be twisted by 180 degrees (so that in Figure 4.1 the anvil would be at the top and the blade at the bottom). A second cut can then be made to give a good surface. Alternatively, the second cut can be made with the fibre shears in the original position (i.e. that shown in Figure 4.1 with the anvil down) by reversing the fibre end-for-end.

The end surface of the fibre should be carefully inspected before gluing. If the end is not perfectly flat and smooth, a new cut must be made, preferably at least one fibre radius down the fibre. There is no point in trying to make joints with poorly cut fibre. The glue has almost no filling power, so any deviation from flatness in the end of the fibre will cause a weak joint at best. Worse, it may cause bubbles, with corresponding major loss of light transmission. Also, a bubble is essentially a crack in the joint, so any joint with a bubble is inherently weak.

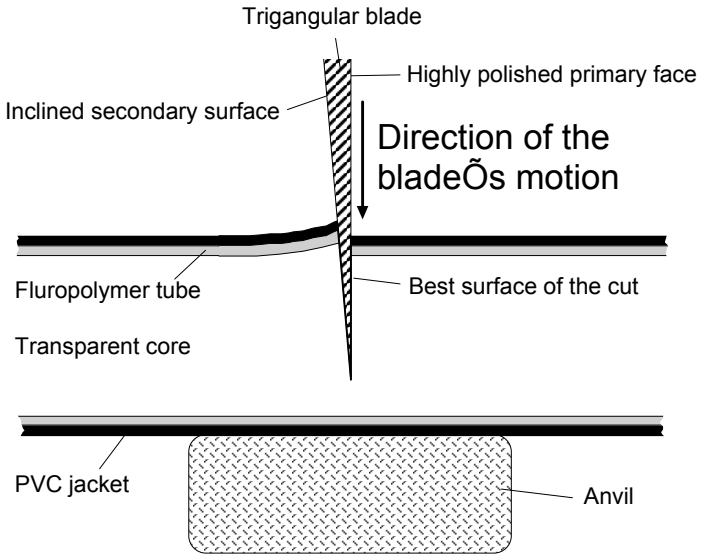

Figure 4.1 Cutting a solid core optical fibre with optical shears such as a *Poly Cutter*™. The surface cut by the highly polished primary face of the chisel-ground blade has a much higher quality than that at the inclined secondary face.

In order to glue the fibre, a measured amount of UV curing epoxy is applied to the centre of the prepared end and smeared over its surface. This end is then pushed gently against the coupler and moved around slightly to make sure that the glue coats the whole of the rough end surface of the coupler. Care should be taken to make sure there are no bubbles in the joint. Moderate pressure is then applied so that the joint is compressed and the fibre is forced into intimate contact with the coupler. The assembly is then clamped in position with a suitable jig

(or by hand if no jig is available – this requires two operators). Excess glue is wiped off (where practical) and then the glue is cured by a suitable UV lamp. (Two-part epoxy glue can also be used, and under optimum conditions can lead to a slightly stronger joint. However, the relatively long cure time requires a high quality jig to align and hold the parts under compression with the correct alignment. UV curing epoxy is much quicker and easier to use.) With a little practice, it is possible for a two-person crew to rapidly make high quality joints without using a jig. One operative holds the fibre in position while the other wipes off the excess glue and illuminates the joint with UV light. However, using a simple jig to control the alignment speeds things up and makes the assembly process more reproducible and less dependent on operator skill.

It is noteworthy that simple butt joints from the fibre to a PMMA block are very strong under tension, often exceeding the tensile strength of the fibre core, while PMMA to PMMA butt joints are very fragile. This appears to be due to the compliance of the core material. The softness of the core relative to the PMMA ensures that the fibre core is in intimate contact with the coupler over the whole surface, with only the thinnest of glue layers between them. Using a thin glue layer leads to a high bond strength. This contrasts with a PMMA to PMMA butt joint where the hardness of each object means that the contact is much less intimate than for a well-made fibre/PMMA bond.

As a practical matter, it is very difficult to avoid using an excess of glue. If the initial amount applied were exactly the same as the final volume of the butt joint, it would be exceedingly difficult to avoid bubbles (which are a potentially major problem). If the fibre is isolated, it is a simple matter to wipe the excess glue from the surrounding surface. However, if the fibre is part of a bundle, it is usually not be feasible to remove the excess glue. This means that it is essential to retain the fibre's fluoropolymer tube, despite the fact that doing so means that the spacing of the fibre cores must be increased accordingly. If one tries to glue naked cores to the collector, excess glue at the circumference of the joint causes very large light losses.

4.3 FIBRE COUPLER/MIXERS

Section 4.1 described the many problems of trying to glue multiple fibres to a stack of thin collector sheets. A better solution is to use a coupler/mixer block, similar to that described in (Franklin & Smith 2007) but with a slightly rough vertical face at the light conduit end, as shown in Figure 4.2. The collector sheets are glued to the stepped surfaces on the collector/mixer and one end of the optical fibres is bonded to the coupler's vertical exit. The exit surface of the optical fibres is bonded to a luminaire. As described in section 3.3.2, the couplers' stepped entry surfaces provide mechanical locators for the collector sheets and makes it simple to construct high strength, low loss optically isolating joints. The bond from the solid core fibre is just a simple butt joint with UV curing epoxy. However, if it is well made, the core will

usually tear before the joint fails under tension. These butt joints are quite weak under sheer loads and are easy to peel off, so adequate stress relief is essential.

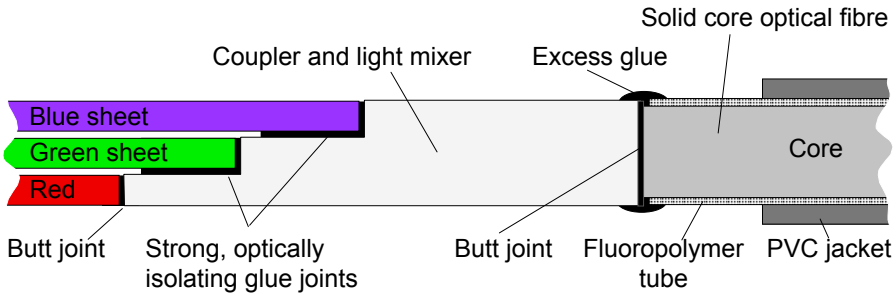

Figure 4.2 A fibre coupler/mixer that provides a good optical and mechanical coupling from a three-layer collector stack to solid core optical fibres (only one fibre is shown in this cross section).

An LSC system using the coupler/mixer of Figure 4.2 was made at FSL by Fabian Bettiol and is illustrated in Figure 4.3. It used twenty-one 6.0 mm diameter optical fibres bonded with UV curing epoxy to a light/mixer coupler at one end, and a luminaire at the other end.

Figure 4.3 (a) Three-layer stack of fluorescent sheets connected via a coupler/mixer to 21 optical fibres. (b) The ends of the fibres are bonded to a luminare. (c) Overview of the system.

There was considerable light loss at the joint between the coupler and the optical fibres. The collector stack has three 2.0 mm sheets so the coupler/mixer required a thickness of 3 x 2.0 mm = 6.0 mm. The fibre diameter was 6.0 mm, but this included the clear outer fluoropolymer jacket (the black outer PVC cladding was stripped away for the last 30 mm of the fibres so that they could be packed more closely). The diameter of the light carrying core was approximately 5.5 mm. Assuming that the fluoropolymer jackets touched, each 6.0 mm x 6.0 mm square at the end of the coupler has a 5.5 mm circular core attached to it. Therefore, the geometric losses are $(6.0^2 - \pi 5.5^2 / 4) / 6.0^2 = 34\%$. There are also significant losses from the glue joints and it is unlikely that transmission reached 50%. To achieve even this figure, it was essential that the outer fluoropolymer jackets touched and this made the assembly a time consuming and delicate task. Note in Figure 4.3(a) how the fibres bulge out from the collector which greatly complicated gluing. In fact, the fibre bundle bulged so much that it was not possible to confine it within the two aluminum clamps that provided strain relief for most of the fibres – strain relief for the three outermost fibres had to be provided with auxiliary green cable ties.

The end of each fibre was bonded to a rectangular block of PMMA that served as a simple luminaire. For ease of assembly, the block was considerably thicker and wider than the collector stack (compare the squeeze of the fibres at the collector in Figure 4.3 (a) with the relaxed layout at the block in Figure 4.3 (c)). This discontinuous increase in optical cross sectional area from the fibres to the block meant that the light from the optical fibres underwent an irreversible increase in étendue, similar to that illustrated in Figure 3.3(b). This increase of étendue made it impractical to include a light extractor of the type outlined in chapter 6. This meant that, as discussed in section 2.3.3, almost half the light reaching the luminaire's exit surface was trapped inside the system by total internal reflection.

4.4 The Cost of Solid Core Optical Fibre

The main problems with this simple many-fibre approach are the difficulty of manufacture and the cost of the fibre. Figure 4.4 shows the cost of solid core optical fibre from the world's largest fibre optics dealer (Fiber Optics Products Inc 2011), normalized to the cost of 10 mm fibre. This graph shows retail prices (OEM discounts tend to be a uniform percentage of the price, so they don't change the curve). All the manufacturers keep their bulk wholesale prices confidential. However, based on more than two decades of experience in the area, I believe that this cost curve is highly representative of typical wholesale prices for bulk purchases.

The cost curve can be divided into two parts. For small diameter fibre, the cost per unit length is almost independent of fibre diameter and may actually be lower for some larger sized

fibres than for the smallest fibres. For larger diameter fibres, the cost is essentially proportional to diameter. The break between the two regimes varies from manufacturer to manufacturer, but is typically at about 5 to 6 mm.

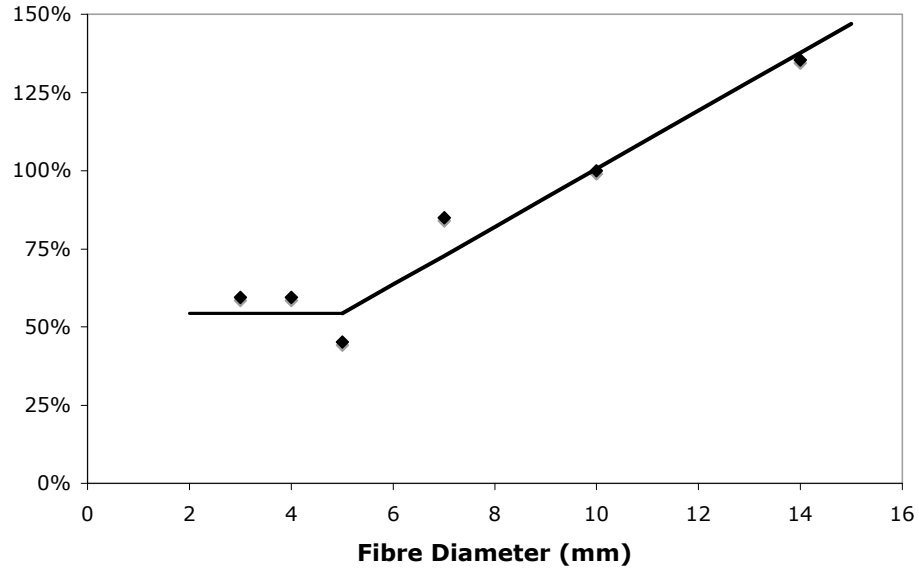

Figure 4.4 Typical cost curve for solid core optical fibre, normalized to prices for 10 mm diameter fibre.

Solid core optical fibres are manufactured by the pressurized casting of a highly transparent polymer core inside a low refractive index fluoropolymer tube. The pressure ensures that the fluropolymer tube is highly circular (provided that the wall thickness is constant). The outer surface of the core is a replicate of the inner surface of the fluoropolymer tube. For a good fibre, this must be smooth on an optical scale. For example, in a long fibre many rays will have more than 5,000 reflections off the core wall. If sidewall losses are to be kept below 10%, this requires a loss per reflection of less than 0.002%. Another way of looking at this problem is to note that after 5,000 deviations we do not want the average accumulated angular deviation to be more than about 5^o. The Central Limit Theorem indicates that the angular deviation around the specular will be approximately Gaussian. Consequently, the mean deviation will be proportional to square root of the number of reflections. Thus to achieve a mean deviation of less than 5^o after 5000 reflections, the mean scattering per reflection must be less than $5^o \div \sqrt{5000} \approx 0.07^o$.

All fluoropolymer tubing is made by extrusion. This is such a critical, but difficult to produce item, that all major fibre companies now manufacture their own fluoropolymer tubing. Different manufactures use somewhat different chemistries for their cores (which are trade secrets) and their individual patented methods to control the cores' polymerization (Joseph & Molitoris 1999; Zarian & Robbins 1989). Many of the important details are closely held trade secrets and the manufacturing process is very much a "black art". There is very little published

material outside the patent literature. In my experience, the latter can at times be quite misleading (although not, to my knowledge, actually untruthful).

The cost of small fibres is almost independent of their diameter because there are certain fixed costs that have to be met, and these fixed costs greatly exceed marginal costs for small fibres. In addition, some aspects of the manufacturing process mean that it is hard to make good quality fibres in the smallest sizes and there is often quite a lot of expensive wastage for these sizes. For various reasons, smaller fibres require very thin walls. This tubing is hard to extrude and is prone to bursting when the fluoropolymer tube is pressurized during the curing process. This means that there is a "sweet spot" for the production process, typically at a diameter of about 5 mm. This is one reason why 5 mm fibre is often cheaper than 3 mm fibre. Another reason is that there is a much larger demand for 5 mm fibre than for 3 mm fibre and this leads to significant economies of scale.

For larger diameters, the cost of finished fibre is almost proportional to its diameter. For larger diameter fibres, by far the greatest expense is the cost of the fluoropolymer tube. For a tube of diameter *d,* and wall thickness *t,* inflated at gauge pressure *p,* the circumferential stress, *s*, is given by (Gordon 1978, pp. 119-23)

$$s = \frac{pd}{2t} \tag{4.1}$$

For various reasons the pressure required for making large diameter fibres is somewhat less than for small ones, so the wall thickness increases a little more slowly than the diameter implied by equation (4.1).

Good quality fluoropolymer tube costs about US$150 per kilogram. (The quantity of chemicals used in the core is proportional to diameter squared, but chemicals are a minor expense, although the purity of the chemicals can have a profound effect on optical quality.) The fluoropolymers are very difficult to extrude with a significant wastage rate during manufacture. Amongst other problems, the molten fluoropolymer excretes a small amount of highly toxic HF gas that rapidly corrodes most steels. So all the hot parts of the extrusion line have to be made from special, *very* expensive, alloys and the entire area requires special ventilation. Another problem is that the range of working temperatures for the fluoropolymer is very small despite its high melting point (about 305^{o}C). Extruding the special thin walled fluoropolymer tubing needed for solid core fibre is right at the edge of existing extrusion technology. The quality of the fluoropolymer tubing is critical to the production process and any hiccups in supply can shut down production. Accordingly, all major fibre manufactures run their own dedicated extrusion lines to keep in-house control of the production of this critical component.

The fine details of the extrusion properties of the fluoropolymers are poorly understood by anyone, including the makers of the resin (although they do provide an invaluable source of advice). Consequently, there can be sudden, major unexpected problems due to variations in the batch-to-batch properties of the resin or small changes in the setup of the extruders. Tuning an extrusion line can be an expensive, time consuming and very frustrating process. So once an extrusion line is working properly, there is a very strong incentive to run it continuously 24 hours per day until the job is finished.

It turns out that while large diameter fibres require thicker walls (which increases material costs), the thicker walled tubes are easier to extrude (which decreases wastage) and these two effects more or less cancel out. The net result is that cost of the fluoropolymer tube is essentially proportional to its diameter and so the cost of large fibre is also approximately proportional to diameter.

We saw from section 3.1.5 that conservation of étendue requires that the combined cross sectional area of the optical fibres must be approximately the same as the cross sectional area of the LSC collector stack. Thus the relevant cost metric is the cost per unit area of the fibres and this is graphed in Figure 4.5 using the data in Figure 4.4. From the discussion above we see that for diameters less than about 5 mm, cost per unit area is inversely proportional to the square of the fibre diameter. For larger fibres the cost is inversely proportional to the fibre diameter. (Production and handling problems mean that the curve rises for diameters >> 20 mm.) Since the cost of the optical conduit dominates system cost, in order to have an economically viable LSC it is essential to use the largest possible diameter of optical fibres.

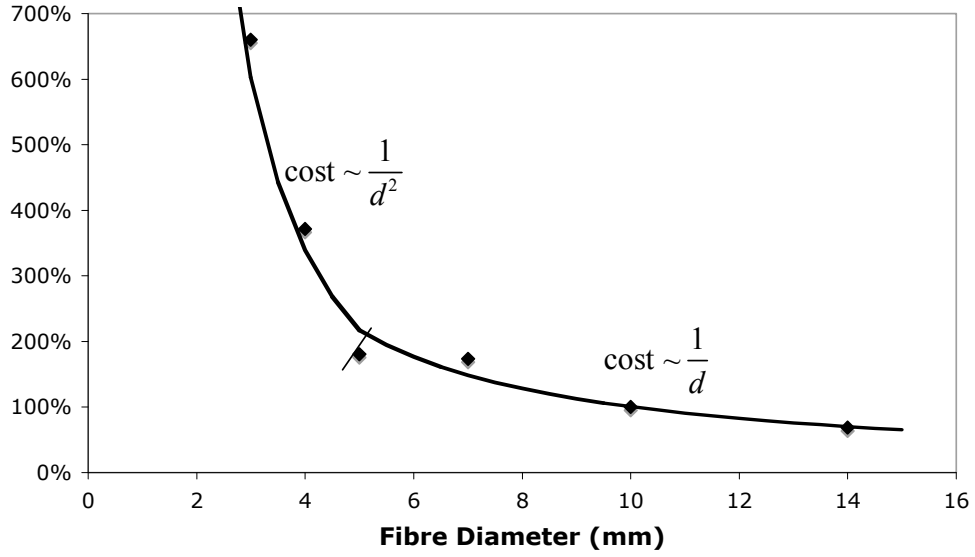

Figure 4.5 Typical cost per unit area of solid core optical fibre, normalized to prices for 10 mm fibre. For small diameters cost ~ $1/d^2$. For large diameters cost ~ 1/d. The break point is at about 5 mm.

Increasing a fibre's diameter requires adjustments to the starting chemistry and polymerization regime. By adjusting the chemistry and polymerization regime, it is possible to modify the Young's modulus (stiffness) of the core and this is essential for making large diameter fibres. A solid core fibre consists of three components: an inner solid cylindrical core, a fluoropolymer tube and an (optional) outer PVC jacket. The outer jacket is usually thin and flexible enough so that it contributes little to the fibre's stiffness. The stiffness of a solid cylinder is proportional to the fourth power of its diameter (Gordon 1978, p. 379). Therefore, the stiffness of the fibre's core is proportional to the fourth power of its diameter. The stiffness of a thin-walled tube is proportional to the product of its wall thickness and the cube of its diameter (Gordon 1978, pp. 379-80). For a solid core fibre, the wall thickness of the fluoropolymer tube is essentially proportional to diameter. Thus the tube's stiffness is proportional to diameter to the fourth power. This means that the stiffness of both the core and the tube are proportional to the fourth power of the diameter and hence the fibre's overall stiffness also scales as the fourth power of the diameter.

This means that for an unmodified core material, the fibre becomes impractically stiff for large diameters. For example, an unmodified 15 mm fibre would be 81 times as stiff as a 5 mm fibre. And an unmodified 40 mm fibre would be a completely impractical 4100 times as stiff as a 5 mm fibre and 50 times stiffer than a 15 mm fibre.

However, serious problems can also arise if the core material is too soft (i.e. it has too small a Young's modulus). Installers often want to use the smallest possible radius when bending the fibre as this simplifies installation and reduces the amount of expensive fibre, hence decreasing their costs. But when the optical fibre is bent on a tight radius, the fluoropolymer tube has a tendency to buckle and kink, which causes a very large, irreversible loss of optical transmission. The fibre's solid core resists the tendency of the fluoropolymer tube to kink and this sets a lower bound on the core material's softness and hence on the fibre's stiffness. Note that simply specifying a minimum bend radius for the fibre is not a viable solution as tradesmen and builder's laborers are renowned for ignoring written installation instructions and using force to make things fit. Any viable optical fibre must be as "builder proof" as possible.

Another problem with an excessively soft fibre core is that a small diameter fibre may be so flexible that it is not self-supporting. This would require the use of rigid conduits with all the added expense and installation problems. (This problem could be overcome by increasing the thickness of the PVC jacket so that it was stiff enough to support the fibre.)

There are often difficulties in reducing the core's Young's modulus for large diameter fibres. Some manufactures do this by reducing the degree of polymerization. The partly cured fibre smells pungently (actually, a better description would be to say that "it stinks"). Joints in this type of fibre tend to age poorly as the abundant residual monomer can attack the glue. In

addition, while the fibre is initially pliable, it becomes rock hard when the polymerization finally occurs. This can take from months to one or two years, depending on the details of the fibre chemistry and the temperature in the field.

A better solution is to add a low molecular weight plasticizer that acts as a lubricant between the polymer chains. By adjusting the amount of plasticizer, it is possible to tailor the material's Young's modulus. One suitable plasticizer is diethyleneglycol bis allylcarbonate (ADC), also widely known by its trade name of CR-39® (*PPG Industries*). It is interesting that this thermoset homopolymer is commonly used to make lens for eyeglasses as it has the highest hardness and scratch resistance of any low-cost optical plastic. However, full polymerization of ADC takes approximately 20 hours with a maximum temperature of 95°C. This is much longer and hotter than the polymerization schedule for making solid core optical fibre so an acrylate/ADC mixture forms a soft, flexible cross-linked polymer that is very stable under field conditions. I have seen many 15 year old samples of solid core fibre made with this technique that are almost as flexible today as the day they were received. Note, however, that if the fibre is exposed to prolonged high temperatures (say several hundred hours at 80°C) it will become rigid.

The cost and manufacturing problems in making solid core fibre are dominated by two problems: the purity of the chemical and issues with the fluoropolymer tubing. The very long optical path lengths mean that contaminants with a concentration of parts per billion can greatly increase attenuation. This is a particular problem if the attenuation is wavelength dependent, as most applications (including LSC's) require uniform transmission across the visible. Excess attenuation of blue light is a problem for all manufactures and the cause is not known. Problems with chemical purity tend to determine whether or not the finished fibre is of adequate quality. Problems with the fluoropolymer tubing often determine whether it can be made at all.

The high cost of optical fibres means that it is worth considering the addition of a light concentrator to the LSC system. If a concentration of say two could be achieved then one would only need half as much fibre to achieve a given luminous output. This could potentially lead to a significant cost saving. This option was explored by constructing a number of LSC's with compound parabolic concentrator troughs and designs with and array of flat reflector mirrors. These concentrators where of necessity very bulky compared to the collector sheets with at least 20 times the volume of a slim housing for the LSC sheets. Focus groups and the sales department of our commercial partner objected very strongly to the bulky "horse troughs" and were unanimous and vociferous in rejecting this approach. The concentrators also lead to high temperatures at the LSC sheets, which raised concerns about sheet stability. Accordingly, the option of external concentrators was rejected.

4.5 FLAT-TO-ROUND CONVERTERS

Experience has shown that the largest practical fibre diameter is 20 mm and 15 mm is much easier to handle. Solid core optical fibres can be made to special order with diameters as large as 40 mm. However, flexibility greatly reduces above 20 mm and the risk of kinking, with a consequent major, irreversible reduction in light transport, also greatly increases for fibres above this limit. The corresponding area on a 6.0 mm thick collector stack has a width of 52 mm. Thus we need a device that will efficiently couple the light from a 52 mm x 6 mm rectangle into a 20 mm diameter cylinder.

It is clear from results R1 to R4 in section 3.1.5 that the local maximum étendue must not decrease between the rectangular entry portion and the circular exit portion. In practice, since the light typically fills the component and everywhere has the largest possible solid angle, this means that the cross sectional area must not decrease. As will be discussed below, some care has to be exercised in how this apparently simple condition is interpreted. What counts is the cross section *seen by the light*, which is not necessarily the same as the geometric cross section. Failure to allow for this subtlety can lead to zones that attempt to "squeeze the light" and hence cause large light losses.

The basic design is shown as an exploded view in Figure 4.6, redrawn from (Franklin & Smith 2004b) with added labels and a coordinate system centered on the entry face. Light from a flat collector stack enters via an optical joint (not shown) to the entry surface which folds in a flat-to-ring converter to form a hollow tubular section. This is joined to a ring-to-solid circle converter which is in turn is connected via an optical joint (not shown) to a solid core optical fibre. It is absolutely essential that the optical train is a solid optical system with no air gaps.

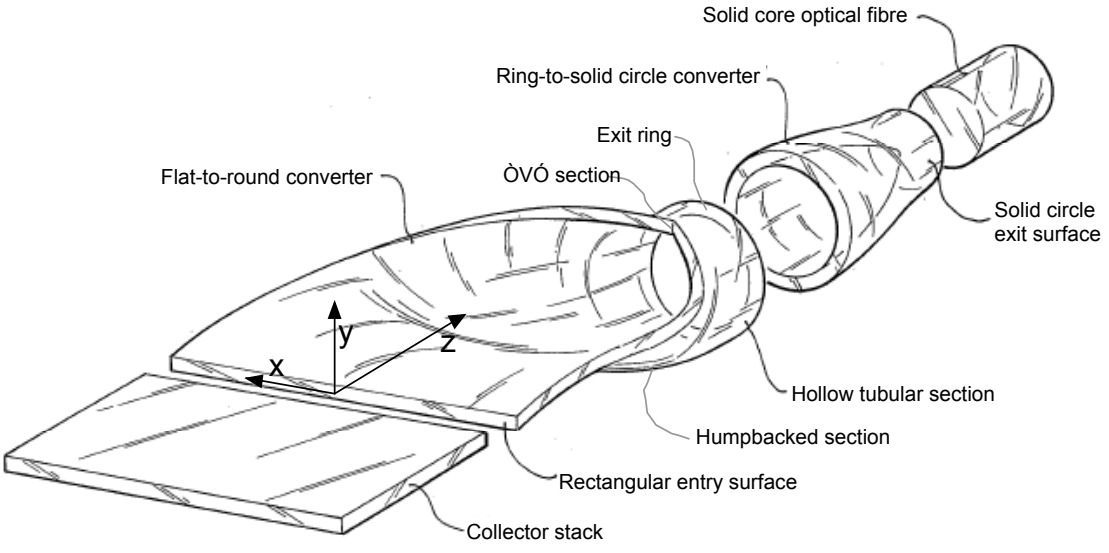

Figure 4.6 Exploded view of a "curled-sheet" flat-to-round converter that couples light from a rectangular entry section to a cylindrical optical fibre.

The ring-to-solid circle converter was described in section 3.3.3 and (Smith & Franklin 1998). The innovation here is the "curled-sheet" flat-to-ring converter and its combination with previously known components. The flat-to-ring converter looks very simple, but there are a number of subtleties. The first is the need to keep the *effective* cross sectional area constant. At the entry and exit zones, the surfaces are parallel to the optic axis. Therefore, the effective cross section in these areas, which is the light carrying area measured perpendicular to the local surface, is the same as the geometric cross section (the light carrying area measured perpendicular to the optic axis). However, at intermediate regions the surface is inclined at an angle, ϕ, to the optic axis. As shown in Figure 4.7, this means that effective cross section can be smaller than the geometric cross section by factor of *cos* ϕ. In some regions, ϕ can exceed 30^o. Thus if the geometric cross section is kept constant, the effective cross section will be reduced by $(1-\cos 30^o) = 13\%$. The light already has the largest possible solid angle. Therefore, by the conservation of étendue, at least 13% of the light must leak out (or be back reflected).

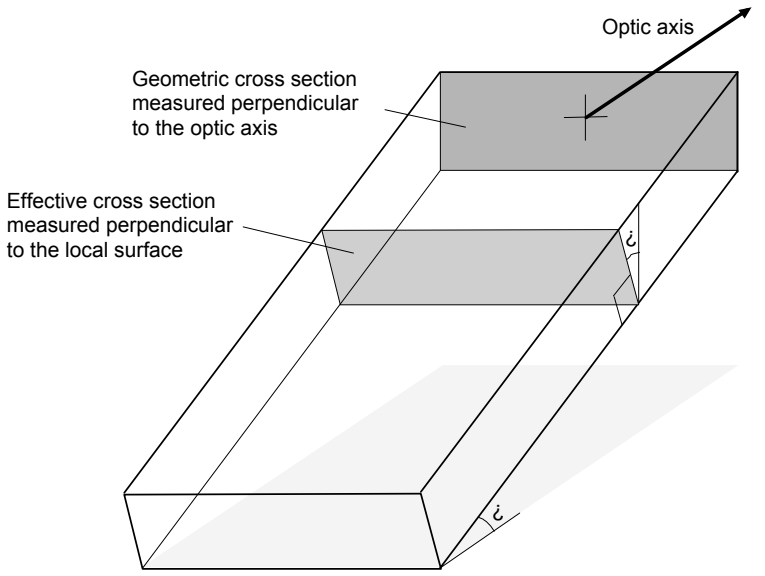

Figure 4.7 The geometric cross section (measured normal to the optic axis) and the effective cross section (measured at right angles to the local surface) differ by the cosine of the inclination, ⌀.

Another subtlety is the inclination of the sidewalls that, as shown in Figure 4.6, have a complicated 180^o twist along their length. Much of the light entering the converter has the maximum angle that can be confined by TIR inside a sheet. If a sidewall is not locally normal to both the inner and outer surfaces, then some light reflecting off a sidewall will acquire an increased angle with respect to the inner (or outer) surface and will escape through it. The complex, three-dimensional twist of the sidewalls means that the "locally normal" condition can be quite hard to meet along the whole of the sidewall. In particular, the skew curvature of the sidewall surface means that in the geometric cross sections the sidewalls are *not* at right angles

to the curves for the top and bottom surfaces. This means that a unit designed with right angles in the geometric cross sections can easily have sidewall inclination errors of 10^o that after TIR would cause a 20^0 change in the light's inclination with a consequent substantial light loss.

4.5.1 Basic Design of Curled-Sheet Converters

One way of making a flat-to-ring converter is to take a thin sheet of flexible transparent material of length *l*, width *w*, and thickness *t,* which has all of its sidewalls perpendicular to the top surface. The aspect ratio of the sheet, *a*, is given by

$$a = \frac{l}{w} \tag{4.2}$$

In order to avoid excessive bending stresses, we require $a > 3$ and $w >> t$. We start by constraining one end to be flat (forming the rectangular entry portion of dimension $w \times t$) and bend the other end into a ring that has the same circumference as the sheet's width. This means that the radius of the ring's neutral surface, r_n is

$$r_n = \frac{w}{2\pi} \tag{4.3}$$

while the radius of the outside surface, r_o, is

$$r_o = \frac{w}{2\pi} + \frac{t}{2} \tag{4.4}$$

and the radius of the inside surface, r_i, is

$$r_i = \frac{w}{2\pi} - \frac{t}{2} \tag{4.5}$$

The ring portion will be joined to a ring-to-solid circle converter (as shown in Figure 4.6). The latter's external surfaces are almost parallel to the optic axis which means that the walls in the sheet's final hollow tubular section must almost be nearly parallel to the optic axis. In order to achieve this, the terminal part of the sheet must be pulled inwards to give an acute "V" where the sheets' opposite edges meet. In order to form a good exit section with a gentle transition to the ring-to-solid circle converter, the "V" should be at least one radius away from the exit ring. We then let the material relax to minimize internal stresses.

The two-dimensional bending results in a "humpbacked" central portion that displaces the optical axis by approximately one radius. This means that the "V" is close to the original optic axis and the centre of the ring is approximately one radius from the original axis. If the sheet's aspect ratio is four or more then the stresses are low and consequently local deformations are also low. This means that the sheet's thickness is almost unchanged by the bending and its

width is also unchanged. Thus the effective cross sectional area is constant for the entire length of the device and étendue is preserved. (The steep inclinations at the entry to the "humpback zone" mean that the *geometric* cross sectional area has substantial changes. However, as pointed out in the previous section, this is irrelevant: from the light's point of view all that counts is the *effective* cross sectional area). The local radius of curvature is everywhere many times the sheet thickness. Consequently, light losses from bending are very small.

The stresses are small along all of the sidewalls, except in the immediate vicinity of the "V". Thus, except for near the "V", local deformations of the sidewalls are also small. In the original flat sheet, the sidewalls are normal to the top and bottom surfaces. The low local stresses in the curled up sheet means that the sidewalls in the bent sheet are also everywhere locally normal, except perhaps near the "V".

The gentle curvature of the sheet means that from the point of view of light inside it, it "looks" locally almost like a flat sheet with "locally normal" sidewalls. Any ray that would be trapped inside a flat sheet by total internal reflection will also be trapped inside the curled sheet. Thus this design provides an almost lossless transition from a rectangular entry to the hollow circular section.

As discussed below in section 4.6, a curled-sheet flat-to-round converter was constructed and gave measured geometric losses of less than 5%. However, this is not a practical method of making a converter since creating optical grade sidewalls in a material resembling jelly was quite challenging. Rather, the interest is in the shape, which can be replicated by more practical methods such as injection moulding. Section 4.7 describes the highly successful injection moulding trials for shapes derived from the curled sheet design.

We now need to turn our attention to the shape of the end zone. The flat-to-round converter of (Franklin & Smith 2004b) illustrated in Figure 4.6 (conceptually) uses a flat-to-ring converter with an optical joint to a ring-to-solid circle converter. It is critical that the axes of the two components are accurately aligned and that the surfaces of each component have the same slope at the joint. Any discontinuities will cause considerable light loss or back reflection. Note that the loss site or reflection zone may not be at the joint, but may be located towards the exit portion of the ring-to-solid circle converter. Misaligning the axis by angle ø causes an increase in the effective cross sectional area of $1/\cos ø$. This increases the étendue by a similar factor and it was shown in section 3.1.1 that increasing the étendue is an irreversible process. The light field is at the limiting angle for confinement by total internal reflection, so the loss of light will be at least of order $(1 - 1/\cos ø)$. However, a much more serious problem can arise when light first strikes the inclined surface and exceeds the critical angle. If ø is small, the loss is approximately $\phi/2\theta_{crit}$. This is potentially a serious loss, so we need to examine in some detail the orientation of the exit ring and the slope of the component near this surface.

If a physical sheet is deformed in the way described above, it will be found that the end ring surface is inclined to the optic axis so that it leans towards the "V". The cause is the difference in the distances from the entry portion to the exit ring. Let z_o be the z coordinate of the sidewall at the ring. The sidewall starts at (w/2, 0, 0) and finishes at approximately (0, 0, z_o). The path taken is a complex three-dimensional curve. We can split the path into three parts: an initial straight segment, a middle portion that has a complex curve, and a final straight section from the "V" to the exit ring. Measurements of curled-sheet flat-to-ring converters showed that the edge remains almost parallel to the z-axis for the first third of its length. The final portion is of length r and is also parallel to the z-axis. Thus, the middle segment has ends at approximately (w/2, 0, l/3) and (0, 0, $z_o - r_n$). The path is parallel to the z-axis at the left hand end and at a small angle at the "V" end. However, as a first approximation we can take a straight line between its two ends although this will tend to overestimate z_o. The total path length is l. Therefore, a slight overestimate of z_o is

$$z_o \approx \frac{l}{3} + r_n + \sqrt{\left(\frac{2l}{3} - r_n\right)^2 - \left(\frac{w}{2}\right)^2} \tag{4.6}$$

Combining (4.6) with (4.2) and (4.3) gives

$$z_o \approx w\left[\frac{a}{3} + \frac{1}{2\pi} + \sqrt{\left(\frac{2a}{3} - \frac{1}{2\pi}\right)^2 - \frac{1}{4}}\right] \tag{4.7}$$

Let z_i be the z be the coordinate of the bottom centre of the ring. This point is at approximately (0, -2r_n, z_i). The shortest path from the origin to this point goes through the "humpback" section, but this bending adds very little extra distance. Thus a good estimate for z_i is

$$z_i \approx \sqrt{l^2 - (2r_n)^2} \tag{4.8}$$

Combining (4.8) with (4.2) and (4.3) gives

$$z_i \approx w\sqrt{a^2 - 1/\pi^2} \tag{4.9}$$

The tilt of the exit surface, ϕ, is approximately

$$\phi = \tan^{-1}\left[\frac{\pi(z_i - z_o)}{w}\right] \tag{4.10}$$

For an aspect ratio of 4.0, equations (4.7) and (4.9) give the differences in the z coordinates from the top to the bottom of the exit ring as 0.038w with a corresponding tilt of the exit surface as 6.7°. The corresponding étendue loss (1 - 1/$cos\phi$) is 0.7% and the loss due to

light exceeding the critical angle ($\approx \phi/2\theta_{crit}$) is approximately 8.0%. Increasing the aspect ration to 5.0 decreases the difference in the z coordinates to $0.030w$ and reduces the end tilt to 5.3^{o}. The corresponding étendue loss is 0.4% and the loss due to light exceeding the critical angle is approximately 6.2%. These losses can be eliminated by trimming the end of the curled sheet so that it is perpendicular to the original optic axis.

4.6 Designing a Curled-Sheet Flat-to-Round Converter

4.6.1 The Basics

Attempts to use the *Strand7*® finite-element analysis software (*Strand7 Pty Ltd*) to calculate the shape of a curled-sheet flat-to-ring converter were unsuccessful. While it is easy to use finite element packages to calculate stresses in a known shape, it is not straightforward to use these programs to generate the shapes described in section 4.5.1. In retrospect, part of the difficulty may have been that it was not understood at the time that for a rectangular sheet bent into a flat-to-ring converter, the exit ring is inclined at angle ø to the optic axis, as described by equations (4.6), (4.9) and (4.10). However, the finite element models assumed that the exit ring was normal to the optic axis. Doing this for a rectangular sheet leads to very high stresses and unreasonable shapes.

Accordingly, it was decided to construct a prototype curled-sheet flat-to-ring converter from a rectangular sheet of flexible transparent polymer and to use this device to test the theory outlined in section 4.5.1. A ring-to-solid circle converter made earlier at my direction by Dr Paul Swift was on hand and is shown in Figure 4.8. Dr Swift measured the efficiency of this device as 85% and ascribed the losses to surface defects from hand polishing and lack of optimal design shape (Smith & Franklin 2002).

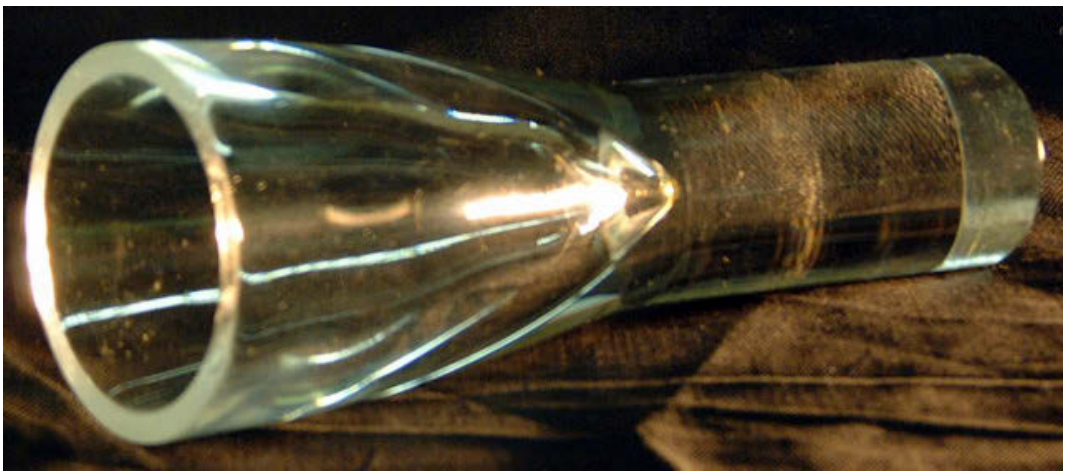

Figure 4.8 A ring-to-solid circle converter with constant solid cross sectional area.

An optimized version of this ring-to-solid circle converter was constructed as a polygon object and ray traced in *Zemax*® (*Radiant Zemax LLC*). Figure 4.9 shows a ray trace for light with the largest possible solid angle that can be confined inside a cylinder by total internal reflection. Losses are about 1%.

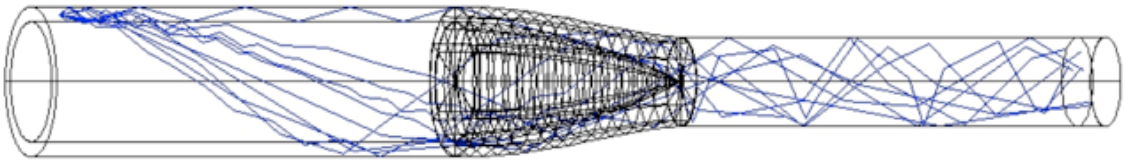

Figure 4.9 Ray tracing a ring-to-solid circle converter in *Zemax*® for light with the maximum solid angle.

The goal was to make a flat-to-ring converter and to couple this to the existing ring-to-solid circle converter to make a complete flat-to-round converter, similar to that illustrated in Figure 4.6. The plan was that if the prototype proved satisfactory, its dimensions would be measured and used for a computer model in the *Zemax*® ray tracing program. The existing ring-to-solid circle converter had an entry-ring with an outside diameter of 50.0 mm and a wall thickness of 5.0 mm. This requires a sheet width of (50.0 – 6.0) x π = 138 mm.

4.6.2 Casting a Flexible Transparent Sheet

The key requirements for the rectangular sheet used in a flat-to-ring converter are:

1. The sheet must be transparent enough so that there is little attenuation over the full length of the model (different rays have quite different path lengths so any significant attenuation would considerably complicate the analysis).

2. The sheet must be flexible enough so that it can be bent into a circular exit ring without kinking. This requires that the sheet is very soft. However, the sheet must be stiff enough so that it is self-supporting.

3. The top and bottom surfaces must be very smooth with a high quality optical finish. Scattering losses of 10% after 65 interactions requires a loss per interaction of less than 0.15% (at 45^{o} incidence) and a mean scattering angle of less than 0.6^{o}.

4. The sidewalls must be accurately perpendicular to the top surface, have sharp edges, and have a moderate quality optical finish. For a sheet aspect ratio of 4, rays have at most 4 interactions with the sidewalls. So a 10% loss requires a loss per interaction of less than 2.5% (at 45^{o} incidence) and a mean scattering angle at the sidewalls of less than 2.5^{o}.

Note that the requirements 2 and 4 are contradictory. The flexibility requirement means that the sheet must be very soft. However, it is difficult to create optical grade sidewalls in very soft materials.

There is no commercially available sheet that meets requirements 1 to 4. So it was decided to cast sheets from the material used for solid core optical fibre. When properly polymerized, this material has a very low attenuation (approximately 3% per metre) and, with the appropriate amount of plasticizer, it is soft enough to meet requirement 2. Note that the casting liquid shrinks by about 10% during polymerization so it is essential that the mould can accommodate this.

Mr. Eddy Joseph kindly provided access to his factory's laboratory at *Poly Optics Pty Ltd* in Burleigh, Queensland. The initial mould (the "*A*" mould) was made by the UTS Science Faculty workshop. It was constructed from two 267 mm x 207 mm x 10 mm aluminum plates with 10 mm thick aluminum sidewalls bolted to both long sides and one short side (the top was left open). All interior surfaces were lined with 2 mm thick *Teflon*® sheet (*Unasco Pty Ltd*) bonded to the aluminum with *Loctite® 770* primer and *Loctite® 431* adhesive (*Henkel AG & Co. KGaA*) leaving a mould cavity 6.0 mm thick that was open at the top.

For optical quality cast sheet, it is essential to avoid any bubbles in the liquid. This was achieved by taking a 5.0 mm diameter *Teflon*® tube and flattening one end. The mould was inclined at about 20^{o} and filled through the *Teflon*® tube with the tube's flattened end held close to the top of the mould so that the casting liquid flowed smoothly down the inside of the mould. The mould was filled to 30 mm from the open top, which was then covered with aluminum foil to exclude moisture.

The filled mould was placed vertically in a 70^{0} C water bath with the surface of the water about 10 mm above the initial surface of the casting liquid inside the mould. After 5 hours, the mould was removed from the water bath and allowed to air cool. The mould was then opened by removing the sidewalls and levering apart the top and bottom sheets. Unfortunately this tended to delaminate the *Teflon*® off the aluminum sheets. Trials with other glues were unsuccessful.

The cast sheets' flexibility was excellent and their bulk optical properties were very satisfactory. The bulk attenuation was too small to measure (<2%) when tested with a laser beam that was aligned parallel to the sheet's top surface so that it did not strike the top or bottom surface. However, these surfaces were not optically smooth and gave unacceptable scattering when tested with a laser beam inclined through the sidewalls so that the internal angle of incidence was more than 5^{o}.

The key problems with the *A* mould were the smoothness and the attachment of the mould liner (*Teflon*® sheet). Attempts to use other polymer sheets as mould liners were

unsatisfactory. Accordingly, trials were conducted with a second mould, the *B* mould, made from 112 mm x 61 mm x18 mm glass blocks and a sidewall consisting of a *Teflon*® coated 50 mm diameter O-ring. Polymerized casting material sticks tenaciously to clean glass, so various mould release agents were tested at UTS using casting solutions kindly donated by *Poly Optics*. Standard release agents used for the commercial cell casting of PMMA on glass did not work as the flexible polymer has a much stronger bond to glass than does cast PMMA. Various agents were trialed and *Helmar H.4000® silicone spray* (*Helmar Australia Pty Ltd)* gave excellent results for the small *B* mould. As will be discussed below, it proved to be less satisfactory for large moulds.

It is important that the glass is completely covered with a very thin layer of release agent. (Too much release agent causes excess scattering in the cast sheet, but any uncoated glass can cause surface defects.) The glass blocks in the *B* mould were prepared by lightly spraying on the release agent and wiping it off. This procedure was repeated three times with a vigorous 2-minute final polish with a very clean cloth. The *B* mould gave 50 mm circular discs that had very glossy top and bottom surfaces and bulk attenuation that was too small to measure.

A third mould, the *C* mould, was made from 300 mm x 210 mm x 12 mm glass sheets held together with 10 "C" clamps. The mould's side seals were a single piece of 6 mm diameter expanded *GORE® Joint Sealant* PTFE cylindrical tape that started at the mould's top centre and followed the complete outer circumference of the glass sheet. "C" clamps proved much more reliable than spring loaded clamps as the *GORE® Joint Sealant* is quite resilient and required larger compressive forces than could readily be provided with spring clamps. Also, the screw action of the "C" clamps permitted a controlled and reproducible pressure on the seal.

Helmar H.4000® silicone spray was used as a release agent. Trials showed that the 30-fold increase in surface area and 33% reduction in thickness for the glass plates in the *C* mould compared to the *B* mould necessitated the use of more release agent. This was achieved by reducing the duration and intensity of the final polish. However, the extra release agent increased the attenuation of the cast sheet although it was still acceptable (approximately 10% loss over the sheet length). In retrospect, it would probably have been better to have used the same amount of release agent as for the *B* mould, and to have separated the casting by chilling the assembly in a freezer (the thermal expansion coefficient of cast sheet is many times that of glass). Lastly, it should be mentioned that after initially satisfactory results, subsequent cast sheets had unacceptable attenuation with a slightly "milky" appearance when viewed edgewise. After extensive (and frustrating) tests of the casting chemicals, cleaning chemicals and the release agent, it turned out that the batch of the "very clean cloth" used for the final polish of the mould was contaminated.

The *C* mould was assembled horizontally by laying a coated glass sheet on the centre of stand so that there was a 40 mm wide space around the whole of the perimeter to provide access for the clamps. A precut length of 6 mm diameter *GORE® Joint Sealant* was positioned around the circumference of the glass sheet so that it formed a complete loop. The final 20 mm of the sealant (where it approached the start of the seal) was bent outwards to provide a gap for filling the mould. The second glass sheet was then placed on top of the sealant and held in place with a "C" clamps at each corner plus two clamps on each long side and one clamp on each short side. The 10 clamps were then tightened to give even compression of the seal. As the clamp pressure was increased, a thin line was observed where the glass came into intimate contact with the cylindrical *GORE® Joint Sealant* and air was forced from the interface. The pressure of individual clamps was adjusted so that this line was about 1.5 mm wide along the whole of the seal. This procedure gave a reliable leak-proof seal and a spacing between the two glass plates uniform to about 0.05 mm. The final sheet thickness of 5.5 mm was slightly less than the goal of 6.0 mm. However, achieving the latter would have required the used of thicker *GORE® Joint Sealant* tape which was not available.

The glass mould was then filled and polymerized by the procedure described above for the *A* mould. One advantage of the glass mould over the aluminum and *Teflon® A* mould is that it was possible to observe the filling process and to make sure that there were no bubbles. After filling, the 20 mm gap in the seal was blocked off by repositioning the bent piece of sealing tape. This procedure gave a good waterproof seal along the whole of the entire mould except for a tiny vent where the two ends of the sealing tape met. The vent is essential as the casting liquid contacts by more than 10% on polymerization.

The transparency of the mould and the presence of a good top seal enabled the mould to be filled to within 10 mm of the top of the glass with the meniscus only 5 mm below the surface of the water bath (c.f. 30 mm and 20 mm respectively for the *A* mould). The transparency of the glass also made it possible to observe the contraction of the casting liquid during the polymerization process. These observations assisted in optimizing the "cooking" time for the sheets. On the one hand, it is essential that the sheet is properly polymerized (excess residual monomer can cause stability problems, difficulties with handling, and OH&S issues). On the other hand, excessive time in the water bath decreases the sheet's flexibility by causing undesired side reactions with the residual monomer. Leaving the mould in the water bath for one hour after the end of visible shrinkage gave good quality sheets that proved odor free and very durable.

After air-cooling, the moulds were easy to open. The *GORE® Joint Sealant* tape pulled cleanly away from the cast sheet and with careful handling could be reused many times (a useful economy as it is quite expensive). A gentle twist with a wooden wedge separated the top half of

the mould. The cast sheet could then be easily peeled off the bottom half of the mould. The sheets were stored in HDPE bags as these proved not to mark the soft surface while *Glad Wrap*® cling film left a residue that marred the surface.

The cast sheets from the *C* mould turned out to be a little short for bending into a curled-sheet flat-to-ring converter. Accordingly, a fourth mould, the *D* mould, was constructed from 380 mm x 250 mm x 12 mm glass plates. Cast sheets from the *D* mould made with the procedures described above were used to make good quality curled-sheet flat-to-ring converters.

4.6.3 Assembling a Curled-Sheet Flat-to-Ring Converter

It was pointed out in section 4.6.2 that a key requirement for a sheet in a flat-to-ring converter is that the sidewalls are accurately perpendicular to the top surface, have sharp edges, and have a moderate quality optical finish. The scattering process is stochastic with about half the interactions causing the light to increase its angle with respect to the optic axis (which may cause loss) while about half the interactions will decrease the angle of the light with respect to the optical axis (which will help to confine the light). Thus the ray random walks towards the loss cones and the fractional loss due to scattering, f_{scat}, will be proportional to the square root of the number of interactions with the sidewalls, I. For light from a LSC the average number of interactions with a converter's sidewalls is approximately equal to the converter's aspect ratio, a. So

$$f_{scat} \sim \sqrt{I} \approx \sqrt{a} \tag{4.11}$$

For a sheet aspect ratio of 4, a 10% loss requires a loss per interaction of less than 5% and a mean deviation from a perfect specular reflection less than 2.2°. The mean deviation will be the RMS sum of scattering from a rough surface and deviation due to incorrect surface inclination. Since the deviation is twice the slope error, this means that the inclination of the sidewall should be correct to within 1°, and preferably to better than 0.5°. This combination of optical finish and correct slope is quite difficult to achieve in a material that resembles a stiff jelly.

It is essential that the sidewalls' edges are as sharp as possible. We may model each edge as a 90-degree arc of radius r_{side}. Approximately half the rays that interact with an edge will be lost from the light guide so the loss fraction from each interaction with edge will be of order $r_{side}/2t$. The edges form only a very small part of the sidewall (the edge radius is much smaller than the sheet thickness, t) so the loss fraction, f_{edge}, will be proportional to the number of interactions. Each sidewall has two edges, so

$$f_{edge} \approx \frac{Ir_{side}}{t} \approx \frac{ar_{side}}{t} \tag{4.12}$$

Thus for a flat-to-round converter with a typical sheet thickness of 6 mm and an aspect ration of 6, achieving a sidewall edge loss of 1% requires edge radius of 10 μm.

Hand held optical shears such as a *Poly Cutter*™ do not give an optical quality surface finish. Also, it is not possible to cut a long edge with this type of tool or to achieve the required accuracy. However, they can be used to cut a small "window" into the side of a cast sheet for laser testing. For testing purposes, the window is coated with a refractive index matching medium (such as glycerin for a temporary window or glue for a permanent one) and covered with a thin sheet of PMMA that provides an optical surface.

After a number of trials it proved possible to produce a high quality sidewalls by using a computer controlled router. This gave planar surfaces with accurate dimensions and a good quality matt finish without any visible chipping or tearing of the edges. Correct clamping is very important as the soft material deforms under low pressure – the final sidewall will not be planar if the sheet is cut when it is deformed by the clamp. Vacuum clamping gave much better results than mechanical clamping. Surface profile and finish degrades markedly if the cutter is more than half a sheet thickness from the vacuum clamp.

Good finish requires:

1. The use of special cutters. Single edge spiral O flute cutters gave the best results.
2. Very sharp cutters. (Note that the material is soft so wear is low.)
3. High angular speeds. 12,000 rpm gave the best results.
4. A good cutting fluid. Liquid hand wash soap gave good results.
5. The correct feed rate (too high or too low gives poor finish).
6. The use of climb cut rather than normal cut. (Normal cut is fine for rough cutting, so a combined rough and finish cut can be made in one machine cycle.)

The surface produced by the router has a matt finish. This was taken to a high gloss by using a fine brush to apply two coats of *Showa X3*™ (*Showa Technocoat Co. Ltd.*, Tokyo, Japan) at 33% concentration in ethoxy propyl acetate (also called propylene glycol ethyl acetate). The resulting sidewalls gave almost no visible scattering when tested with a laser.

A curled-sheet flat-to-ring converter was assembled from a 330 mm x 137 mm x 5.0 mm flexible sheet made by the *D* mould with cut, but uncoated edges. One end of the sheet was clamped flat and the other end was curled around a 40 mm diameter plastic mandrel. The position of the mandrel was adjusted to minimize the stress in the sheet while holding the mandrel axis parallel to the sheet's entry axis. The area of the mandrel beneath the sidewalls was covered with a light coat of *Helmar H4000® silicone spray* as a release agent. The final 30 mm of the sidewalls was glued together with *Loctite® 349 Impruv®* (*Henkel AG & Co. KGaA)* optically clear UV curing adhesive.

As described in section 4.5.1 and equation (4.10), the tubular end of the unit was noticeably inclined towards the V section. The end ring was squared off normal to the optic axis by using a very sharp 42 mm fly cutter in a milling machine at 2,500 rpm using WD-40 as a cutting fluid. The resulting surface was much rougher than the sidewalls produced by the high-speed router but this was not important as it was ultimately to be glued to a ring-to-solid cylinder converter.

After assembly, the sidewalls were given two coats of *Showa X3*^{TM} dissolved at 33% concentration in ethoxy propyl acetate. This was done after assembly to avoid the damage that might occur by bending a coated edge.

Figure 4.10 shows a side view of the curled-sheet flat-to-ring converter. Note that it is rotated 180^{o} about its long axis compared to the converter in Figure 4.6, which makes the "humpbacked section" much more obvious.

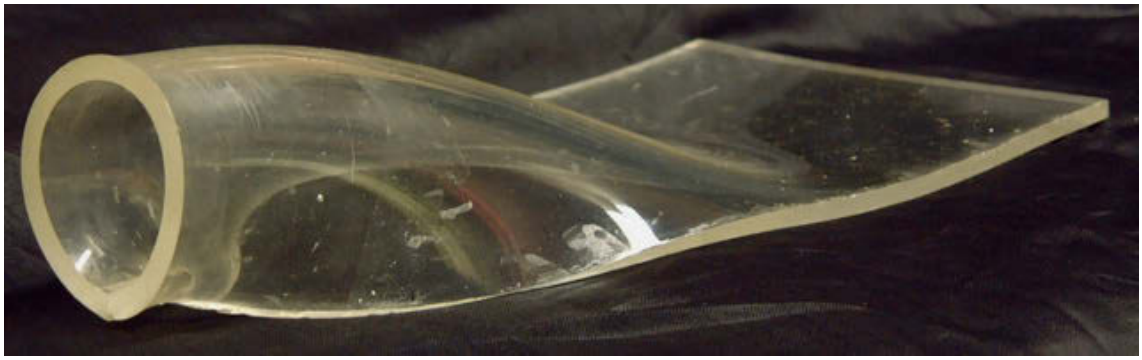

Figure 4.10 Side view of a curled-sheet flat-to-ring converter. Note the distortion of the exit ring.

The end ring in Figure 4.10 is noticeably deformed by residual stresses from the desired circular shape. Also, as described in section 4.2, the UV cured glue joints are very strong in tension but somewhat prone to peeling. Accordingly, the cylindrical end section was covered in HDPE (to act as an optical isolator) and tightly wrapped with PVC tape. This resulted in a much more circular end profile as shown in Figure 4.11

For optical testing, a 500 mm x 125 mm x 2.0 mm green fluorescent PMMA sheet was glued to the converter's entry surface as shown in Figure 4.11. This photograph indicates that the converter is working very well. The light from the short fluorescent sheet has the largest possible solid angle for light trapped by total internal reflection. The high angle light inside the sheet and the converter mercilessly illuminates every surface blemish. However, what is very noticeable is the complete absence of bright patches *not* due to surface blemishes. In particular, the sidewalls of the converter are actually darker than the diamond polished edges of the fluorescent sheet. In fact, there are no visible geometric losses.

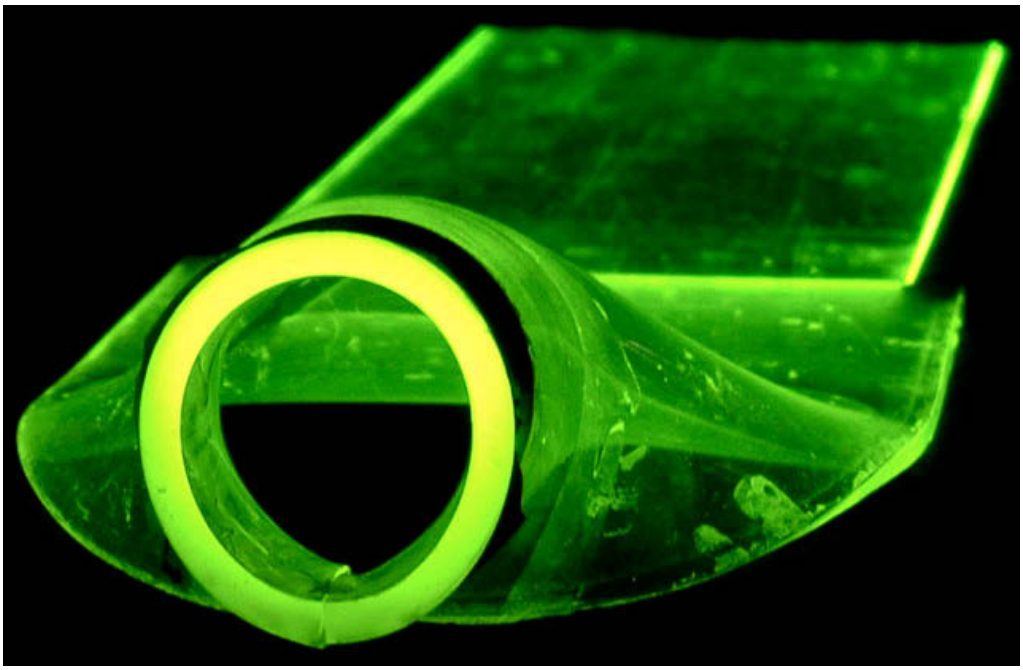

Figure 4.11 Curled-sheet flat-to-ring coupler attached to a fluorescent sheet. The output is then fed into an integrating sphere and compared to that from a similar luminescent sheet without a coupler.

The performance of the converter was measured by feeding the light from the exit ring into an integrating sphere. This was then compared with the light from a similar sized flat flexible sheet from the *D* mould that was glued to a 500 mm x 125 mm x 2.0 mm green fluorescent PMMA sheet. The converter's output was 95% of that from the flat flexible sheet. This is a very satisfactory performance given the inevitable surface blemishes that accumulate during the bending and gluing process.

A complete flat-to-round converter, similar to Figure 4.6, was made by gluing the flat-to-ring converter of Figure 4.11 to the ring-to-solid circle converter of Figure 4.8. The assembled unit had an efficiency of approximately 80%, which agrees well with the combination of flat-to-ring converter efficiency of 95% and a ring-to-solid circle efficiency of 85% (0.95 x 0.85 = 0.81). Note that as discussed in section 4.6.1, ray tracing with *Zemax*® indicated that with improved design, geometric losses in a ring-to-solid circle converter can be reduced to about 1%. So these results indicated the prospect of a very high performance flat-to-round converter.

4.6.4 Modelling a Curled-Sheet Flat-To-Round Converter

The exterior surface of the physical model illustrated in Figure 4.11 was measured on a 10 mm grid. A smoothed 3D curve was fitted to this data.. The requirements for conservation of étendue discussed in sections 4.5 and 4.5.1 were then used to calculate the location of the interior surface and co-ordinates of the sidewalls. This mathematical model was then used to calculate the vertices of a *polygon object* that was ray traced in *Zemax*®. (A polygon object is a user-defined object in *Zemax*® that can be used to define a polygon volume. The polygon object

is based on a collection of 3D triangles or rectangles whose vertices are placed in a suitable ASCII file. The polygon volume may optionally be open or closed. For details see (Zemax 2006, p. 335) and (Zemax 2006, pp. 393-5).

Inspection of the measured coordinates of the flat-to-ring converter's outer (exterior) surface showed that all the measured transverse cross sections were well approximated by arcs of circles. The transverse radius of curvature, $r_o(z)$, varied smoothly from infinity at the flat entry surface to the value given by equation (4.4) at the exit ring. Equations fitted to the transverse radius of curvature had poor numerical stability. However, changing the variable to the transverse curvature, $c_o(z) = 1/r_o(z)$, gave very good results. An excellent fit was obtained for a cubic constrained to have zero at the entrance surface ($z = 0$) and the value implied by equation (4.4) at the exit ring.

In order to develop a mathematical model of the converter, for each value of z along the optic axis we need to determine: the transverse radius of curvature of the outer surface, $r_o(z)$, the position of that centre of curvature, $\boldsymbol{C_0}(z)$, the arc length of the transverse cross section, $w_o(z)$, the radius of curvature of the inner surface, $r_i(z)$, the position of that centre of curvature, $\boldsymbol{C}_i(z)$, and the location of the sidewalls.

The y value of the exterior surface in the y-z plane, $y_o(z)$, was also well described by a cubic. (Note that the converter of Figure 4.11 is inverted compared to that in Figure 4.6 so $y_o(z)$ is negative.)

Fixing both the y value of the outer surface on the y-z plane and the transverse radius of curvature of that surface determines that the centre of curvature for the outer surface, $\boldsymbol{C}_o(z)$, is at

$$\boldsymbol{C}_o(z) = \left(0, 1/c_o(z) + y_o(z), z\right) \tag{4.13}$$

The inner, neutral and outer surfaces are concentric at the exit ring. So as a first approximation we will assume that the inner, neutral and outer surfaces are concentric everywhere and so

$$\boldsymbol{C}_i(z) = \boldsymbol{C}_o(z) \tag{4.14}$$

The outer surface is inclined at some angle ϕ to the z-axis, with ϕ varying slightly along the transverse cross section. As a simplifying assumption, we may approximate the inclination by the value of ϕ at the y-z midplane. From Figure 4.7, if the sheet has a constant thickness of t, (measured perpendicular to the surface) the distance between the outer and inner surfaces in a transverse plane, $T(z)$, is

$$T(z) = \frac{t}{\cos\phi(z)} \tag{4.15}$$

The inclination angle, $\phi(z)$, can be found by differentiating $y_o(z)$,

$$\phi(z) = \tan^{-1} \frac{dy_o(z)}{dz} \tag{4.16}$$

For concentric inner and outer surfaces, relationship between the inner, neutral and outer surfaces are shown in Figure 4.12. We see that the radius of the inner surface, $r_i(z)$, is

$$r_i(z) = r_o(z) - T(z) \tag{4.17}$$

while the radius of curvature of the neutral surface, $r_n(z)$, is

$$r_n(z) = r_o(z) - \frac{1}{2} T(z) \tag{4.18}$$

Now the arc length of the neutral surface has a fixed value of w. The neutral and outer surfaces are concentric. So from Figure 4.12 and equations (4.15) and (4.18) the arc length of the outer surface, $w_o(z)$, is

$$w_o(z) = \frac{w r_o(z)}{r_n(z)} = \frac{w r_o(z)}{r_o(z) - \dfrac{t}{2\cos\phi(z)}} \tag{4.19}$$

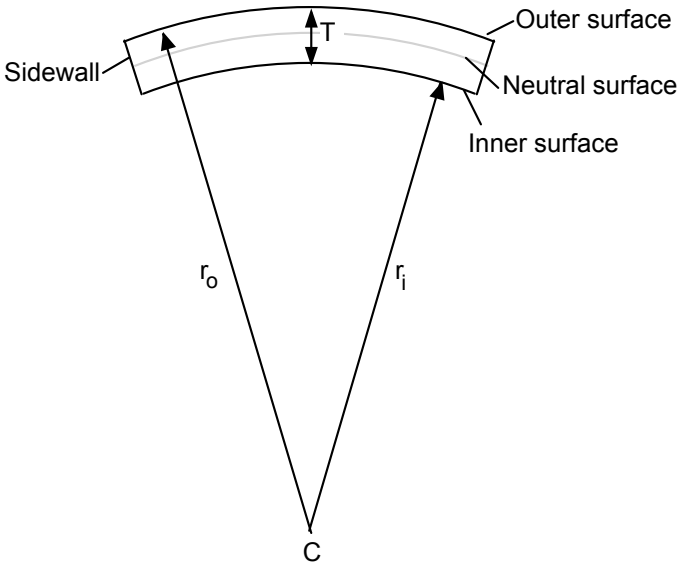

Figure 4.12 Transverse cross section of a flat-to-round converter with the inner and outer surfaces having a common centre of curvature at *C*. The mean direction of the light is inclined to this cross section by (90 - ϕ). Note that the converter's thickness in this plane, *T*, has been exaggerated for the sake of clarity.

It might be thought from Figure 4.12 that the arc length of the inner surface, and hence the position of the sidewalls, could analogously be calculated by

$$w_i(z) = \frac{wr_i(z)}{r_n(z)} = \frac{w\left(r_o(z) - \dfrac{t}{\cos\phi(z)}\right)}{r_o(z) - \dfrac{t}{2\cos\phi(z)}} \tag{4.20}$$

However, doing this would create large losses in the converter because the sidewalls would not be perpendicular to either the outer or inner surfaces. The problem is that those surfaces are inclined by angle ϕ to the transverse cross section shown in Figure 4.12. Indeed, a unit designed with right angles in the geometric cross sections can easily have sidewall inclination errors of 10^o that would cause a 20^0 change in the light's inclination at each reflection and a hence massive light loss after multiple interactions with the sidewalls.

Instead, the procedure adopted was to use equations (4.13) and (4.19) to calculate the position of a point ***P*** at the intersection of the outer surface with the sidewall. Auxiliary points $\boldsymbol{Q}_1$, $\boldsymbol{Q}_2$ and $\boldsymbol{Q}_3$ were then chosen as shown in Figure 4.13 with $\boldsymbol{Q}_1$ and $\boldsymbol{Q}_3$ on the edge of the outer surface and $\boldsymbol{Q}_2$ having the same z value as ***P***, but located away from the sidewall. Let ***S*** be a vector normal to the surface at ***P*** of length t. Then point ***I*** on the inner sidewall edge corresponding to ***P*** is given by

$$\boldsymbol{I} = \boldsymbol{P} + \boldsymbol{S} \tag{4.21}$$

A good estimate of ***S*** is

$$\boldsymbol{S} = \frac{t}{2}(Q_1P \times Q_2P + Q_2P \times Q_3P) \tag{4.22}$$

which is formed by averaging unit vectors for the $\boldsymbol{Q}_1$, ***P***, $\boldsymbol{Q}_2$ and $\boldsymbol{Q}_2$, ***P***, $\boldsymbol{Q}_3$ triplets. (Numerical trials show that only using one triplet to form the unit vector leads to considerable errors and unacceptable light losses in the polygon object). Once a number of points on the inner edge of the sidewall have been found from equations (4.21) and (4.22), it is simple to fit a curve to these values to calculate $w_i(z)$. These values turn out to be significantly different to those of equation (4.20).

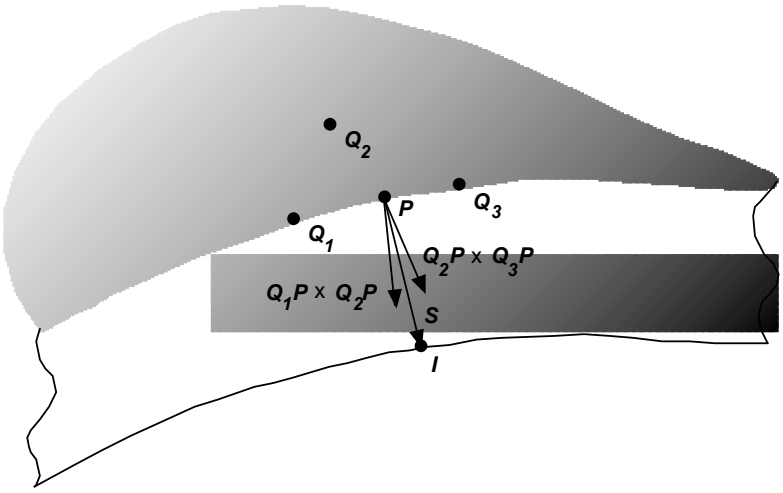

Figure 4.13 Calculating the sidewall. For a point ***P*** on the upper edge of the sidewall, auxiliary points $\boldsymbol{Q}_1$, $\boldsymbol{Q}_2$ and $\boldsymbol{Q}_3$ are used to construct a vector ***S*** that is perpendicular to the outer surface and has a length equal to the sheet thickness, *t*. The point on the inner edge of the sidewall, ***I***, corresponding to ***P*** is $\boldsymbol{I} = \boldsymbol{P} + \boldsymbol{S}$.

The procedure described above was used to calculate a grid of points on a mathematical model based on measurements of the flat-to-ring converter illustrated in Figure 4.11. A closed polygon object for the *Zemax*® program was then written in *Excel*® using the procedures of (Zemax 2006, pp. 393-5). Figure 4.14 shows a typical ray tracing. In this example, taken from the patent (Franklin & Smith 2004b), the source has the largest possible range of angles for light to be confined by total internal reflection inside a flat sheet. More than 98% of the rays reach the exit ring.

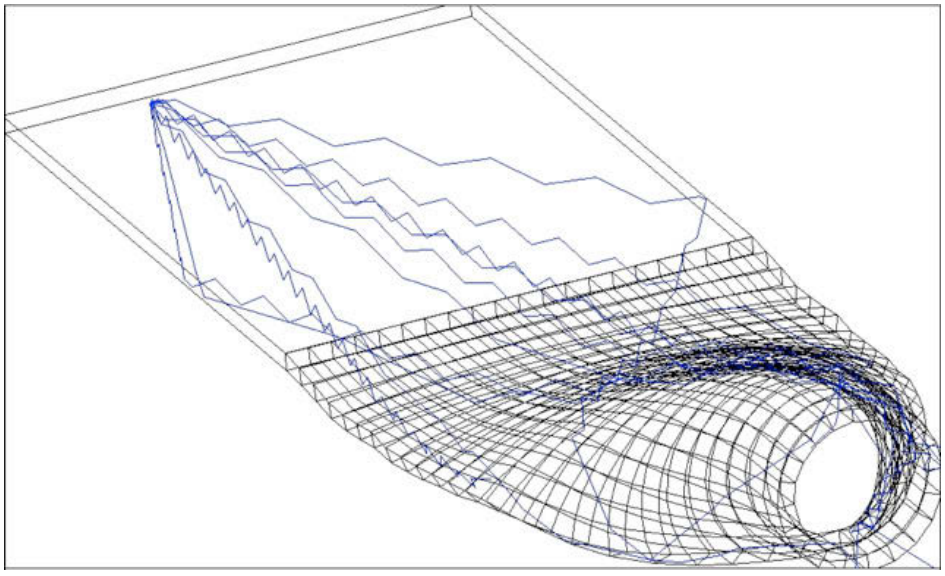

Figure 4.14 Ray tracing in *Zemax*® of a curled-sheet flat-to-ring converter. The source has the largest possible range of angles for light to be confined by TIR inside a flat sheet. More than 98% of the rays reach the exit ring.

This polygon object model was then combined with the polygon object model of a ring-to-solid circle converter of Figure 4.8 so that the combination formed a flat-to-round converter, similar to Figure 4.6. There were no significant extra losses in the flat-to-ring section.

4.7 MASS PRODUCTION OF FLAT-TO-ROUND CONVERTERS

The curled-sheet optical model described in section 4.6.4 was satisfactory for proof of principle, and for developing the basic mathematics of the design. However, this is not a practical method for mass-producing flat-to-round converters. Not only did the sheet matrix have relatively poor optical quality (which could have been improved by better casting technique), but also forming the sidewalls was extremely challenging (as previously mentioned, it was like machining jelly to an optical finish) and would be far too expensive for mass production. The only feasible mass-production technique is injection moulding. However, injection moulding presented a number of significant problems including:

- Making a suitable tool and running injection-moulding trials was estimated to cost on the order of $50,000. Budgetary constraints meant that there had to be a very high confidence of success before committing these funds. If there were major problems it was unlikely that money would be available for a new design.
- The design shown in Figure 4.6 would require significant modification if it was to be made by injection moulding because the "humpbacked" nature and compound curvature of the flat-to-ring section means that there is no unobstructed extraction path for the tool which would make the interior surface.
- It would be technically challenging to achieve a homogeneous optical-grade matrix, optical grade surface finish, accurate surfaces and precision edges over such a large component.

The relatively poor optical quality of the matrix and sidewalls in the curled-sheet optical model described in section 4.6 meant that measurements were necessarily limited. Accordingly, in the commercialization phase of this project it was decided to commission several optical grade flat-to-round converters from *Arrk Australia and New Zealand Pty Ltd* to prove the design of section 4.6.4. (The actual manufacture of the rapid prototypes was undertaken by *Arrk's*® facilities in Taiwan). The plan was to first build and measure a complete flat-to-round converter. If that proved satisfactory, the design would be optimized for mass production by injection moulding. A series of rapid prototypes would be commissioned of the modified design until FSL were confident of both its optical performance and the feasibility of mass-production by injection moulding. Only then would the injection moulding tool and trials be commissioned.

The methods outlined in sections 4.5.1 and 4.6.4 were used as the basis of a *SolidWorks*® model (*Dassault Systèmes SolidWorks Corporation*) created at my direction by Russell Collier at Fluorosolar Systems Ltd. The humpback nature of the design meant that *Arrk Rapid Prototyping* had to make each converter in two pieces that were glued together. Despite concerns about losses from the glue joints, and scattering from the sidewalls (whose skew curves made them very hard to polish), measured transfer efficiency from a LSC sheet glued to the input surface exceeded 92%. As Figure 4.15 shows, geometric losses were very small. In this photograph, the prototype is resting on a smooth sheet of black PMMA (*Plexiglas*®) and reflection off this surface provides a partial view of the underside of the LSC and the flat-to-round converter. In order to facilitate comparison with Figure 4.6, Figure 4.14 and Figure 4.16, this photo and those in Figure 4.17 and Figure 4.18 have been reflected about a vertical axis (interchanging left and right) so that in all figures the source is on the left.

QuickTime™ and a
decompressor
are needed to see this picture.

[Production Note: This figure is not included in this digital copy.
The print copy of the thesis is available for consultation at UTS Library.]

Figure 4.15 The *Arrk*® prototype glued to a red LSC and fitted with a conical light extractor. The glued joints between the upper and lower pieces are visible as a bright line at the exit surface.

Although the designs of sections 4.5.1 and 4.6.4 performed well in both theory and practice, the "humpbacked" nature and compound curvature of the flat-to-ring section made this design impractical to mass produce by injection moulding because there is no unobstructed extraction path for the tool which would make the interior shape (see Figure 4.6). Now the "humpback" section arises from the stress relief of the bent sheet. However, in an injection moulded component there are no stresses, so we can displace cross sections in the x-y plane to eliminate the hump.

For ease of injection moulding, it is desirable that the intersection of the outer surface with the *y*-*z* plane is a straight line. This can be thought of as taking the design of section 4.6.4 and displacing each transverse cross section by $y_o(z)$ so that they all lines up in the *y*-*z* plane. This can be achieved by replacing the centre of curvature given by equation (4.13) with a displaced centre, $\boldsymbol{C}'_o(z)$, at

$$\boldsymbol{C}'_o(z) = \boldsymbol{C}'_o(0, r_o(z), z) \tag{4.23}$$

and using all the other parameters as described in section 4.6.4.

A flat-to-round *Solidworks*® model on this basis is shown in Figure 4.16. This unit is designed to couple a 50 mm x 6 mm stack of three LSC sheets to a 20 mm diameter solid core optical fibre. Note that there is an unobstructed longitudinal extraction path for a tool forming the central cavity. The parting lines for this tool are the edges of the sidewall that are initially at the bottom corner of the entry surface and twist through 180° to form the top of the V. *Zemax*® ray tracing of this model gave losses of about 1%.

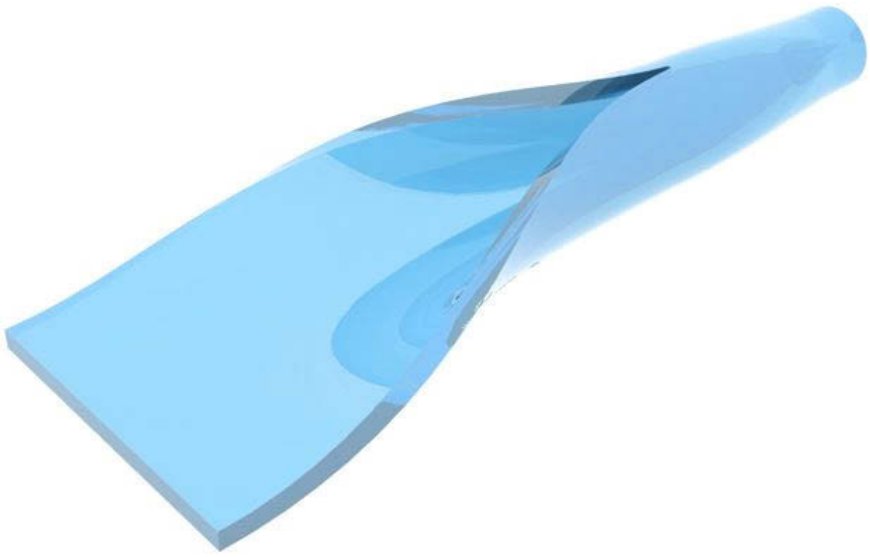

Figure 4.16 A *Solidworks*® model of a flat-to-round converter designed to couple a 50 mm x 6 mm stack of three LSC sheets to a 20 mm diameter solid core optical fibre.

Two rapid prototypes of this design were fabricated by *Arrk Rapid Prototyping*. Figure 4.17 shows one of these optical models glued to a green LSC sheet. The interior cavity at the exit end meant that it was necessary to fabricate each prototype in two pieces to provide access for a polishing tool. The glued joint between the upper and lower pieces is visible in the photo as a series of bright lines. The green triangular streak to the bottom left of the converter is a reflection of the sidewall by the smooth black sheet (*Plexiglas*®) supporting the converter. Geometric losses for this prototype were less than the measurement limit of about 1% i.e. all losses could be attributed to matrix attenuation, surface defects, scattering at the glue joints, etc.

QuickTime™ and a
decompressor
are needed to see this picture.

[Production Note: This figure is not included in this digital copy.
The print copy of the thesis is available for consultation at UTS Library.]

Figure 4.17 An *Arrk*® rapid prototype of the design shown in Figure 4.16 glued on the left to a green LSC. The glued joints between the upper and lower pieces of the optical model are visible as bright lines. The green triangular streak to the bottom left of the converter is a reflection of the sidewall by the smooth black sheet supporting the prototype.

The good optical performance of these prototypes led to a decision to undertake the considerable expense of making flat-to-round converters by injection moulding and *Accura Engineering Pty Ltd* was commissioned to make a suitable tool. One problem with mass-producing this component by injection moulding is the cycle time for the injection-moulding machine. The plastic at the round end has a thickness of 18 mm which caused the predicted cycle time to be very long (with a correspondingly very high unit cost). Accordingly, the design was modified by adding a 2 mm diameter axial hole at the round exit face. This reduced the maximum plastic thickness to only 8 mm and very greatly decreased both the cycle time and the cost. Ray tracing showed that adding the axial hole reduced the light output by < 0.3%. The reduction in cross sectional area is 1.2% which, from étendue arguments, would lead one to expect a loss of 1.0%. This apparent paradox is discussed below.

Two key issues in injection moulding a flat-to-round converter are the optical quality of plastic (which must be as homogeneous as possible) and the precision of the moulding, particularly the edges of the sidewalls. These requirements were achieved by using a side-gate to fill the two-part mould, and then ramming the filled mould with a hydraulic ram across the full face of the exit surface (the end surface of the ram included a 2 mm diameter pin that created the axial hole). The pressure was held at its initial value for about 30 seconds and then slowly decreased as the mould cooled. This procedure gave a very good optical finish over the whole moulding with high surface and edge precision.

Figure 4.18 shows an injection moulded flat-to-round coupler with a green LSC sheet glued to the entry unit and an 18 mm solid core optical fibre glued to the exit cylinder. Note that the entry unit includes a series of steps for an “offset T joint” coupling to a three sheet LSC stack as described section 3.3.2 and the (Franklin & Smith 2007) patent application. The

rectangular piece of plastic near the optical fibre is the injection-moulding gate that is normally removed before adding LSC sheets.

In section 3.1.7 it was shown that conservation of étendue means that it is not possible to "squeeze" light. This means that the cross sectional area of a light guide coupled to a LSC must not decrease along the optical path if losses are to be avoided. However, not all light is equally valuable. In particular, very high angle light is readily lost from optical fibres. Accordingly, the design of the flat-to-round converter was modified to maximize the amount of low angle light, accepting a trade-off of a slightly lower throughput of 96% rather than the better than 99% that can be achieved with a "non-squeezing" design. The resulting injection moulded curled-sheet flat-to-round converter is shown in Figure 4.18. It has a measured transfer efficiency of about 95% percent, which is in good agreement with the calculated value of 96% from ray tracing.

QuickTime™ and a
decompressor
are needed to see this picture.

[Production Note: This figure is not included in this digital copy.
The print copy of the thesis is available for consultation at UTS Library.]

Figure 4.18 An injection moulded flat-to-round coupler fed by a green LSC sheet. The rectangular piece of plastic near the optical fibre is the injection-moulding gate, which is normally removed. Also seen at the bottom left hand corner of the photo are the stepped surfaces used to make an "offset-T joint" from the LSC sheets to the coupler.

It was pointed out earlier that adding the 2.0 mm axis hole to the exit surface decreases the optical cross sectional area of the system by 1.2% but causes a light loss of less than 0.3%. At first glance this would seem to conflict with the conservation of étendue outlined in section 3.1.1. However, detailed ray tracing showed that the "squeezing" optimisation described above caused most of this light to be lost before it reached the axial hole. This is a good illustration of the important fact that the performance of an LSC system is indeed a *system* parameter and cannot be optimized by considering individual components in isolation.

5 TRIMM DOPED SHEETS AND LIGHT GUIDES

5.1 INTRODUCTION

Controlled diffusion of light is a key part of many modern lighting systems. It is a particular problem with the luminaires for the hybrid-LSC system described in section 3.3.4. These light extractors combine red and green light from LSC's with light from a blue LED to make a uniform white light. The problem is that the LED's are high intensity sources while the LSC's light is diffuse. Efficient mixing of light that has such very different distributions to create uniform white light with constant colour is difficult with traditional materials because high diffusion usually implies high backscatter, which causes unacceptable losses. This requires the use of new materials that combine good diffusion with a very high ratio of forward scatter to back scatter.

Forward scattering translucent polymer materials are increasingly used in many areas of light control including skylights, diffusers for luminaires, architectural panels, side-scattering optical fibres and light mixers. Traditional materials for these applications use inorganic additives and pigments such as $CaCO_3$, TiO_2 and $BaSO_4$. Traditional Mie scattering theory modified to include multiple scattering effects is able to semi-quantitatively describe their spectral transmittance and reflectance, and light spreading (Vargas 1999). The combined effects of the mismatch of these particles' refractive index relative to the polymer host and the concentration required to achieve a reasonable spread of transmitted light, intrinsically results in a significant degree of backscattering with consequent reduction of hemispherical transmittance. This is also why sheets doped with these materials look quite milky or creamy when viewed in reflectance. Additionally, sheets doped with micron-sized particles can have objectionable tints because of the strong variation of scattering intensity with wavelength.

For some applications dealing with high intensity sources, such as the sun or high power LED's, a key requirement is that the specular transmittance is very low to reduce unacceptable glare and to provide uniform illumination. Achieving this with traditional diffuser materials requires doping concentrations that give a high degree of backscatter. For instance, in the opal PMMA sheets as used for skylights and the pigmented polycarbonate widely used in roof glazing, it is common to find that at usual pigment levels needed for low specular transmittance (which is much preferred where clear skies dominate), total transmittance of visible light can be down to approximately 50% (Smith, Jonsson & Franklin 2003). This means that a low hemispherical transmittance will often require larger roof openings and hence higher solar gain for a given interior illumination level.

For light fittings, the result of high doping levels with traditional diffuser materials is low Light Output Ratios (LOR's) that then requires larger lamp powers to achieve design illuminance. This is a particular problem for luminaires using high intensity LED's where specular transmittance of 1% may cause intolerable glare and aesthetics may require specular transmittance of less than 0.1% to avoid unacceptable bright spots.

The high ratio of backscatter to forward scatter for polymers doped with traditional diffuser pigments causes unacceptable loss rates with distance traveled in side-scattering optical fibres and light mixer rods made with these materials. Additionally, mixer rods placed stringent demands on the constancy of scattering properties with wavelength that can be very hard to meet with traditional materials. Mixer rods also place very stringent requirements on specular transmittance since even specular transmission levels as low as 0.00002% may lead to a central bright spot on the projected image.

Clearly, there is a need for a doping material for polymer sheets, rods, and side-scattering light guides (which leak light over an extended distance), that have a very high ratio of forward scatter to backscatter, low absorbance, very low specular transmittance and scattering properties that are as nearly wavelength independent over the visible as possible. A material approaching these characteristics is now available. The additive is itself a clear polymer particle and it is embedded in a clear polymer.

This class of new materials has several applications for LSC systems including high efficiency light extractors (discussed in section 6.5), high performance luminaires, and side-scattering light guides coupled to luminaires (section 6.5.3). Additionally, the theory for TRIMM doped light guides turns out to helpful in understanding some types of scattering losses in LSC sheets, see section 8.2.1 and section A.1 of Appendix A.

This chapter will explore the specular and hemispherical optical properties of smooth surface PMMA sheets and rods for various geometries. Section 5.2 outlines the basic optical properties of TRIMM doped materials and explores how these properties can be calculated by ray tracing. Section 5.3 then examines the light diffusion pattern for multi-particle interactions. This leads to a formula for the required geometry and doping concentration to achieve specified levels of diffusion and specular transmittance. Section 5.3.1 explores the light field inside a heavily doped polymer and shows the need to introduce *side transmittance* as a component in addition to reflectance, transmittance and absorptance to completely define and understand the optical properties of these systems. It is shown that the presence of significant side transmittance causes the standard measurements of hemispherical spectral transmittance to significantly underestimate the transmittance of a uniformly illuminated sheet in a way that can lead to very large errors in calculated absorbance. Section 5.4.1 explores the light field inside

and outside light mixer rods and the requirements for achieving high performance light mixer systems. Finally, section 5.4.2 discusses use of these materials for side-scattering optical fibres.

5.2 Optical Properties of Transparent Microparticles in a Transparent Matrix

Low loss, with almost negligible backscattering, can be achieved using a new type of transmission diffusing element, for which we coined the acronym TRIMM (Transparent Refractive Index Matched Microparticle) (Deller et al. 2002). This acronym embodies the key physical features of the particle and matrix - namely (i) each additive particle is several microns in diameter (preferably over 6 μm and typically in the range of 10 μm to 50 μm), (ii) the particle does not absorb visible light and hence is visibly clear and transparent if smooth, and (iii) its refractive index is close to that of the host polymer. It is also of course desirable that the host polymer be highly transparent at visible wavelengths.

In this chapter, we will first analytically calculate in section 5.2.1 the optical properties of individual microparticles in a TRIMM doped matrix. We will then consider how to carry out ray tracing for TRIMM systems using programs such as *Mathematica*® (*Wolfram Research, Inc*) or the *Zemax*® (*Radiant Zemax, LLC*) and compares results from simulations with the relevant analytic expressions.

5.2.1 Single Particle Interactions in a TRIMM System

Van de Hulst devotes chapters 8 and 9 of his classic "*Light Scattering by Small Particles*" (van de Hulst 1981) to a detailed treatment of the large sphere (relative to wavelength) limit of Mie scattering. It is shown that in this limit one can either use ray optics or equivalently take the asymptotic limit of the Mie scattering equations. A basic parameter in these models is the refractive index ratio, m,

$$m = \frac{n_{particle}}{n_{host}} \tag{5.1}$$

For our purposes, it is more convenient to use the difference in the relative refractive index, μ,

$$\mu = \frac{n_{particle} - n_{host}}{n_{host}} = m - 1 \tag{5.2}$$

Note that in principle μ can be positive (when $n_{particle} > n_{host}$) or negative ($n_{particle} < n_{host}$). Currently available TRIMM systems use microparticles of cross-linked PMMA in a PMMA host. The act of cross-linking tends to increase the refractive index slightly, so in all these

systems μ is positive for the whole of the visible spectrum. However, the theory developed below is equally applicable for materials with negative μ provided that $|\mu| \ll 0.1$.

The optical properties of the TRIMM sheets used for this study were determined, by using an Abbe refractometer with TRIMM particles in refractive index matching liquid (Deller 2005, pp. 43-7; Deller, Smith & Franklin 2004a; Smith, Jonsson & Franklin 2003), using an ellipsometer to measure the local refractive index at the polished end of a PMMA rod doped with TRIMM (Deller 2005, pp. 47 - 9) and by fitting scattering data with models based on the theory discussed in this chapter (Deller 2005, pp. 49-51). At 589 nm all methods gave $\mu = 0.0114$. The mean particle diameter was 35 μm. Unless otherwise stated; all calculations below use these values.

The two key parameters for TRIMM systems are the mean deviation per particle interaction, $\bar{\delta}$, and the mean reflectance from the interaction with a single microsphere, $\bar{R}_1$. It is shown below that $\bar{\delta} \propto \mu$ while $\bar{R}_1 \propto \mu^2$. This means that for small enough μ, we can achieve good diffusion of the light with negligible backscattering.

In order to calculate the transmittance pattern, multiple ray tracing is used, with each ray encountering several spheres. The deviation of any ray at a sphere can be simulated from either a single ray analysis or from the Mie result. For the rest of this chapter, unless otherwise stated, we will assume that geometric optics can be used.

The deviation angle, δ, for light scattered by a single TRIMM sphere can be calculated from Figure 5.1 which shows a ray incident at angle θ_1 on a sphere of radius r, at point A, at distance H from the parallel ray that passes though the sphere's centre, C. It is convenient to do calculations in terms of the dimensionless impact ratio, $h = H/r$. Since μ (and hence $\bar{R}_1$) is so small, all rays that enter the sphere are assumed to exit the first time they strike the surface at B.

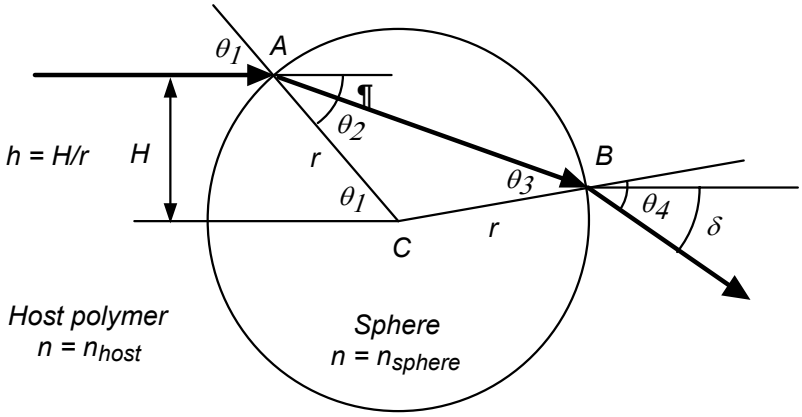

Figure 5.1 Definition of different parameters when a single ray enters a TRIMM sphere. The final deviation angle, δ, is greatly magnified compared to that in the materials discussed in this chapter.

Now triangle ABC is isosceles, so $\theta_2 = \theta_3$. Hence by Snell's Law,

$$n_{host} \sin\theta_1 = n_{particle} \sin\theta_2 = n_{particle} \sin\theta_3 = n_{host} \sin\theta_4 \tag{5.3}$$

so

$$\theta_1 = \theta_4 \tag{5.4}$$

and

$$\theta_2 = \theta_3 \ . \tag{5.5}$$

The deviation at A is $\partial = (\theta_1 - \theta_2)$, which is also the deviation at B. Thus the total deviation, δ, is

$$\delta = 2(\theta_1 - \theta_2) \tag{5.6}$$

Now it is clear from Figure 5.1 that

$$h = \sin\theta_1 \tag{5.7}$$

While from equations (5.2), (5.3) and (5.7) we see that

$$\sin\theta_2 = \frac{n_{host}}{n_{particle}} \sin\theta_1 = \frac{h}{1+\mu} \tag{5.8}$$

So combining equations (5.6), (5.7) and (5.8) gives the fundamental equation for TRIMM optical systems,

$$\delta = 2\left[\sin^{-1}(h) - \sin^{-1}\left(\frac{h}{1+\mu} \right) \right] \tag{5.9}$$

It is noteworthy that δ depends only on h and μ. This means that (in the geometric limit) the single-particle scattering pattern is completely independent of the particle size distribution – it depends only on μ. Accordingly, any variation in the scattering pattern that is wavelength dependent follows solely from changes in μ with respect to wavelength. Note that small changes in the absolute refractive index of either the particle or of the host can give rise to significant changes in μ, and hence in the particles' scattering properties. This means that in order to achieve weak dispersion in scattering properties for a TRIMM doped system, we require a close match in the host's and the particles' dispersive indices over the wavelength region of interest.

Currently available TRIMM systems use microparticles of cross-linked PMMA in a PMMA host. The refractive index of the TRIMM particles may be divided into two components: a dominant primary contribution from the PMMA chains and a small secondary positive component from the crosslinking. Now both the host and the microparticles contain similar PMMA chains so the primary components of the refractive index are the same at all

wavelengths. And the secondary component from the cross-linking is almost wavelength independent. Consequently, the *difference* in the refractive index between the particle and the host, and hence μ, varies much less with wavelength than does the refractive index (Deller 2005, pp. 47-52).

Strictly speaking, Mie theory should be used to calculate the deviation. However, geometric optics is a good approximation provided the ray is more than about a wavelength from the sphere's edge (van de Hulst 1981, p. 209). For a sphere of radius r and light of wavelength λ, the corresponding geometric limit, δ_{geom}, is

$$\delta_{geom} = \delta\left(1 - \lambda/r\right) = 2\left[\sin^{-1}\left(1 - \lambda/r\right) - \sin^{-1}\left(\frac{1 - \lambda/r}{1 + \mu}\right)\right] \tag{5.10}$$

and the fraction of rays that are within the geometric limit, f_{geom}, is

$$f_{geom} = (1 - \lambda/r)^2 \tag{5.11}$$

For a 35 μm diameter microsphere sphere with $\mu = 0.0114$, the geometric limit at 589 nm is $h_{geom} = 0.966$ which corresponds to and angle of incidence of 75°. Note that 93% of the incident rays have $h < 0.966$ and so are well approximated by equation (5.9).

Equation (5.9) may be simplified by taking a Taylor expansion in $(1 + \mu)$. Dropping higher order terms leads to the useful approximation for δ of

$$\delta \approx \frac{2\mu h}{\sqrt{1 - h^2}} \tag{5.12}$$

For $\mu = 0.0114$ the error in this approximation is less than 0.25% for h < 0.75, rising to 1.0% at the geometric limit.

We can use Figure 5.1 and equations (5.2) to (5.8) to calculate the TRIMM sphere's refection coefficient, R_1. The Fresnel Equations indicate that a plane wave incident on a non-magnetic dielectric surface with the transverse electric polarisation (i.e. the electric vector in the plane of the surface has a reflection coefficient, R_{TE}, of

$$R_{TE} = \left[\frac{\sin(\theta_i - \theta_t)}{\sin(\theta_i + \theta_t)}\right]^2 \tag{5.13}$$

where θ_i is the angle of incidence and θ_t is the angle of the transmitted refracted ray (Hecht 2002, p. 115). The reflectance coefficient for light with the transverse magnetic polarisation (i.e. the magnetic vector in the plane of the surface) has a reflection coefficient, R_{TM}, of

$$R_{TM} = \left[\frac{\tan(\theta_i - \theta_t)}{\tan(\theta_i + \theta_t)} \right]^2 \tag{5.14}$$

In Figure 5.1 the incidence plane at the entry point A is parallel to the incidence plane at the exit point B. Now μ is small so only a tiny fraction of the incident energy is reflected at A. Thus the reflectance coefficient is very nearly just the sum of the reflectance coefficients at A and B. Hence from equations (5.6), (5.13) and (5.14),

$$R_{1TE} = 2\left[\frac{\sin(\delta/2)}{\sin(2\theta_1 - \delta/2)} \right]^2 \tag{5.15}$$

$$R_{1TM} = 2\left[\frac{\tan(\delta/2)}{\tan(2\theta_1 - \delta/2)} \right]^2 \tag{5.16}$$

Whether a particular ray has TE or TM polarisation depends on the orientation of the surface with respect to the ray's electric vector. However, the orientation of the microsphere's surfaces is random so the polarisation is also random (a given ray may strike one sphere with TE polarisation and another with TM). So the single particle reflectance coefficient, R_1, is just the average of the coefficients for each polarisation and

$$R_1 = \left[\frac{\sin(\delta/2)}{\sin(2\theta_1 - \delta/2)} \right]^2 + \left[\frac{\tan(\delta/2)}{\tan(2\theta_1 - \delta/2)} \right]^2 \tag{5.17}$$

Note that some earlier work has effectively neglected to include the internal reflection at the particle/host surface and so underestimates the reflection coefficient by a factor of two (Deller 2005, p. 24; Deller & Franklin 2005; Smith, Jonsson & Franklin 2003). However, the very small value of the back reflection coefficient means that this is not an important error – twice an infinitesimal is still an infinitesimal.

Equation (5.17) gives the reflectance in terms of δ. The reflectance at a given impact ratio can be found by using equation (5.9) to first calculate $\delta(h)$ then substituting this into equation (5.17). The result is plotted in Figure 5.2 for $\mu = 0.0114$. We see that for $h < 0.5$ (angle of incidence < 30°) the reflectance is essentially constant at 0.065%. The maximum back reflectance of 0.126% occurs for h= 0.707 (angle of incidence = 45°). Reflectance increases for rapidly $h > 0.9$, but is still less than 1% at the geometric limit of h=0.966 for 35 μm diameter microspheres.

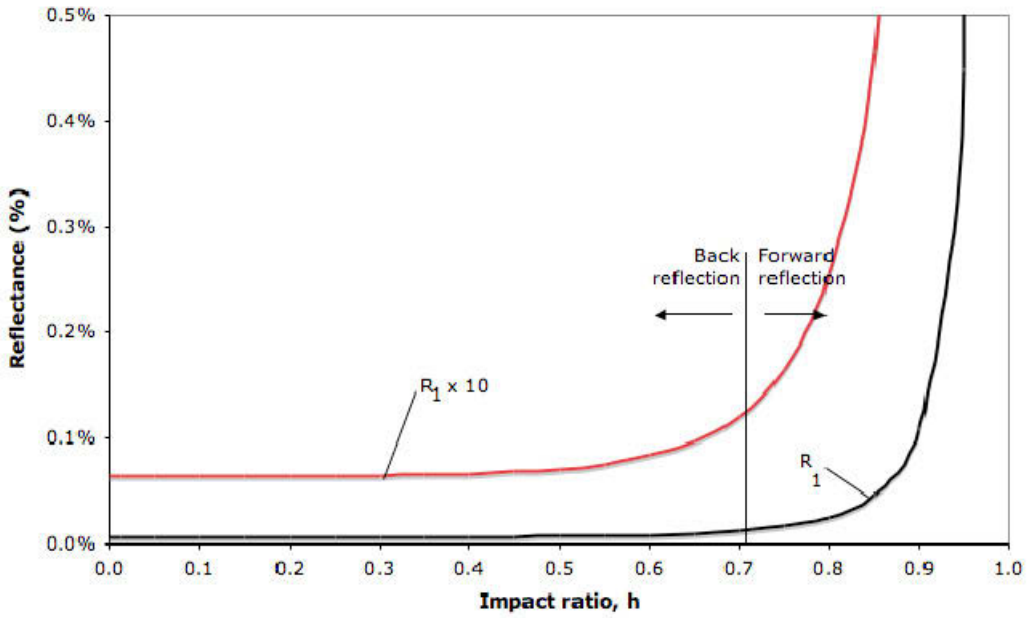

Figure 5.2 Reflectance from a TRIMM sphere for $\mu = 0.0114$ for various impact ratios. Rays with $h < 0.71$ are back reflected. The geometric limit for 35 μm particles is $h = 0.966$.

It is easy to show (Hecht 2002, p. 121) that at normal incidence equation (5.17) simplifies to

$$R_{1\ normal} = 2\left(\frac{n_{paticle} - n_{host}}{n_{paticle} + n_{host}}\right)^2 = 2\left(\frac{\mu}{2+\mu}\right)^2 \approx \frac{\mu^2}{2} \tag{5.18}$$

We see from Figure 5.2 that the back reflectance increases with impact parameter and reaches twice this value for the extreme back reflected rays.

For back reflection to occur the rays must strike the surface of the sphere at an angle of incidence smaller than 45° ($h = 1/\sqrt{2}$). We note from Figure 5.3(a) that the probability of an incident ray having a fractional radial contact value in the interval h to $h+dh$ is $2\pi h dh$. Thus the mean back reflectance of a ray striking a single sphere is

$$\overline{R}_1 = \frac{\int_0^{1/\sqrt{2}} 2\pi R_1(h) h\, dh}{\int_0^{1/\sqrt{2}} 2\pi h\, dh} = 4\int_0^{1/\sqrt{2}} R_1(h) h\, dh \tag{5.19}$$

This can be evaluated numerically by using equation (5.9) to give $\delta(h)$ in equation (5.17) and then numerically integrating (5.19). For $\mu = 0.0114$, $\overline{R_1} = 0.0087\%$. A good approximation for $0.007 < \mu < 0.020$ is

$$\overline{R_1} \approx 0.670\,\mu^2 \qquad (5.20)$$

which has a RMS error of 0.8% over this range.

If the TRIMM particle is in a sheet then only light reflected back at less than the critical angle will escape the sheet. For a ray normal to the sheet's surface this corresponds to an angle of incidence at the microsphere of half the critical angle or $h = 1/(2n)$. For PMMA this is $h = 0.34$. Inspection of Figure 5.2 shows that the reflectance is almost constant up to this value. So after correction for Fresnel reflection at the sheet air interface of approximately 9%, equation (5.18) is a good estimate of external reflection from a single microsphere.

The practical result of all of the above is that the reflectance from a TRIMM particle is so small that under most circumstances we can safely ignore it. For most practical purposes, TRIMM materials diffuse the rays with negligible back reflection.

We can now investigate the details of the deviation function for single particles. As outlined above, in the geometric optic limit equation (5.9) calculates the deviation δ of a ray striking a TRIMM sphere at fraction h of a radius. The corresponding probability density function, $f(\delta)$, is derived below and is graphed in Figure 5.3(b). Note the high degree of asymmetry and the pronounced tail.

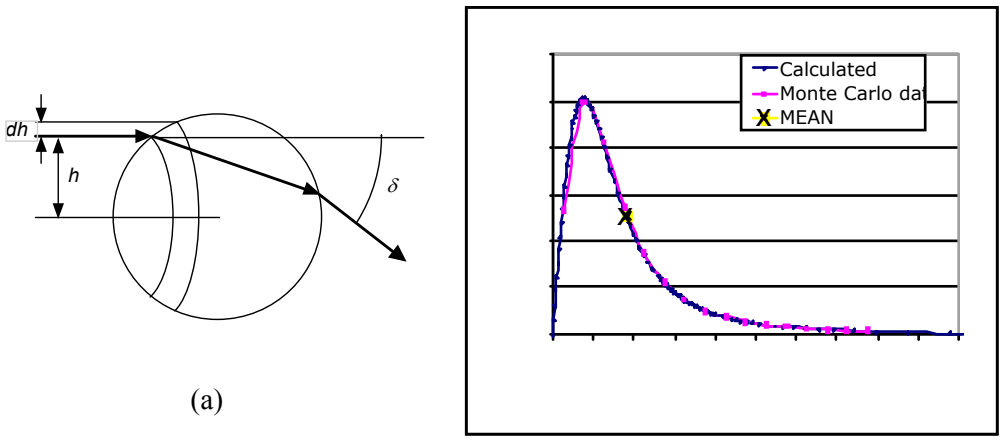

(a)

(b)

Figure 5.3 (a) Angular deviation of a single ray striking a TRIMM sphere of unit radius.
(b) The probability density distribution of the deviation, $f(\delta)$ for $\mu = 0.0114$.

In order to calculate the mean deviation, $\overline{\delta}$, we note from Figure 5.3(a) that the probability of an incident ray having a fractional radial contact value in the interval h to $h+dh$ is $2\pi h dh$. Thus the mean deviation of a ray striking a single sphere is

$$\bar{\delta} = \frac{\int_0^1 \delta(h) 2\pi h\, dh}{\int_0^1 2\pi h\, dh}$$
$$= 4\int_0^1 h\left[\sin^{-1}(h) - \sin^{-1}\left(\frac{h}{1+\mu}\right)\right] dh \qquad (5.21)$$
$$= \frac{\pi}{2} - \left[2 - (1+\mu)^2\right]\sin^{-1}\left(\frac{1}{1+\mu}\right) - \sqrt{2\mu+\mu^2}$$

where for the final step in (5.21) we have used the fact that for $a > 0$ (Dwight 1961, p. 122),

$$\int x \sin^{-1}\left(\frac{x}{a}\right) dx = \left(\frac{x^2}{2} - \frac{a^2}{4}\right)\sin^{-1}\left(\frac{x}{a}\right) + \frac{x}{4}\sqrt{a^2 - x^2} \qquad (5.22)$$

Equation (5.21) is rather cumbersome. However, by using equation (5.12) as an approximate expression for δ in the first line of equation (5.21), we see that

$$\bar{\delta} = \frac{\int_0^1 \delta(h) 2\pi h\, dh}{\int_0^1 2\pi h\, dh} \approx \frac{\int_0^1 \frac{4\pi\mu h^2}{\sqrt{1-h^2}}\, dh}{\pi} = \pi\mu \qquad (5.23)$$

Over the range of $0.010 < \mu < 0.020$ (the typical range for TRIMM doped PMMA sheets and mixer rods) the average error in $\bar{\delta}$ ranges from 13% to 19 % with an average error of 16%. For μ close to our standard value of 0.0114, a better estimate is

$$\bar{\delta} = 2.76\,\mu \qquad (5.24)$$

A typical TRIMM material is 35 μm diameter cross-linked PMMA spheres in a PMMA matrix, which has $\mu = 0.0114$ at $\lambda = 589$ nm (Deller et al. 2002). For this material, $\bar{\delta} = 1.80^o$ and $\delta_{geom} = 4.5^o$.

The probability density distribution, $f(\delta)$, can be calculated analytically. The cumulative probability density, $P(h)$, is

$$P(h) = \int_0^{\delta(h)} f(\delta)\, d\delta \qquad (5.25)$$

Now from Figure 5.3(a) it is clear that $P(h)$ is also the ratio of the projected area for rays with impact ratios less than h, compared to the projected area of the sphere's extremity. So

$$P(h) = \frac{\int_0^h 2\pi h\, dh}{\int_0^1 2\pi h\, dh} = h^2 \qquad (5.26)$$

Combining equations (5.25) and (5.26) with equation (5.9) leads to

$$f(\delta) = \frac{\partial P}{\partial \delta} = \frac{\partial P}{\partial h} \cdot \frac{\partial h}{\partial \delta} = \frac{h}{\frac{1}{\sqrt{1-h^2}} - \frac{1}{\sqrt{(1+\mu^2)-h^2}}} \tag{5.27}$$

Note that from equation (5.26), the median deviation ($P(h) = 0.5$) occurs for $h = 1/\sqrt{2}$. Therefore, from equation (5.9) the median deviation, δ_{median}, is

$$\delta_{median} = \frac{\pi}{2} - 2\sin^{-1}\left(\frac{1/\sqrt{2}}{1+\mu}\right) \approx 2\mu \tag{5.28}$$

where the approximation comes from applying equation (5.12). The error is approximately 0.16% for $\mu = 0.0114$.

Figure 5.3(b) shows $f(\delta)$ as calculated using equation (5.27), and $f(\delta)$ as derived using Monte Carlo simulations in *Mathematica*® for ~100,000 deviations (Deller & Franklin 2005). The Monte Carlo data is sorted into 0.5° bins, hence the slight inaccuracy of the fitted curve in the 0-1° range. There is excellent agreement between the analytic calculations and the simulations.

An alternative approach for a single sphere is to work with the scattered intensity distribution function, $I(\delta)$, in the limit of small μ and a large sphere radius (van de Hulst 1981, pp. 203-6). The results from this approach relate directly to measurements made with a photogoniometer of scattering in TRIMM doped systems.

Figure 5.4 illustrates the geometry for a sphere of radius r illuminated by collimated light beam of intensity I_{in}. The flux of energy, F_{in}, into the annulus of radius H and width dH, is

$$F_{in} = I_{in} 2\pi H dH \tag{5.29}$$

This light is refracted by the TRIMM sphere exits with deviation angles ranging from δ to $\delta+d\delta$. At large distance l from the sphere ($l >> r$) the flux of energy is spread over an annulus of width $ld\delta$ and radius $l\sin\delta$. So the intensity of the scattered light by a single sphere, $i(\delta,l)$ is

$$i(\delta,l) = \frac{F_{in}}{2\pi l^2 \sin\delta d\delta} = \frac{I_{in} H}{2\pi l^2 \sin\delta} \frac{dH}{d\delta} = \frac{I_{in} r^2 h}{2\pi l^2 \sin\delta} \frac{dh}{d\delta} = I_{in}\left(\frac{r^2}{2\pi l^2}\right) D \tag{5.30}$$

where

$$D(\delta) = \frac{h}{\sin\delta} \frac{dh}{d\delta} \tag{5.31}$$

is called the particle's divergence.

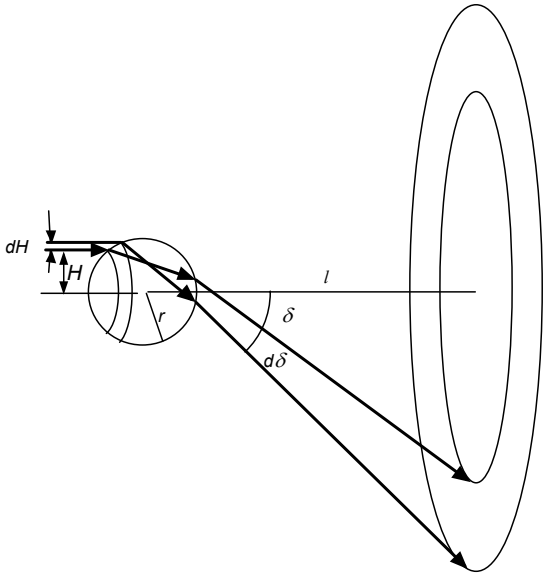

Figure 5.4 Geometry for a sphere of radius r illuminated by collimated light.

Note that the final expression in equation (5.30) is the product of the intensity of the illuminating beam, fixed geometric factors (grouped in the round brackets) and the divergence. So the divergence completely describes the distribution function of the scattered light. Now h is dimensionless and it was shown by equation (5.9) that δ is purely a function of h and μ. Hence equation (5.31) implies that D does not depend on the particle's radius: in the geometric limit all TRIMM particles of the same μ have exactly the same scattering pattern. Thus the intensity of the light scattered by an optically thin array of TRIMM particles, $I(\delta)$, is

$$I(\delta) = I_0 D(\delta) \tag{5.32}$$

where I_0 is the intensity of the scattered light in the direction of the illuminating beam. Note that $I(\delta)$ is the intensity of the light inside the host material. If the scattering pattern of thin sheet of TRIMM doped material is measured in air, say with a photogoniometer, it is of course necessary to use Snell's Law to calculate the effect of refraction at the exit surface on the deviation angle and the measured external intensity. It is also important to note that I_0 refers to the intensity of the *scattered* light, which is completely different to the intensity of the *specular* light (i.e. light not deviated by the TRIMM particles), even though both beams are in the same direction. The specular beam is the subject of section 5.3.2.

Figure 5.5 shows the intensity distribution for single particle TRIMM scattering calculated from equations (5.32), (5.31) and (5.9) for $\mu = 0.0114$. The figure also shows the best-fit Gaussian distribution with a standard deviation of 0.760^o. To aid comparison at larger deviation angles, the scattering is also plotted using the right hand scale that has a displaced origin and 10 times the sensitivity of the left hand scale. The TRIMM distribution has considerably more light at large angles than the Gaussian distribution, increasing from 10x at

2.5° to more than 400x at 3.5°. As we will see in section 5.3.3, this large angle scattering has important implications for light diffusion in TRIMM doped systems.

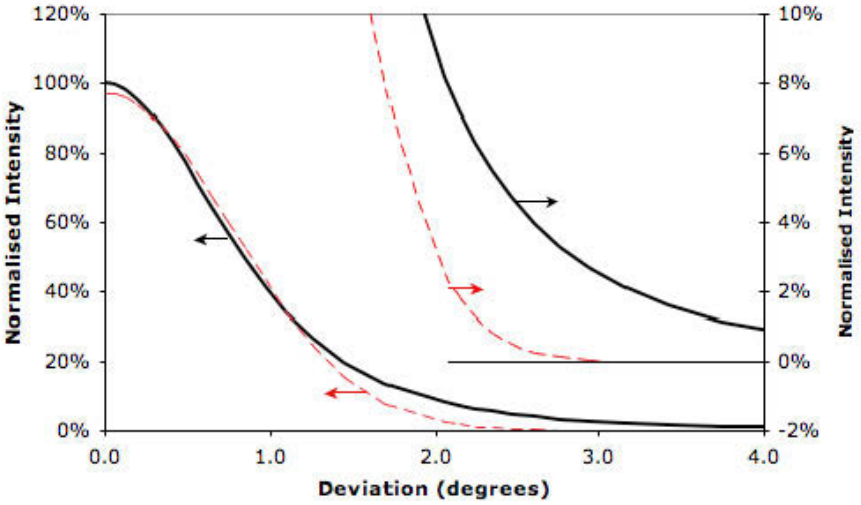

Figure 5.5 Normalised intensity distribution of light scattered by a TRIMM microsphere with $\mu = 0.0114$ (solid black line) and a best fit Gaussian distribution with a standard deviation of 0.760° (dashed red line). The large angle scattering is also plotted on the right hand scale at 10x sensitivity.

It is clear by inspection of Figure 5.5 that the light scattered by a TRIMM microsphere is not well described by a single Gaussian distribution. However, as Figure 5.6 shows, a good fit to this distribution can found for the sum of two Gaussians that have central heights of 0.690 and 0.305 and standard deviations 0.587° and 1.294° respectively. The difference is not visible on the standard scale. There is no obvious physical significance to the second Gaussian.

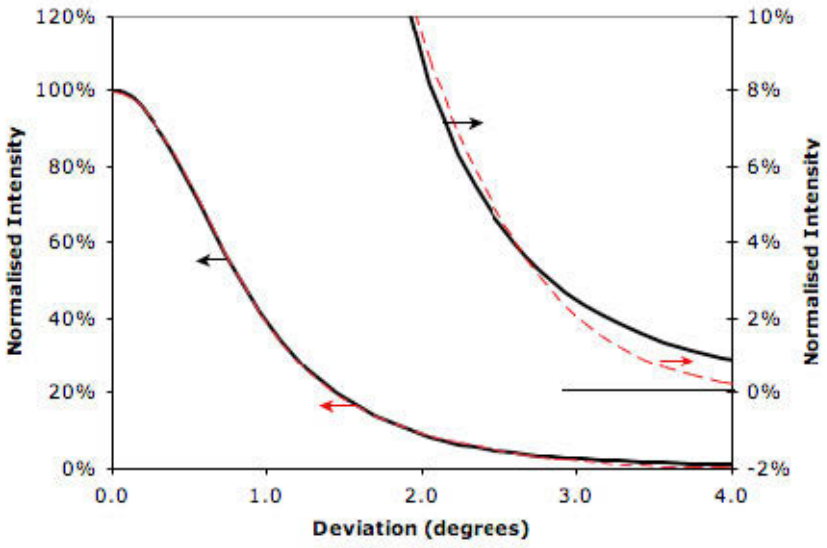

Figure 5.6 Normalised intensity distribution of light scattered by a TRIMM microsphere with $\mu = 0.0114$ (solid black line). Also plotted is a best-fit sum of two Gaussian distributions (dashed red line) that have central heights of 0.690 and 0.305 and standard deviations 0.587° and 1.294° respectively.

5.3 MULTI-PARTICLE INTERACTIONS IN A TRIMM SYSTEM

Consider a block of polymer doped with TRIMM at a linear particle density of α particles per metre such as Figure 5.7. We initially assume that the block is wide enough so that there is negligible interaction with the sidewalls.

The light undergoes a number of processes. At the air-polymer interface there is Fresnel reflection as described by equations (5.13) and (5.14). For an unpolarised incident beam, the specular reflection coefficient is an almost constant 4% for angles of incidence up to 60^{o}. Most of the light is refracted into the polymer where it undergoes multiple scattering from microparticles and emerges as diffusely transmitted light. However, a small fraction of the rays miss all the microparticles and are transmitted without deviation. This specular transmission is so important that it will be discussed at length in section 5.3.2. On the other hand, some of the light interacts with so many microparticles that when it reaches the polymer-air interface it has an angle of incidence greater than the critical angle and so it is trapped inside the polymer by total internal reflection. These rays form the subject of the next section.

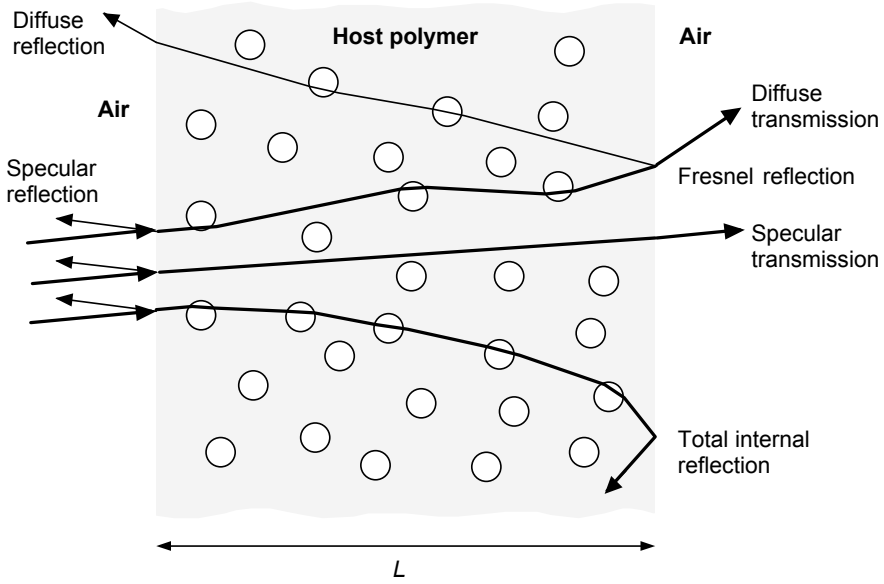

Figure 5.7 Schematic of rays traversing a block of clear polymer of thickness L doped with clear spheres. A ray is shown that is totally internally reflected.

5.3.1 Side-Loss in TRIMM Systems

For most optical systems the absorbance, A, is calculated by measuring the transmission, T, the reflectance, R, and assuming that

$$A = 1 - T - R \tag{5.33}$$

The measurements of transmission and reflectance are simple for non-diffusing samples. For diffusing materials it is necessary to use integrating spheres to capture the diffusely reflected and transmitted light. However, intrinsic limitations of conventional equipment mean that a simple application of equation (5.33) to measurements of TRIMM doped materials can give profoundly inaccurate results.

Figure 5.8(a) is a photograph of a TRIMM doped sheet obliquely illuminated with a narrow HeNe laser beam. Total internal refection at the exit face traps a substantial fraction of the light. Part of this light is further scattered so that, as shown in Figure 5.8(b), it can escape though the entry face and contribute to enhanced reflection. Another part of the light is trapped by TIR at both surfaces and so it is transported laterally for a significant distance before it escapes. If the lateral transport distance exceeds the entry aperture to the detector, then as shown in Figure 5.8(b), this *side-loss* light will not be detected by the detector. Conventional analysis using equation (5.33) will incorrectly ascribe all this side-loss light to absorption. Instead one should calculate absorbance as

$$A = 1 - T - R - S_T \tag{5.34}$$

where S_T is the fraction of the incident light that undergoes side-loss.

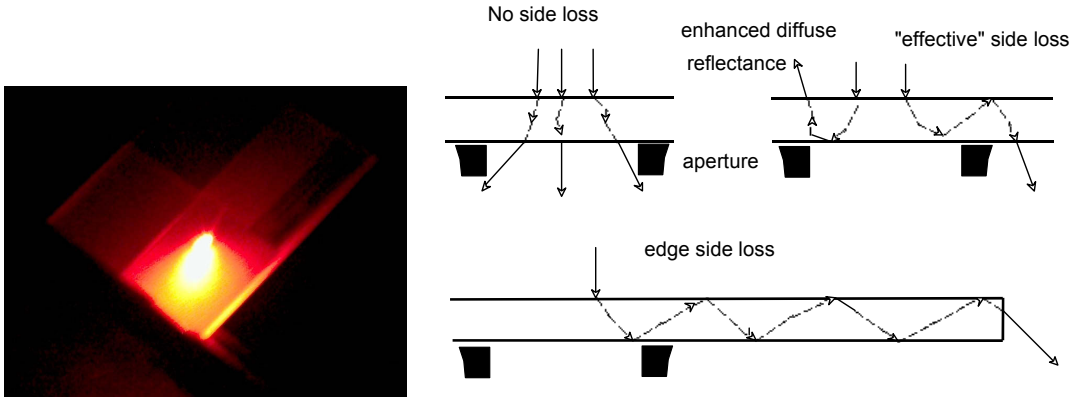

(a) (b)

Figure 5.8 (a) Photograph of a TRIMM doped sheet obliquely illuminated with a narrow HeNe laser beam. Both rays that transmit and exit after a single pass and those that make up the side-loss component can be seen. (b) Schematic of some different categories of ray paths in TRIMM dope systems according to their contribution to measured components. The black rectangles under the sheet represent the cross section of the spectrometer's entrance aperture.

It should be noted that S_T depends in a complex non-linear way on a large number of factors including: (i) the diameter of the entry beam, (ii) the angle of incidence, (iii) the sheet thickness, (iv) the refractive index of the PMMA matrix, (v) the relative refractive index of the microparticles, (vi) the size of the entry aperture to the spectrometer's integrating sphere, and (vii) the distance between the sheet's exit surface and the spectrometer's entry aperture.

An illustration of how important side-loss can be in measuring absorbance is the measurements shown in Figure 5.9 from (Smith, Jonsson & Franklin 2003). This diagram shows the measured side-loss of four samples of thickness 1.00, 2.00, 3.00, and 4.00 mm that were prepared by *Röhm Degussa GmbH* in Darmstadt, Germany. The matrix was optical-grade clear type 7N PMMA molding beads mixed with 7% by weight 1011F *Plexiglas*® molding beads that are doped with clear transparent crosslinked PMMA spheres with an average diameter of 15 μm. The absorbance of this system, designated N77, is known in the visible to be <<1% for a 4 mm path length. (We have not been able to measure the true absorbance, but on theoretical grounds it is probably less than 0.1% for a path length of 4 mm.)

The diffuse reflectance and transmission were measured with *a Perkin-Elmer Lambda 900*® spectrophotometer at visible and NIR wavelengths. The spectrophotometer was equipped with a *Labsphere*® 150-mm-radius *Spectralon*® integrating sphere *PELA-1000*®. The angle of incidence was 8° in the reflectance mode and normal in the transmittance mode. The sphere entrance ports are circular with a diameter of 20 and 25 mm for transmittance and reflectance, respectively. The incident beam was smaller than the exit sphere's entrance port.

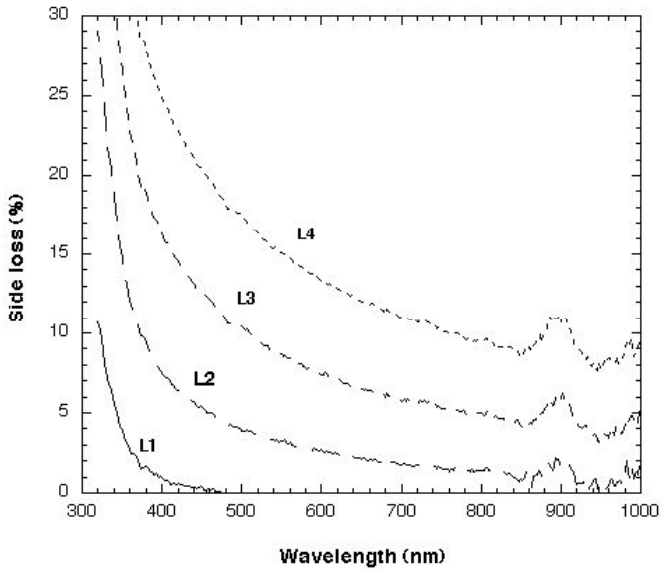

Figure 5.9 Side-loss S_T spectra from 300 to 1000 nm at 1, 2, 3, and 4-mm thickness of N77 TRIMM doped PMMA plotted in curves L1 – L4 respectively.

The side-loss was computed using equation (5.34). If the side-loss had been ignored and a conventional analysis had been applied using equation (5.33), all of the side-loss would have been attributed to absorbance and the vertical scale in Figure 5.9 would be absorbance. This would give an absorbance at 450 nm for the 4 mm thick L4 sample of 20%, which is an

overestimate by a factor of at least 20, and probably by a factor of at least 200. Clearly, side-loss cannot be neglected when measuring TRIMM doped systems.

Jonsson et al have added sideloss to the standard corrections used for measuring reflectance and transmittance with single integrating spheres (Jonsson et al. 2005). The revised theory has excellent agreement with observations of TRIMM for: scattering functions, hemispheric transmittance and reflectance at multiple wavelengths, and hemispheric transmittance and reflectance at multiple angles of incidence.

5.3.2 Specular Transmittance of TRIMM Doped Systems

For some applications dealing with high intensity sources such as the sun or LED's, reducing glare from specular transmission is a key requirement. For example, Figure 5.10 shows the typical radiance from a conventional skylight under solar illumination. Specular solar radiation has an average half-width θ_{sun} of 0.26^{o} (Woan 2000, p. 176), so any specular transmission leads to a spike in the radiance. Similar radiance curves can occur for the luminaires in the hybrid LSC-LED system described in section 3.3.4 where specular transmission of the intense light from the LED's causes the spike. Analogous curves can also occur in LED projector systems that mix red, green and blue LED's to form a white light source that is projected onto a screen. If the light mixer has a significant specular component then the specular beam will be projected as a bright dot on the screen. For an LED projector the horizontal axis in Figure 5.10 would be labeled pixel number, the vertical axis "luminance per pixel" and the "diffuse component" would be the ordinary output that forms the image on the screen.

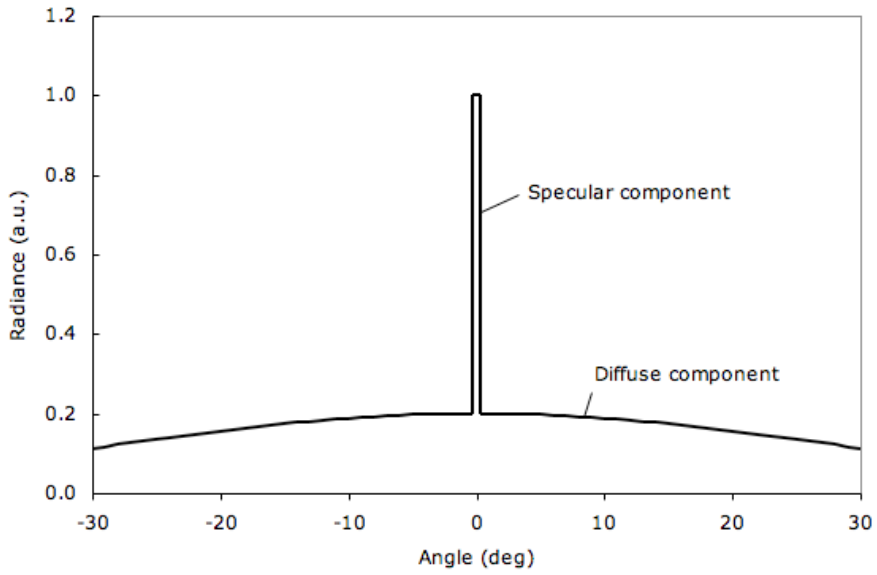

Figure 5.10 Radiance of a conventional diffuser illuminated with an intense light source. Examples include: a skylight illuminated by the sun, a luminaire in a hybrid LSC-LED system, and a LED projector.

A useful parameter for characterizing all of these systems is the specular contrast ratio, C, defined as the ratio of the maximum radiance with the specular component, L_{max} to the radiance of the surrounding area, L_{local}

$$C = \frac{L_{max} - L_{local}}{L_{local}} \tag{5.35}$$

For a skylight or a luminaire in the hybrid LSC-LED system, we can rewrite this as

$$C = \frac{L_{specular}}{L_{diffuse}} \tag{5.36}$$

where the peak total radiance is split in to the maximum specular radiance, $L_{specular}$, and the diffuse radiance, $L_{diffuse}$, with the latter being interpolated to the angle of maximum radiance.

For a LED projector, strictly speaking we need to work in terms of the luminance per pixel on the screen, L_v, and so

$$C_{projector} = \frac{L_{v\ specular}}{L_{v\ image}} \tag{5.37}$$

where the $L_{v\ image}$ is the luminance of the image near the specular spot and $L_{v\ specular}$ is the additional luminance contributed by the specular beam. However, the efficiency of the projection optics is essentially constant over the small angular region of interest so we may write

$$C_{projector} \approx \frac{L_{proj\ specular}}{L_{proj\ image}} \tag{5.38}$$

where the $L_{proj\ image}$ is the radiance of the mixer at angles close to the specular beam and $L_{proj\ specular}$ is the radiance of the specular beam.

The acceptable value of the specular contrast ratio is very much a function of the particularities of the application. If a skylight has $C = 1.0$ then someone looking at the diffuser will see the disk of the sun as twice as bright as the surrounding area. In order to hide the sun (so that the diffuser appears to have a uniform radiance) we need $C < 10\%$. A projector system has a more stringent requirement because a fixed spot in an image can be very objectionable. So a reasonable requirement is $C_{projector} < 2\%$. We will see that even this stringent requirement can readily be achieved by using TRIMM doped materials.

If we neglect inclination effects, the radiance, L, of a source of area, A, emitting a radiant flux, Φ, uniformly into a solid angle Ω is (Klein 1970, p. 123)

$$L = \frac{\Phi}{A\Omega} \tag{5.39}$$

A source with a half width of θ subtends a solid angle, Ω, of

$$\Omega = 2\pi(1-\cos\theta) \tag{5.40}$$

Solar radiation has an average half-width θ_{sun} of 0.26° (Woan 2000, p. 176). Opal PMMA and pigmented polycarbonate sheets used for skylights employing conventional pigments typically have a total transmittance of visible light of approximately 50% (Smith, Jonsson & Franklin 2003). The diffused light from these sheets is nearly Lambertian with $\theta_{diffuse}$ approximately 45°.

Consider a skylight of area, A, that has a diffuse transmittance, $T_{diffuse}$, and a specular transmittance, $T_{specular}$. Now from equations (5.36) and (5.39), if the incident luminous flux is Φ, then

$$L_{specular} = CL_{diffuse}$$

$$\frac{T_{specular}\Phi}{A\Omega_{specular}} = \frac{CT_{diffuse}\Phi}{A\Omega_{diffuse}}$$

and so

$$T_{specular} = \frac{CT_{diffuse}\Omega_{specular}}{\Omega_{diffuse}} \tag{5.41}$$

Thus from equations (5.40) and (5.41)

$$T_{specular} = \frac{CT_{diffuse}(1-\cos\theta_{sun})}{(1-\cos\theta_{diffuse})} \tag{5.42}$$

Thus achieving C = 10% for a skylight requires $T_{specular}$ = 0.000 18%. Achieving this with traditional diffuser materials requires doping concentrations that give a high degree of backscatter and typically reduces hemispherical transmittance to just 50% (Smith, Jonsson & Franklin 2003). For skylights, a reduction in hemispherical transmittance requires larger roof openings for a given interior illumination level which in turn cause problems with heat gain in summer and heat loss in winter (Smith et al. 2001; Smith et al. 2000; Smith, Jonsson & Franklin 2003).

One of the LSC designs explored for this project is the hybrid LSC-LED system described in section 3.3.4. In order to reduce light guide costs, this system has only a green and a red LSC sheet with a set of solar powered blue LED's providing the small amount of blue light required for colour balance. The light from the LSC and the LED's is combined and mixed in the light extractor illustrated in Figure 3.23 and reproduced here as Figure 5.11 for the sake of convenience. One problem with the hybrid luminaire is that the LED's are a very intense light source and hence could cause unacceptable glare. To solve this problem, a sheet of TRIMM diffuser is optically bonded to the front of the extractor. As can be seen in Figure 5.11(b), this successfully eliminates the otherwise intense glare from the LED chips. The design shown in Figure 5.11 uses 8 LED's on each side of the planar light guides to distribute the blue LED light as evenly as possible.

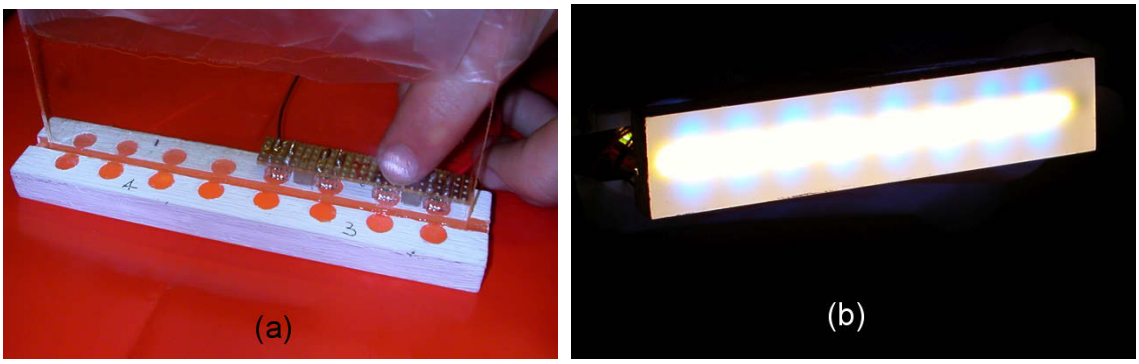

Figure 5.11 (a) Assembly of a hybrid light extractor showing the LED's at the back of the extractor. There is a TRIMM diffuser sheet optically bonded to the front surface to reduce the glare from the LED's. (b) The hybrid light extractor in operation with the LED's viewed through the front TRIMM diffuser. Note the absence of glare from the high intensity LED chips.

We wish to choose a TRIMM diffuser for the front of the extractor so that specular radiance of each LED chip, L_{LED}, has a specified specular contrast factor compared to the diffuse light from the extractor. The exit face of the light extractor has an area of $A_{extractor}$. The N_{LED} LED chips each has an area of A_{LED} and their combined output provides a small fraction, B, of the total lumens (typically $B \approx 5\%$ (Earp et al. 2004b; Smith & Franklin 2004)). It can be seen from Figure 5.11(b) that the radiance of the LSC derived light is not uniform across the face of the extractor. The detailed operation of the extractor is discussed in section 6.5.3. Here we simply note that the LSC light can be thought of as combination of "end-light" that forms the bright central stripe and uniformly distributed "trapped light". The net result is that the radiance from the LSC light in the vicinity of the LED's is some fraction $f_{diffuse}$ of the mean radiance, $\overline{L}_{extractor}$. For the design illustrated, $f_{diffuse} \approx 0.38$.

Now from equations (5.36) and (5.39), for an extractor emitting a luminous flux, Φ,

$$L_{LED} = Cf_{diffuse}\overline{L}_{extractor}$$

so

$$\frac{T_{specular}B\Phi}{N_{LED}A_{LED}\Omega_{LED}} = \frac{Cf_{diffuse}\Phi}{A_{extractor}\Omega_{extractor}} \qquad (5.43)$$

Good colour rendering requires that the ratio of blue LED light to red and green light from the LSC is the same at all angles. To achieve this, the emission pattern of the light extractor for LSC light was measured with a photogoniometer. The photogoniometer was then used to record the emission pattern of different types of LED's. LED's were then selected that matched the extractor's emission pattern of the LSC light within $\approx 2^o$ so that $\Omega_{LED} \approx \Omega_{extractor}$. (Note that known large differences between LED manufacturers' specifications for emission patterns and the measured patterns (Deller, Franklin & Smith 2006b) made it essential to measure each type of LED.)

Thus from equation (5.43),

$$T_{specular} = \frac{Cf_{diffuse} N_{LED} A_{LED}}{BA_{extractor}} \tag{5.44}$$

For the hybrid light extractor illustrated in Figure 5.11, $f_{diffuse} \approx 0.38$, N_{LED} = 16, the chips are 0.5 mm x 0.5 mm, B = 0.050 and the front face of the extractor is 25 mm x 130 mm. So to achieve a specular contrast factor of 1.1 we need $T_{specular}$ = 0.10%.

For LED mixer systems the requirements are much more stringent. With some designs the optics focus the specular transmission onto a very small number of pixels, n_{pix}. If the display has N_{pix} pixels then we require that

$$T_{specular} = \frac{C_{projector} n_{pix}}{N_{pix}} \tag{5.45}$$

For example, for a display with 10^6 pixels where the specular light is focused (as a worst case) onto one pixel, in order to achieve a specular contrast ratio of 2% requires $T_{specular} = 2.0 \times 10^{-8}$. Conventional diffuser materials with such a low a specular transmission also have intrinsically low diffuse transmittance and hence greatly degrade system performance. It is a unique feature of TRIMM doped materials that they can give exceedingly low specular transmittance while still having a diffuse transmittance that is close to 100%.

A ray's path through a TRIMM doped material, as it deviates with every sphere interaction, can be described as a random walk. Multiple interactions will tend to randomly deviate the ray. If, x, is the number of interactions in a path of length, l, a light ray will on average encounter $\bar{x} = \alpha l$ particles with a mean deviation of $\bar{\delta}$. Now $\bar{\delta}$ is small so the path length of rays traversing the bock, l, is very close to the block's thickness, L. We call

$$a = \alpha L \tag{5.46}$$

the axial particle number of the TRIMM doped volume. Note that since $l \approx L$, $a \approx \bar{x}$.

To a good approximation, the particles are randomly distributed throughout the sheet (this approximation is not quite true near the sheet's surfaces). So the actual number of particles encountered will have a Poisson distribution with a mean of a. The probability of a ray striking exactly x particles, $P_a(x)$, is

$$P_a(x) = \frac{a^x e^{-a}}{x!} \qquad x = 0, 1, 2, \ldots \tag{5.47}$$

A specular ray is, by definition, one that encounters precisely zero particles. The probability of this happening, which is the same as the specular transmission coefficient, $T_{specular}$, is

$$T_{specular} = P_a(0) = e^{-a} = e^{-\alpha L} \tag{5.48}$$

and so the required axial particle number, a, is

$$a = -\ln(T_{specular}) \tag{5.49}$$

The calculated axial particle numbers for a skylight, hybrid LSC-LED light extractor and a LED projector system are shown in **Table 5-1**.

The next section discusses how to calculate the mean deviation angle. Applying equation (5.58) from that section with $\mu = 0.0114$ gives the mean deviation angles shown in **Table 5-1**.

The mean reflectance per particle as given by equation (5.18) is small enough so that back reflection has only a negligible effect on forward energy transfer. Thus the mean total back reflectance from the a microparticles, $R_{particles}$, is

$$R_{particles} = a\bar{R}_1 \approx \frac{a\mu^2}{2} \tag{5.50}$$

The calculated back reflectances are given in **Table 5-1**. All are negligible compared to the Fresnel reflection of 3.9% at both the front and back surfaces.

Table 5-1 Optical properties of various TRIMM based diffuser systems with specified specular contrast ratios.

System	Skylight	Hybrid LSC-LED	LED Projector
Required contrast ratio, C	10%	10%	2%
Specular transmission limit	0.000 020%	0.104%	2.0×10^{-8}
Axial particle number, a	13.1	6.9	17.7
Mean diffusion angle	8.3^o	6.0^o	9.7^o
Back reflectance	0.085%	0.045%	0.12%

It is interesting to contrast the linear dependence of the back reflectance upon axial particle number (equation (5.50)) with relationship for the contrast ratio. If we substitute the expression for $T_{specular}$ into equations (5.42), (5.44) or (5.45) we see that for all these systems

$$a \approx -\ln(C) + K \tag{5.51}$$

where K is a constant that depends only on the physical parameters of the particular system. Thus,

$$C \sim e^{-a} \tag{5.52}$$

This relationship is in fact quite general because if $C << 1$ then $T_{specular} \sim C$ and so from equation (5.48),

$$C \sim T_{specular} \sim e^{-a} \tag{5.53}$$

This exponential dependence of contrast ratio means that we can achieve almost any required contrast ratio without significant back reflectance. **Table 5-1** shows the parameters for systems with contrast ratios of 0.1% - a level that would be hard to detect with even high quality instruments.

Table 5-2 Optical properties of various TRIMM based diffuser systems that have specular contrast ratios of 0.10%.

System	Skylight	Hybrid LSC-LED	LED Projector
Required contrast ratio, C	0.10%	0.10%	0.10%
Specular transmission limit	1.8×10^{-8}	9.4×10^{-6}	1.0×10^{-9}
Axial particle number, a	17.9	11.6	20.7
Mean diffusion angle	9.7^{o}	7.8^{o}	10.5^{o}
Back reflectance	0.12%	0.075%	0.13%

5.3.3 Light Diffusion Inside TRIMM Doped Systems

The distribution of light inside the block shown in Figure 5.7 will be the convolution of the source emission function with the point-spread function of the propagating light. As a preliminary estimate of the total angular spread of rays reaching the end of a TRIMM system, one may consider the propagation of rays entering the sheet at normal incidence.

To optimize design parameters to obtain uniform light output, we wish to determine the angular distribution of light at a certain propagation distance along the optic axis. A ray's path through a TRIMM doped material, as it deviates with every sphere interaction, can be described as a random walk. Multiple interactions will tend to randomly deviate the ray. In a path of length l a light ray will on average encounter $\bar{x} = \alpha l$ particles. The Central Limit Theorem suggests that the mean half-cone angular spread, $\bar{\Sigma}$, of light in the cross-sectional plane when it reaches the end of a TRIMM doped block can be approximated by

$$\bar{\Sigma} \approx \bar{\delta}\sqrt{\bar{x}} \tag{5.54}$$

Now $\bar{\delta}$ is small so the path length of rays traversing the bock, *l,* is very close to the block's thickness, *L*. Thus, from (5.46),

$$a = \alpha L \approx \alpha l = \bar{x} \tag{5.55}$$

So by using equation (5.23) as an approximation for $\bar{\delta}$ and equation (5.55) as an approximation for $\bar{x}$, we see from equation (5.54) that

$$\bar{\Sigma} \approx \pi \mu \sqrt{a} = \pi \mu \sqrt{\alpha L} \tag{5.56}$$

There are several approximations in the derivation of equation (5.56), so it is interesting to model a best fit for *a* independent additions of deviations given by equation (5.9) with

$$\bar{\Sigma} = k \mu a^{p} \tag{5.57}$$

There are a number of reasons for expecting that the constant *k* will be a significantly larger than π, the estimate in equation (5.56), and that the power *p* will be slightly larger than equation (5.56)'s prediction of 0.5. Firstly, the random walk of the rays' paths means that the actual number of particles encountered will on average be slightly larger than the axial particle number, *a*. This error will grow with increasing axial particle number which will tend to slightly increase *p*. Secondly, it can be seen from Figure 5.5 that the scattering from TRIMM particles has significantly more light at large scattering angles than an equivalent Gaussian distribution. Consequently, equation (5.56) will tend to somewhat underestimate the mean angular spread. This effect increases *k* but does not greatly impact on *p.* Finally, and more fundamentally, the Central Limit Theorem implicitly assumes a plane in a Cartesian coordinate system. However, δ is measured in spherical coordinates. The difference does not matter for small $\bar{\Sigma}$. However, for large spread angles, the curvature of the coordinate surface becomes important. This means that in angle space, points with equal Σ are significantly closer together (and hence more probable) than is predicted by the Central Limit Theorem. This effect tends to increase both *k* and *p* above the values predicted by equation (5.56).

The optimized fit of equation (5.57) to Monte Carlo simulations of TRIMM doped systems in *Mathematica*® was calculated (Deller & Franklin 2005) for $0.01 < \mu < 0.02$, and $50 < a < 130$, the typical experimental range of these parameters for light mixer rods. A good fit is

$$\bar{\Sigma} \approx 3.39 \mu a^{0.514} \tag{5.58}$$

where the error in the sum of the squares of the residuals varies from 1.1% to 6.2% over the optimized range of μ and *a*. We note that the difference in the values of *k* and *p* in equation (5.58) from the estimates in equation (5.56) are both of the predicted sign and are 7.3% and 2.7% respectively, with the difference in *p* being comparable to the fitting error. Examination of

the ray paths in the previously described simulations and detailed simulations carried out with Alan Earp at my direction (Earp 2001) strongly suggest that the primary source of error is the curvature of the coordinate surface at large spread angles.

5.4 Applications of TRIMM Doped Systems

5.4.1 Mixing in TRIMM Doped Light Guides

For a high performance LSC system it is not enough to just supply adequate lumens – the red, green and blue light from the collector sheets must also be combined and mixed to give white light that has a high colour rendering index. For aesthetic reasons, it is important that there is no perceptible colour shift across the illuminated region. One way of achieving this is to use the TRIMM doped light mixers described below.

A similar mixing problem occurs when using red, green and blue LED's for illumination. Light sources using fully mixed red, green and blue LED's have been judged superior to halogen, incandescent and phosphor white LED sources as reading and task lights (Narendran & Deng 2002). The problem is to come up with a compact design that can completely mix the light without causing excessive losses. Attempts to use TIR inside clear acrylic rods gave no significant improvement in illuminance, color, or beam uniformity compared to a bare LED array (Zhao, Narendran & Van Derlofske 2002) while, as discussed in the preceding section, conventional diffusers have very high losses. It will be shown below that TRIMM doped rods can provide very good colour mixing in a short rod with very low losses. A patent has been granted for this design (Franklin, Smith & Joseph 2007).

As part of another project, we arranged for the manufacture by a commercial extruder of 12.7 mm diameter PMMA rods doped with the TRIMM particles described section 5.2.1. The average diameter of the particles was 35 μm with a relative refractive index at 589 nm of $\mu = 1.0114$. Rods were prepared with a linear particle density of 0.25 ± 0.03 mm^{-1} and 1.33 ± 0.08 mm^{-1}. A clear PMMA rod from the same extruder was used as a control. Rods were cut to a length of 100 mm and the ends were optically polished.

The experimental set up shown in Figure 5.12 was jointly designed with Chris Deller who carried out most of the measurements described below and in (Deller, Smith & Franklin 2004a). A triad of red, green and blue 3 mm LED's were mounted as close together as possible at one end of the mixing rod. The centre point of the LED array was aligned with the rod's axis. A frosted glass screen was positioned 100 mm from the exit end of the light guide. Photographs of the output light distributions transmitted through the screen were taken with an *Olympus® C-4000 ZOOM* digital camera. For quantitative observations, the screen was removed and replaced with a translational stage, carrying the detector of a *Hagner S3®* universal photometer (*B.Hagner SB)*. The detector size was reduced to ~1 mm diameter with a cover. The illuminance

of each LED was measured every millimetre in a horizontal direction through the centre axis of the guide, to form a strip 80 mm long. Each measurement corresponds to one pixel. The source luminous flux of each of the LED's was measured using the *Hagner*® photometer coupled to an *Oriel 70491*® integrating sphere.

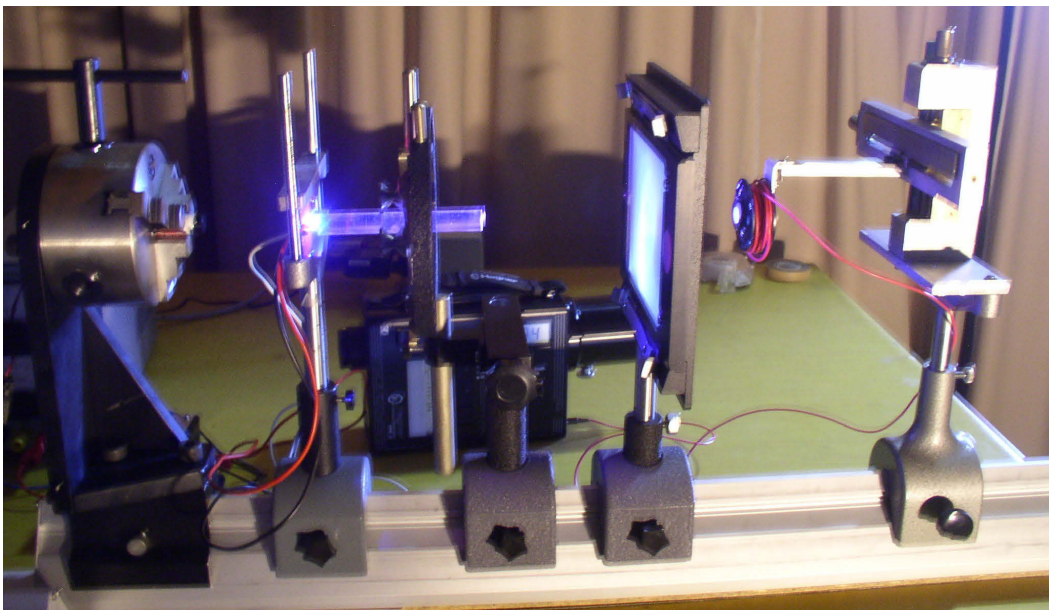

Figure 5.12 Experimental set-up, showing (from the left): alignment laser, LED array, PMMA mixing rod, frosted glass screen and the translational stage with a photometric detector.

The clear and TRIMM doped cylindrical light guides were ray traced with *Mathematica*® using the TRIMM scattering theory from section 5.2.1 (Deller, Franklin & Smith 2006a; Deller et al. 2002). Figure 5.13 shows the photographed (a) & (b) and modelled (c) colour distributions at a distance of 100 mm from the exit end of the clear rod. Notice the excellent qualitative agreement between modelled data Figure 5.13(c) and the photograph Figure 5.13(a), although some colour in the white, slightly overexposed parts of the photograph was visible to the naked eye. It is interesting to note that the visual pattern is strongly dependant on the viewing angle: Figure 5.13(a) and (b) are the same set-up photographed from slightly different angles (photograph (b) also has a slightly shorter exposure to show the colour variation in the central region that is overexposed in (a)). This considerable colour variation with viewing angle shows that undoped PMMA light guides are not suitable as LED mixers. Similar problems occur when LSC sheets are coupled to clear light guides.

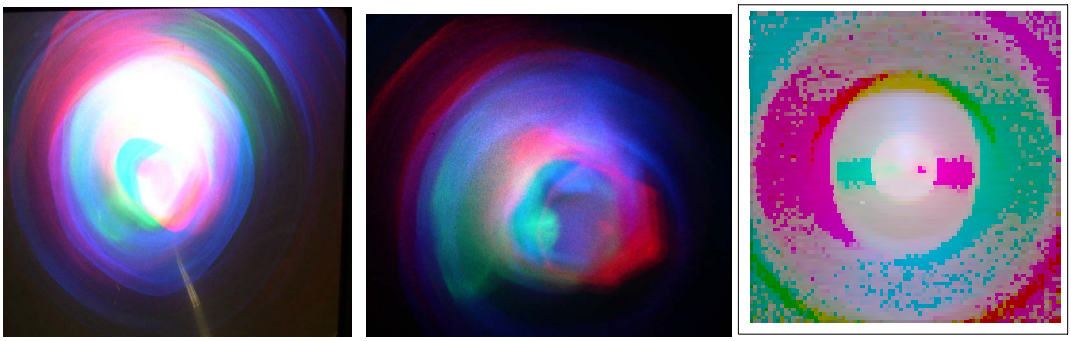

(a) (b) (c)

Figure 5.13 (a) & (b) Photographed output from a clear 100 mm long PMMA rod observed on a screen 100 mm from the end of the rod, viewed from different viewing angles. (c) Modelled output.

Figure 5.14 shows the photographed, modelled and measured colour distributions of the TRIMM doped rod projected onto a ground glass screen 100 mm from the exit end of the rod. There was a no perceptible colour variation in the light across the ground glass screen and no visible localized changes with observing angle. The slight colour variations in the photograph were not detected in the photometric measurements and appear to be due to due to imperfect white calibration of the camera.

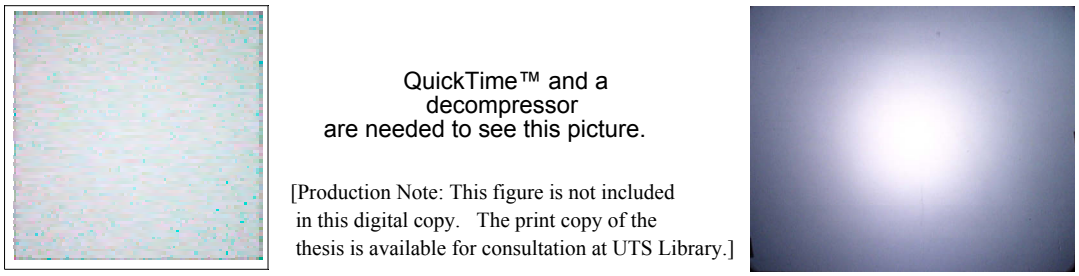

(a) (b) (c)

Figure 5.14 (a) Photographed output from a 88 mm TRIMM doped PMMA rod observed on a screen 100 mm from the end of the rod. (b) Modelled output from the TRIMM doped rod. (c) Measured CIE coordinates for a 1 mm central strip of (a) and (b).

A convenient parameter for TRIMM mixer design is the critical length, L_{crit}. This is defined as the length, for a given μ and α, where $\bar{\Sigma}$ is equal to θ_{crit}, the ray angle with respect to the rod axis where rays will escape out of the walls due to the critical condition. For meridional rays in a circular light guide, or for a guide with square walls, $\theta_{crit} = \pi/2 - \sin^{-1}(1/n)$, assuming the medium outside the mixer is air. From equations (5.56) and (5.58) it can be seen that a preliminary estimate of the critical length, assuming a Gaussian distribution of $\bar{\delta}$, is

$$L_{crit} = \frac{\theta_{crit}^{1.946}}{10.8\alpha\mu^{1.946}} \tag{5.59}$$

However, numerical studies suggest that this is an overestimate by a factor of about two (Deller & Franklin 2005) for $\mu = 0.0114$ and the error increases as μ increases.

It is not necessary for the TRIMM to be uniformly distributed along the entire mixer rod. Excellent results have been achieved with a TRIMM doped sheet at the end of a clear PMMA rod (Deller, Smith & Franklin 2004b). For the experiment described in that paper, a 2.94 mm sheet of TRIMM doped PMMA was glued with *Loctite® IMPRUV 34931®* glue to the end of a clear PMMA rod that had a diameter of 25.5 mm and a length of 58.9 mm. No air bubbles or defects were visible at the interface, which is indicative of a good optical joint.

The rod was measured with the set-up described in Figure 5.12. It was illuminated with a triad of red, green and blue 5 mm LED's that had been measured with a photogoniometer and selected to have similar emission patterns. For this experiment the ground glass screen was positioned 150 mm from the TRIMM sheet's exit surface.

A clear PMMA rod without the TRIMM diffuser was used as a control with the modelled and photographed colour distribution shown in Figure 5.15. The visual pattern was strongly dependant on the viewing angle.

Figure 5.15 (a) Modelled and (b) measured output from a clear 25.5 mm diameter, 58.9 mm long rod viewed 150 mm from the output surface.

Figure 5.16 shows the modelled and photographed output of the rod with a thin TRIMM diffuser sheet bonded to one end. An important feature is that the visual pattern was independent of the viewing angle.

An artifact of the photographs is the inability to display colour over a large brightness range. This means that the blue halo in Figure 5.16(b), although slightly visible in the experimental system, appears much less prominent to the eye. In addition, it was difficult to generate a sufficiently high intensity from the green LED to achieve a desirable colour balance,

as is evident in both the modelled and photographed results. Overall, the results are not quite as good as for a uniformly doped rod, but they are acceptable for many purposes.

The system illustrated in Figure 5.16 had a measured transmittance of 83%, which compares well with the measured transmittance of the clear control rods of 87%. The mixer's measured side-escape loss was 6.0%. Thus by using antireflection coatings, the mixer's transmittance could potentially be boosted to 94%.

The cost and mass of the clear light guide is restrictive for large diameter applications. One possible alternative design is to replace the PMMA rod with a hollow cylinder lined with a highly efficiency specular reflector (such as *3M® Silverlux®*) and have a TRIMM doped sheet at the output end. Very good results have been achieved with a similar design for mirror skylights where the sun acts as intense narrow angle source (Swift, Smith & Franklin 2006). However, the design has not been test with LED's.

QuickTime™ and a
decompressor
are needed to see this picture.

[Production Note: This figure is not included in this digital copy.
The print copy of the thesis is available for consultation at UTS Library.]

Figure 5.16 Output colour distribution transmitted through the frosted glass screen 150 mm from the end of the TRIMM sheet. (a) Modelled. (b) Photographed.

5.4.2 TRIMM Based Side-scattering Optical Fibres

The primary goal of this project was to find a way to couple light from a luminescent solar concentrator into a solid core optical fibre and to use that fibre to distribute light over long distances inside a building. At the start of the project available solid core optical fibres suffered from significant wavelength dependant losses that often varied from batch to batch. Accordingly, considerable time was spent working with Australia's leading manufacturer, Poly Optics Australia Pty Ltd, on ways of improving fibre performance. This work was very successful and lead to numerous applications for end-light fibre including: chandeliers, lighting for swimming pools, and decorative architectural lighting.

There has long been a demand for high efficiency side-scattering optical fibres to compliment endlight fibres. However, despite the effort of many workers, previous designs of side-scattering fibres suffer from high backscatter and low transport efficiency.

United States Patent No. 5,067,831 (Robbins, Zarian & Willford 1989) describes the general concept of side scattering light guides. Robbins discloses a polymer core that is encased within a transparent fluoropolymer cladding. Robbins relies on the leakage of light from the cladding with passage of light through the core.

United States Patent No. 4,422,719 (Orcutt 1981) discloses a transparent semi-solid core that is encased within a tubular cladding. Orcutt discloses a number of ways of providing side scattering capabilities including:

- Scoring the surface of the cylindrical core with angular cuts or discontinuities. The cuts and discontinuities deflect light beams circumferentially outwardly of the tubular core. The inside of the tubular cladding is etched or otherwise treated chemically or mechanically to cause light striking the inner surface of the tubular cladding to diffuse.

- Introducing bubbles or foreign materials into the cylindrical core material while the cylindrical core is still molten.

- Introducing a high refractive index scattering powder into the tubular cladding material such as titanium dioxide.

In order to achieve sufficient side scattering, prior additives to the core all had excessive opacity so that light could not be transmitted for more than a small distance from the light source and light output and hence brightness would vary very strongly with distance. To achieve sufficient length of light transport, conventional additives would have to be added at such low concentrations that little scattered sidelight would emerge. In addition bubbles and other foreign materials are often very difficult to add uniformly into the core because the difference in their density compared to the liquid polymer.

United States Patent No. 6,091,878 (Abramowicz, Daecher & Hallden-Abberton 1997) from Rohm & Haas Company limits the concentration of additives that are added to the tubular cladding to increase the effectiveness with which light is transmitted circumferentially out of a cylindrical light guide. While the Rohm & Haas design addresses some of the deficiencies of Orcutt, the light guides of Rohm & Haas suffer from a lack of efficiency due to the large angles at which light is scattered by their additive and the uncontrolled nature of the primary light extraction from the fibre's core.

It was shown in section 5.2.1 that TRIMM systems have controlled forward scattering with almost no backscatter, which is ideal for a side-scattering optical fibre. In addition, the density of the cross-linked PMMA microparticles is similar to that of the casting liquor used to make solid core optical fibres. This suggested that a superior side-scattering optical fibre could be made by doping conventional optical fibre with cross-linked PMMA microparticles. Trial

batches made at Poly Optics Australia Pty Ltd had excellent performance and led to a number of patents. (Franklin, Smith & Joseph 2003) describes the basic design and methods of manufacturing the side-scattering optical fibre. It was found that the appearance of the fibre could be improved by adding an appropriate diffusing jacket (Franklin, Joseph & Smith 2004). The side-scattering fibre has been in continuous production since it was patented and has a wide range of applications, including stair lights illustrated in Figure 5.17 and illumination strips for bicycle helmets shown in Figure 5.18. Another proposed application is to simplify the tracing of telecommunications cables by adding a side-scattering fibre to the cable's jacket. By illuminating the cable at one end, the cable can be caused to glow along its length, greatly simplifying circuit tracing without having to disrupt the circuit (Henderson, Franklin & Smith 2005).

The intensity of the side scattered light falls off exponentially with distance along the fibre. However, as Figure 5.17 and Figure 5.18 show, by illuminating the fibre from both ends it is possible to achieve a uniform output. Another method is to position a high reflectivity mirror at the remote end of the fibre. If the concentration of TRIMM is chosen so that the optical fibre is one half-length long, then the combination of forward and reflected light gives uniform side scattered emission along the whole length of the fibre.

Figure 5.17 Stair lights at UTS using TRIMM doped side-scattering optical fibre.

Figure 5.18 Bicycle helmet using LED's and TRIMM doped side-scattering optical fibre. Note the even brightness achieved by using a LED at each end of the fibre.

The theory of scattering from TRIMM systems described in 5.2.1 and 5.3.1 has been applied to TRIMM doped side-scattering optical fibres with excellent agreement between the modeled and measured optical properties (Deller 2005; Deller, Franklin & Smith 2006a; Deller et al. 2002).

TRIMM doped side-scattering optical fibre has several applications for LSC systems. The simplest is as a high efficiency light extractor at the end of an optical fibre coupled to LSC's (see section 6.5 for details). A more sophisticated application is in a luminaire that combines light from a LSC with electrically generated light.

When a dense cloud obscures the sun the light from a LSC will drop. It is desirable to be able to supplement the light from the LSC with additional electrically generated light to keep the room lighting constant. However, it is not enough to keep the total lumens constant. Experience has shown that people are very sensitive to rapid changes in the directional properties of light. One case where this problem often occurs is where the primary source of room lighting is from windows and the electrical lights are automatically adjusted to keep lux levels constant. The very different directions of the window light and electrical light mean that switching between the two sources changes the directional properties of the illumination, even though the total amount of light remains fixed. Many users find this directional change highly

objectionable and it is not uncommon to find that they either switch off the automatic light tracking or disable the system.

One unique feature of side-scattering optical fibres is that they are transparent to external light incident from any direction. This means that, as shown in Figure 5.19 they can be placed inside a luminaire that also has electrically generated light. As described in (Smith & Franklin 2007), the control system can adjust the output of the electrically generated light to keep total lumens constant without changing the angular distribution of light from the luminaire or illumination pattern of the room.

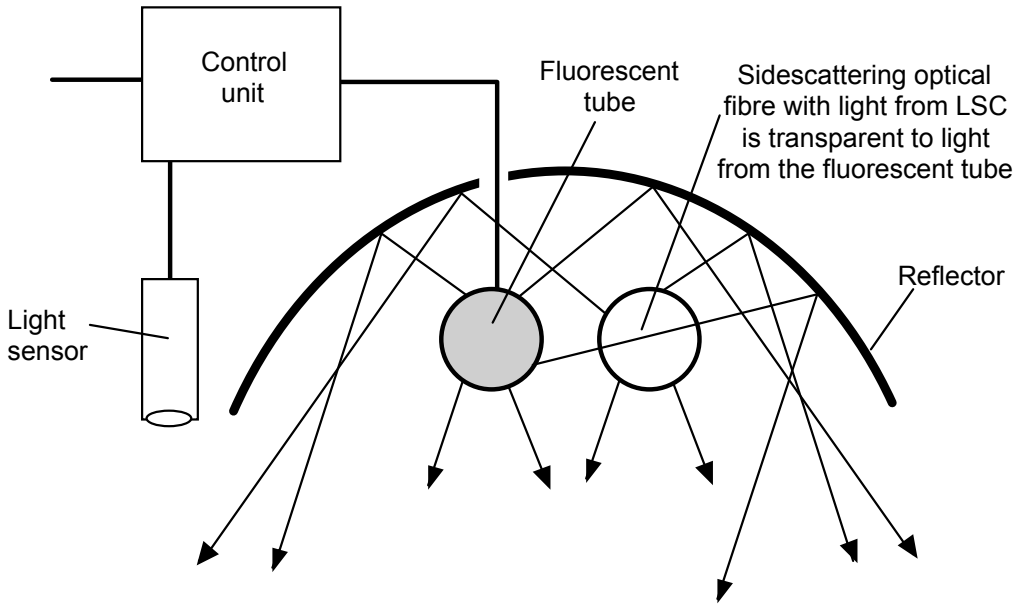

Figure 5.19 Diagram of a luminare with a side-scattering optical fibre (delivering light from a LSC) integrated with an electrically driven fluorescent tube in a common housing. The control system senses the light level in the room and can adjust the output of the fluorescent tube to keep the light level constant without changing the illumination pattern. The side-scattering fibre is transparent to light from the fluorescent tube, which makes it easier to integrate the two light sources to give constant illumination pattern.

6 LIGHT EXTRACTION FROM SOLID OPTICAL SYSTEMS

6.1 INTRODUCTION

In many modern light sources such as LSC's and light emitting diodes, light is emitted within a high refractive index light-guiding structure. Some of this light is trapped, and will not be able to escape (Saleh & Teich 2007, pp. 689 - 90). Similar problems are observed when collecting fluorescent radiation in waveguides (Ratner 1994) and scintillation detectors (Smith 1971). For lighting applications, this trapped light should be able to escape the light-guiding structure. In LED's this is commonly achieved with a special profile in the active zone or with special surface nanostructures (Saleh & Teich 2007, pp. 690 - 2). However, in LSC lighting systems, the small light-emitting zone is coupled to the large light collector by an extended light guide, so a different approach must be taken. This chapter will focus on the extraction of emitted light from rectangular LSC coupled to extended light guides and explores ways of extracting a large fraction of the trapped light at the end of the light guide and directing it as useful illumination.

6.2 WHAT IS TRAPPED LIGHT?

It is a fundamental principle of linear optics that no optical system in which all the light enters from outside the system can ever have any trapped light. This is because light trapping requires that once light is generated within a system, it must be totally internally reflected off all surfaces. However, all linear optical systems are time reversible (Pedrotti & Pedrotti 1987). So in these systems, if light can pass in through a surface at a particular angle, then light traveling in the exact opposite direction will pass out through that surface.

If light enters a light guide system from the outside and is reflected from the far end, it will tend to reach the entry surface with an angle similar to that with which it started, and will thus be able to pass through that surface and so escape from the system. This means that any optical system in which the light enters from an external source can have no trapped light.

Only light sources that generate light inside a material can produce internally trapped light. Examples of internal light sources are fluorescent molecules and electron–hole pairs in semiconductor light emitting diodes. A substantial portion of the emission from such sources is often completely trapped within the system by total internal reflection (Saleh & Teich 2007, pp. 689 - 92). The key point is that this internally generated light can travel on a closed path that cannot be duplicated by light entering from the outside.

Another simple argument based on fundamental thermodynamics can be used to show that no type of linear optical system can have trapped light enter from the outside. For if it were

possible for a linear system to losslessly accumulate light produced externally, then the light would be continuously accumulated without limit and so the energy density inside would also increase without limit. Such a system could be used to generate temperatures that were arbitrarily larger than the source temperature—a clear violation of the Second Law of Thermodynamics. Internal source systems do not suffer from this problem because the accumulation of trapped light changes the properties of the system in a way that prevents the endless accumulation of light. For example, fluorescent dyes become opaque to their own emissions at large enough photon densities due to non-linear effects and so a system using these dyes will eventually cease to accumulate trapped light.

However, it is possible in such systems to achieve high internal flux densities, possibly even super-generation (Reisfeld et al. 1989; Reisfeld, Yariv & Minti 1997). To achieve and utilize such enhanced fluxes special light extraction procedures are need in which the amount of trapped light escaping is controlled to low enough fraction to ensure gain, but not so high that gain is not possible. Output optical switching analogous to Q-switching lasers might also be possible to achieve gain.

6.3 ENDLIGHT VS. TRAPPED LIGHT

Before going any further, it is important to make distinctions between the different categories of light within the light guide of a LSC system (Earp, Franklin & Smith 2005). Consider a LSC consisting of a rectangular block of transparent dielectric with perfectly parallel sides, doped with a fluorescent dye. The fluorescently emitted light is essentially isotropic[2], so a small fraction (referred to as 'endlight') will strike the end surface inside the critical angle cone and escape, as shown in Figure 2.5(a), previously introduced as Figure 2.5 and reproduced here for convenience. By connecting a clear light guide to this surface, the endlight can be used as a lighting source. As shown in Figure 3.6, a considerably larger fraction (referred to as 'side loss') will escape through critical angle loss cones at the top, bottom and sides of the block. Some of the side loss cones can be converted to endlight using suitable reflectors (Franklin 2001b). The remainder of the light is 'trapped light', and does not escape at any of the surfaces of the LSC. When a clear light guide is attached to the end of the LSC sheet, without any air gap (however small), both the endlight and the trapped light enter the light guide and will undergo total internal reflection and travel to the end of the light guide. Approximately 91% of the endlight will escape upon striking the end surface with the remaining 9% being trapped by Fresnel reflectance. It has been shown elsewhere that the light reaching the end of the light guide is approximately half endlight and half trapped light (Earp et al. 2004b; Franklin 2001b).

[2] See section 3.1.3 for a discussion angular distribution of the fluorescently emitted light.

Therefore approximately half of the available light remains trapped within the light guide (as illustrated in Figure 2.5(b)), unless the end surface of the LSC is given special treatment.

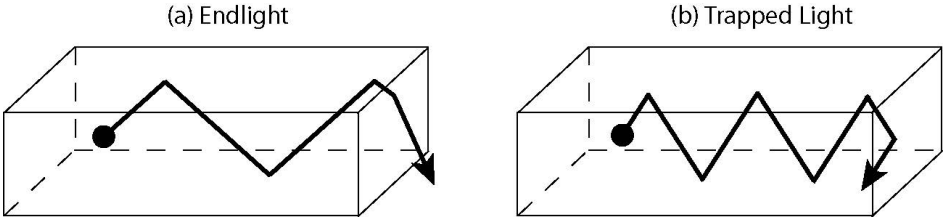

Figure 6.1 (a) Endlight can pass through an end surface, whereas (b) trapped light is totally internally reflected at all surfaces.

6.4 CALCULATION OF AMOUNT OF EACH FORM OF TRAPPED LIGHT

Figure 6.2 illustrates the distribution of the light emitted by dye molecules in a rectangular LSC sheet of relative refractive index, n with a mirror with a reflectivity of, r, at one end. There are six escape cones aligned along the sheet's three principal axes (the two sideloss cones along axes 5 and 6 have been omitted for the sake of clarity). We saw in equation 3.6 that the solid angle of each escape cone, Ω_{escape}, is

$$\Omega_{escape} = 2\pi(1-\cos\theta_{crit}) = 2\pi\left(1-\sqrt{1-1/n^2}\right) \tag{6.1}$$

Now the fluorescently emitted light is isotropic. So the fraction of the emission in each escape cone, f_{cone}, is the ratio of the solid angle of the escape cone to 4π steradians. Thus,

$$f_{cone} = \frac{\Omega_{escape}}{4\pi} = 1/2\left(1-\sqrt{1-1/n^2}\right) \tag{6.2}$$

Immediate losses occur through the top and bottom surfaces and the two sides. The fraction of emission that escapes in this way, f_{escape}, is the ratio of combined solid angle of the four escape cones to 4π steradians. So from equation (6.2) and (6.2),

$$f_{escape} = 4f_{cone} = 2\left(1-\sqrt{1-1/n^2}\right) \tag{6.3}$$

If we ignore absorption and scattering inside the LSC sheet, the fraction of the emission that reaches the light guide as end light, f_{end}, is the ratio of the total solid angle of the two endlight cones (corrected for reflection at the mirror) to 4π steradians. So, from equation (6.1),

$$f_{end} = \frac{(1+r)\Omega_{escape}}{4\pi} = \frac{(1+r)}{2}\left(1-\sqrt{1-1/n^2}\right) \tag{6.4}$$

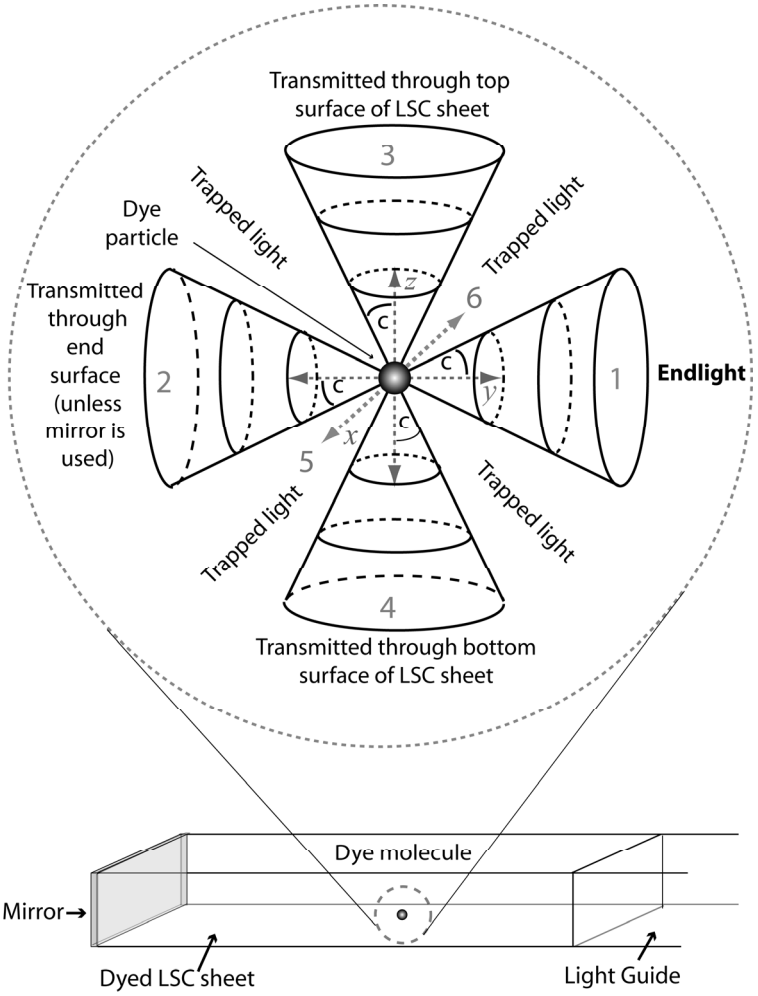

Figure 6.2 Distribution of the light emitted by dye molecules in an LSC sheet. The sideloss cones (cones 5 and 6) have been omitted for clarity.

Now trapped light is, by definition, that fraction of the emitted light that is not in an escape cone and is not absorbed at the mirror. In the forward direction there is one full cone of end light and four half cones of sideloss light (see figure 3.6). There is a similar amount of light emitted in the backwards direction that it reflected forward with an efficiency of r. Thus from equation (6.1), the fraction of emission that reaches the light guide in the form of trapped light, $f_{trapped}$, is

$$\begin{aligned} f_{trapped} &= \frac{(1+r)[2\pi - (1+4\times 0.5)\Omega_{escape}]}{2\pi} \\ &= \frac{1}{2}(1+r)\left(3\sqrt{1-1/n^2} - 2\right) \end{aligned} \tag{6.5}$$

From equations (6.4) and (6.5), the ratio of the total amount of light reaching the light guide (i.e. the sum of endlight and trapped light) to the endlight, F_{all}, is

$$F_{all} = \frac{f_{trapped} + f_{end}}{f_{end}} = \frac{2\sqrt{1 - 1/n^2} - 1}{1 - \sqrt{1 - 1/n^2}} \tag{6.6}$$

Table 6-1 summarizes the results for PMMA light guide that has a refractive index of 1.49 (MatWeb-Cast 2011; MatWeb-Extruded 2011) and a mirror with a reflectivity of 0.90. We see that the amount of trapped light is slightly less than the amount of endlight. Thus if the LSC is coupled to a rectangular light guide, as illustrated in Figure 6.2, the end surface of the light guide will reflect all the trapped light and so will waste nearly half of the available light. What is required is a way of extracting the trapped light at the end of the light guide. This is the job of the light extractor, and will form the basis for the rest of this chapter.

Table 6-1 Light fractions for a non-absorbing, non- scattering PMMA LSC that has a refractive index of 1.49 and a mirror reflectivity of 90%.

Quantity	**Fraction of light**
f_{cone}	12.9%
f_{escape}	51.6%
f_{end}	24.6%
$f_{trapped}$	21.3%
Mirror absorption	2.2%
F_{all}	1.86

However, before we consider the details of light extractors, we need to explore how realistic equations (6.1) to (6.6) are. Important simplifying assumptions in deriving these expressions were that:

i) The cones do not overlap,

ii) The mirror is a perfectly specular reflector with a high reflectivity,

iii) There is no absorption in the LSC, and

iv) There is no scattering in the LSC.

We will look at each of these assumptions in turn.

The condition for the cones not to overlap is that the critical angle is less than 45^o, which is true when $n > \sqrt{2}$. This is satisfied for all practical polymer LSC's surrounded by air (only fluoropolymers have refractive indices less than 1.41 and all known fluoropolymers are both far too expensive and scatter excessively for practical LSC's). Overlap of the cones will occur for LSC sheets in water, and LSC's with low refractive index surface layers (such as sol-gel or fluoropolymer). However, for the rest of this chapter we will assume that the LSC sheet is surrounded by air, which means that the escape cones do not overlap.

Good end mirrors can almost double the amount of light exiting the LSC (and hence double useful light output). However, to do this they must have a high specular reflectivity as scattering will cause losses by converting low-angle light to high-angle light that is not trapped by total internal reflection. Achieving specular end mirrors is technically quite demanding. The main problem is the thinness of the LSC sheets, typically about 2.0 mm. Two techniques have proved satisfactory. The first is to coat a high reflectivity *3M® Silverlux®* film with a transparent self-adhesive film, die cut the film into 6.0 mm wide strips, bond the reflective strips to the diamond polished end of the LSC, and then use a scalpel to trim off excess reflector film. Specular reflectivity at normal incidence measured with HeNe laser exceeds 95%. The second method is to vacuum coat the diamond-polished end of the LSC with aluminum. Specular reflectivity at normal incidence measured with HeNe laser was about 85%. The main problem with vacuum coating is ensuring that the coating is restricted to the end of the LSC sheet. Trials at my direction by a vacuum coating firm in Sydney showed that this could be achieved by tightly packing a stack of LSC sheets in the vacuum coater so that other sheets shielded all but the top and bottom surfaces of the stack while the side surfaces were protected by a mask.

The self-adhesive reflective film method is a labour intensive process. This means that it is best suited to prototypes and small-scale production. Evaporative aluminum coatings (with a suitable protective over-coating) requires expensive specialized equipment and has a slightly lower performance. However, it is much more suited to mass production.

Absorption in an LSC reduces the amount of light that reaches the light guide. Trapped light has a larger angle to the sheet axis than endlight, which means that on average it travels further and hence experiences somewhat more absorption. Thus the effect of absorption is to slightly reduce the ratio of total exiting light to endlight below the value of equation (6.6).

The effect of scattering is quite complex. Briefly, scattering causes diffusion in a ray's angular coordinates. When a ray reaches one of the escape cones (i.e. its angle with respect to any side surface is less than the critical angle) it will be very rapidly lost. Trapped light is closer to the escape cones so it experiences a higher loss rate than endlight. Thus scattering also reduces the ratio of total exiting light to endlight below the value of equation (6.6), which assumes no scattering. For a high quality PMMA LSC, measured values of F_{all} are typically about 1.7 rather than the 1.86 predicted by equation (6.6).

Light trapping and refraction at interfaces mean that it is not possible to measure the angular distribution of light inside a LSC sheet by observations from a planar end surface. This problem was largely overcome with the experimental set-up shown in Figure 6.3 and Figure 6.4, similar to that of (Zastrow 1981). The apparatus used a 100 mm diameter hemispherical lens bonded to a mask with an aperture at the lenses centre of curvature. The mask was in turn bonded to a LSC sheet so that the LSC sheet and lens formed a solid optical system. The curved

surface of the lens allowed all LSC light that passed through the aperture to enter the surrounding air without significant deviation.

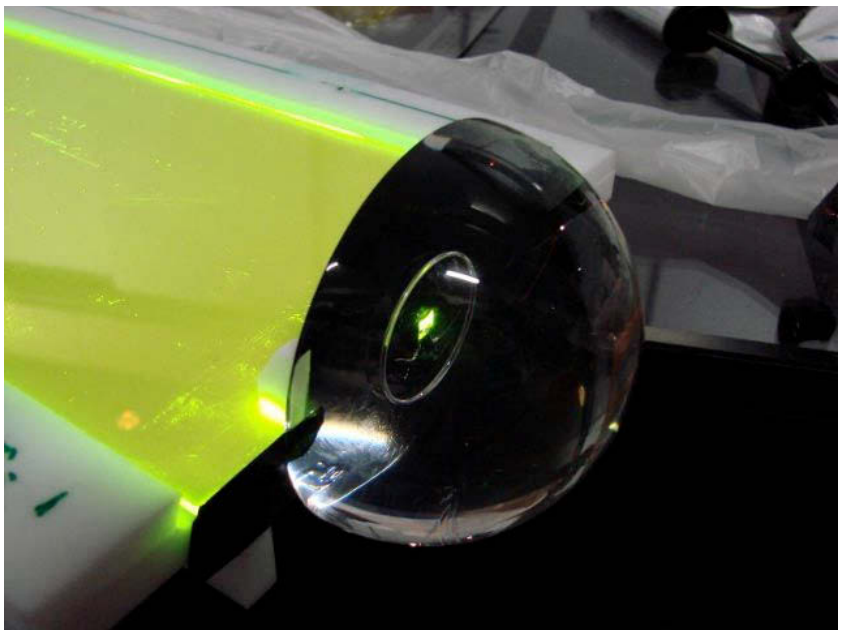

Figure 6.3 A hemispherical lens is coupled to the end of a LSC to observe and measure the light field inside a LSC. There is a 2.0 mm x 2.0 mm emission window from the LSC at the centre of the hemisphere. The LSC and lens form a solid optical system. The black cloth that usually covers the LSC and the hemispherical diffuser screen that usually covers the lens been removed for the sake of clarity.

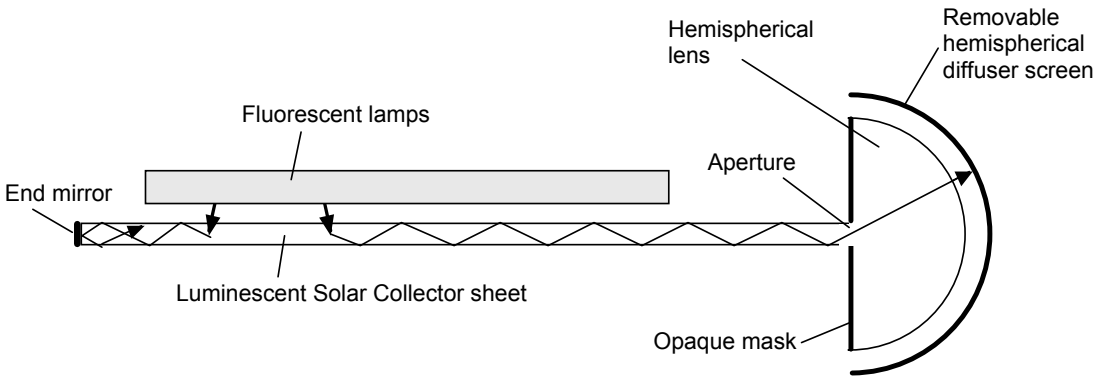

Figure 6.4 Schematic of the experimental set-up for observing and measuring the light field inside a LSC.

The LSC sheet was a 1200 mm x 150 mm x 2.0 mm PMMA sheet doped with 60 ppm *Lumogen*® F083. The sheet was illuminated with two 900 mm long fluorescent lamps orientated parallel to the sheet's axis. In order to increase the light intensity and to reduce stray light, the lamps were housed under a 99% reflective housing (not shown) that was extend to the edges of the LSC. The reflector and the entire sheet were covered with a black cloth (not shown) so that there was no visible stray light. The sheet had a specular end mirror so that the light field was representative of a full-sized collector sheet.

The planar surface of the 100 mm diameter clear PMMA hemispherical lens was covered with an opaque mask of thin black self-adhesive film that contained a 2.0 mm x 2.0 mm aperture concentric with the lenses centre of curvature. The LSC sheet was glued to the mask with *Dymax* OP-29® UV-curing adhesive and a *Dymax Blue Wave 50*® UV Lamp. Care was taken to ensure that there was a good optical joint at the aperture between the sheet and the hemispherical lens. Auxiliary support blocks (not shown) provided mechanical support for the lens so that there were no stresses on the glue that filled the aperture.

The radius of the lens is so large compared to the size of the aperture that all light passing though the aperture reaches the lenses hemispherical exit surface at essentially normal incidence and so is not deviated by refraction upon entering the surrounding air. Also, all rays experience the same Fresnel reflection losses of 3.9% at the hemispherical surface.

In order to visualize the light field, the hemispherical lens was covered with a removable hemispherical diffuser shell, as shown in Figure 6.4 and Figure 6.5. In Figure 6.5(b) the four sideloss cones (top, bottom, left and right) are clearly visible. The endlight cone has been marked as the central white circle. Light between that circle and the sideloss cones is trapped light. To help clarify the photograph, the hemispherical diffuser shell in Figure 6.5 is partially illuminated with white light from the top right, with the brightest illumination occurring in Figure 6.5(a).

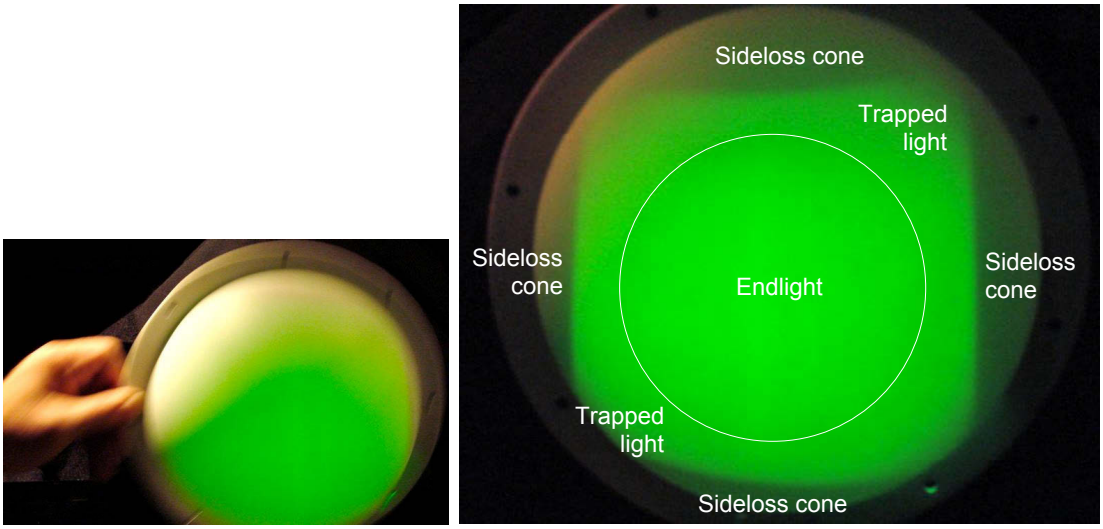

Figure 6.5 Left: a Hemispherical diffuser screen that is placed over the hemispherical lens to help visualise the light pattern inside a LSC. Right: Projected light distribution inside a LSC. The white circle shows the endlight cone. The four sideloss cones are clearly visible. Light between the endlight circle and the sideloss cones is trapped light.

The emission pattern was measured quantitatively with the UTS photogoniometer, described in (Earp, Smith & Franklin 2007; Smith, Jonsson & Franklin 2003), by removing the diffuser screen and positioning the apparatus so that the aperture in the mask was at the

photogoniometer's centre of rotation. Scans with a detector 580 mm from the centre of rotation were made in the plane of the horizontal LSC sheet, at right angles to that plane, and at ±45° to the plane of the sheet. The results are shown in Figure 6.6.

If γ is the angle from the normal to the aperture's surface, then areal projection means that the aperture will reduce the illuminance at the detector by a factor of cos γ. Thus the field luminance of the light inside the sheet is proportional to detector signal divided by cos γ. For an ideal system, the field luminance should be constant up to the escape cones and zero in the escape cones. Note that γ is also the angle of a ray with respect to the sheet's longitudinal axis.

As can be seen from Figure 6.6, the measured field luminance for the in-plane scan is close to this ideal, being constant to within about 3% up to the escape cones, and then falling to zero within 4°. For the perpendicular-to-plane scan, the field luminance is almost constant to 20° but then falls increasingly rapidly to 60% of the central value at 40°. The reason for the loss of the high angle light is almost certainly scattering from the sheet's upper and lower surface: light with γ = 30° averages over 350 interactions with the sheet's top and bottom surfaces. The measured luminance in the ±45° planes is intermediate between that of the in-plane and perpendicular-to-plane up to the critical angle. It then decreases linearly with γ, falling to 15% of the central value at 80°, the highest angle measured.

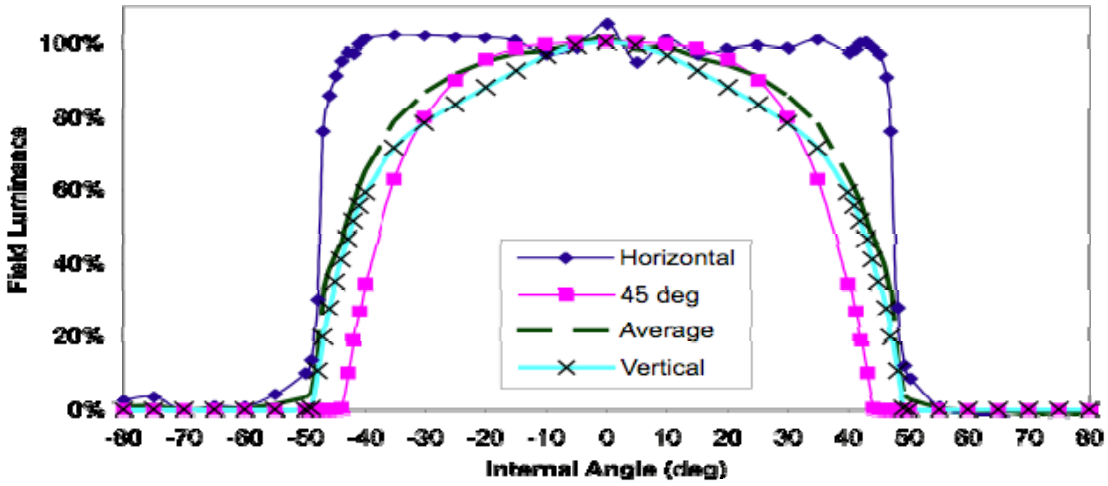

Figure 6.6 Measured internal field luminance for a LSC in various scan directions.

6.5 TYPES OF LIGHT EXTRACTORS

6.5.1 The Importance of Étendue

Étendue is a fundamental tool for analyzing LSC's systems for daylighting. To briefly summarize from section 3.1, we saw in equation 3.1 that the étendue, G, for a homogeneous light guide of refractive index, n, is

$$G = \int_A n^2 \mathbf{\Omega} \bullet \mathbf{dA} \tag{6.7}$$

where the light crossing an infinitesimal area, dA, with associated area vector, **dA** has a solid angle of Ω. The vector **Ω** of magnitude Ω is in the central direction of the light. (In analyzing light extractors the light field is not uniform and the integration surface for equation (6.7) is often not normal to the optic axis, so it is not possible to simply our expression for étendue to equation 3.2.)

It was shown in table 3.2 that the limiting étendue per unit area of a rectangular PMMA light guide is 6.75 sr while the value for an end surface perpendicular to the sheet's axis is only 3.61 sr. Now étendue is conserved by transmission across a boundary. So this means that for light inside a light guide with that maximum solid angle, only about half of the internal light can cross a perpendicular end surface, with the rest being reflected as trapped light. Section 3.1.4 shows that inclining the end surface gives only a small improvement.

6.5.2 Increasing the Cross Sectional Area

Equation (6.7) suggests a number of approaches to of extracting the trapped light from the light guide. First we note that, as Figure 6.7(a) shows, simply increasing the area does not work because the light strikes the exit surface with unchanged angle and so the fraction of trapped light is unchanged. See Figure 4.3 for an illustration of this type of system.

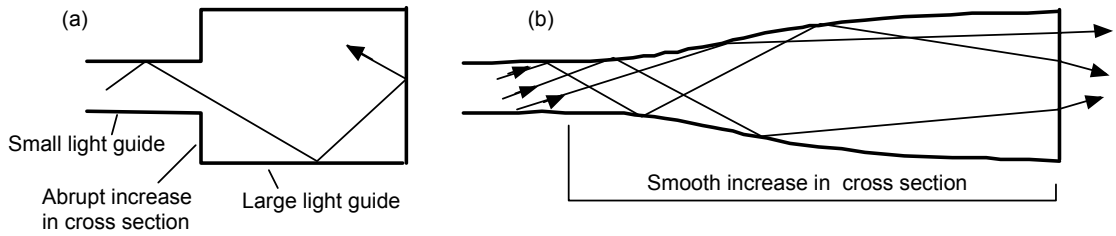

Figure 6.7 Light extractors. (a) A simple increase in area does not work. (b) A smooth increase in area can give good light extraction.

A better approach is an adiabatic expansion of cross sectional area that trades increased area for decreased solid angle, illustrated in Figure 6.7(b). For a cylindrical optical fibre this can reduce the angle of incidence at the exit surface below the critical angle, allowing good

extraction of trapped light. However, the great thickness of the extractor means it is hard to make by injection moulding or other mass production techniques.

A better solution is shown is Figure 6.8 copied from the granted patent (Franklin 2001a) and briefly mentioned earlier as figure 2.6. This light extractor expands the area but also curves the exit surface. The curvature reduces the angle of incidence at this surface, which increases Ω.dA in equation (6.7). The curvature also increases the integrated area in equation (6.7). Both of these effects raise the étendue at the end surface. However, the component of the solid angle in the plane of the light guides is unchanged. So unless the light extractor is broadened sideways (which is not usually practical) about half the trapped light cannot be extracted.

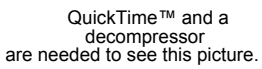

[Production Note: This figure is not included in this digital copy.
The print copy of the thesis is available for consultation at UTS Library.]

Figure 6.8 Expanded area light extractor (66) with a cylindrically curved exit face.

6.5.3 Light Extractors Using Multiple Interactions

An alternative approach is to use multiple interactions, each of which extracts some portion of the light. To put it colloquially, if the étendue is too big, we take lots of small bites. In terms of equation (6.7), we are changing the surface over which the light escapes, and hence the area integrated, from the light guide's small transverse cross section to the light extractor's much larger longitudinal areas. For this approach to work there has to be some part of the system that changes the angle of the light as it moves along the light path. Otherwise total internal reflection would not permit the light to exit through the longitudinal surfaces.

The first light extractor built on this principle is shown in Figure 6.9, copied from the granted patent (Franklin 2001a). The main aim of the experiments describe below was to demonstrate that is was possible to convert trapped light in LSC's to useful illumination. A 270 mm x 20 mm x 2.0 mm concentrator sheet 40 dyed with 70 ppm *BASF Lumogen*® F083 dye was exposed to a fluorescent lamp in a reflective housing 41 at one end, with the middle portion 44 of the sheet serving as an optical conduit 42 as it did not have any light exposure. The total light output from the optical conduit was measured with an integrating sphere 43.

The final 50 mm of the optical conduit was treated in various ways so that the totally internally reflected light 45 could be scattered and released. Treatments tested included:

(a) roughening one or more surfaces with 1200 grade, 600 grade, 400 grade, 240 grade and 120 grade "wet and dry" abrasive papers; (b) attaching "diffuse" sticky tape to the top and bottom side surfaces; (c) gluing various diffuser sheets to the surfaces; and (d) dipping the final 50 mm into acetone for various intervals, which roughens the surfaces. The grooves made with abrasive papers were mostly perpendicular to the long axis of the conduit and their direction seemed not to be important.

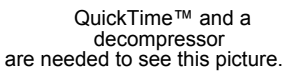

[Production Note: This figure is not included in this digital copy.
The print copy of the thesis is available for consultation at UTS Library.]

Figure 6.9 System used to measure the gain in output from a treated end (46) of a LSC (42) illuminated with a lamp (41). Light output is measured with an integrating sphere (43). From (Franklin 2001a).

All of the above treatments gave more light output than no treatment, where the only light output was through the conduit's end surface as end light. The best results of 63% more light were obtained when 1200 grade paper was used to roughen the topside surface only. However, even 120-grade paper on all side surfaces gave 43% more light than no treatment. In the conduit treated with 1200 grade paper, the sidelight leaked out over the first 30 or 40 millimetres of the 50 mm treated length. This corresponds to an emission area about 18 times that of the untreated sheet with about 10 interactions of light with the rough surface.

In the more roughly treated conduits, the side light leaked out within the first 10 mm of the 50 mm treated length of conduit. However, in all of the conduits treated with abrasive paper, about one quarter of the light came out the end surface 46. This is probably because even rough surfaces become specular reflectors at grazing incidence.

The above experiments were primarily useful as a proof-of-principle (and for convincing patent examiners of the reality and usefulness of trapped light). However, sheet roughening is not a commercially viable method of light extraction.

A better solution is to use a block of highly diffusing polymer to randomize the light, as shown in Figure 6.10 from (Franklin 2001a). The diagram is schematic in that étendue considerations require that the diffuser block must be several times as long as it is high. Traditional diffuser materials have high back scatter which would greatly reduce the output. However, the TRIMM doped materials discussed in chapter 5 combine excellent diffusion with little backscatter. Good results were obtained with TRIMM blocks that had a length 10 times the

height of the light guide stack. Several light extractors were constructed and used with tri-colour LSC systems and hybrid-LSC systems. Measured extraction efficiency was better than 90%, and there was no visually detectable change in colour with angle. The visual appearance was judged to be very superior.

QuickTime™ and a
decompressor
are needed to see this picture.

[Production Note: This figure is not included in this digital copy.
The print copy of the thesis is available for consultation at UTS Library.]

Figure 6.10 A TRIMM based light extractor at the end of a light guide stack.

The analogous design for a cylindrical optical fibre is a short rod of highly doped TRIMM polymer. This was not tested directly, as the available TRIMM doped PMMA rods had too small a diameter. However, excellent results were obtained with ordinary TRIMM doped sidescattering optical fibre Poly Optics Australia Pty Ltd.

An alternative approach is shown in Figure 2.7(b), briefly introduced earlier as Figure 2.7, and reproduced here for the sake of convenience. This light extractor utilises a diffusely reflecting white coating on its rear and side surfaces. Trapped light entering the extractor undergoes total internal reflection at the exit face and is reflected back to the diffusely reflecting white back surface. This reflects the light with a random orientation so that much of it now pass though the exit face. The fraction that does not escape returns to the rear-diffusing reflector and the process continues until (i) the light enters free space via the exit face, (ii) the light is reflected back down the light guide, or (iii) the light is absorbed by the matrix or the white diffuser.

This design uses an extraction surface with about 8 times the cross sectional area of the light guide and much of the light also has multiple interactions with the extraction face. So there are no problems in satisfying the étendue requirements of equation (6.7) for near total light extraction. The main loss mechanism is reflection of trapped light back down the light guide, which can be minimised by a careful choice of the extractor's thickness (measured along the light guide axis) and height (measured perpendicular to the light guide axis).

Design of these light extractors requires a detailed knowledge of the BRDF of the diffusely reflecting white back surface. This was measured with the UTS photogoniometer (Earp, Smith & Franklin 2007) and incorporated into numerical models in *Mathematica*®. A number of prototypes were constructed. Measured extraction efficiencies were ≈ 86%.

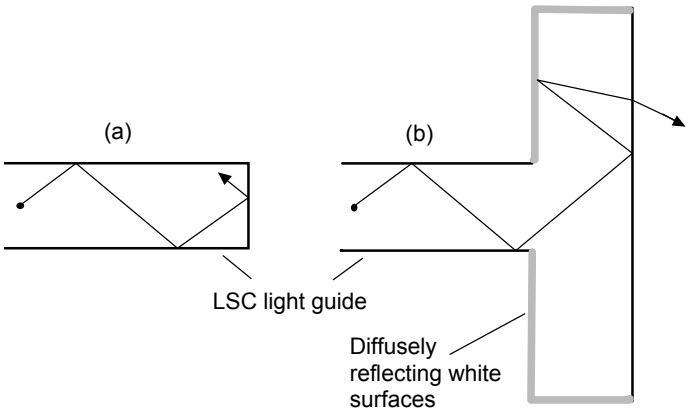

Figure 6.11 (a) A perpendicular end surface reflects almost half of the available light. (b) Extraction of trapped light by a luminare with expanded area and diffusely reflecting white surfaces.

Up until now the light extractors have used diffusion at a surface (Figure 6.9 and Figure 2.7) or in the matrix (Figure 6.10) to change the angle of the light as it strikes successive surfaces. An alternative approach is to use the geometry of the light guide.

Figure 6.12 illustrates a wedge type light extractor for planar light guides. Light reflected off the inclined surfaces increases its angle with respect to the optic axis. The angle of incidence with the surfaces keeps increasing until the light is no longer contained by total internal reflection. Extraction efficiency is very close to 100%. However, a serious drawback of a simple wedge as a luminaire is that most of the light is strongly forward peaked in quite narrow beams either side of the wedge axis. This directionality of emission is not a problem if the light extractor is just to be used to measure system efficiency.

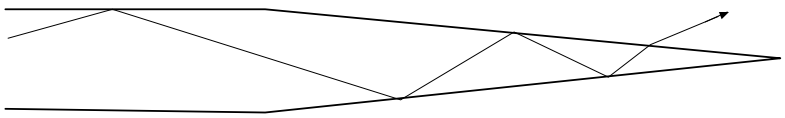

Figure 6.12 A wedge-type light extractor. Light moving down the extractor strikes the surfaces at increasing angles until it is no longer confined by total internal reflection.

The analogous design for a cylindrical optical fibre is a cone, although some modifications are required to take into account the difference in the light field and the geometry, as the latter causes total internal reflection of some rays in the cylindrical system that are not reflected in the planar system.

The light from the curled-sheet flat-to-round converters discussed in sections 4.5 and 4.6 has a significant amount of skew rays that are at more than 50^{o} to the fibre's axis. Much of this light is back reflected by a simple cone. However, close to 100% extraction efficiencies can be achieved with the design illustrated in Figure 6.13. This light extractor has a cylindrical entry portion with a diameter about twice that of the fibre and a length of about one fibre diameter.

This section is followed by a conical element that has a length of about five fibre diameters. A substantial fraction of the light is emitted close to the cone's tip so it important that the tip has as small a radius as possible. The flat surface of the cylindrical portion acts as a mirror for any skew rays that are initially back reflected by the conical element, redirecting them into the cone.

This design is not practical as a light extractor for fibre optic LSC systems because (i) the light is strongly concentrated in an annulus about the cone's axis, (ii) the sharp tip is fragile, and (iii) the device's considerable thickness (40 mm for a 20 mm fibre) means that it is not suitable for injection moulding and would be expensive to make by machining and polishing. However, the measured and modeled efficiencies are close to 100%. So it is suitable for measuring the efficiency of an LSC system.

A conical light extractor along these lines was illustrated in Figure 4.15 being used to measure the output of a flat-to-round converter. Conical light extractors without the cylindrical element have been used with LED's to boost output light (Saleh & Teich 2007, p. 691).

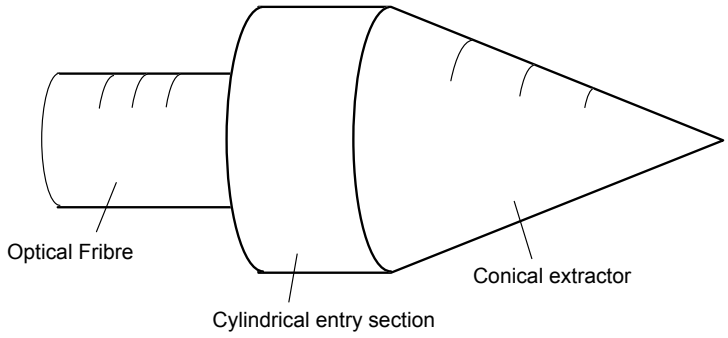

Figure 6.13 A conical light extractor for an optical fibre.

The problem of the non-uniform distribution of the emitted light from the wedge-type light extractor for sheet light guides can be overcome by using the more complicated geometry of the "Scimitar" light extractors, here illustrated in Figure 6.14. These rapid prototypes were made by *Arrk Australia and New Zealand Pty Ltd* from *SolidWorks*® models (*Dassault Systèmes SolidWorks Corporation*) created at my direction by Fluorosolar Systems Ltd. Ray tracing with *Zemax*® gave a theoretical extraction efficiency of 99.2% and a light pattern uniformity factor (defined as the ratio of the standard deviation of the output signals detected in the forward direction, above, below, to the left and to the right of the light extractor) of 95.7%. Dr Alan Earp at FSL measured the extraction efficiency of the light extractor for the green LSC as approximately 99%. His photograph of the output of an extractor coupled to a green LSC illuminating a white screen is shown in Figure 6.14. The measured light distribution was significantly more uneven than for the ray tracing calculations, with the difference believed to be due to inaccuracies in the rapid prototype.

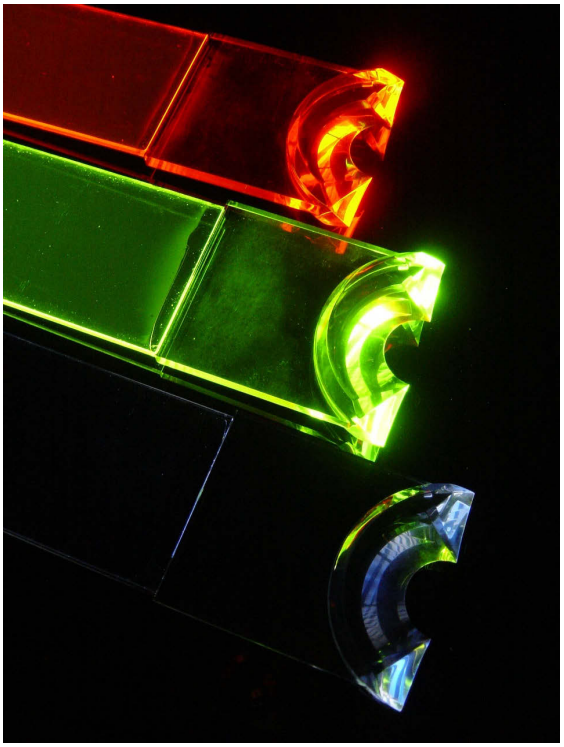

QuickTime™ and a
decompressor
are needed to see this picture.

[Production Note: This figure is not included in this digital copy. The print copy of the thesis is available for consultation at UTS Library.]

Figure 6.14 "Scimitar" light extractors made by *Arrk*® (left) with the observed output for the green LSC illuminating a white screen (right).

For optical fibres an excellent design is the hollow cone extractor illustrated in Figure 6.15. By including an axial hole in the initial cylindrical section the maximum wall thickness is reduced to less than one quarter of the diameter of the optical fibre. For an 18 mm fibre with a 2 mm axial hole the maximum thickness is 4 mm. This is small enough to permit low cost production by injection moulding. Including the axial hole reduces the measure and modelled extraction efficiency to about 95%, but this is an excellent trade off. By adjusting the dimensions of the cone it is possible to achieve a very uniform light distribution over a wide range of angles.

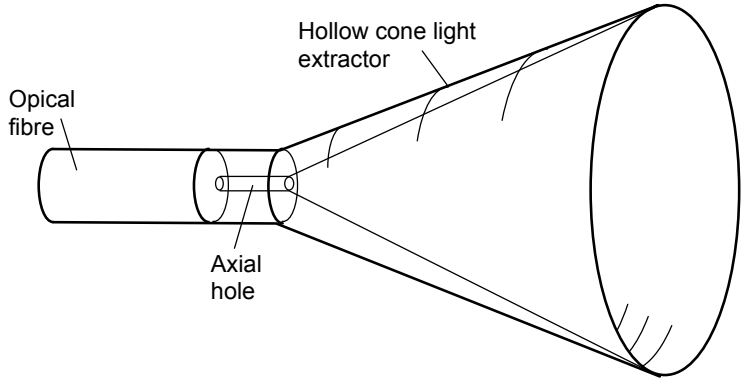

Figure 6.15 Hollow cone light extractor.

The strengths, weaknesses and extraction efficiency for the various types of light extractor are summarized in **Table 6-2**.

Table 6-2 Comparison of Different Types of Light Extractor

Type	Strengths	Weaknesses	Extraction Efficiency
Simple increase in cross sectional area		Bulky and hard to mass produce	< 50%
Roughened light guide	Simple to manufacture	Does not extract low angle light	43%
TRIMM block or cylinder	Excellent visual appearance	Angular distribution set by RI of microparticles	90%
Diffuse white light trap	Simple to manufacture	No control over light's angular distribution	86%
Wedge	• Simple to make • Very high efficiency	Light distribution is strongly forward peaked in twin beams	Almost 100%
Cone with cylindrical entry	• Simple to make in small quantities • Useful for system testing	Light distribution is strongly forward peaked	Almost 100%
"Scimitar" for flat light guides	Good angular distribution	Bulky and hard to mass produce	99%
Hollow cone	Excellent angular distribution that can be readily tailored	Somewhat delicate edge	95%

7 LIGHT TRANSPORT IN LSC SHEETS

7.1 INTRODUCTION

In earlier chapters we have explored the physics of luminescent solar collector systems including: the fundamental limitations of étendue that require the use of high aspect ratio collector sheets (sections 3.1 and 3.2), methods for coupling rectangular cross-section collector stacks to optical fibres for long distance light distribution into buildings (chapter 4), and methods for extracting trapped light to increase useful luminous output (chapter 6). Up until this point, we have essentially treated LSC sheets as a "black box" that absorbs sunlight and emits concentrated fluorescent emission along one edge. However, the collector sheets are the heart of any LSC and the system's luminous output is proportional to their efficiency. Accordingly, the next four chapters will explore the physics and some the chemistry of LSC sheets. This chapter will discuss the details of light transport in LSC sheets. Chapter 8 then describes how collector sheets are made and testing methods for ensuring their high optical performance. Chapter 9 explores extinction mechanisms in LSC sheets and chapter 10 then goes on to describe the problem of long-term photodegradation in LSC sheets and its impact on system performance.

Maximising transport efficiency of light within the collector sheets is essential because on average useful fluorescent emission has to travel a considerable distance to the collection edge. Transport efficiency always involves dependence on sample dimensions, in our case length being the main factor. A noteworthy feature of LSC systems is that their output (unlike most solar collector systems) does not scale linearly with collection area. In other words, net LSC output is not a linear function of area or length. However, the higher the transport efficiency, the larger the useful area, and hence the higher the luminous output. Furthermore we often find that output usually stabilises if length is increased too much. Hence actual transport efficiency determines the optimum length for maximum output.

For lighting applications of LSC's, the key performance parameter for the collection sheets is their lumens-to-lumens efficiency (lumens at collection edge divided by incident solar lumens). In this chapter, LSC performance is here described mainly in terms of lumens-to-lumens efficiency and total lumen transport loss within the LSC (see section 2.2 for a discussion of LSC's used for photovoltaic applications). Modelling that takes account of individual photon processes is presented in section 7.2, while the efficiency and transport parameters describing total visible spectral performance are discussed in section 7.4.

In order to optimise the luminous output of an LSC, it is important to distinguish between dye-related losses and losses intrinsic to the as-produced undoped matrix. In this chapter, the

emphasis is on the characterisation of dye-related loss processes and their effect on performance. Because the luminous output from an LSC depends both on the absorption and emission spectra of the dye, finding the optimum dye concentration is a central aspect of the maximisation of the light output.

As noted in chapter 2, the main impact of dye concentration on loss is due to self-absorption. Self-absorption occurs when the dye's extinction and emission bands overlap (see Figure 2.1 which shows the absorption and emission spectra for the green fluorescent dye *Lumogen*® F083). Hence if some emitted photons are re-absorbed, two factors must be considered: (a) the resulting shift in the output spectrum, and (b) the resulting loss from those output photons no longer trapped by TIR. Self-absorption is the main component of dye related extinction before outdoor exposure, but the possibility of scattering linked to the addition of the dye cannot be ignored. Clustering of dye molecules may induce weak scattering losses. Total extinction as a function of wavelength can be determined by measuring the specular transmittance, which is reduced by absorption and any scattering. The relative importance of absorption vs scattering will be explored in chapter 9.

Dye related photodegradation can also cause additional absorption and this will be discussed in chapters 9 and 10. For this chapter, we will largely restrict our attention to extinction processes in as-prepared LSC sheets.

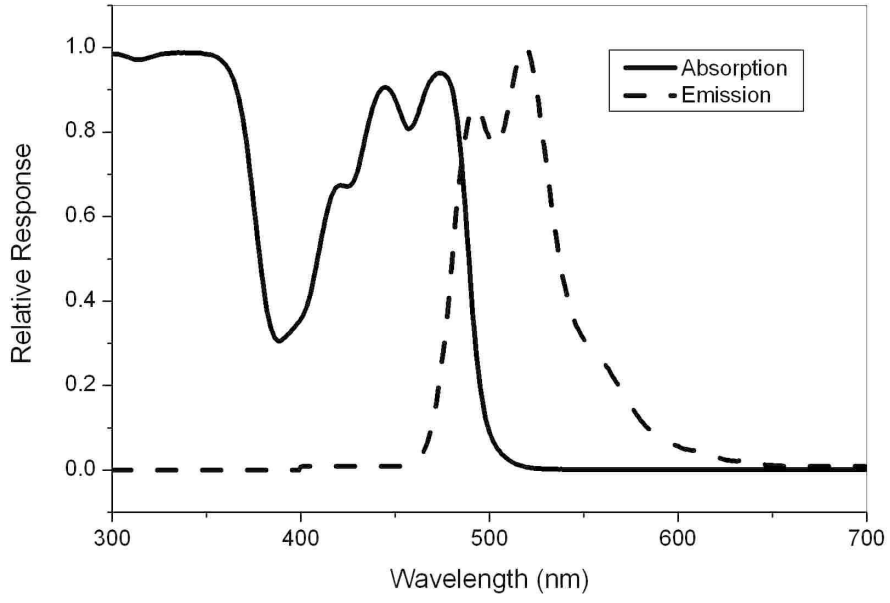

Figure 7.1 Absorption and emission spectra of the green fluorescent dye *Lumogen*® F083 at 60 ppm.

Attenuation that is independent of the dye concentration may arise from scattering losses due to impurities in the matrix, surface and edge roughness, or variations in the flatness of the LSC sheet. Because scattering should vary slowly with wavelength over the emission band, the

effect on output spectra will be small, but it does reduce the number of output photons. These matrix losses can quite significantly limit the light output of an LSC (Thomas, Drake & Lesiecki 1983a). If the dye is mono-molecularly dispersed, scattering sources are expected to be confined to those in the clear polymer matrix. The most likely source of attenuation in the emission band largely clear of the transition zone ($\lambda > 520$ nm in Figure 2.1) is from the very weak tails of the absorption band, which vary slowly with wavelength. In most early work, data similar to Figure 2.1 was collected from samples a few millimetres thick. While these tails may appear to be very small in such data, our models using transmittance data on much thicker samples indicate that they are in fact very important.

In an earlier paper (Swift, Smith & Franklin 1999a) we underestimated the potential practical output for the collector because the non dye-related losses were over-estimated. Treating the measured fall off in output for long collectors as due to scattering, this light loss was attributed predominantly to matrix losses. However, the analysis presented in this chapter and chapter 9 shows that this loss is in fact mainly due to previously neglected impacts of dye-related loss. Assuming non dye-related losses are constant for a given matrix, dye-related losses can be minimised by careful selection of dye concentration. One of the primary aims of this work is to find the optimum dye concentration to promote a high level of light output by minimising dye-related attenuation while maintaining satisfactory absorption. The light collected from a stack of coloured LSC's can then be coupled to a flexible light guide and transported over several metres, giving effective natural room lighting in areas where natural sunlight is not readily available (Earp et al. 2004b).

7.2 MODELLING OF LSC OUTPUT

The luminous output of an LSC can be theoretically modelled, using the spectral absorption and emission spectra of the dye (Swift, Smith & Franklin 1999a). This section builds upon that work and takes the opportunity to recast the mathematics into standard coordinates and to include a number of small effects that were neglected in the original study. The improved theory and the experiments described below formed the basis for a patent on methods for optimising the dye concentration of an LSC sheet (Franklin & Smith 2004a).

We start by considering the emission of a single dye molecule in a rectangular light guide of refractive index, n, length, L, width, w and thickness, t, with the dye molecule distance, l, from the collection edge (as shown in Figure 7.2). We will use standard spherical coordinates with angular co-ordinates ϕ and θ as illustrated. This is a different coordinate system to earlier chapters. So for the sake of clarity, for this chapter we denote the critical angle of the matrix by χ rather than θ_{crit}.

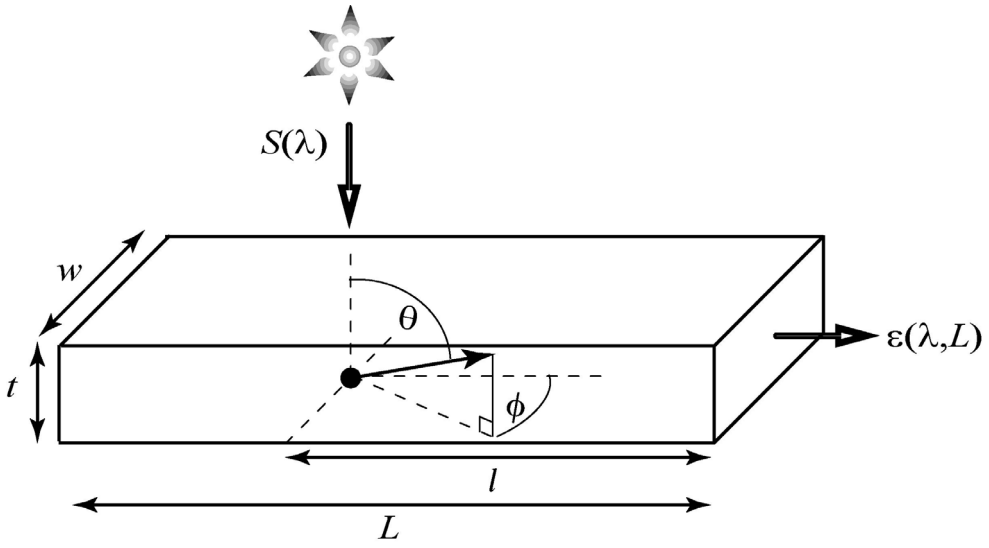

Figure 7.2 Luminescent Solar Concentrator of length L, illuminated by source $S(\lambda)$, produces end emission $\varepsilon(\lambda,L)$ at collection edge.

For a ray of trapped light, reflection off the top and bottom surfaces changes the sign of θ but leaves the magnitude of θ unchanged. Similarly, reflection off the side surfaces changes the sign of ϕ but leaves the magnitude of ϕ unchanged. Thus the distance travelled by a particular ray emitted from the dye molecule before it reaches the collection edge is $l/\sin\phi\cos\theta$. This ray will be attenuated by the combined effects of the matrix, the light guide geometry and the dye which have attenuation constants of $\alpha_m(\lambda)$, $\alpha_g(\theta,\phi, l)$ and $\alpha_d(\lambda)$ respectively. The attenuation of the polymer matrix is here assumed here to be independent of wavelength (this assumption is relaxed in chapter 9).

Deviations of the light guide from the ideal geometry (perfectly smooth surfaces, constant thickness, parallel sides, sides normal to the top surface, etc) cause attenuation $\alpha_g(\theta,\phi, l)$ (the l dependence arises primarily from local variations in surface quality and sheet thickness). In a properly manufactured sheet with diamond polished edges, α_g is almost constant and is of the order of 1% m^{-1}, and so can be neglected. However, as discussed in section 2.3.2, deviations in thickness in poorly cast sheets can cause geometric losses of a few percent. It will also be shown in section 8.5 and section A.4 of Appendix A that using flame polishing or mechanical polishing for the edges rather than diamond polishing leads to large geometric losses (see also (Earp et al. 2004c)).

The dye-related loss coefficient at the nominal dye concentration, $\alpha_d(\lambda)$, also includes any effects of dye-photodegradation. The variation of $\alpha_d(\lambda)$ with dye concentration is discussed in section 7.5.1 while the effects of photodegradation on the dye-related losses form the basis for chapters 9 and 10. However, for a given sheet at a particular time we can treat $\alpha_d(\lambda)$ as a quantity that varies only with wavelength.

Let the fluorescent dye have an emission power spectrum $\varepsilon_o(\lambda)$ (with SI units W m^{-2} nm^{-1}, at wavelength λ where the subscript "o" denotes the "original" spectrum of emitted radiation prior to encountering other dye molecules). The spectral intensity at the collection edge of the collector resulting from the illumination of the sheet by an external source is,

$$\varepsilon(\lambda, L) = \frac{\varepsilon_o(\lambda)}{\int \varepsilon_o(\lambda')d\lambda'} \frac{2E_e}{\pi wt} \frac{1}{L} \int_0^L dl \int_{\chi}^{\pi/2} \sin\theta d\theta \int_0^{\sin^{-1}\left(\frac{\cos\chi}{\sin\theta}\right)} \exp\left(\frac{-[\alpha_d(\lambda)+\alpha_m(\lambda)+\alpha_g(\theta,\phi,l)]l}{\sin\theta\cos\phi}\right) d\phi \quad (7.1)$$

where E_e is the total power emitted by the dye molecules. With the simplifying assumptions for the matrix and geometric attenuation constants described above, for most purposes we can simplify equation (7.1) to

$$\varepsilon(\lambda, L) = \frac{\varepsilon_o(\lambda)}{\int \varepsilon_o(\lambda')d\lambda'} \frac{2E_e}{\pi wt} \frac{1}{L} \int_0^L dl \int_{\chi}^{\pi/2} \sin\theta d\theta \int_0^{\sin^{-1}\left(\frac{\cos\chi}{\sin\theta}\right)} \exp\left(\frac{-(\alpha_d(\lambda)+\alpha_m)l}{\sin\theta\cos\phi}\right) d\phi \quad (7.2)$$

For the case in which sunlight at normal incidence with spectral intensity $S(\Psi)$ is distributed uniformly over the top surface of the collector (with area wL and front surface reflectance R_c), the total power emitted by the dye molecules E_e is given by

$$E_e = wL(1-R_c)\int (1-e^{-\alpha(\Psi)t})S(\Psi)\eta_e(\Psi)d\Psi \quad (7.3)$$

which is the sum of the absorbed energy at each incident wavelength Ψ multiplied by the energy-to-energy conversion efficiency of the dye $\eta_e(\Psi)$,

$$\eta_e(\Psi) = \eta_{quant}\frac{\langle\lambda\rangle}{\Psi} \quad (7.4)$$

where η_{quant} is the ratio of emitted photons to absorbed photons, Ψ is the wavelength of the incident photon and $\langle\lambda\rangle$ is the average wavelength of photons emitted by the dye molecule, defined as

$$\langle\lambda\rangle = \frac{\int \lambda\varepsilon_o(\lambda)d\lambda}{\int \varepsilon_o(\lambda)d\lambda} \quad (7.5)$$

If the incident light is not normal but has an angle of incidence of θ_i, then equation (7.3) must be modified by replacing the sheet thickness, t, with the path length of the incident light in the LSC sheet, $p(\theta_i)$. From Snell's Law,

$$p(\theta_i) = \frac{t}{\cos\left[\sin^{-1}\left(\frac{\sin\theta_i}{n}\right)\right]} \tag{7.6}$$

However, this added complexity is seldom necessary because: (i) the sheet is optically thick enough at most of the wavelengths of interest so an increase in path length adds little to the fluorescent emission; and (ii) the operation of Snell's Law means that $p(\theta_i)/t < \sec\chi$. For PMMA (n = 1.49) this means that $1 \le p(\theta_i)/t < 1.35$.

In equation (7.3) there is also a dependence of the front surface reflectance, R_c, with the angle of incidence. However, for PMMA R_c is only 3.9% at normal incidence and is almost constant up to angles of incidence of 60°. Thus for most purposes equation (7.3) is an adequate approximation for non-normal incidence.

In the experiments described in section 7.3, the LSC has the dimensions L = 1200 mm, w = 135 mm and t = 2.0 mm. Sunlight is collected on the largest face, absorbed by the dye and emitted isotropically. The emitted light either undergoes total internal reflection, leaves the collector through one of the surfaces or it is absorbed by another dye particle and re-emitted. Without total internal reflection, the random emission angle from the dye would give the same amount of fluorescent emission per unit area exiting each surface. However, as discussed in section 3.1.2, due to total internal reflection a large fraction of rays are directed towards the smaller surfaces, such that the surface with the smallest area has the largest concentration of light rays. Hence the luminous output is measured at one of the small edges (135 mm × 2.0 mm), which is called the collection edge. In principle, all light reaching the collection edge can be extracted. Chapter 6 showed that practical light extractors can have a very high efficiency and only a weak dependence on θ and ϕ. Accordingly, the theoretical model of this chapter assumes that the light extraction efficiency has a constant value of 100%.

LSC light output and hence performance can be improved by increasing the amount of light absorbed by the dye. This can be achieved by having the large bottom face over a highly reflective surface, or by increasing the dye concentration. However, the use of a reflector allows a higher total absorption with less dye, which in turn improves transport properties (Franklin & Smith 2004a; Smith & Franklin 1996; Smith & Franklin 1998; Smith & Franklin 2000). Thus overall output is higher using the reflector, which can be either a separate specular mirror or a diffuse white reflector. Specular mirrors can be metal based, but recently special all-dielectric structures with exceptionally high reflectance have been used with LSC's (Slooff, Burgers & Debije 2008).

The reflective surface must not be in direct intimate contact with the collector sheet as this would greatly reduce total internal reflection transport efficiency. The typical ray averages

over 150 reflections from the bottom surface. So a specular reflectivity of 90% for a reflector in intimate contact with the bottom surface would lead to a forward transfer coefficient of less than $0.90^{150} = 1.4\text{x } 10^{-7}$, i.e. a catastrophic loss of light. Even with a specular reflectivity of 99%, the output is reduced by least 78%. Thus it is essential with most mirrors to have an air gap between the reflector and the LSC sheet.

For simplicity in modelling, we have neglected the losses at this reflector. Reflectance from the mirror is taken to be specular, so t in equation (7.3) becomes $2t$, increasing the absorbed energy. The total error in E_e in this approximation is typically below 1.0%, since for a typical LSC it is a small error in a contribution that is of order 10% for violet and green sheets and less than 30% for a pink or red sheet. For a diffuse reflector one should apply equation (7.6) to equation (7.3).

The fraction of emitted rays collected can also be significantly increased by attaching a specular reflector in intimate contact with the small edge opposite the collection edge. This mirror enables the collection of some of the rays originally travelling away from the collection edge. If there was no attenuation in the LSC sheet, a perfect mirror would double the systems luminous output. Gains approaching the mirror reflectivity can be achieved with short LSC's. However, the long LSC's required for practical daylighting have significant extinction for internal light and the practical boost for these systems is about 45%.

7.3 Spectral Shift Due to Self-Absorption

Self-absorption by the dye molecules has a considerable impact on both the spectrum and total luminous flux output from a LSC sheet. In this section the spectral output of LSC sheets are measured experimentally and compared with spectra using the theory outlined above. Section 7.4 then examines the luminous flux from LSC's.

7.3.1 Experimental

The dyes investigated in this work were *Lumogen*® F300 (red) at a concentration of 40 ppm, *Lumogen*® F083 (green) at 70 ppm, and *Lumogen*® F570 (violet) at 140 ppm. These well-known dyes are commercially available from *BASF*, and have good photostability. Their quantum efficiencies are respectively 0.96, 0.91, and 0.92 (Seybold & Wagenblast 1989).

For this study, LSC's were produced from 2.0 mm thick cast PMMA sheets. Since we required the collector sheet's long axis to be at least one metre in length, the sample had to be obtained from a commercial supplier in Spain. Their casting solution involves pure pre-polymer and fully dispersed dye. Initial polymerisation takes place in a temperature controlled water bath, followed by an extended air anneal to ensure residual monomer levels are below 0.5%. LSC samples with dimensions of 1200 mm x 150 mm x 2.0 mm were produced by cutting

sections from the master sheets and diamond polishing the four thin edges with a diamond polisher (*C.R. Clarke 1550)*. Samples for emission measurements were produced with all edges diamond polished and dimensions of 40 x 20 x 2.0 mm.

The emission spectra were measured using a *Perkin Elmer LS 50* fluorescent spectrophotometer. The diamond polished edge of the sample was placed so that its normal was normal to the excitation beam and in a position such that approximately half the width of the excitation beam did not pass through the sheets. This arrangement allowed the measured spectra to be not affected by self-absorption — this was confirmed by observation that the spectrum did not vary with the dye concentration. The absorption spectra were measured using a *Cary 5E* UV-Vis-NIR spectrophotometer.

The spectral output of the 1200 mm long LSC sheets was measured using the *Perkin Elmer LS 50* fluorescent spectrophotometer. The sheets were illuminated in room light and light from the collection edge of the FPC fed into the fluorescent spectrophotometer via an optical fiber.

7.3.2 Results and Discussion

The measured dye emission spectra, dye absorption spectra and the measured output spectra for 1.2 m long LSC sheets doped with the three *Lumogen*® dyes are shown in Figure 7.3. Theoretical output spectra calculated using equations (7.2) to (7.5) are also plotted. The agreement between the calculated and measured spectra for each of the LSC sheets is very close. The noisy nature of the calculated spectra is due to the noise in the measured absorption spectra — small variations in the measured transmission in a 2.0 mm thick sample give rise to large variations of the calculated spectral output since light travels through an average distances of approximately 700 mm. It is noteworthy that there are considerable shifts in the colour of the output spectrum as compared to that of the dye for each of the LSC sheets. In the cases of the violet and green sheets, the self-absorption leads the spectrum being shifted toward the peak sensitivity of the eye, so that there is an increase in the luminous efficacy of the spectra.

QuickTime™ and a
decompressor
are needed to see this picture.

[Production Note: This figure is not included in this digital copy.
The print copy of the thesis is available for consultation at UTS Library.]

Figure 7.3 Measured spectra of dye absorption (**- - -**) and dye emission (⋯⋯) along with the associated measured (—) and calculated (**—**) emission spectra for a 1.2 m LSC for: (a) *Lumogen*® F300 (red), (b) *Lumogen*® F083 (green), and (c) *Lumogen*® F570 (violet). The measured spectra are normalized and the calculated spectra are fitted by eye.

7.4 LIGHT TRANSPORT PERFORMANCE

7.4.1 Assessing Sheet Quality for Lighting

Up to this point, we have been using radiometric quantities (which is the appropriate tool for LSC's used for solar cells). In order to calculate the illumination performance of the LSC, we now need to introduce photometric quantities. In ordinary operation, the top surface of the LSC is uniformly illuminated by sunlight, producing a luminous flux F_L, at the collection edge.

$$F_L = \kappa \int \varepsilon(\lambda, L) y(\lambda) \, d\lambda \tag{7.7}$$

where $\kappa = 683$ lumens per Watt is the standard photometric conversion factor and $y(\lambda)$ is the standard photoptic response of the human eye.

The quality of an LSC sheet for daylighting applications is assessed via two key parameters: luminous output (or lumens-to-lumens efficiency) and half-length. For optimum performance each of these parameters should be maximised for a given size collector. A useful parameter for characterization of an LSC daylighting system is the lumens-to-lumens efficiency $\eta_{l\text{-}l}$, defined as follows:

$$\eta_{l-l} = \frac{F_L}{I_{sol} w L} \tag{7.8}$$

where F_L (as defined in equation (7.7)) is the luminous power leaving the LSC sheet at the collection edge, I_{sol} is the solar luminous intensity (in lux) incident on the top surface of the collector. In earlier work (Earp et al. 2004b; Earp et al. 2004c; Swift, Smith & Franklin 1999b) we called this term "light-to-light efficiency". However, that term is more appropriate for the radiometric quantities used in photovoltaic LSC theory, rather than for LSC systems used for daylighting.

Lumens-to-lumens efficiencies ranging from 5-10% are predicted in our computations for the material geometry described and practically achievable material properties. This translates to around 1100-1200 lumens in clear sky conditions, which is sufficient for indoor lighting. From equations (7.1), (7.3) and (7.7) it is seen that F_L is proportional to the collector area, $w \times L$, however it also depends on L via the integral in equation (7.1), resulting in a strong dependence of $\eta_{l\text{-}l}$ on L.

If dye absorption is high, the transport efficiency of the fluorescent sheet makes the most significant impact on LSC performance. While measurement of total output under solar illumination is the central performance parameter, it is useful to have a light transport efficiency parameter that can be measured in a simple experiment under fixed conditions. Thus a simple measurement scheme has been devised, with an associated parameter known as the LSC sheet's half-length, $L_{½}$, which gives a useful guide to the light transport efficiency. $L_{½}$ is the transport distance over which the emitted light intensity falls by 50%. This parameter can be very useful in quality control and for comparison of the transport efficiency of different LSC samples. Since it can be predicted theoretically, it provides an additional test of the basic models, as demonstrated in section 7.4.3.

7.4.2 Measurement of $L_{½}$

Figure 7.4 shows the arrangement used to determine $L_{½}$ experimentally. The LSC sheet was illuminated with a small fluorescent lamp orientated parallel to the collection edge at a distance *l.* In order get a well-defined value of *l,* and to minimise stray light, the lamp had an opaque housing (not shown) with a 10 mm wide slit parallel to the sheet's collection edge. The interior of the lamp housing was lined with a 99% reflective film to maximise the lamp's output. Stray light from the lamp was minimised by covering it with a black cloth (not shown).

In an effort to ensure that any light leaving the bottom surface of the collector did not re-enter the collector, the fluorescent sheet was placed on top of a clear PMMA sheet, which in turn lay on top of a sheet of black cardboard. (In subsequent work, it was found that using a single sheet of black PMMA (*Plexiglas*®) gave slightly improved results.)

Reflectance from the back edge of the fluorescent sheet was removed by placing black tape nearby on the top surface, as shown in the diagram. A 500 mm diameter integrating sphere was used to measure the luminous output of the collection edge when the LSC sheet was illuminated at a range of *l* values from 100 mm to 1100 mm. Thus luminous output could be recorded as a function of *l*, excluding the first and last 100 mm of the sheet.

In order to minimize stray light, a small back cloth (not shown) was placed around the integrating sphere's entrance slit. A baffle was used inside the integrating sphere to ensure that the detector only picked up light scattered inside the sphere and that all direct emission was excluded from the measurement (eliminating direct emission greatly reduces sensitivity to the angular distribution of the emitted light). It was found that LSC sheet output falls off as an approximately exponential function of *l*, so the exponential slope, γ, can be used directly to calculate $L_{½}$, as described in the following section.

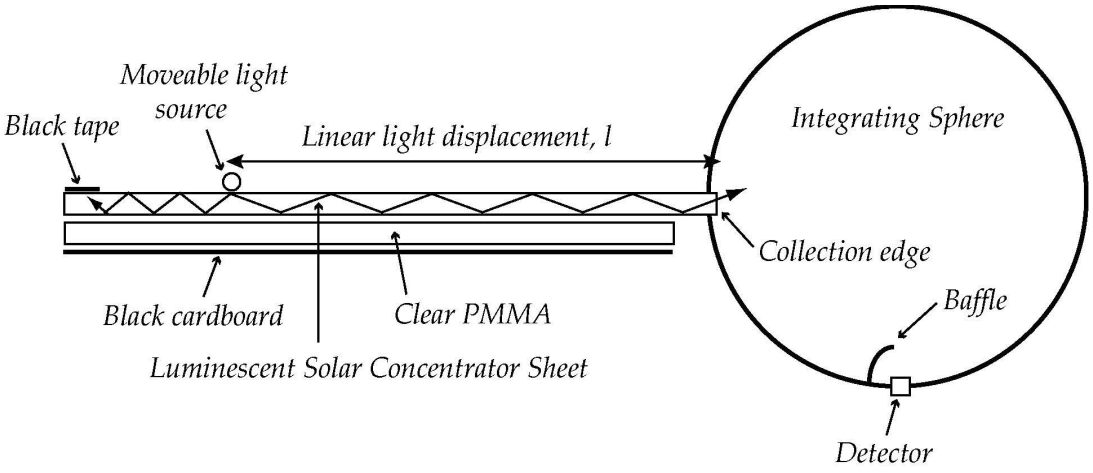

Figure 7.4 Experimental set-up for measurement of the half-length of an LSC.

7.4.3 Theoretical Calculation of $L_{½}$

By simulating the half-length experiment described above from first principles using transmission and emission data, we can model the behaviour of γ and $L_{½}$. These simulations help in defining $L_{½}$ from experiment and also test if our direct measurements of total attenuation are in accord with basic models. This output model is different from the radiant flux model mentioned in section 7.2, which assumes the LSC is uniformly illuminated over the whole of the top surface. In this case, the length integral is unnecessary, as the LSC sheet is now only illuminated at a single line spanning the width of the collector. Therefore, the emission power spectrum at the collection edge in equation (7.2) can be simplified to the following form:

$$\varepsilon(\lambda,l) \sim \varepsilon_o(\lambda) \int_{\chi}^{\pi/2} \sin\theta \, d\theta \int_{0}^{\sin^{-1}\left(\frac{\cos\chi}{\sin\theta}\right)} \exp\left(\frac{-(\alpha(\lambda)+\alpha_m)l}{\sin\theta\cos\phi}\right) d\phi \tag{7.9}$$

Thus the output lumens, F_l, at the collection edge of an LSC that is illuminated at a plane of constant distance l from the collection edge is given by simplifying (7.7),

$$F_l = \kappa \int \varepsilon(\lambda,l) y(\lambda) \, d\lambda \tag{7.10}$$

For modelling of the luminous output, F_l may be written approximately as an exponential function of l (as defined in Figure 7.2 and Figure 7.4) with

$$F_l \sim F_o e^{-\gamma(l)l} \tag{7.11}$$

where F_o is the (constant) intensity of the fluorescent lamp and $\gamma(l)$ is the wavelength and path length averaged attenuation parameter since it includes the full emission spectrum and all paths that would allow light to exit through the collection edge. (From section 6.4 we see that this is approximately 1/8 of all fluorescently emitted light in the experiment described in section 7.4.2). Thus using equations (7.9) and (7.10), F_l (which is equivalent to the output measured in the half-length experiment) is calculated as a function of l, and a modelled value of $\gamma(l)$ may be obtained from the slope of a plot of log (F_l) vs. l. The effects of l on γ are discussed in more detail in section 7.4.4 where it is seen that γ can be considered to be a constant over a specified range of l values. Finally, the loss coefficient γ is standardised to a set range of l values, and used to calculate the half-length parameter $L_{½}$.

$$L_{½} = \frac{\ln 2}{\gamma} \tag{7.12}$$

Now the decay is actually not a simple exponential decay since many paths and wavelengths contribute to output in equation (7.9) via integral sums over wavelength dependent

attenuation and the many path lengths defined by (θ, ϕ, l) at a given l. Thus for collector modelling and design, rigorous quality control, and especially extraction of the matrix or scattering component of total output, a more detailed analysis of the theory behind output vs. l data is needed. In brief, (7.9) leads to γ and half-length as a slowly changing functions of l. Hence if $L_{½}$ is to be quoted as a quality control measure, then a fixed l range and precisely specified data collection and analysis must be applied. This topic is considered in more depth in section 7.4.4.

In order to separate the dye-related, matrix-related and geometric attenuation of light in an LSC, $L_{½}$ can be broken down into three components to account for the various processes. The matrix component $L_{m½}$ accounts for losses intrinsic to the matrix, including absorption, internal scattering from impurities and total internal reflection losses from rough surfaces or edges. The dye-related loss component $L_{d½}$, accounts for losses due solely to the dye, including self-absorption and scattering from clustered dye molecules. The small geometric component, $L_{g½}$, accounts for losses due to deviation of the light guide from the ideal geometry (perfectly smooth surfaces, constant thickness, parallel sides, sides normal to the top surface, etc).

From equations (7.1), (7.9) and (7.11) it is clear that the components add inversely and

$$\frac{1}{L_{½}} = \frac{1}{L_{m_{½}}} + \frac{1}{L_{d_{½}}} + \frac{1}{L_{g_{½}}} \tag{7.13}$$

Although $L_{½}$ itself is not directly substituted into the theoretical model, the subdivision of $L_{½}$ into dye-related, matrix-related and geometric components does enable these losses to be addressed separately. Dye related losses vary with wavelength and are described by the measured extinction coefficient $\alpha(\lambda)$ in equation (7.9). The matrix related loss coefficient, α_m, is assumed to be independent of wavelength and is thus linked directly to $L_{m½}$, which can be calculated using (7.12) with a loss coefficient $\gamma = \gamma_m = \alpha_m$. In *high quality* sheets with diamond polished edges, the measured geometric attenuation, α_g, is almost constant and is of the order of 1% m^{-1} with a corresponding half-length of close to 70 m. This is so large in comparison to the matrix and dye-related half-lengths that geometric losses can usually be neglected and will be omitted from the rest of this chapter.

Half-length data is not only useful for direct quality control but also to help refine the key parameter α_m (or γ_m). Given the sensitivity of output to small changes in $\alpha(\lambda)$ (to be discussed in section 7.5), the ability to estimate α_m from two distinct types of measurements is of considerable value. For the practical design of LSC's, half-length is often the key design parameter. In particular, it will be shown in section 7.6 that there is little to be gained in luminous output by increasing the size of the collector sheets much beyond one half-length.

7.4.4 Experimental and Theoretical $L_{½}$ Results

For this study, LSC's were produced from 2.0 mm thick cast PMMA sheets containing *Lumogen*® F083 fluorescent dye at a concentration of 60 ppm. The samples were custom manufactured by a commercial supplier in Japan who was selected after extensive negotiations and several on-site visits. A different supplier was used to that used for the spectral studies in section 7.3 as it was felt that the Spanish sheets had an inferior matrix. The Japanese manufacturer's casting solution involves starting with a very pure pre-polymer and dye dispersed by the methods described in section 8.3. Initial polymerisation took place in a temperature controlled water bath, followed by an extended anneal to ensure residual monomer levels are below 0.5%. LSC samples with dimensions 1200 mm x 150 mm x 2.0 mm were produced by cutting sections from the master sheets and diamond polishing the four thin edges with a diamond polisher (*C.R. Clarke 1550)*.

The luminous output of a 1.20 metre-long green LSC was measured as a function of linear displacement l over the range 0.1 m < l < 1.1 m. These measurements are represented in Figure 7.5 by the triangular data points. Note that the graph has a logarithmic scale for luminous output, so an exponential function with a constant exponent would plot as a straight line.

Using equations (7.9) and (7.10), the same luminous output was also simulated as a function of l, over the range 0.1 m < l < 2.0 m. The larger length range was used to simulate light rays with longer path lengths within the 1.2 m long collector. In an LSC sheet equipped with a specular end mirror, some photons emitted near the collection edge may traverse the length of the sheet and reflect off the end mirror before returning to the collection edge, experiencing a linear displacement of around 2 m. Light rays with a greater displacement than the length of the collector cannot be measured separately, but their related loss coefficient may be estimated using the theoretical model. These simulated results for a standard matrix with matrix half-length $L_{m½}$ = 5 m are represented by the solid curve in Figure 7.5.

One of the chief aims of this study is to distinguish between dye-related and non-dye related losses in LSC sheets. This is made possible by separating the two dominant loss components in the model (geometric losses can usually be ignored). Hence the contribution of matrix losses can be extracted to theoretically predict the performance of an LSC with a perfect non-scattering matrix. In the model this corresponds to an infinite matrix half-length, approximated here by $L_{m½}$ = 10,000 m. Theoretical output for the same green LSC as above, but with a perfect matrix, is represented by the dashed curve in Figure 7.5.

For this investigation, the magnitude of the luminous output was of little interest – it is the slope γ that is required for calculation of $L_{½}$. The luminous output has arbitrary units, as the integrating sphere measurement is proportional to lumens by an undetermined calibration factor. The output is only an *approximately* exponential function of l: the slope actually varies slightly

over the course of 2.0 m. However, this slow variation of slope does give the basis for a useful standard "test" on sample lengths that are not too unwieldy for a laboratory bench. Test collector lengths are fixed at 1.2 m, as this is the size, or close to the size, of commercially feasible designs.

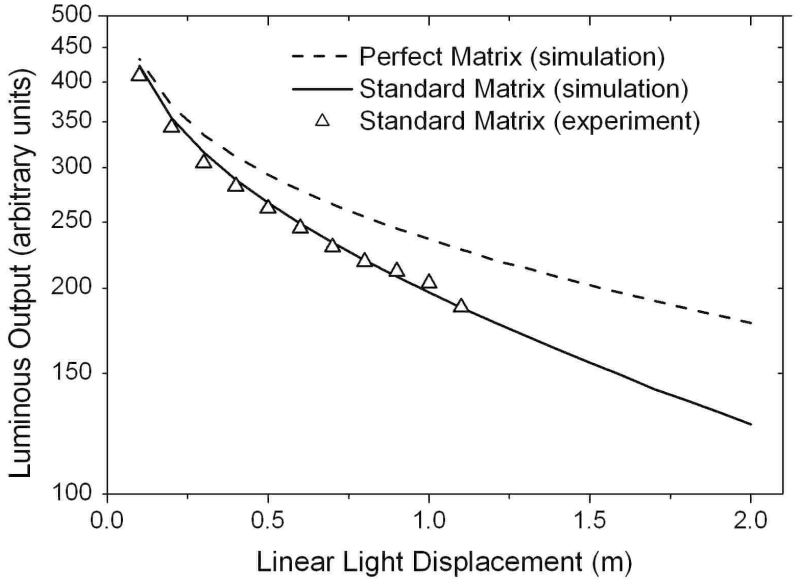

Figure 7.5 Luminous output as a function of length for a 1.2 m green LSC doped with 60 ppm *Lumogen*® F083. Here a perfect non-scattering matrix is compared with a standard matrix ($L_{m½}$ = 5 m).

As in the data shown in Figure 7.5, a reasonable "constant" γ fit can be obtained on samples 1.2 m long over the range 0.4 m to 0.9 m. A distance of about 0.3 m is required for light emitted in the main overlapping region between the absorption and emission spectra to be fully self-absorbed. Transport losses per unit length are thus high for $l < 0.3$ m. Hence the data in the region $l \leq 0.30$ m are excluded from the line of best fit. At the other end of the collector, the black tape on the top surface may not be sufficient to absorb all reflectance from the back edge (note that the reflectance of this surface is 3.8% for normally incident light but 100% for high-angle trapped light). Thus there is a slight overestimation of output lumens at the collection edge due to residual end reflectance, so the end region from 1.0 m to 1.10 m in the 1.20 m sample (represented by the two last triangle data points in Figure 7.5) is also excluded from the line of best fit.

Linear slopes have been fitted to the output curves ($R^2 > 0.99$), giving γ values for two separate regions. $L_{½}$ is then calculated by substitution into equation (7.12) (see Table 7-1). The experimental curve in the region $0.40 \leq l \leq 0.90$ m (with a slope of $\gamma = 0.58$ m^{-1}) corresponds to the approximately linear range from the experimental measurements for a 1.20 m sheet, and shows good correlation with the theoretical value of $\gamma = 0.59$ m^{-1} in this region. In the region $1.0 \leq l \leq 2.0$ m, output was theoretically modelled to give an estimate of $L_{½}$ for photons

reflected from the back edge mirror. The slope is smaller in this region ($\gamma = 0.44\ m^{-1}$) and the simulated $L_{½}$ value is longer because light remaining after these distances is confined to wavelengths of weak attenuation. Because of this $L_{½}$ has not reached the expected asymptotic limit (which is the value of $L_{m½}$), due to the effect of the weak absorption tails.

Table 7-1 Theoretical and experimental LSC half-length, $L_{½}$ (in metres), for a green LSC doped with 60 ppm *Lumogen*® F083. The sheet dimensions are 1200 x 135 x 2.0 mm. Results are shown for both a standard matrix ($L_{m½} = 5$ m) and a simulated perfect non-scattering matrix ($L_{m½} \approx \infty$), using γ values derived from the curves in Figure 7.5.

Collector Length Range (m)	**LSC Half-Length, $L_{½}$**		
	Experiment	*Simulation*	
	$L_{m½} = 5$ m	$L_{m½} = 5$ m	$L_{m½} \approx \infty$
0.40 – 0.90	1.20	1.17	1.61
1.00 - 2.00	–	1.58	2.48

7.5 Separating Dye and Matrix Effects

There are a number of variables involved in the design of an LSC system - perhaps the most significant are the choice of matrix material, the concentration of the fluorescent dye, and the dimensions of the collector. To optimise these parameters, LSC output was simulated using the model described in section 7.2 However, to ensure that appropriate values are used for the loss parameters in the model, dye-related and matrix-related losses must be separated. It is important to know if the dye is introducing any new scattering or loss processes over the whole emission band not present in the undoped matrix. At the extremely high accuracy levels needed to reliably predict performance, it will be seen that dye-related attenuation loss is difficult to directly measure from standard spectral data on thin samples.

By addressing dye and matrix related losses separately, LSC's can be studied to determine which source of loss has the greater impact on the light transport performance. The inability to easily separate dye and matrix effects can lead to errors. This led in earlier work (Swift, Smith & Franklin 1999a) to an underestimation of potential output since the measured half-length for $l > 0.30$ m was attributed entirely to matrix losses . It was assumed then that self-absorption losses vanished for the region $l > 0.3$ m. In section 7.6 where total output is examined under solar illumination, a reduction of matrix impact is thus required, since the measured half-length continues to be affected by the very weak tail of the dye absorption spectrum and possibly dye linked scattering in these good samples for $l > 0.3$ m.

7.5.1 Dye-Related Losses

Light loss from an as-produced LSC sheet can be attributed to both scattering and absorption. In general, scattering arises from the matrix and absorption losses arise from the dye, but doping the matrix with dye may induce additional scattering, even if the dye appears to be fully dispersed. The reader should keep in mind that the normal reabsorption/reemission process of the dye molecules, even in the case of 100% quantum yield, behaves like an inelastic scattering process. Every re-emission redistributes the propagation angles of light nearly isotropically over the whole solid angle (assuming that the dye molecules have random orientation). A fraction of the light is not guided and leaves the collector (see section 3.1.8 for details). The remainder is trapped in the collector and may be re-absorbed and re-emitted, resulting in longer average path lengths.

Dye-related losses are observed chiefly via self-absorption in the overlapping region between the dye attenuation $\alpha(\lambda)$ and emission $\varepsilon_o(\lambda)$ spectra (see Figure 2.1 and Figure 7.3). $\alpha(\lambda)$ consists of the dye absorption spectrum and possibly a very small wavelength-independent scattering component, and is calculated from transmission measurements made with a *Cary 5E* UV-Vis-NIR spectrophotometer. The fluorescent emission spectrum of the dye $\varepsilon_o(\lambda)$, was measured with a *Perkin Elmer LS50* Luminescence Spectrometer.

As self-absorption is the major cause of dye-related losses, the emission region is the most important region for studying the absorption losses. For the green dye studied here, the emission region is approx. 470 nm < λ < 600 nm, and most of the dye absorption is observed between 400 nm and 500 nm. In the 'tails', attenuation region above 550 nm the dye does not significantly absorb, and transmission is very close to unity. The very small, almost wavelength independent attenuation may be due to dye scattering, or to the slowly varying absorption tails. Because this region overlaps with the dye's emission peak, it has a large impact on output in the long LSC's needed for useful architectural illumination (it may be less important for short LSC's used for solar cells). This means that it must be carefully investigated.

The tails region of the green dye transmission spectrum in a 2.0 mm thick sample is shown in Figure 7.6, previously introduced as Figure 2.9 and reproduced here for the sake of convenience. The solid line represents the measured transmittance with the Fresnel reflectance removed. The dashed line is the same spectrum, except that the transmission in the 'tails region' beyond 550 nm has been artificially set to 100% as a reference. The attenuation of the dye in PMMA (excluding reflectance loss at the top and bottom surfaces) was determined by comparing measurements from dyed and non-dyed samples. With this method, these measurements are at the upper accuracy limit of the *Cary* spectrophotometer. Chapter 9 further investigations dye related scattering and evaluates the extent to which it affects the attenuation in the tails region, and hence overall LSC performance.

The spectra in Figure 7.6 are used in our models in section 7.6 to compare the effect of small changes in tails attenuation to the overall performance of the LSC.

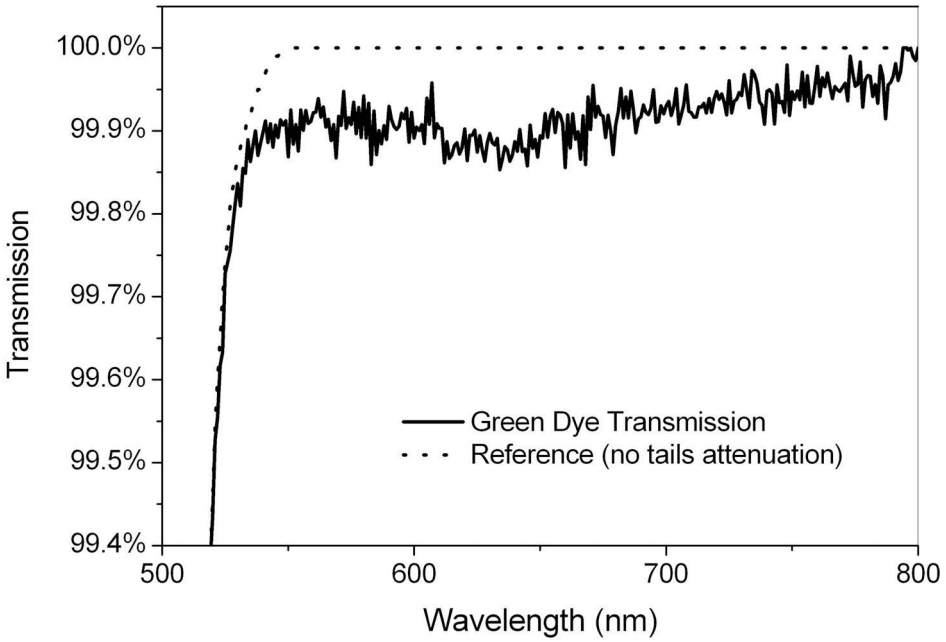

Figure 7.6 Transmission tails measured through a 2.00 mm thick LSC sheet doped with 60 ppm *Lumogen*® F083. The solid line represents the measured transmission of the green dye (excluding Fresnel reflectance), and the dashed line is the same spectrum, except that the transmission in the 'tails region' beyond 520 nm has been artificially set to 100% as a reference.

7.5.2 Matrix-Related Losses

A different approach to half-length measurement is needed for a clear matrix as there is no internal fluorescence to provide the light. $L_{m½}$ is also more difficult to measure, as it is much longer than $L_{½}$, so the attenuation per metre is considerably smaller. Attenuation measurements over different long lengths (up to several metres) of clear matrix material from the same batch are needed for this purpose. These accurate measurements have not been made for the samples discussed here, but some rough measurements indicate that $L_{m½}$ is between 5 and 10 metres, which is lower than expected. The clear matrix used in this study is not the best quality matrix available, so it should be possible to achieve much better half-length values with a better matrix.

In Figure 7.7 theoretical half-length values for the green LSC are shown as a function of dye concentration, with both a perfect matrix and a typical matrix half-length of 5 m, and with and without the presence of dye 'tails' attenuation beyond 520 nm. The model predicts that the half-length of a typical system increases two-fold if all matrix losses are removed. Matrix related losses could be reduced by careful material selection and manufacture, to minimise the extent of chemical and physical impurities. For minimal geometric losses, it is essential that all surfaces of the sheet are clean, smooth, flat and parallel. Thickness variations of up to 6% have

been observed in some samples, leading to 6% losses in output. Edge finish quality can also have quite a significant effect on $L_{½}$: the half-length of an LSC sheet can be doubled by diamond polishing the edges as opposed to mechanical polishing (Earp et al. 2004b). As a good clear matrix material is also used as a light guide, it should be manufactured with minimal scattering losses. With careful selection of chemicals and controlled production reactions, matrix absorption and scattering can be minimised, increasing the matrix half-length. All these factors must be considered for comprehensive optimisation of an LSC matrix.

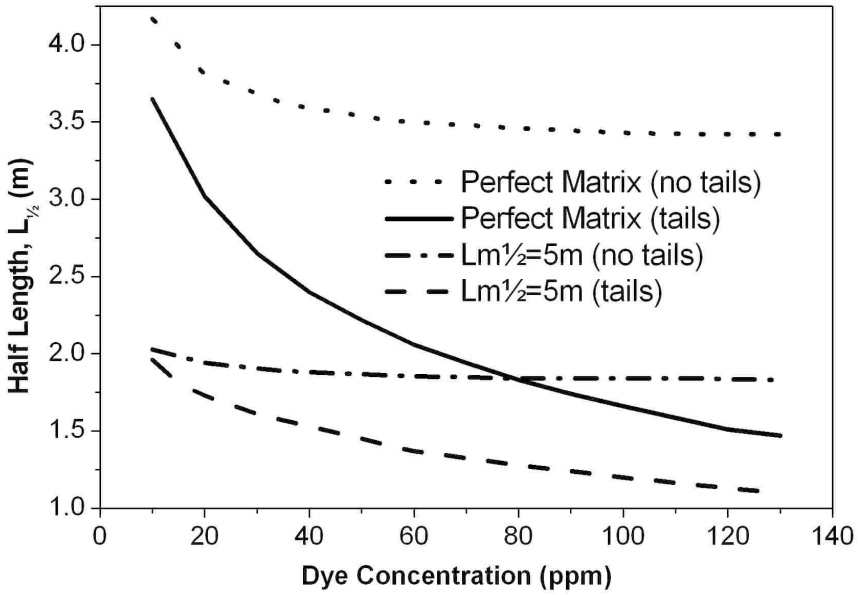

Figure 7.7 Theoretical half-length for a 1.2 m green LSC as a function of *Lumogen*® F083 dye concentration, for standard ($L_{m½}$ = 5 m) and perfect (non-scattering) matrices with and without tails attenuation.

7.6 Optimisation of Collector Properties

When designing an LSC system, dye concentration is important because it affects not only absorption but also total attenuation at each emission wavelength, which directly controls the light output of the LSC sheet (see Figure 7.8). Modelling using the absorption and emission data at various concentrations has shown that LSC luminous output is extremely sensitive to the very weak scattering and/or absorption in the 'tails region' of the attenuation spectrum. Hence $L_{½}$ is acutely dependent on dye concentration, as demonstrated by the much slower than expected approach to the asymptotic values of $L_{½}$ and γ in Figure 7.7. The spectral region up to around 550 nm causes the sharp fall off in γ up to l = 0.30 m (see Figure 7.5). This was expected, but the change beyond l = 0.30 m could not be explained simply by matrix effects. Finding $L_{½}$ by measurement is much easier than using spectral data on a thin sheet, which requires accuracy of better than one part in 10^4 to accurately predict output. The problems with the spectral

measurements described above lead to the development on the improved methods outlined in chapter 9. However, measuring half-lengths still has a place as a quick and simple technique.

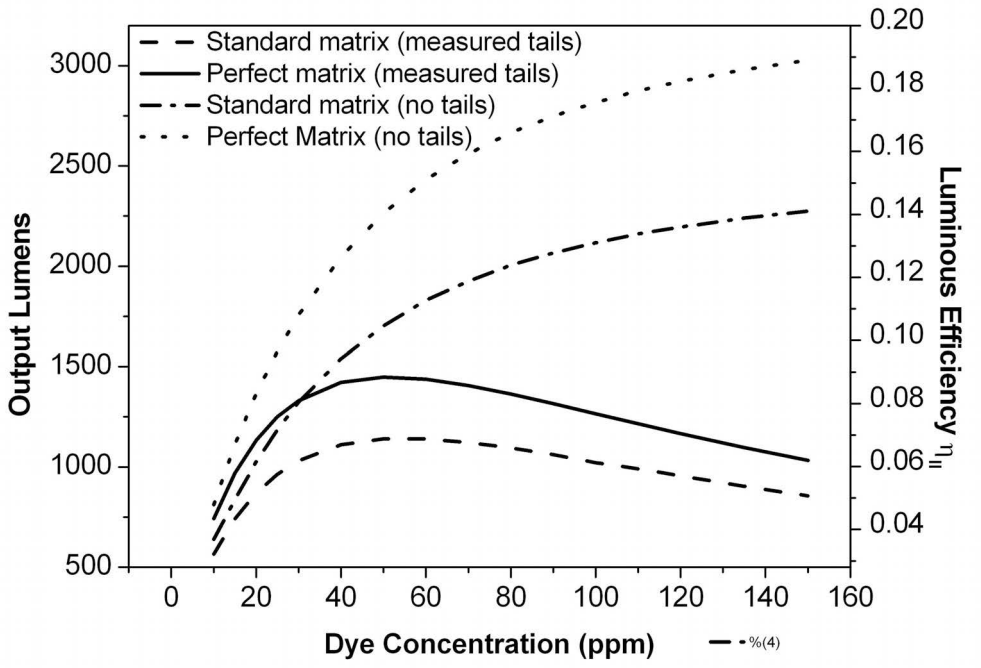

Figure 7.8 Theoretical luminous output as a function of dye concentration for a 1.2 m green LSC for standard ($L_{m½}$ = 5 m) and perfect (non-scattering) matrices with and without tails attenuation.

In Figure 7.8 the output of a LSC sheet is plotted as a function of dye concentration for the measured and reference transmission spectra shown in Figure 7.6, with two values of $L_{m½}$ corresponding to a typical matrix ($L_{m½}$ = 5 m) and an ideal matrix with no scattering ($L_{m½}$ = 10,000 m, approximating an infinite half-length). From this graph, it can be seen that both increased matrix half-length and increased tails transmission are favourable for a high luminous output. The optimum dye concentration is also sensitive to the difference in tails transmission. With the measured tails transmission, the optimum concentration is around 60 ppm, but when the tails transmittance is set to 100%, output continues to increase with dye concentration right up to 150 ppm. Therefore a high accuracy measurement of the tails transmittance is crucial if the ideal dye concentration is to be determined and the LSC performance is to be successfully optimised. Nonetheless, the current measurements have been used to predict the output of a single LSC sheet under direct solar illumination of 100,000 lux. For the 60 ppm green LSC sheet with the measured tails attenuation and a standard matrix of $L_{m½}$ = 5 m, the theoretical output of 1,140 lumens is in good agreement with the measured value of 1,122 lumens.

Up until now we have assumed that the dye is uniformly dispersed thought the matrix. One possible alternative is to have the dye concentrated in a thin layer with the rest of the matrix acting as a clear light guide. However, in order to achieve the same absorption as an isotropic

sheet, the dye concentration in the layer would have to be increased in inverse proportional to the thickness of the dyed layer. The turnover of Figure 7.8 shows that the high concentration would lead to somewhat reduced system output. The high dye concentration would also increase the risk of forming molecular complexes with adverse impact on light transport and hence output lumens.

Figure 7.9 shows the theoretical luminous output of the green LSC sheet as a function of collector length, using the measured transmission spectrum shown Figure 7.6, for three different concentrations with an ideal non-scattering matrix and a typical matrix. It is seen that for longer collectors the correct selection of dye concentration becomes more important. From the output vs. concentration plots in Figure 7.8 assuming the measured tails attenuation, the optimal concentration for the green LSC is 60 ppm of *Lumogen*® F083. If the dye concentration is below the optimum value (e.g. 30 ppm), the absorbed light is relatively low, but the losses are less significant. Alternatively, (as shown in Figure 7.9) if the dye concentration is too high (e.g. 100 ppm), the output is good for short LSC's, but for LSC's longer than one metre it begins to level off with length as the dye loss becomes increasingly significant. Again, it is clear that the ideal non-scattering matrix produces a significantly higher light output than the typical matrix in samples with $L_{m½}$ = 5 m, reinforcing the fact that a low-scattering matrix is as important as selection of dye concentration. Overall, it can be seen that optimum dye concentration thus depends on both thickness and length of the collector, and is a balance between increasing absorption and reducing losses.

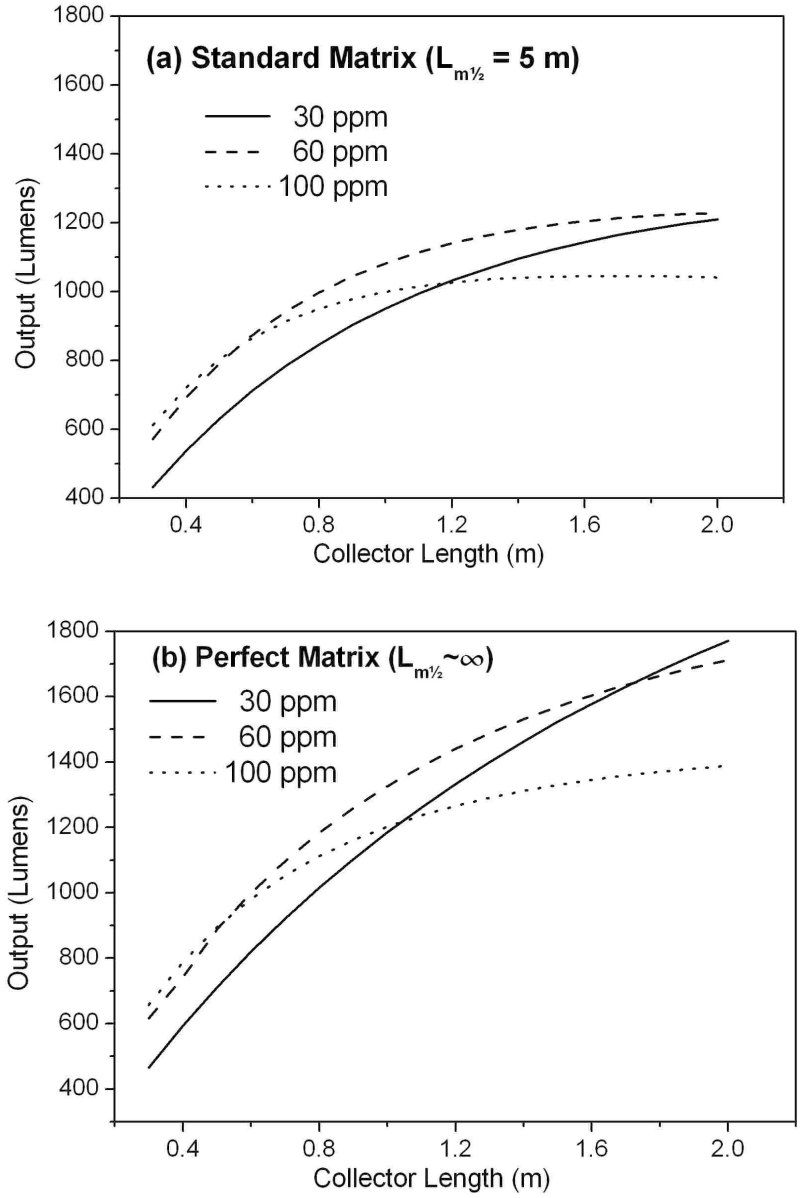

Figure 7.9 Theoretical luminous output vs. collector length for a green LSC doped with *Lumogen*® F083 fluorescent dye at concentrations of 30 ppm, 60 ppm and 100 ppm in (a) a standard matrix of half-length $L_{m½}$ = 5 m, and (b) a perfect non-scattering matrix.

Collector parameters are studied further in Figure 7.10, where theoretical luminous efficiency is plotted as a function of dye concentration and collector length. High lumens-to-lumens efficiencies between 10-16% are observed for short collectors under 0.6 m in length, and efficiency decreases with collector length, at varying rates depending on the dye concentration and matrix quality. The fall-off in efficiency with length is slowest for collectors with the optimum dye concentration of 60 ppm, and for collectors with a perfect matrix. Thus with the correct selection of dye concentration and matrix quality, the sensitivity of collector efficiency to length can be minimised. Crossovers of curves in Figure 7.10(a) and Figure 7.10(b) indicate that optimum dye concentration decreases with collector length *L*.

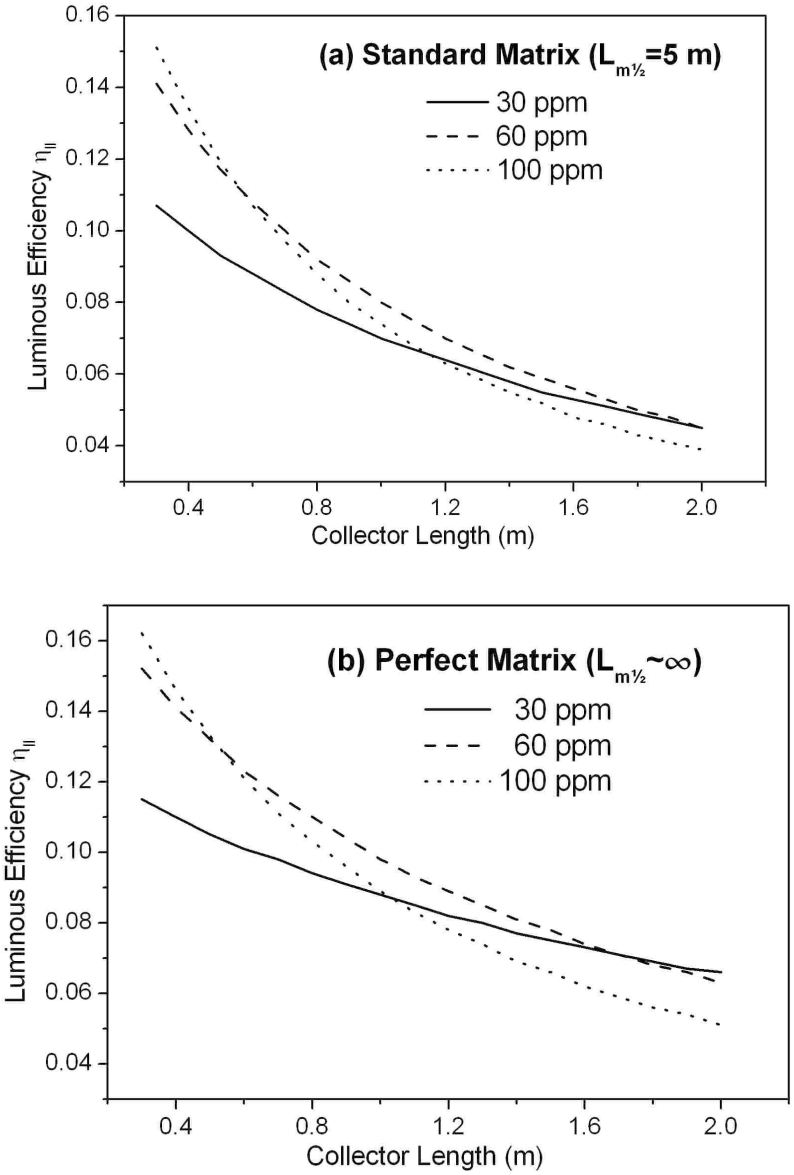

Figure 7.10 Theoretical lumens-to-lumens efficiency vs. collector length for a green LSC doped with *Lumogen*® F083 fluorescent dye at concentrations of 30 ppm, 60 ppm and 100 ppm in (a) a standard matrix of half-length $L_{m½}$ = 5 m, and (b) a perfect non-scattering matrix.

7.7 CONCLUSION

The optimum combination of dye concentration and collector length requires very accurate assessment of the transport losses in the emission region for a fixed matrix optical quality and collector thickness. A model has been developed that can predict performance accurately, provided the attenuation parameters are known with sufficient accuracy. Simulations and measurements show that when exposed to sunlight a green LSC is capable of producing sufficient illumination levels for natural indoor lighting. The model and data also indicate that

without improvement in the matrix, extension of the collector length beyond 1.2 m is of little value.

Three different coloured LSC collector sheets, such as pink, green and violet, are required if white light is desired for room illumination. Near-white light output of over 1500 lumens is achievable for a small system around 1 metre long in carefully manufactured sheets (Earp et al. 2004b). This multi-colour LSC analysis is made possible by the extension of the current model. Ongoing studies of LSC scattering in a photogoniometer and in an integrating sphere spectrometer in the region $\lambda > 550$ nm will promote a better understanding of the subtle changes in transmission in this region, which are very significant for collector performance. Since green dominates output lumens in a three-layer stack, its optimisation is crucial. The addition of two other colours for white output should raise the total lumens-to-lumens efficiency well above that for the individual green LSC reported here.

8 MAKING LSC SHEETS

The quality of the collector sheets in a LSC dominates system performance: if the collector sheets are unsatisfactory then there is no possibility of producing a high performance LSC system. At the start of this project no commercially available fluorescent sheets had the half-lengths required for a LSC daylighting system. So much work throughout this project was devoted to developing methods to manufacture and test suitable fluorescent sheets.

Such was the breadth of commercial interest in this project that we were able either to be present at and direct actual dyed LSC sheet production trials, or to set specific guidelines that the various companies involved were to follow. Companies in six countries participated in these studies and we were present for and directed multiple full-scale production line trials in Australia, Spain and Japan. Initial trials involved integrating our UTS based scientific developments with existing company capabilities.

Lessons learned led to several later production refinements, better understanding of the relevant optical and materials science, and to major improvements in performance of LSC sheets made with commercial faculties. These developments embody many useful guidelines and important details for anyone attempting similar activities. The full details are in *Appendix A: Mass Production of High Performance LSC Sheets*. The core lessons and science from these studies are summarized in this chapter.

8.1 CHOICE OF LUMINOPHORE

The key requirements for the wavelength shifting luminophore are that it must have: a high quantum efficiency (luminous output is proportional to quantum efficiency), a large Stokes shift (to minimise self-absorption), emission at wavelengths that can be readily combined to make good quality white light that has a high colour rendering index, good compatibility with the matrix (so that light transport is not degraded), and good photostability. Photostability is so important for the commercial viability of a LSC that it will be discussed at length in chapters 9 and 10.

Quantum dots (QDs) have considerable long-term potential as wavelength shifting elements for LSC's. However, at present they are very expensive (currently US$3,000 to $10,000 per gram, but this is expected to decline (Sanderson 2009)), have high re-absorption losses and low quantum yields (typically < 0.8) (Debije & Verbunt 2012; Earp et al. 2004b; Earp et al. 2004c). They are also difficult to disperse in polymer matrices (van Sark et al. 2008b). Another possible long-term solution is the new rare earth doped inorganic fluorescent nanoparticle pigments that are sufficiently small (< 50 nm) to not significantly scatter light (de

Boer et al. 2011). Laser dyes are not a viable solution because of their small Stokes shifts (Cahill 1993) and poor quantum yields (Reda 2007). Some organic dyes have near unity quantum efficiencies, and moderate to good dye molecule photostability (Cahill 1993; Seybold & Wagenblast 1989), making them one of the most suitable fluorescent species currently available for use in LSC's. The best available organic dyes at the start of the project were the *Lumogen*® series from *BASF* and they form the basis of this chapter, although most of the comments are applicable to any organic dye and to most inorganic wavelength shifting systems.

There are a number of basic and somewhat conflicting requirements that all must be satisfied for the production of high quality LSC collector sheets:

- The undoped matrix must have good optical properties with a half-length of at least 5 m, and preferably more than 10 m. It was shown in section 7.6 that using a matrix with a half-length less than 5 m materially reduces the collector's luminous output.
- Strips cut from the master sheets must have low geometric losses. This requires: (i) smooth top and bottom surfaces, (ii) constant thickness for the sheets, and (iii) good machining properties so that one can form low-loss sides, say by diamond polishing.
- The sheets need to be as thin as possible. The basic geometry of the LSC sheets is determined by the conservation of étendue. It follows from section 3.1 that for a three-layer collector stack, conservation of étendue requires that the cross sectional area of each collector sheet must not exceed one third of the cross sectional area of the light guides. It was also shown in section 4.4 that the cost of the light guides dominates system cost, and that the cost of a light guide is a linear function of its cross sectional area. This means that system cost is almost inversely proportional to sheet thickness, so there is a big premium on making the collector sheets as thin as possible. However, there are several problems if the sheets are too thin. First, edge forming can be difficult in thin sheets due to chipping at the corners. The effect is aggravated by the fact that for a given size of chip, side geometric losses are inversely proportional to sheet thickness. Second, it was shown in section 2.3.2 that light loss from thin spots is proportional to the fractional change in thickness. Now for most sheet production processes the absolute error in thickness is at best independent of sheet thickness and may actually increase as thickness declines. So the fractional error is at least inversely proportional to thickness and hence this geometric loss scales similarly. Finally, we saw in section 3.3.2 that practical LSC designs require at least one high-efficiency butt joint (to a light guide or flat-to-round converter), which are hard to make reliably with very thin sheets. The standard minimum thickness for extruded sheet on a full sized extrusion line is two millimetres. However, somewhat thinner sheet can be produced

on small "laboratory" extrusion lines. The minimum thickness for continuous casting is 2.00 mm and there are no prospects for reducing this. The practical limit for cell casting is a thickness of about two millimetres3.

- The fluorescent dye needs to have good quantum efficiency, a large Stokes shift (to minimize self-absorption), and good photostability. The best dyes at this time are the *Lumogen*® series from BASF.
- The dye needs to absorb incident light over a path length of 2 mm but not attenuate fluorescently emitted light over a path length of over 1000 mm. No known organic dye completely satisfies this requirement. However, it was shown in section 7.3 that the *Lumogen*® series of dyes come reasonably close at longer wavelengths.
- Low attenuation of fluorescently emitted light transported inside a collector sheet requires that the dye is completely dispersed at a monomolecular level since dye aggregates absorb and scatter light (Meseguer et al. 1981) and have adverse effects on photostability (Wilson et al. 2010b). Unfortunately, the Lumogen® dyes have a very low solubility within bulk MMA and a strong tendency to form molecular complexes (Bleasby 1995). Once formed, these complexes can be very hard to remove.
- Photostability requires low levels of residual monomer (Kinderman et al. 2007a). Photoquenching in *Lumogen*® dyes is greatly reduced if the residual monomer level is less than 0.5% (Bleasby 1995; Böhm 2000).

[3] One Japanese company I visited has a specialist cell casting line that produces sheets with a thickness of < 1.0 mm with a tolerance of about ± 0.05 mm. However, it is restricted to sheet sizes of less than 150 mm x 150 mm and the cost per unit area is more than 10 times that for standard cell cast sheet. They said that it would not be possible to scale the process to make full sized sheets.

8.2 DISPERSING THE DYE

In order to make ultra-high quality fluorescent sheets, it is essential that the dye is completely dissolved and dispersed at a monomolecular level. Unfortunately, most of the *Lumogen*® series of dyes have a tendency to form molecular complexes that absorb the light fluorescently emitted by single dye molecules (Bleasby 1995). Tiny quantities of these molecular complexes can greatly reduce the fluorescent emission from a large sheet of dyed PMMA. So part of the art in making fluorescent sheets for a LSC is to dissolve the fluorescent dyes at a molecular level in a way that minimises the formation of molecular complexes. This section will describe proven methods for making and testing the dye solutions.

The ordinary way of dissolving sparingly soluble materials, such as the *Lumogen*® series of dyes, is to make up a masterbatch at high concentration in a good solvent. However, extensive trials by BASF in Germany and Australia have shown that this leads to poor optical quality sheets (Bleasby 1995; Böhm 2000). The only suitable solvent finally identified by UTS and BASF is MMA or "pre-pol" (partly polymerized MMA). An additional problem is that the laser scattering tests (described below in section 8.3) show that high dye concentrations rapidly lead to the creation of molecular complexes. These complexes are hard to remove once they have formed. This problem is most acute with the green F086 dye, less serious with the pink F285 dye and least serious with the violet 570 dye. It has been found that the formation of these molecular complexes can be avoided if the maximum concentration is always kept below 10x the final sheet concentrations. Note that because of photopic response of the human eye is peaked in the green, the green sheet supplies most of the lumens for the LSC with the principle roles of the violet and pink sheets being restricted to providing colour balance (Earp et al. 2004b; Swift & Smith 2003; Swift, Smith & Franklin 1999b). Thus any diminution of the output of the green sheet has a large adverse effect on both luminous output and colour balance.

The best way of dissolving *Lumogen*® dyes is to use ultrasonic agitation (Franklin & Swift 1997). Unfortunately few manufactures have this capability for mass production although following the success of our work at UTS, BASF GmbH have built multi-million euro plants with this capability (Böhm 2000). However, good results can be achieved with traditional high-shear mechanical agitation. The rest of this section assumes that mechanical agitation is used for mass production. All reference dye solutions must be made by ultrasonic agitation as this gives almost perfect dye dissolution. A small, cheap ultrasonic agitator of the type used for cleaning tools is suitable for this purpose and was used in our work in Australia and demonstrated to factory staff in Spain, Germany and Japan.

Clear control sheets should always be made simultaneously with the fluorescent collector sheets using an identical process (except for the addition of the dye). The clear control sheets are very helpful in diagnosing whether problems are due to dye dissolution, sheet

polymerisation, contamination, packaging problems, handling errors, or to some other process. All stirring cycles and agitation cycles must be identical for dyed and control sheets. The importance of the clear control sheets for de-bugging the sheet production process cannot be over emphasized.

LSC sheets doped with fluorescent dyes are ***extremely*** sensitive to cross-contamination with other fluorescent dyes whose absorption spectra overlap their emission spectrum. For example, the long path length inside a sheet mean that a contamination level of a few parts per billion of pink dye in a green sheet will lead to a loss of almost all the green output light (whereas 1000 ppb of green dye in a pink sheet would have little effect). Accordingly, extreme care must be taken to ensure that all equipment is cleaned before it is used with a different dye.

In order to reduce any likelihood of cross-contamination and to simplify contamination tests, batches of fluorescent collector sheets should be made in the same order as the wavelength of their mean absorption wavelengths. For *Lumogen*® dyes this means that sheets should be made in the following sequence: (i) clear control sheet (essential for *every* production run in the development phase), (ii) violet *Lumogen*® F570 dye, (iii) green *Lumogen*® F083 dye, and finally (iv) pink *Lumogen*® F285 dye.

Additionally, if possible one should minimise the possibility of cross-contamination by using separate, dedicated containers for mixing each type of fluorescent dye and for making up final batches prior to casting. While this is feasible for small-scale tests, it may not be practical for mass production.

One interesting feature of the *Lumogen*® green F086 dye is that a sonicated 600 ppm solution (i.e. x 10 standard concentration) stored for 3 months at a temperature of 4 ^{o}C has the same laser scattering properties (as measured by the methods of section 8.3) as a freshly sonicated solution. However, a sonicated solution with twice this concentration (i.e. x 20 standard concentration) stored at 4 ^{o}C has increased scattering after two days and forms particles visible to the naked eye after a fortnight. One possible explanation is that the sonicated x 10 solution has no nucleation centres, the dye being perfectly dispersed to a monomolecular level, whereas the x 20 solution has significant numbers of nucleation centres despite the ultrasonic agitation.

The procedure described below for dissolving the dye stresses the importance of always keeping the dye concentration at not more than 10 times the final concentration. Small scale casting experiments at Poly Optics Pty Ltd yielded bad results for x 20 concentration, poor results at x 15 concentration (with the green dye showing the worst results) and excellent results for x 10 concentrations for all dyes. So x 10 concentration was adopted for this project.

8.2.1 Procedure for Dissolving the Dye

Check the purity of the MMA and "pre-pol" by the laser testing procedure described in section 8.3 using ultra-pure distilled MMA as a standard.

Use pure MMA at a temperature of 60 - 65 ^{o}C as a solvent. ***Do not use any other solvent to dissolve the dye.***

Add the dye to the warm MMA while stirring constantly.

Make sure that the dye concentration never exceeds 10 times final concentration (e.g. for the green dye the concentration must never exceed 600 ppm; for the pink dye the concentration must always be less than 500 ppm). Higher dye concentrations rapidly lead to the creation of molecular complexes. These complexes are hard to remove once they have formed. This problem is most acute with the green dye.

Take a 50 ml sample of the dye concentrate solution and ultrasonically agitate it for 5 minutes to completely dissolve the dye. This ***A*** sample (with perfectly dissolved dye) will serve as the standard for the mechanically agitated solution.

Check the quality of the ***A*** sample from step 5 by the laser testing procedure described in section 8.3. The sample should have very little scattering. Significant scattering suggests contamination.

Mechanically agitate the bulk MMA mixture to completely dissolve the dye. 30 minutes in a high-shear stirring machine is usually enough. Note that excessive agitation can cause problems.

Take a ***B*** sample of the mechanically agitated dye solution. Use the laser testing procedure described in section 8.3 to compare the ***B*** solution with the sonicated ***A*** solution from step 5. If the mechanical agitation process has worked properly then the two solutions will have identical scattering. The time and intensity of mechanical agitation should be adjusted to minimise the difference between the solutions. Also compare the solutions to reference solutions of ultra-pure distilled MMA. Visual comparisons between solutions are much easier and more informative than tests of a solution by itself.

Dilute the dyed MMA to the final concentration. This final dilution may be with pure MMA, "pre-pol", or any convenient mixture of the two.

Add initiator if this is not already in the "pre-pol".

Mechanically agitate the casting solution to thoroughly mix the casting liquor. This is typically for a minimum of 5 minutes.

Vacuum degasses the casting solution.

Take two samples of the dyed casting solution, the ***C*** and ***D*** samples. Ultrasonically agitate the ***C*** sample for 5 minutes. Use the laser testing procedure described in section 8.3 to compare

the ***D*** solution with the sonicated ***C*** sample. If everything is satisfactory, then the two solutions should have identical scattering.

Polymerise the sheet.

Heat-treat the sheets to reduce residual monomer levels to at most 0.5 %. (This step may be omitted for laboratory test sheets.)

8.3 LASER TESTING DYED MMA AND PMMA

A good way to test both the purity of the monomer and the quality of dye dissolution is to visually observe the scattering of a linearly polarized laser beam. A red laser is used for the green or violet dyed solutions so that there is no fluorescence. A 2 mW HeNe laser is ideal, but a well-collimated red diode laser can be used. It is essential that the laser is 100% polarized with a known plane of polarization. Note that some HeNe lasers are unpolarised while in others the plane of polarization is not fixed, but varies randomly.

In this method, a sample is illuminated with a polarised laser beam and observed from a point that is at right angles to the laser beam and in a plane orthogonal to that of the laser's polarisation. Figure 8.1 illustrates a vertically polarised horizontal laser beam, which is the best setup for observing fluids. However, for sheets it is often more convenient to use a horizontally polarised horizontal laser beam and to view the sheet from above.

When viewed with either setup, light scattered by micron-sized particles is essentially unpolarised. Light scattered by nanoscale particles (i.e. with a size <100 nm) is 100% polarised with the same polarisation orientation as the laser beam (Hecht 2002, pp. 346-7).

Total scattering can be estimated by observing the laser beam in a dark place against a dark background. These observations should be compared to the scattering from a sample of known properties such as vacuum distilled monomer. In good quality MMA and "pre-pol" the laser beam should be almost invisible. Any undissolved dye particles, dust particles, etc in dye solutions or cast sheet stand out very clearly.

Reference dye solutions should be made by ultrasonic agitation as this gives almost perfect dye dissolution. A small, ultrasonic agitator of the type used for cleaning tools is suitable.

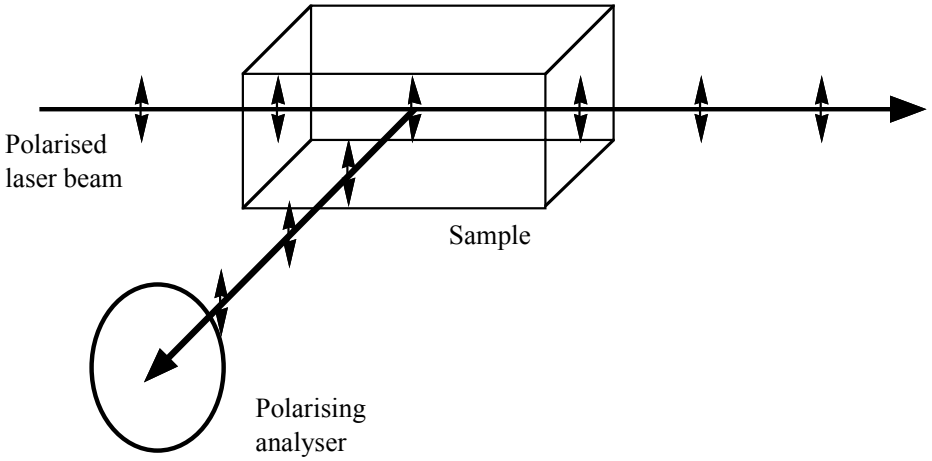

Figure 8.1 Set-up for laser testing using a polarized laser beam. The observer is located so that the scattering angle is a right angle and the laser is polarized perpendicular to the line of sight. By rotating the polarizing analyser the observer can estimate the degree of polarisation in the scattered light. Scattering from nanoscale particles is 100% polarised. Scattering from micron-sized is almost unpolarised.

The nature of the scattering centres can be found by measuring the scattered light's degree of polarisation (Hecht 2002, pp. 346-7). If the scattered light is 100% polarised then the scattering is due purely to particles with a size <100 nm. However, if the scattered light is completely unpolarised then the scattering is due purely to micron-sized with a diameter typically > 5 μm. Partial polarisation can be caused by the simultaneous presence of both nanoscale and micron-sized particles, or by particles of intermediate size.

With practice one can estimate the degree of polarisation by viewing the laser beam through a polarising filter and rotating the filter to find the maximum and minimum beam brightness. Alternatively, one can rotate the laser beam along its axis and look for changes of scattered light. Visual observations are usually satisfactory for comparative purposes.

The object of the exercise is to make dyed PMMA sheets that have very little scattering. An essential requirement for this is that the MMA and dyed solutions have very low levels of scattering since the final sheet is seldom better than the casting solution. Significant scattering in the MMA or dyed solutions invariably leads to poor quality polymer sheets.

In properly made dyed PMMA there is very little scattering. The small amount of scattering that does occur is almost purely from nanoscale defects. If a dyed sheet has measurable non-nanoscale scattering then there is probably something wrong with the manufacturing process, even if the overall level of scattering is acceptable. Clear control sheets that are made by exactly the same polymerisation process as the dyed sheets (except for the addition of the dye) are invaluable for diagnosing problems, particularly whether the problem is primarily with the matrix or with dye dissolution.

8.4 MANUFACTURING METHODS FOR DYED PMMA SHEETS

There are currently three methods of making dyed PMMA sheets of a size suitable for LSC's: extrusion, continuous casting and cell casting. Some of the advantages and disadvantages of each method are compared in **Table 8-1** in section 8.4.4. Optical quality is highest for cell casting and lowest for extrusion. Minimum batch sizes are lowest for cell casting and highest for extrusion. For mass production the most important factors are performance and photostability (cost per sheet is a secondary factor because this is only a modest part of system cost). However, for a test programme, minimum batch size is also important since a test programme must explore many different possibilities.

8.4.1 Extruded Sheet

Extruded PMMA is manufactured on a multi-million dollar, highly automated production lines consisting of: a screw extruder, a sheet die, a calendaring roller stack, a cooling unit, a coating line and a packing unit. In standard operation, the screw extruder mixes and melts pellets of very dry clear matrix with pellets of dyed masterbatch. The mix is dispensed through a sheet dye block that extrudes a two millimetres thick strip of high viscosity molten plastic in a ribbon that is up to three metres wide. The ribbon enters the calendaring roller stack that cools it and imparts a high quality finish due to the differential motion of the rollers. In a good production line, the surface finish of the final sheet is dominated by the performance of the calendaring rollers with many complex interacting factors including: the rollers' surface finish, the uniformity of the temperature along each roller, the smoothness of the mechanical drives, alignment tolerances, operator skill and the quality of the integration with the rest of the line. A good calendaring roller stack typically costs well over one million dollars.

The warm sheet is peeled off the final calendaring roller and air cooled to room temperature as it runs along a series of small rollers. The warm sheet then passes from the cooling unit to a coating line that applies protective films to the sheet's top and bottom surfaces. Some manufactures ordinarily use coated paper. However, this tends to leave residual adhesive and much better optical quality is achieved by using special (but more expensive) low-tack polymer films. Saws at the end of the line cut the material "on the fly" to it's final size.

Extruded dyed LSC sheet has considerable promise for low-cost LSC's. Because of the method's high degree of automation, extrusion is the lowest cost way of mass-producing sheets. It can readily achieve matrix half-lengths of more than 5 metres. Good surface finishes for the top and bottom surfaces are readily achieved and thickness control for a 2.00 mm thick sheet of ± 0.01 mm is routine. Mechanical properties are acceptable although somewhat inferior to continuous cast or cell cast sheets, although chipped edges in the diamond polisher can sometimes be an issue. However, the key problem is its light transport properties.

The standard method of making dyed extruded sheet is to use a masterbatch of pellets that have a high dye concentration (typically x100). The masterbatch pellets are mixed with an appropriate fraction of clear pellets and the combination is extruded, relying on the screw in the extruder to homogenize the mixture. This method works well for ordinary sheets so masterbatches were made at UTS and were also commissioned from three Australian and three German companies. Unfortunately, all masterbatches gave sheets that had very high levels of scattering. The problem is the tendency of the *Lumogen*® dyes at high concentration to form scattering complexes. The only solution appears to be to incorporate the dyes into the polymer at the time of polymerization.

A more fundamental problem is that it is extraordinarily difficult to produce masterbatch pellets that have the same molecular weight distribution as the virgin clear pellets. If the molecular weights are slightly different then the refractive indices will also differ which causes scattering losses. This is because although the extruder's screw melts and stretches each masterbatch pellet, the high viscosity of the melt means that the mixing is incomplete at a micro scale. Thus the final sheet has micro-regions that are masterbatch pellet, and micro-regions that are standard pellet. The small differences in refractive index cause scattering similar to the TRIMM microparticles discussed in chapter 5.

Multiple attempts by various Australian and German companies to produce suitable dyed masterbatch were all unsuccessful. The only apparent solution is to dope the matrix pellets with the final dye concentration at the time of polymerisation. This is technically straightforward, but is relatively expensive. Unfortunately, it is not feasible on a small scale. Section A.1 of Appendix A describes an unsuccessful attempt at producing extruded sheets using custom manufactured pellets doped with the final dye concentration. This section also discusses a number of practical issues for making LSC sheets by extrusion including: moisture levels in the pellets, residual monomer in the final sheets, design requirements for the extruder barrel, the harmful effects of trace quantities of "re-grind", and contamination issues with masterbatch.

8.4.2 Continuous Casting

Continuous casting of dyed sheets starts with the batch preparation of dyed partially polymerised MMA, often called "pre-pol". The reduction in volume from MMA to PMMA is about 17%. However, by partially polymerising the casting liquor before casting, the volume reduction in the mould is minimized. It is difficult to seal the edges of the moving moulds used for continuous casting, so the "pre-pol" for this process is made with a relatively high degree of polymerisation and a viscosity similar to that of honey, say 2,500 centipoise. This high viscosity makes the "pre-pol" hard to handle and bubbles can be a serious problem, but it greatly reduces

leakage and shrinkage in the mould. Cell casting moulds have much better edge sealing, so that process uses “pre-pol” with a lower degree of polymerisation and hence a lower viscosity.

In continuous casting, large batches of dyed viscous “pre-pol” are poured between pairs of horizontal mirror-polished stainless steel belts about three metres wide and over 200 m long. The pairs of belts are separated by gaskets to form a space equal to the thickness of the material desired, plus an allowance for shrinkage (Graf 2000; Rustin 2000). These twin belts continuously convey the material through a series of cooling and heating units that regulate the polymerisation of the PMMA and perform the heat treatment to reduce residual MMA. Saws at the end of the line cut the material "on the fly" to it's final size.

The cost comparison with other methods can be a little complex. On the one hand, the cost per kilogram of the MMA used to make continuous cast sheet is considerably less that the cost per kilogram of optical-grade extrusion pellets. On the other hand, there is a very large capital investment to build a continuous cast sheet line (the highly polished stainless steel belts are *very* expensive). The cost of capital tends to outweigh the low material costs and cell cast sheet typically costs more than extruded sheet, although the differences reduce as sheet quality is increased. The high capital costs of continuous casting lines mean that in 2000 there were only two continuous casting plants in the USA, but dozens of major extruders (Graf 2000). Continuous casting is highly automated, so it is cheaper than cell casting.

Clear continuous cast sheets usually have good optical quality with a half-length significantly superior to that for extruded sheets. The thickness tolerance for most manufacturers for 2.00 mm sheet is ± 0.02 mm, although the best Japanese sheets typically have their thickness constant to a remarkable ± 0.01 mm. Mechanical properties are excellent, almost as good as cell cast sheets.

The minimum batch size is about 400 kg so it was not possible in this project to make LSC sheets by continuous casting for experimental trials. However, just as with cell casting, the dye is dissolved in MMA or “pre-pol”. Thus by using the techniques described in sections 8.2 and 8.3, it should be possible to achieve the same half-lengths for continuous casting as for cell casting while achieving much better thickness control.

One possible concern is residual monomer. Cell casting can readily increase the final anneal time to reduce residual monomer to the lowest possible level, but this is not feasible on the inflexible continuous cast line However, many lines use higher anneal temperatures than for most cell cast lines, so this may not be a problem.

The good optical quality and excellent thickness control make continuous casting a strong contender for volume production of LSC sheets provided one can overcome the residual monomer level mentioned above, the photostability issues described in chapters 9 and 10, and the problems of industrial culture described in section A.3 of Appendix A.

8.4.3 Cell Casting

Cell cast sheets are produced by assembling a mould for each individual sheet, and then pouring the casting solution into the mould. Factories typically use 3 m x 1.5 m tempered glass sheets for moulds. The glass is only 6.0 mm thick and hence is somewhat flexible because of the large sheet size. Edge sealing is achieved with a continuous sacrificial PVC gasket held in place with numerous strong spring clamps. For filling, the mould is placed in a vertical position on a weighbridge. The sheets are wedged a few millimeters apart at the top centre of the mould and the mould cavity is filled with a measured mass of dyed "pre-pol" casting liquid. The viscosity of the "pre-pol" ensures that there is no leakage from the side gaskets. The wedge is removed and the sheets snap back to give a good seal. In the "as filled condition", the sheets bulge noticeably. However, the volume of the casting liquid reduces by about 7% on polymerisation and this causes the final sheet to have parallel surfaces (this compares to a reduction in volume from MMA to PMMA of about 17%). The moulds are polymerized in a water bath and are then heat treated to reduce the level of residual monomer. The newer method is to use an oven with tightly controlled airflows. This method of annealing (also called "post-cure") is relatively expensive but it permits high temperatures and hence very low residual monomer. Levels as low as 0.2% can be achieved in routine production (Acrylics USA 2011). The older and cheaper method of annealing is to use an unpressurised water bath, which limits temperatures to just below 100 ^{o}C and so gives a somewhat higher level of residual monomer.

The cast sheets are then given a protective film. Some manufactures ordinary use coated paper. However, as was mentioned in section 8.4.1, this tends to leave residual adhesive and much better optical quality is achieved by using special (but more expensive) low-tack polymer films. Choosing the correct protective film is also important for achieving high-quality diamond polished edges for the LSC collector strips and this topic is discussed in section A.4 of Appendix A.

Cell cast sheets have the highest optical quality and best mechanical properties of all the production processes discussed. By using the procedures described in section 8.2, it is possible to disperse *Lumogen*® dyes to a monomolecular level. The cell casting process requires significant skilled labour and this makes it relatively expensive. However, the batch size can be as small as a few sheets and some manufacturers will even cast a single custom sheet for a small premium (Acrylics USA 2011). This means that it is the best process for experimental work or small-scale LSC production.

A major problem with cell cast sheets is the variation in sheet thickness. The standard specification for premium quality 2.0 mm thick sheet is ± 0.2 mm. For some manufactures the specification may be -0.2/+0.3 mm. Actual sheets may be significantly thicker than specification, although seldom thinner. However, when a collector stack is glued to a flat-to-

round converter, what counts is the worst-case sum of tolerances for all the components and parts thereof. With three sheets at + 0.2 mm and allowance for each step on the injection moulded converter of +0.02 mm, the midpoint of the converter must be at least 0.66 mm more than the mean stack thickness. This increases the light guides' cross sectional area by 11% with a similar increase in the system cost.

Even more important, if a sheet is too thick it will prevent proper assembly of the flat-to-round converter. The tight tolerances mean that the end thickness of every LSC collector strip should be measured before it is glued to a flat-to-round converter.

The better LSC manufacturers routinely measure the thickness of every cast sheet at a large number of points to help improve their manufacturing process. This thickness data can be used to select sheets that meet the tolerance. It may also permit the cutting of in-spec strips from parts of full sized sheets that would otherwise have to be rejected. Most rejected sheets have superior visual appearance, so they may be suitable for other applications.

Uniformly thin sheets do not cause difficulties with assembly. However, a thickness reduction gives a corresponding reduction in the areal density of the dye molecules and hence reduces light absorption in that sheet. This can upset the system's colour balance. Also, as discussed in section 2.3.2, thin spots in a sheet reduce light output from that sheet which can also upset the system's colour balance.

By negotiating hard with the sheet manufacturer we managed to achieve a tolerance of ± 0.1 mm, i.e. about 10 times the standard for extruded or continuous cast sheets. Maintaining this tolerance was a constant battle and could prove burdensome with mass production.

Section A.2 of Appendix A has describes some of the problems encountered in making sheets by cell casting and the lessons learnt.

8.4.4 Comparison of Sheet Production Methods

Table 8-1 compares some of the advantages and disadvantages of making PMMA LSC's by extrusion, continuous casting and cell casting. Note that for a test programme, minimum batch size is very important, as a test programme must explore many different possibilities. For mass production the key parameters are luminous output and photostability – cost is not a key issue as the sheets are a relatively small part to the total cost of a LSC system.

To summarize: cell casting looks like the best option for initial small-scale production, although some waste sheets (or re-use for other applications) may need to be tolerated. Continuous casting is probably the best short-term option for mass production, with extrusion offering good prospects for low-cost mass production of LSC collector sheets.

Table 8-1 Key parameters for various manufacturing methods for PMMA sheet.

	Method of Sheet Manufacture		
Parameter	**Extruded**	**Continuous Cast**	**Cell Cast**
Optical quality of matrix	Worst	Good	Best
Ease of dye dissolution	Hard	Straightforward	Straightforward
Residual monomer concentration	Highest	Medium	Lowest
Molecular weight	Lowest	Medium	Highest
Hardness	Lowest	Medium	Highest
Machinability	Lowest	Medium	Highest
Cost of sheet	Lowest	Medium	Highest
Capital cost of plant	Medium	Very high	Lowest
Cost of raw materials	Highest	Lowest	Medium/Low
Minimum batch size	Large	Large	Small
Thickness variation (standard)	± 0.03 mm	± 0.02 mm	± 0.20 mm
Thickness variation (possible)	± 0.01 mm	± 0.01 mm	± 0.10 mm

8.5 Mass Production of Optical-Grade Edges for LSC's

The half-length of a LSC sheet is greatly affected by the surface finish of its sides (Earp et al. 2004b). The standard industrial method for achieving a good side finish is flame polishing. However, the half-length of flame polished sheets is usually quite low and after considerable experiment in the early parts of the project we found that diamond polishing gave low-loss side surfaces. The preferred tool is a *C.R. Clarke 1550*® (CR Clarke & Co. (UK) Ltd), which gave the best results of all the machines tested. Measured edge losses for LSC sheets polished with this machine are << 1% per metre, which is small enough to be neglected.

Section A.4 in Appendix A describes the *C.R. Clarke 1550*® diamond polishing machine, its application to making optical grade edges for LSC collector sheets, problems with protective sheet films, and the tolerances on strips that are to be diamond polished.

It was mentioned earlier that flame polishing is the standard industrial technique for giving a good edge finish. In the hands of a skilled operator this technique can produce a very attractive finish that looks better to the eye than most "as produced" diamond polishing.

However, appearances are deceptive and with flame polishing there is significant loss from the corners that are inherently rounded, and a lack of surface flatness. The eye is also deceived by the fine striations left by diamond polishing. Our measurements show that the striations cause very little light loss. However, the human eye is exceedingly sensitive to fine lines and so people greatly overestimate the importance of the fine striations.

For commercial decorative work, the fine lines from diamond polishing are often removed by giving the edges a light hand polish that can take the surfaces to an attractive high gloss. However, this is unnecessary for LSC's, as experience has shown that it adds negligibly to the half-length and can sometimes materially decrease the half-length by rounding the sheets' corners. The human eye is not very sensitive to the losses caused by rounded corners, so this is another case where appearances are deceptive. For LSC's, "as-produced" diamond polishing is best.

9 EXTINCTION MECHANISMS IN LSC'S

9.1 INTRODUCTION

One of the most significant remaining technical obstacles preventing widespread utilisation of LSC's is the limited photostability of the fluorescent species (Deshpande & Namdas 2000; Earp et al. 2010; Mansour 1998a; Mansour 1998b). Quantum dots (QDs) are advantageous in that they are inherently more stable than organic dyes, and provide broader and more easily tunable absorption bands (Hyldahl, Bailey & Wittmershaus 2009; Klampaftis et al. 2009; van Sark et al. 2008b). However, QDs are presently very expensive (currently US$3,000 to $10,000 per gram, but this is expected to decline when QD's achieve mass production (Sanderson 2009)), have high re-absorption losses and low quantum yields (typically < 0.8) (Debije & Verbunt 2012; Earp et al. 2004a; Earp et al. 2004c), and can be difficult to disperse in polymer matrices (van Sark et al. 2008b). Another possible solution is inorganic fluorescent nanoparticle pigments that are sufficiently small (say < 50 nm) to not significantly scatter light. Until recently most of these candidates did not have high enough quantum yields, but the latest developments (de Boer et al. 2011) with select rare earth doped nanoparticles may have overcome this limitation. Laser dyes also show good photostability, but generally exhibit small Stokes shifts (Cahill 1993) and poor quantum yields (Reda 2007). Some organic dyes have near unity quantum efficiencies, and moderate to good dye molecule photostability (Cahill 1993; Seybold & Wagenblast 1989), making them one of the most suitable fluorescent species currently available for use in LSC's. Organic dye doped LSC's are thus the focus of this extinction study.

Photostability is the key issue holding back the use of LSC's in real applications as most other issues impacting on initial performance can now be managed. It requires not only dye molecule stability, but also the maintenance of low-loss light transport within the dye-doped polymer. Photodegradation of LSC's and the associated reductions in LSC efficiency can therefore be broken down into two main processes:

1) *Fluorescence quenching* – photoexcited dye molecules gradually break down due to interactions with impurities in the matrix or with ultraviolet (UV) radiation (if present) resulting in reduced absorption and fluorescence intensities with exposure.
2) *The formation of photoproducts* – photodegradation can lead to the formation of byproducts or aggregates, causing increased 'tails' absorption at longer wavelengths than the main dye absorption edge and hence a reduction in internal transport efficiency of fluorescently emitted light (Goetzberger & Wittwer 1981; Seybold & Wagenblast 1989; Wittwer, Stahl & Goetzberger 1984).

From earlier work in section 7.5 on LSC's it is evident that low levels of extinction in the 'tails region' (defined as wavelengths longer than the main dye absorption peak) reduces the net transport within a dyed sheet of fluorescently emitted light. The result is a significant reduction in LSC luminous output (Earp et al. 2004a; Earp et al. 2004c) and overall optical efficiency (Wilson et al. 2010a). Hence measuring changes in the tails extinction in exposed LSC's and identifying the origins of such changes is an important exercise that can highlight significant sources of loss and provide valuable information about the degradation mechanism.

This chapter focuses on the analysis of the additional extinction caused by photoproducts, in particular its break up into scattering and absorption components. If photoproducts form in an LSC during exposure, an important step in the remedial process is to identify the light loss mechanism. The next chapter will explore in more detail potential sources of degradation including ultraviolet radiation, UV additives, antioxidants, heat, and visible illumination. Until this work, most efforts, including our own, had focused on limiting initial loss of output due to scattering and ongoing degradation loss resulting from UV degradation of dye molecules. We had learnt to satisfactorily manage these impacts, but found after long-term outdoor exposure that other unknown loss processes were arising over time. The first step is to better understand their source and relative impact.

Depending on the nature of the dye degradation mechanism, photoproducts may cause extinction losses either by increased non-fluorescing absorption or by increased scattering. Matrix scattering losses in an LSC can be experimentally measured (Thomas, Drake & Lesiecki 1983b), as can total extinction losses via measurements of transmission along the LSC long axis (Wittwer, Stahl & Goetzberger 1984). However, experimental measurements of absorption and scattering generally require two different sets of equipment and two differently sized samples. The advantage of the experimental method presented below is that it enables the subdivision of light traveling longitudinally inside an LSC into transmitted, absorbed and scattered components, using the same LSC sample with a single set of equipment. This analysis technique enables the identification of the primary light loss mechanism in an exposed LSC, which can help determine the particular degradation mechanism at work. The theory and some example experimental results are presented below.

9.2 Experimental Method and Theory

9.2.1 Sample Preparation

For this study, LSC's were produced from 2.0 mm thick cast PMMA sheets containing *Lumogen*® F083 fluorescent dye (*BASF*) at a concentration of 60 ppm. Since we required the collector long axis to be at least one metre in length, the sample had to be obtained from a

commercial supplier. Their casting solution involves very pure pre-polymer (inorganic impurities at parts per billion level, organic molecule impurities such as ketones under 1 ppm), peroxide initiator and fully dispersed dye. Initial polymerisation took place in a temperature controlled water bath, followed by an extended air anneal to ensure that residual monomer levels were below 0.5%. The *Lumogen*® F08*3* green dye has absorption and emission maxima at 472 nm and 518 nm respectively. Clear reference sheets were also produced with exactly the same process and ingredients, but omitting the dye. The clear sheets have very high optical quality in terms of measured light transmittance over a 1.2 meter path length. Clear and dyed LSC samples with dimensions 1200 mm x 150 mm x 2.0 mm were produced by cutting sections from the master sheets and diamond polishing the four thin edges with a diamond polisher (*C.R. Clarke 1550*®*)*.

9.2.2 Test Equipment

The following equipment was used to experimentally isolate the extinction losses due to scattering and absorption. As schematically represented in Figure 9.1, LSC samples of length *L* were illuminated with an optic fibre illuminator containing a 50 W tungsten halide lamp, connected to a 1.0 m long, 18 mm diameter polymer optic fibre (*Lumenyte*®) and a 1.0 mm x 20 mm slit. Output spectra were measured with a fibre optic integrating sphere (*Ocean Optics*®*, FOIS-1*®*),* consisting of a 38 mm diameter integrating sphere with a 9.5 mm diameter sample port, connected via a 50 μm diameter optic fibre to an *Ocean Optics*® *USB2000*® UV-Visible spectrometer. Spectra were recorded with a PC using *Spectrasuite*® software (*Ocean Optics*®*)*. Stray light was excluded from the measurement by placing a black cloth over the top surface of the LSC adjacent to the integrating sphere port, and by using a black PMMA base sheet (*Plexiglas*®).

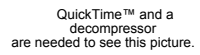

[Production Note: This figure is not included in this digital copy.
The print copy of the thesis is available for consultation at UTS Library.]

Figure 9.1 Experimental set-up for transmission measurements.

9.2.3 Transmission Measurements

The tails transmission of the LSC was measured as follows. Initially, the light source was coupled into the clear reference sheet, and the output signal at its end surface, $E_C(\lambda)$, was

measured with the integrating sphere and spectrometer according to the setup shown in Figure 9.1. The spectral power entering the sample is not easily measured directly due to geometrical coupling losses at the entry surface. Hence the spectral power $P_o(\lambda)$ entering the sample, which is the power immediately inside the entry surface of the clear reference sample, was calculated from the output signal as follows:

$$P_o(\lambda) = \frac{E_C(\lambda) w_C}{w_{\text{det}} \tau (1-f) \Delta\lambda} \quad (\text{counts.sec}^{-1}.\text{nm}^{-1}) \tag{9.1}$$

where $E_C(\lambda)$ is the measured spectrometer signal from clear reference sheet (counts); w_C is the width of clear reference sheet (m); w_{det} is the width of detector port on integrating sphere (m); τ is the spectrometer integration time (sec) (a value of 50 msec was used for the transmission measurements); $\Delta\lambda$ is the wavelength interval (nm) and f is the matrix loss factor (the fraction of the light source lost in the clear reference sheet due to matrix extinction and Fresnel reflection at the far end).

The matrix loss factor, f, was calculated as follows:

$$f = R_{end} + \left(1 - e^{-L\alpha_m}\right) \tag{9.2}$$

Where R_{end} is the Fresnel reflection loss at the far end surface of the LSC (for this study, $n_{PMMA} = 1.492$ and $n_{air} = 1.000$, so $R_{end} = 0.039$); L is the length of clear reference sheet (m) and α_m is the extinction coefficient of clear matrix (measured with a monochromatic laser).

For the LSC sample in this study, a representative value of $\alpha_m = 0.098$ m^{-1} was measured with a green laser at $\lambda = 532$ nm, which is near the two primary emission peak wavelengths of *Lumogen*® F083 (492 nm and 516 nm respectively). (From equation 7.12, the corresponding half-length is 7.1 m.) Calculation of equation (9.2) for a 1.2 m long LSC yielded a matrix loss factor of $f = 0.151$ for the clear reference sample.

The light source was then coupled into the dyed LSC using the same setup shown in Figure 9.1, and the output signal from its end surface, $E_D(\lambda)$, was recorded. The spectral power transmitted by the LSC, $P_T(\lambda)$, was calculated as follows:

$$P_T(\lambda) = \frac{E_D(\lambda) w_D}{w_{\text{det}} \tau (1-R_{end}) \Delta\lambda} \quad (\text{counts.s}^{-1}.\text{nm}^{-1}) \tag{9.3}$$

where $E_D(\lambda)$ is the measured spectrometer signal at the far end of the dyed LSC (counts); w_D is the width of dyed LSC (m) and R_{end} is the Fresnel reflection losses at end surface of LSC ($R_{end} = 0.039$). Note that unlike equation (9.1), the correction factor in brackets in equation (9.3) does not include intrinsic matrix losses, so that the LSC matrix losses are included in the transmission measurement.

The transmission spectrum of the LSC, $T(\lambda)$, was calculated by dividing the transmitted spectral power, $P_T(\lambda)$, by the input spectral power, $P_o(\lambda)$,:

$$T(\lambda) = \frac{P_T(\lambda)}{P_O(\lambda)} \tag{9.4}$$

The mean tails transmission, $\overline{T}$, was calculated by averaging $T(\lambda)$ over the tails wavelength region for the particular dye. For the *Lumogen*® F083 dye used in this study, the full tails region is 550 nm ≤ λ ≤ 750 nm, which includes a significant part of the emission spectrum but also extends beyond it. As described below in sections 9.2.5 and 9.3.1, calculations were restricted to the wavelength range 600 nm ≤ λ ≤ 750 nm in order to avoid contributions from excess emission below 600 nm.

9.2.4 Scattering Measurements

One of the advantages of the experimental method presented in this chapter is that the same equipment can be used to measure both the transmitted light at tails wavelengths that reaches the end of the LSC and the scattering intensity from the side of the LSC. As illustrated in Figure 9.2, the scattering intensity, $E_x(\lambda)$, was recorded at a various lateral distances, x, from the LSC entry surface, with the integrating sphere positioned at the side of the LSC. $E_x(\lambda)$ was measured at N different positions, spaced evenly along the side of the LSC, with an integration time of 1.2 seconds. For this study, the collector length was L = 1200 mm, and $E_x(\lambda)$ was measured at 100 mm intervals between x = 100 mm and x = 1100 mm ($N = 11$). To ensure that the scattering measurements only contain light traveling in the forward direction, back-reflected light from the LSC end surface was excluded by placing black absorbing tape across the entire width of the LSC, on the top surface near the output end.

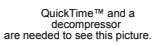

[Production Note: This figure is not included in this digital copy.
The print copy of the thesis is available for consultation at UTS Library.]

Figure 9.2 Side view of the experimental set-up for scattering measurements.

The total spectral power scattered from the top, bottom and sides of the sheet, $P_s(\lambda)$, was calculated by summing the measured values of $E_x(\lambda)$ over all x positions, and multiplying by four,

$$P_S(\lambda) = 4\sum_{x_1}^{x_N} \frac{E_x(\lambda)dx}{w_{\text{det}}\tau\Delta\lambda} \quad (\text{counts.s}^{-1}.\text{nm}^{-1}) \tag{9.5}$$

where $E_x(\lambda)$ is the spectral intensity at the LSC side surface (counts); x the distance from its entry surface(m); τ is the spectrometer integration time used for measurement of $E_x(\lambda)$ (sec) and dx is the length interval represented by each measurement (m). Note that the sum in equation (9.5) is multiplied by four because isotropic scattering leads to equal amounts of scattered light escaping from the top, bottom, left and right hand sides of the LSC.

The scattering spectrum, $S(\lambda)$, was calculated by dividing the scattered spectral power $P_S(\lambda)$ by the input spectral power $P_o(\lambda)$:

$$S(\lambda) = \frac{P_S(\lambda)}{P_O(\lambda)} \tag{9.6}$$

The mean scattered fraction, $\overline{S}$, was calculated by averaging $S(\lambda)$ over the effective tails region of the dye.

9.2.5 Absorption

After measuring the transmission and scattering spectra, calculation of the absorption spectrum, $A(\lambda)$, was straightforward. Photons traveling lengthwise through an LSC must be either transmitted, scattered or absorbed. Therefore, to uphold the conservation of energy principle, the three components must sum to unity at each wavelength:

$$T(\lambda) + S(\lambda) + A(\lambda) = 1 \tag{9.7}$$

Note that equations (9.3) to (9.7) do not hold for wavelengths where dye emission is present, as some photons at these wavelengths have been converted by fluorescence from lower wavelength photons. So this type of analysis is best applied to the tails region where dye emission is negligible. Methods of extending the analysis to wavelengths where there is dye emission are discussed in section 9.3.1.

It follows from equation (9.7) that the mean values of the three components must also sum to unity:

$$\overline{T} + \overline{S} + \overline{A} = 1 \tag{9.8}$$

Therefore, the absorption spectrum, $A(\lambda)$, and the mean tails absorption $\overline{A}$ are calculated by substitution of the measured tails transmission and scattering values into equations (9.7) and (9.8) respectively.

When properly dissolved, most suitable dyes for LSC's appear to have negligible absorption in the tails region for transmission across standard sheet thicknesses of a few millimetres. However, for typical transport distances inside a useful LSC (often > 1000 mm), we show below that tails absorption in as-prepared LSC sheets extends across the whole emission spectrum. This tails absorption, though small, is important and such tails absorption was also recently found by Wilson et al (Wilson et al. 2010b) at shorter LSC lengths. This absorption tail is slowly varying with wavelength and thus does not affect the output spectrum that largely attains its asymptotic value after a few centimetres of travel due to re-absorption from overlap of the main absorption peak with the emission spectrum. However, though weak, we show below that initial tails absorption is strong enough to significantly reduce edge output approximately in proportion to length. A key feature in this chapter is the significant growth in tails absorption and hence loss of output resulting from visible light induced photoproducts.

9.2.6 Stability Testing

Before and after various periods of outdoor exposure, the overall performance of the LSC's was tested by measuring the dye absorption, output luminous flux, half-length and mean tails transmission. Photometric quantities are of primary interest in this study rather than radiometric quantities, as the LSC's under test were being used for a lighting system. Therefore, during outdoor exposure, the solar illuminance was monitored with a lux meter, tuned to the spectral response of the human eye (*Li-Cor® LI-210®*). Dye absorption was monitored in 50 mm x 65 mm x 2.0 mm samples by measuring the attenuation coefficient, α (m^{-1}), over a 2.0 mm path length, at the dye's peak absorption wavelength of 472 nm, with a *Cary 5E® UV-VIS-NIR* spectrometer. The output luminous flux, F, and half-length, $L_{½}$, were measured using the same LSC sample analyzed in section 9.3.1 below, with dimensions 1200 mm x 150 mm x 2.0 mm. $L_{½}$ was defined in section 7.4.1 as the path length over which 50% of the fluorescently emitted light is lost due to extinction. Half-lengths were measured using the experimental method described in section 7.4.2 and (Earp et al. 2004a). F was measured from one of the narrow end surfaces using a *Minolta® CL-200®* lux meter and a 500 mm diameter integrating sphere, by illuminating the sample with two 1.2 m long fluorescent tubes (one UV tube and one 'Daylight' tube). The performance results for a green LSC are discussed in section 9.3.2.

9.3 Results and Discussion

9.3.1 Tails Extinction

Experimental results are presented below for the green LSC described in section 9.2.1. The LSC was initially tested before exposure, then again after six days' exposure to sunlight underneath a

UV cover, which blocks all UV radiation below 340 nm. The total illuminance was 2.4 Mlux.h. The measured spectra are presented in Figure 9.3 that was earlier presented as Figure 2.10 and is repeated here for the sake of convenience. In the region from 500 nm ≤ λ ≤ 600 nm, the measured scattering component contains excess signal above a Rayleigh scattering curve ($S(\lambda) \sim \lambda^{-4}$) fitted to the scattering data for λ > 600 nm (dotted line). The scattered light spectrum has two peaks at 525 nm and 555 nm, which correspond to the characteristic secondary and tertiary emission peaks of the *Lumogen*® F083 dye. Therefore, this portion of the side-scattered spectrum above a Rayleigh plot can be attributed to dye emission, and was consequently excluded from the energy balance sum to conform with the assumptions underlying equations (9.7) and (9.8). Hence for this sample, for the sake of simplicity, calculations of $\overline{T}$, $\overline{S}$ and $\overline{A}$ have been restricted to the region 600 nm ≤ λ ≤ 750 nm to avoid interference from dye emission. The apparatus could be improved to allow a study of extinction over the complete tails zone by reducing or eliminating the emitted radiation component. This could be done by adding a long pass filter, or by adding a small piece of the same LSC material orthogonal to the input light source optic fibre, between the fibre and the LSC. This filter would absorb a large portion of the photons within the absorption region of the dye, eliminating or significantly reducing fluorescent emission from the sample.

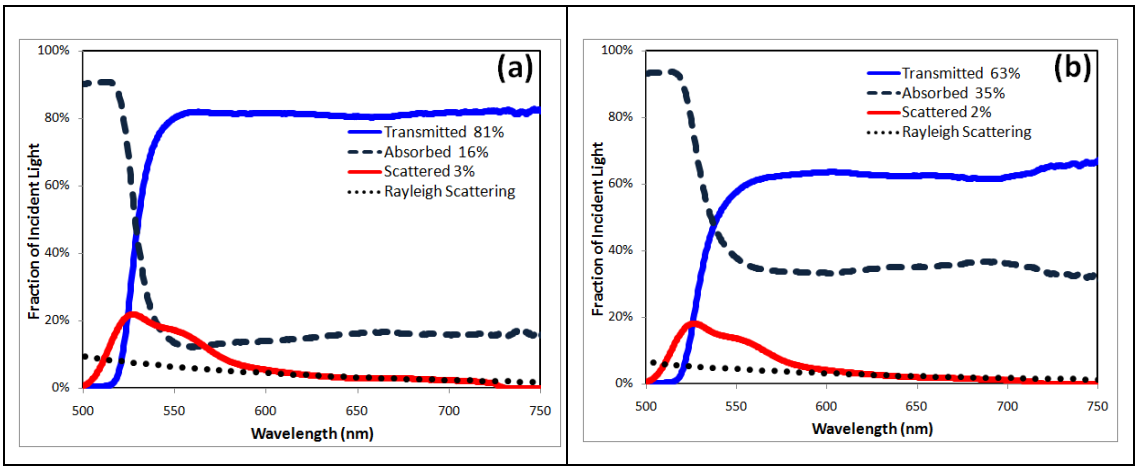

Figure 9.3 Tails extinction measurements for a 1.2 m long green LSC (a) before exposure, (b) after 6 days outdoor exposure. A Rayleigh scattering function has been fitted for λ > 600 nm.

Table 9-1 shows the mean tails transmission, absorption and scattering components for the LSC before and after outdoor exposure. Before exposure, the 1.2 metre long LSC's showed high transmission in the tails region ($\overline{T}$= 81.6 ± 0.5%), with 2.6 ± 0.5% extinction due to scattering and 15.8 ± 0.5% due to absorption. After outdoor exposure, the tails transmission dropped considerably ($\overline{T}$= 63.5 ± 0.5%), while the scattering component remained small ($\overline{S}$=

1.6 ± 0.5%). The initial mean scattering value of $\overline{S}$ = 2.6 ± 0.5% would be expected to drop to $\overline{S}$ = 2.0 ± 0.5% due to the measured reduction in LSC transmission (if more light is absorbed, less is available for scattering so the amount of light scattered will decrease, even if the scattering probability is unchanged). This expected scattering value is not significantly different from the observed scattering component after exposure, $\overline{S}$ = 1.6 ± 0.5%. In other words, the scattering component after outdoor exposure was not significantly different from the initial value. Therefore, by deduction, the marked decrease in transmission observed for this LSC sample after exposure is wholly due to increased tails absorption (from $\overline{A}$ = 15.8 ± 0.5% to $\overline{A}$ = 34.9 ± 0.5%). Hence though the fluorescently active dye loss was small at only a few %, the severe loss of ability of this 1.2 metre long LSC sample to transport light after solar exposure renders it unsuitable for applications in which the LSC is more than about 20 cm long. The tails absorption, which is approximately constant across the emission band, more than doubled after only 6 days outdoors despite the LSC being underneath a UV blocking cover.

Table 9-1 Mean transmission and extinction components in the wavelength range 600 nm – 750 nm for a green LSC containing *Lumogen*® F083 fluorescent dye, before and after outdoor exposure.

Treatment	Exposure (Mlux.h)	$\overline{T}$	$\overline{S}$	$\overline{A}$
Initial	0	81.6 ± 0.5%	2.6 ± 0.5%	15.8 ± 0.7%
Exposed 6 days	2.43	63.5 ± 0.5%	1.6± 0.5%	34.9 ± 0.7%

The observed degradation does not appear to be specific to the dye colour, as similar degradation was observed for three different *Lumogen*® dyes (F083 yellow, F285 pink and F570 violet, all made by BASF) in the same PMMA matrix with the same preparation method. Nor does the photodegradation appear to be due to UV radiation, as all radiation below 340 nm in wavelength was blocked, with a series of thicker UV cover sheets also having no effect. Similar bleaching of organic dyes under visible light exposure has been observed in the absence of UV light (Kinderman et al. 2007a; van Sark et al. 2008a).

One possibility is that the poor photostability to light transport in this LSC is due to products resulting from photooxidation of dye molecules from interactions with impurities in the matrix during photoexcitation. Another possible source of absorbing photoproducts is residual monomer, which is the largest contaminant even though present at under 0.3% by weight. LSC stability is known to be strongly sensitive to minor ingredients in the matrix including additives and residual monomer (Kinderman et al. 2007a). Thermal gravimetric

analysis (TGA) of these LSC samples indicated the presence of nontrivial levels of residual monomer. Thus further annealing of LSC samples prior to exposure may help reduce residual monomer levels and thus improve their stability

Ketone impurities in the matrix are one possibility though only very low levels are present. Some of our published experimental results show that ketones can cause significant photodegradation in *Lumogen*® F083 dye solutions, and also that photostability may be improved by adding an anti-oxidant such as DABCO (1,4-diazabicyclo-[2.2.2] octane) (Earp et al. 2010). The presence of oxygen has been linked to increased degradation rates for both organic dyes (Seybold & Wagenblast 1989) and quantum dots (van Sark et al. 2002). Thus antioxidants are commonly used to improve stability in solar energy applications, such as polymer encapsulants for photovoltaic modules, particularly in combination with UV stabilisers (Pern 1996a). Further work is required to confirm the benefit of using antioxidants in solid PMMA LSC samples and to clearly identify the origins of the tails absorption

Nonetheless, the data in Figure 9.3 and Table 9-1 confirm that the photoproducts formed in this LSC during outdoor exposure are predominantly absorbing in nature, rather than scattering. What is intriguing is that this absorption band is broad and flat (which also tends to rule out scattering). This is also indicative of formation of a range of absorbing species, or of large molecules or molecular clusters forming, rather than the molecular break up expected with normal photoquenching. As shown below, these absorbing photoproducts cause a significant reduction in LSC luminous output at the desired end. This is accompanied by a relatively small decrease in fluorescent absorption. Further work is required to confirm the cause of the instability, its link if any to the small drop in dye absorption, and hence to identify potential means of improving photostability in PMMA LSC's.

9.3.2 Overall Performance

Four performance parameters (dye absorption, luminous output, half-length and mean tails transmission) were measured for the LSC tested above, using different sized LSC samples before exposure and after exposure outdoors underneath a UV blocking cover. Each measurement was repeated three times at each exposure condition, and average values were calculated. All samples were cut from the same master sheet, and exposed simultaneously with the same conditions, so the photodegradation curves are directly comparable. The mean tails transmission ($\overline{T}$) was measured over a 300 mm path length using a 300 mm x 100 mm x 2.0 mm sample, and the measured attenuation losses were scaled to the same path length as the full-sized LSC (1200 mm), for comparison to $L_{½}$ and F. Each parameter was divided by its initial

value to give relative performance after exposure, and the degradation curves are plotted in Figure 9.4.

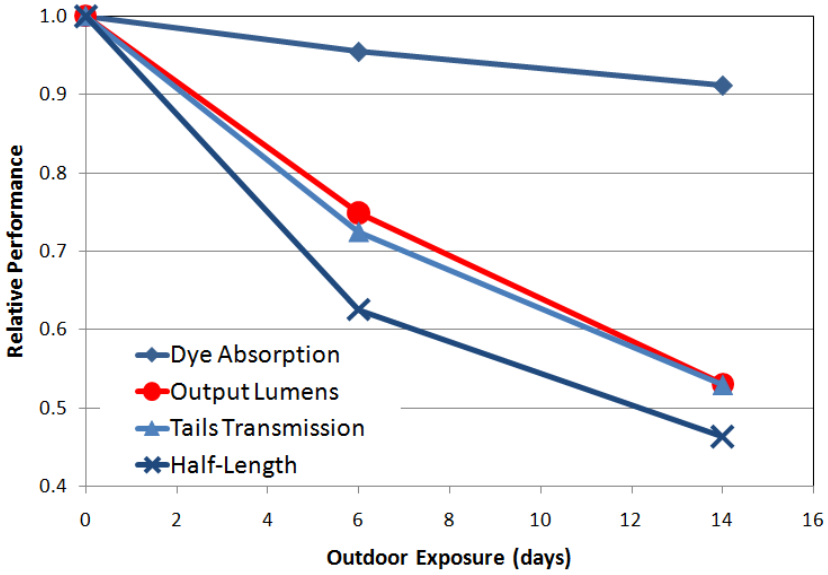

Figure 9.4 Relative performance of green LSC after outdoor exposure for dye absorption, output luminous flux, mean tails transmission and half-length.

From Figure 9.4 it is evident that the Lumogen F 083 dye in PMMA experienced some fluorescence quenching, as the dye absorption dropped by 9% after two weeks exposure with UV blocking (averaging 4.5% loss per week). For the same dye in a PMMA/ HEMA matrix, Kinderman et al. (Kinderman et al. 2007a) measured a 31% reduction in relative absorption after the equivalent of 8 months outdoor exposure, (averaging <1% loss per week). However, when the same dye was cast in a commercially available *Plexit* 55® PMMA matrix (which was believed to contain additives such as UV stabilisers), an 80% reduction in absorption was observed after only 2 months (> 10% loss per week). The above results highlight the sensitivity of organic dye stability to minor components in the matrix. van Sark et al. (van Sark et al. 2008a) found that the absorbance of *Lumogen*® Red F305 dye in PMMA only dropped by 3% after 85 weeks outdoor exposure, when the monomer was distilled to remove minor impurities prior to casting. However, for the same dye in *Plexit* 55®, the absorbance reduced by 15% over the same time period. Thus distillation of the monomer prior to casting is promising as a means of increasing matrix purity and improving dye stability in a LSC. Some alternative organic dyes have been shown to have poor stability in PMMA, such as *CRS040*® blue dye in distilled PMMA and *Pyrromethen* 580® dye in *Plexit* 55® (van Sark et al. 2008a) and *Fluorescence Red G*® and *S13*® by *Macrolex*® (Kinderman et al. 2007a). Thus purifying the matrix should improve LSC stability, but only if the dye itself exhibits good inherent stability.

However, the best indicator of overall LSC performance for daylighting applications is not the dye absorbance, but the output luminous flux, F, which dropped by approximately 50% over the same time period. These measurements indicate that the reduced dye photostability of this dye/PMMA combination and the increasing tails absorption may be linked. Furthermore, L½ and T are both strongly correlated with the output luminous flux, showing similar reductions of about 50% after 14 days — approximately five times the corresponding reduction observed in dye absorption. Hence for large area LSC's, the output luminous flux is around five times more sensitive to changes in tails absorption than it is to fluorescence quenching.

This is an important result with strong implications for the way LSC's are tested for photostability. As indicators of overall LSC performance, F, $L_{½}$ and $\overline{T}$ are more informative than dye absorption, as they are each sensitive to small changes in the light transport properties within the LSC, whereas dye absorption measurements only give information about fluorescence quenching. The products of fluorescence quenching may be the source of the observed enhanced tails absorption, but other photoproducts cannot be ruled out. It is noteworthy that, as seen in Figure 9.3, these tails (although less intense) exist in as prepared samples but were *not* found in un-doped PMMA. So it is possible that a sub-set of dye molecules which are not fully dispersed but aggregated from the outset is involved, as proposed by (Wilson et al. 2010b), and that the energy provided by illumination allows more such clusters to form. Given we have taken great care to monitor dye dispersion in solution prior to casting it is quite possible that some dye aggregates are forming during polymerisation with mobility provided by the heat involved during polymerisation and subsequent thermal annealing, and either mobility or dye aggregation could be aided by trace impurities, given the benefits noted above of ultra high purity. Heat is also generated under solar illumination from both the dye Stokes shift and from various NIR absorption peaks in PMMA. If this is the case limiting dye molecule mobility should enhance stability. The influence of details of the internal crystal structure of the PMMA, possibly including trace impurities and residual monomer, are worth investigating in this regard.

For photovoltaic applications of LSC's, the wavelength range of interest is not limited to visible light, so the ultimate performance parameter is the power generated by the solar cells, rather than the luminous flux. In this case, the wavelength range for measurement of $L_{½}$ and $\overline{T}$, may be chosen to suit a particular dye or solar cell response and smaller LSC lengths may suffice. Nonetheless, whatever the wavelength range, $L_{½}$ and $\overline{T}$ are valuable parameters for describing overall LSC efficiency, particularly for larger area LSC's, due to their high sensitivity to tails extinction and direct impact on lumens produced.

9.4 CONCLUSIONS

An experimental method is described above for measuring the extinction tails that extend across the whole emission band in LSC's, and mathematically subdividing this extinction into scattering and absorption components. The scattering component has classic Rayleigh spectral dispersion while the absorption component is almost spectrally flat. Measurements on a green PMMA LSC containing *Lumogen*® F083 dye indicated a sharp rise in tails absorption after only 6 days exposure outdoors underneath a UV blocking cover. However, the scattering component remained essentially constant after exposure, indicating that the main source of photoinduced extinction losses for this LSC was an absorbing photoproduct.

By comparing the dye absorption, light transport properties and output luminous flux of the same LSC after exposure, it was found that the overall LSC performance was approximately five times more sensitive to growth in tails absorption than to fluorescence quenching. Hence maintaining low tails absorption levels is crucial for maintaining high collector output. These results highlight the importance of monitoring tails absorption in LSC's after outdoor exposure, as a sensitive test for the onset of degradation and the presence of absorbing photoproducts. Simply checking for dye quenching, as is often done, is clearly from this work a misleading indicator of long-term stability. Identification of the species responsible for this growth in tails absorption and their formation mechanism is a difficult task but would greatly aid in developing LSC's that are sufficiently stable for various long term outdoors applications. The absence of these absorption tails in as prepared PMMA and their presence at significant but much weaker levels in as prepared dye doped samples indicates one strong possibility is dye molecule aggregation induced by heat or illumination. Given the enhanced stability found in some reported PMMA made from ultra pure monomer this dye molecule aggregation may be aided by trace impurities with the heat from solar illumination by itself insufficient to form the problem photoproducts. If dye aggregation is not the main problem, either heat or visible light could be facilitating dye reactions with impurities by enhancing impurity mobility and dye-impurity reaction kinetics.

10 PHOTODEGRADATION OF FLUORESCENT SHEETS

10.1 INTRODUCTION

Chapter 9 showed that the dominant extinction mechanism in LSC's is spectrally flat absorption extending across the emission band. This chapter explores in detail the photostability of PMMA LSC's containing organic dyes in order to identify the most significant factors resulting in the photodegradation of dye absorption and the ensuing growth of tails absorption with increased exposure. The effects of ultraviolet radiation, UV additives, antioxidants, heat and illumination are all assessed for their impact on LSC photostability.

10.2 EXPERIMENTAL METHOD AND THEORY

10.2.1 Sample Preparation

For this study, two batches of LSC's were produced from 2.0 mm thick cast PMMA sheets, each containing one of the following *Lumogen*® fluorescent dyes (by *BASF*), violet F570 (at a concentration of 120 ppm), green F083 (at 60 ppm), pink F285 (at 50 ppm). The peak wavelengths of the absorption and emission spectra and the tails regions of the three dyes are shown in Table 10-1 below. Clear cast sheets were also made with the same protocol but no dye, to serve as controls.

Table 10-1 Fluorescence peak wavelengths and tails absorption regions for the dyes used in this study

Lumogen® Dye	Absorption maximum (nm)	Emission Maximum (nm)	Tails region (nm)
Violet F570	377	415	500 – 800
Green F083	472	504	590 – 800
Pink F285	549	579	650 – 800

Since using LSC's for lighting requires the collector long axis to be at least one metre in length, the sample had to be obtained from a commercial supplier in Japan. The production process is described Chapter 8 and sections A.1 and A.4 of Appendix A. The dye was first completely dissolved in pure MMA at about 10 times the sheet concentration. The methods and test procedures outlined in sections 8.2 and 8.3 were used to ensure that the dye was completely

dissolved. The dyed MMA was then added to pure pre-polymer and an initiator. Initial polymerisation took place in a temperature controlled water bath, followed by an air anneal to reduce the concentration of residual monomer.

The experiments described in section 9.3.1 and (Earp et al. 2009) suggested that ketones and/or excess residual monomer could be contributors to the photodegradation and that the antioxidant DABCO (1,4-diazabicyclo-[2.2.2] octane) could be added to improve photostability. Accordingly, the sheets were made from a casting solution of very pure pre-polymer (inorganic impurities at parts per billion level, organic molecule impurities such as ketones under 1 ppm), peroxide initiator and fully dispersed dye. (Peroxide initiator was used as earlier work showed that this gave superior half-lengths (Franklin & Swift 1997).) Two batches of LSC's were made for this study, both containing a UV stabiliser, the nature of which was not disclosed by the LSC manufacturer. The second batch also contains the antioxidant DABCO with an approximately equimolar concentration to the F083 dye (0.2 mM). Initial polymerisation takes place in a temperature controlled water bath, followed by an extended air anneal to ensure residual monomer levels were below 0.5%.

Clear and dyed LSC samples were produced by cutting sections from the master sheets and diamond polishing the four thin edges with a diamond polisher (*C.R. Clarke 1550*®). Samples were prepared with dimensions of 300 mm x 100 mm x 2.0 mm. This sample size has the advantage of being suitable for measuring dye absorption over the thickness of the sheets (a 2.0 mm path length) as well as tails transmission over the 300 mm longitudinal path length, and it is also large enough to use for luminous output measurements. Thus all three performance parameters could be readily monitored as a function of exposure time with these samples.

10.2.2 Spectral Measurements

The tails transmission of the LSC samples was measured using an experimental method similar to that described in section 9.2.2, although based on the findings of section 9.3, the additional tails extinction with exposure is almost entirely attributed to absorption. Thus it was not necessary to separate extinction into scattering and absorption components, simplifying the technique and analysis. As illustrated in Figure 10.1, LSC samples were illuminated with an optic fibre illuminator containing a 50W tungsten halide lamp, connected to a 1 m long, 18 mm diameter polymer optic fibre (*Lumenyte*®) and a 1.0 mm x 20 mm slit. The main difference of this setup to that of Figure 9.1 is the addition of a 500 mm diameter integrating sphere with a rectangular entry port that was used to collect the entire output from the small end surface of the LSC (100 mm x 2 mm). Output spectra were measured at a 25 mm diameter detector port using a 38 mm diameter *FOIS-1*® fibre optic integrating sphere (*Ocean Optics*®*),* with a 9.5 mm diameter sample port, connected via a 50 μm diameter optic fibre to a *USB2000*® UV-visible

spectrometer (*Ocean Optics*®). Spectra were recorded over the range 350 – 1000 nm with a PC using *Spectrasuite*® software (*Ocean Optics*®). Stray light was excluded from the measurement by placing a black cloth over the top surface of the LSC adjacent to the integrating sphere port, and by using a black PMMA base sheet (*Plexiglas*®).

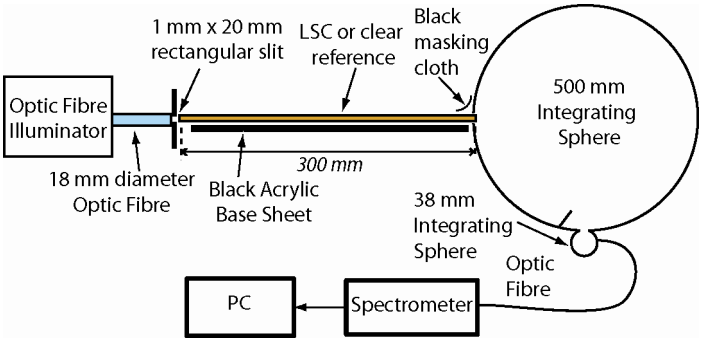

Figure 10.1 Experimental setup for tails transmission measurements.

Initially, the light source was coupled into the clear reference sheet, and after subtracting the background signal, the output signal at its end surface, $E_C(\lambda)$, was measured with the integrating sphere and spectrometer according to the setup shown in Figure 10.1. The clear sample was then replaced with a dyed LSC, and the output signal from its end surface, $E_D(\lambda)$, was recorded. As the sample geometry and production method are identical for the clear and dyed samples, the only difference between these measurements is the presence of the dye. Hence the transmission spectrum of the LSC, $T(\lambda)$, was calculated by dividing the transmitted signal from the dyed LSC by that of the clear reference:

$$T(\lambda) = \frac{E_D(\lambda)}{E_C(\lambda)} \tag{10.1}$$

$T(\lambda)$ was measured three times for each sample, and the average value was calculated.

When properly dissolved, most suitable dyes for LSC's appear to have negligible absorption in the tails region for transmission across standard sheet thicknesses of a few millimetres. However, as discussed in section 9.3, for typical transport distances inside a useful LSC length, tails absorption in as-prepared LSC sheets, although weak, has a significant impact that extends across the whole emission spectrum (Earp, Smith & Franklin 2010). Similar tails absorption was also found recently by Wilson et al. (Wilson et al. 2010a) at shorter LSC lengths. This chapter expands upon our published work as outlined in chapter 9 and (Earp, Smith & Franklin 2010) and shows that long wavelength dye absorption can increase significantly with exposure, and also addresses some of the potential factors contributing to dye degradation.

Dye attenuation coefficients α (m^{-1}) were measured with a *Cary 5E® UV-VIS-NIR* spectrometer for 2.0 mm path lengths over the wavelength range 250 nm – 800 nm, using 50 mm x 65 mm x 2.0 mm samples. Emission spectra were measured with an *LS50®* fluorescence spectrometer (*Perkin Elmer®*) using 50 mm x 10 mm x 2.0 mm samples. Each spectrum was measured three times and the average value was calculated. The specular transmission of the UV blocking cover sheet was measured in the wavelength range 250 – 800 nm with a *Cary 5E®* UV-VIS-NIR spectrometer, and the total hemispherical transmittance was measured by Alan Earp at UNSW in the wavelength range 210 – 800 nm with a *Cary 5G® UV-VIS-NIR* spectrometer, using an integrating sphere fitting.

10.2.3 Luminous Output

Luminous output was measured using a similar setup to the tails transmission measurement in Figure 10.1. However in this case, the sample was illuminated from above with two 1.2 m long fluorescent tubes (one UV tube and one 'Daylight' tube), and the fluorescent emission from one of the narrow end surfaces was collected with the 500 mm diameter integrating sphere and the illuminance was measured with a *Minolta® CL-200®* lux meter. A lux-to-lumens conversion factor was calculated for the integrating sphere using direct sunlight, by comparing the illuminance measured at the detector port to the luminous flux entering the rectangular slit of known size. Hence for each sample, the illuminance measurements (lux) at the detector port of the integrating sphere were converted to luminous flux (lm). As the LSC emission spectrum requires a path length of approximately 300 mm to stabilise due to the overlap of the dye absorption and emission regions, the 300 mm long samples used here are the minimum sample length suitable for luminous output measurements.

10.2.4 Stability Testing

The LSC samples were initially tested prior to exposure, then installed outdoors in Sydney, inside a weatherproof housing underneath a UV blocking cover, which blocks all UV radiation below 330 nm. The overall performance of each LSC was tested before and after various periods of outdoor exposure by measuring the dye absorption, output luminous flux, and tails transmission as described above. Photometric quantities are of primary interest in this study rather than radiometric quantities, as the LSC's under test were being used for a lighting system. Therefore, during outdoor exposure, the solar illuminance was monitored with a *Li-Cor® LI-210®* that has a spectral response similar to the photopic response of the human eye.

For this study, two batches of LSC's were tested during different months with varying sunlight conditions. Hence in order to compare the two sets of results, the total exposure was quoted not in terms of calendar days, but in terms of a standard typical clear sky reference day

during the initial exposure period with a total illuminance of 560 klux.h. Hence the degradation rates (per day) resulting from these curves will be slightly overestimated, as some days were overcast or partly cloudy. Nonetheless, the standard reference day was used for ease of comparison from one set of measurements to the next.

10.3 Results and Discussion

10.3.1 Stability of Dye and Tails Absorption

Experimental results are presented below for 2.0 mm thick samples of the three different coloured PMMA LSC's described in section 10.2.1. The measured dye attenuation spectra before and after outdoor exposure are presented in Figure 10.2, for three *Lumogen*® dyes in PMMA: (a) violet F570, (b) green F083, and (c) pink F285. A logarithmic scale was used to highlight the changes in three spectral regions: i) ultraviolet, ii) the dye absorption peak, and iii) the tails region. Measurements are shown for the samples before exposure (black) and after exposure periods of 10 'standard' days (dark blue) and 71 days (light blue). For reference, the relative emission spectra for each dye are shown as a dotted line.

From Figure 10.2, three distinct outcomes of photodegradation can be seen for each of the dyes. As exposure increases, 1) the dye peak absorption drops gradually due to fluorescence quenching, 2) the ultraviolet absorption at shorter wavelengths than the dye absorption peaks gradually increases, and 3) the tails absorption gradually increases. This combination of effects has been observed in other organic dye based LSC's after exposure (Wittwer, Stahl & Goetzberger 1984). In the present study, after 71 days exposure the tails absorption has increased by a factor of 5 to 10 – the largest increase here being for the green dye F083. As indicated by the dotted lines in Figure 10.2, a significant portion of the dye emission region overlaps with the growing tails absorption. Hence as demonstrated below, this photoinduced tails absorption will lead to significant reductions in luminous output for these samples.

Process 1 (fluorescence quenching) is one of the key physical observations primarily used to monitor dye stability. With the logarithmic scale used here, fluorescence quenching is only clearly visible after 71 days. Processes 1 and 2 are directly related, as the small fragments that form when dye molecules break down increase absorption, most noticeably at 300 to 350 nm, which is below the dye peak and in the UV region. Hence increases in UV absorption with exposure should correspond directly to decreases in dye peak absorption. It is possible that the products of fluorescence quenching (with high UV absorption due to smaller molecules) may also cluster together to form aggregates causing a weak long-wavelength tail. These absorption tails, though less intense, exist in as-prepared dyed samples but were not found in un-doped PMMA. At small optical path lengths of a few millimetres this tails absorption is not significant, but for path lengths >100 mm, tails absorption becomes very significant. Thus the increases in

both UV absorption and tails absorption with exposure may both stem from fluorescence quenching, but other photoproducts cannot be ruled out at this stage. The broad and flat shape of the tails absorption band is indicative of formation of a range of absorbing species, or of large molecules or molecular clusters forming, rather than the molecular break up expected with normal photo-quenching. As demonstrated previously in section 9.3.2 and (Earp, Smith & Franklin 2010; Goetzberger & Wittwer 1981), and confirmed above, these absorbing photoproducts cause a significant reduction in LSC output at the desired end, accompanied by a relatively small decrease in fluorescent absorption.

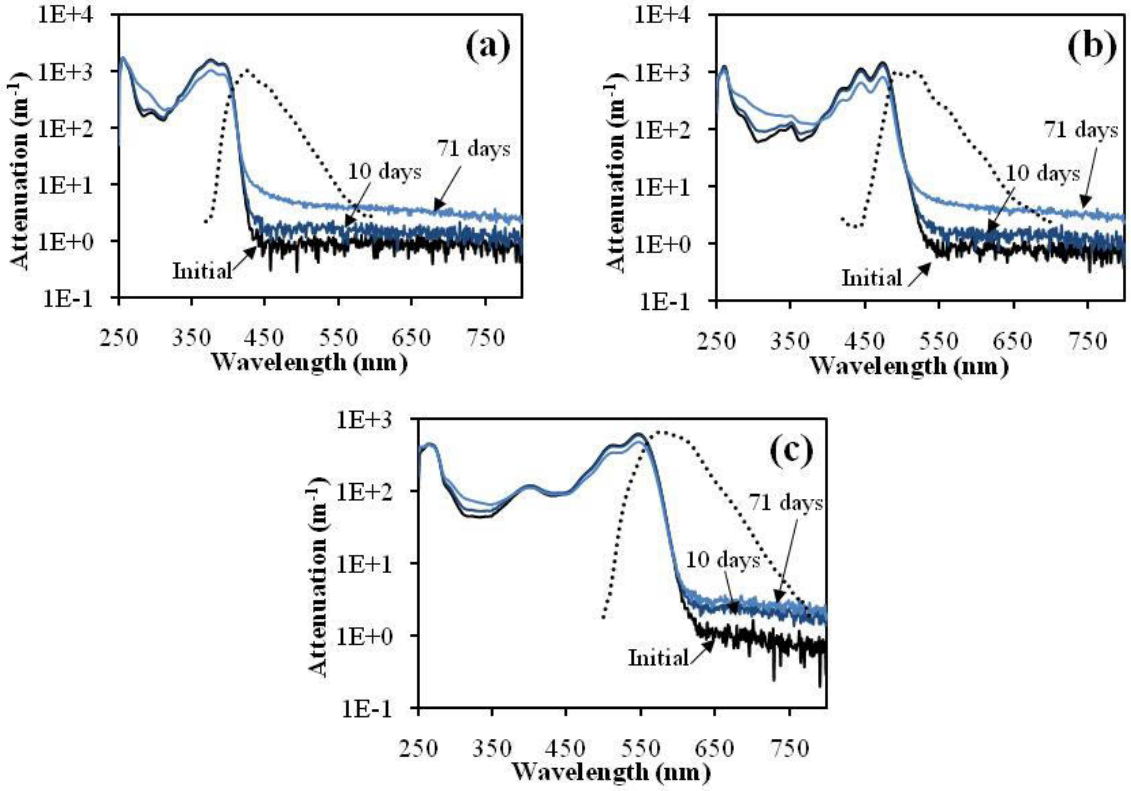

Figure 10.2 LSC dye absorption before and after outdoor exposure underneath a UV cover sheet, for three *Lumogen*® dyes in PMMA: (a) violet F570, (b) green F083, and (c) pink F285. Attenuation spectra are shown on a logarithmic scale for 2.0 mm thick samples before exposure (solid black line) and after exposure periods of 10 days (dark blue line) and 71 days (light blue line). For reference, the relative emission spectra for each dye are shown as a dotted line.

One intriguing result is that for the pink dye in Figure 10.2(c) after 10 days exposure, the dye absorption continues to drop due to fluorescence quenching, while the tails absorption stabilises, with almost no additional tails absorption after 71 days. This strongly suggests that there is another factor involved in the growth of tails absorption, and that it is not solely linked to fluorescence quenching. At this stage, the responsible mechanism is not known, although it is believed that the tails absorption growth is due to interaction between the photoexcited dye molecules and impurities in the matrix, such as residual monomer. The presence of absorption

tails in LSC's that increase with exposure has been known for almost 30 years (Goetzberger & Wittwer 1981), although as far as the authors know, no satisfactory explanation has been offered for the growth of tails absorption with exposure. Further work in isolating the particular mechanism responsible for the growth in tails absorption would play an important part in improving LSC photostability.

The noisy data in the tails region in Figure 10.2 is due to the fact that the samples have negligible tails absorption over a two mm path length. Longer integration times in the spectrometer would help increase the signal to noise ratio, but a better approach would be to increase the path length (as for the samples in Figure 10.3). Nonetheless, the differences between the tails spectra in Figure 10.2 are larger than the noise levels, so the trend of increasing tails absorption with exposure can be reliably discerned above the noise. Although the tails data in Figure 10.2 are only indicative, the observed trend of a growing absorption tail is confirmed in the more sensitive data in Figure 10.3 below.

Figure 10.3 shows the tails transmission of the same PMMA LSC's over a 300 mm path length, before and after outdoor exposure: (a) violet F570, (b) green F083, (c) pink F285, and (d) a clear reference sample. The dye emission spectra are plotted as a dotted line for reference. In some cases the nominal transmission exceeds unity due to a small contribution from dye emission. This artifact only occurs at wavelengths that overlap the dye's emission spectrum and it can be attributed to dye emission. Section 9.3.1 has some suggestions for improvements to the apparatus that would remove this artifact and allow a study of extinction over the complete tails zone.

Figure 10.3 also clearly shows that although the tails absorption over a two millimetre path length is very small, for all three dyes it correlates closely with the large reductions in LSC transmission over a 300 mm path length. This also corresponds to significant reductions in luminous output, as illustrated in Figure 10.4 for LSC's containing the violet (diamonds), green (squares) and pink (circles) dyes, as well as a three layer LSC stack consisting of violet above green above pink (triangles). As the bulk of the lumens come from the green LSC, the photodegradation curve of the three-layer stack luminous output follows that of the green LSC most closely. After 71 days exposure, the luminous outputs of the various LSC's have dropped to between 15% and 50% of their initial levels. This is an unacceptably high degradation rate; so further work must be done to improve the stability of commercially manufactured LSC's.

The unacceptable photodegradation of all the dyed samples is in stark contrast the excellent performance of the clear sheet. As Figure 10.3(d) shows, transmission in the clear sheets remained constant to within 1% for the whole of the experiment and any slight decrease can probably be attributed to minor surface damage associated with the multiple measurements experienced by this sheet (three removals from the weatherproof housing followed by at least

three independent transmission measurements at each epoch). In fact, Figure 10.3(d) strongly suggests that: (i) any change in transmission in the clear sheets due to photodegradation of the clear matrix over 71 days is << 1%, and (ii) the reduction in LSC transmission due to surface damage associated with the transmission measurements is < 0.3% per measurement cycle.

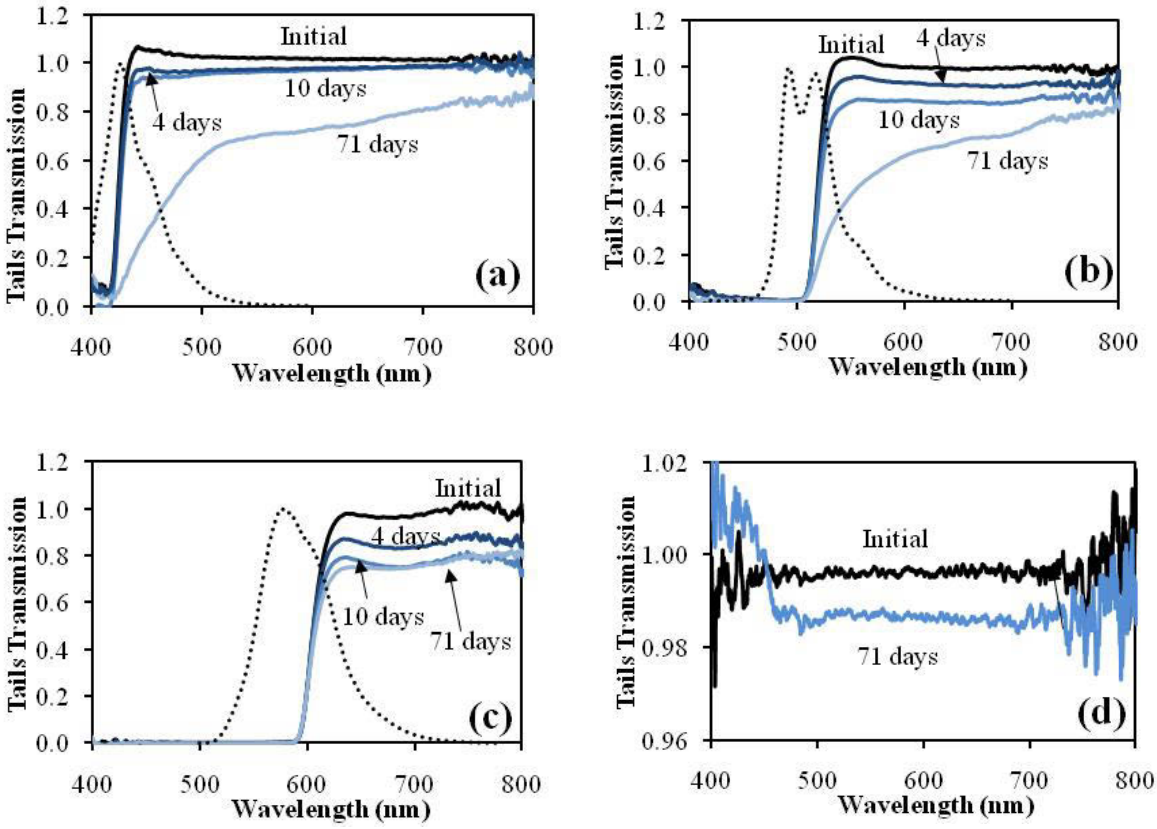

Figure 10.3 Tails transmission of PMMA LSC's containing *Lumogen*® dyes over a path length of 300 mm, before and after outdoor illumination under a UV cover sheet: (a) violet F570, (b) green F083, (c) pink F285, and (d) clear reference. (Note the 20-fold change of vertical scale for (d)). Transmission spectra were measured before exposure (solid black line), after 4 days (dark blue), 10 days (blue) and 71 days exposure (light blue). Relative dye emission spectra are shown for reference as a dotted line.

For the pink LSC, although the tails absorption stabilises after approximately 10 days (Figure 10.3c), fluorescence quenching continues to occur (Figure 10.2c), resulting in further reductions in luminous output after 71 days (Figure 10.4). Hence luminous output is sensitive to both dye absorption and tails transmission, and both properties must be stabilised for satisfactory LSC photostability. From Figure 10.3(d) it is evident that the tails absorption growth process requires the presence of the dye, as a clear matrix sample exposed for the same time period (71 days) showed less than 1% reduction in transmission over the visible wavelength region. Hence matrix instability seems at first sight not the primary cause of the photodegradation observed here, in accordance with prior studies (Hermann 1982). However

thermal or chemical impacts on the matrix structure due to dye related processes under illumination are not ruled out by studies on undoped PMMA.

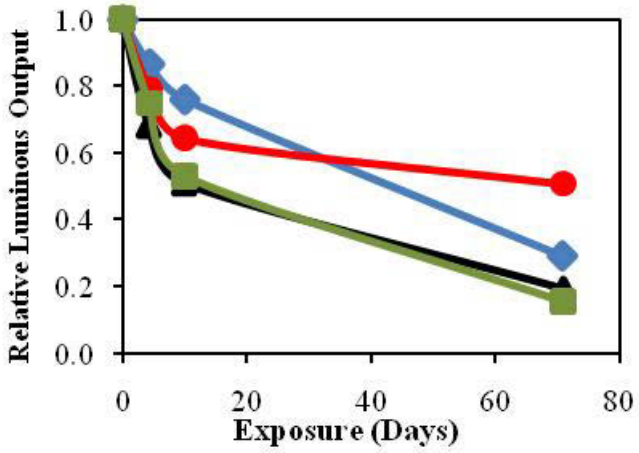

Figure 10.4 Luminous output degradation of PMMA LSC's after exposure under a UV cover sheet. Three different dyes were used: *Lumogen*® violet F570 (blue diamonds); *Lumogen*® green F083 (green squares); *Lumogen*® pink F285 (red circles); and a three layer LSC stack consisting of violet above green, above pink (black triangles).

It is noteworthy that the observed photodegradation is not limited to one dye, as similar degradation was observed for all three *Lumogen*® dyes (F083 green, F285 pink and F570 violet) in the same PMMA matrix with the same preparation method. Earlier degradation studies via dye quenching linked to lack of blocking of solar UV showed in contrast that degradation decreased noticeably in the progression violet, green and pink/red with the latter photostable in small samples, even if unprotected. This means another degradation mechanism is at work here. The remainder of this chapter investigates a number of potential contributing factors to the instability of these LSC's.

10.3.2 Impact of an Antioxidant

One possibility is that the poor photostability to light transport in these LSC's is due to products resulting from photo-oxidation of dye molecules from interactions with impurities in the matrix during photoexcitation. If this were the case, then one would expect to see improvements in stability with the use of an antioxidant. The presence of oxygen during manufacture has been linked to increased degradation rates for both organic dyes (Seybold & Wagenblast 1989) and quantum dots (van Sark et al. 2002). Antioxidants are also commonly used to improve stability in solar energy applications, such as polymer encapsulants for photovoltaic modules, particularly in combination with UV stabilisers (Pern 1996b). Antioxidants have been used to improve photostability of the F083 dye in a solvent (Earp et al. 2010). However, for this benefit to be applicable to LSC's, the antioxidant must improve dye stability in solid PMMA. The singlet oxygen quencher 1,4-diazobicyclo [2,2,2] octane (DABCO) improves the photostability

of a laser dye in PMMA, and the best results were achieved with a concentration of approximately 0.1 mM (Ahmad, Rahn & King 1999). Hence for this study, another batch of PMMA LSC's was produced using the same production method as the first, but including the antioxidant DABCO at a concentration of approximately 0.2 mM. This second batch of LSC's was tested with the same methods as outlined above, and the photodegradation curves were compared to the previous batch by plotting the exposure for both datasets in terms of standard days of 560 klux.h each.

The photodegradation curves results are plotted in Figure 10.5 for the two batches of LSC's for (a) dye absorption and (b) tails transmission, with no antioxidants (dotted lines, open shapes) and containing 0.2 mM DABCO (solid lines, closed shapes). Three dyes were tested: violet F570 (blue diamonds), green F083 (green squares), and pink F285 (red circles). After 71 days outdoors, the dye absorption dropped to 79% of its initial value for the pink dye, 69% for the violet dye and 59% for the green dye. Hence the average weekly photodegradation rates were approximately 1.8% (pink dye), 3.2% (violet dye) and 3.8% (green dye). For the green and violet dyes in a PMMA/HEMA matrix, Kinderman et al measured absorption losses of 30-35% after the equivalent of 8 months outdoor exposure (approximately 1% loss per week) (Kinderman et al. 2007b). Hence this photodegradation is three to four times faster than that observed in a similar study. No reference stability data for the pink dye could be found in the literature, although as expected from past studies with red dyes, this longer wavelength dye was more stable than the green and violet dyes. Kinderman et al also found that when the green and violet dyes were cast in a commercially available *Plexit 55*® PMMA matrix, (which was believed to contain additives such as UV stabilisers), fluorescence quenching occurred much faster than in PMMA/HEMA, particularly for the green dye. The above results highlight the sensitivity of organic dye stability to minor components in the matrix. Van Sark et al. recently found that the absorbance of *Lumogen*® Red F305 dye in PMMA only dropped by 3% after 85 weeks outdoor exposure, when the monomer was distilled to remove minor impurities prior to casting (van Sark et al. 2008b). However, for the same dye in *Plexit 55*® (*Evonik Industries AG*), the absorbance reduced by 15% over the same time period. Thus distillation of the monomer prior to casting is promising as a means of increasing matrix purity and improving dye stability in a LSC.

Figure 10.5(a) shows that the addition of the antioxidant DABCO made no significant difference to the rate of fluorescence quenching for any of these dyes in PMMA. In contrast, Figure 10.5(b) shows that for all three dyes, the use of DABCO significantly improved the stability of the tails transmission. This result suggests that the tails absorbing photoproducts form as a result of oxidation, as the use of an antioxidant slows their formation. Moreover, DABCO reduces photo-quenching for the green F083 dye in a solvent (Earp et al. 2010), but

here in solid PMMA it had no significant effect on photo-quenching. This suggests that dye breakdown in these solid samples is caused by a mechanism other than photo-oxidation, or that there is another impurity present in solid samples, which inhibits the stabilising effect of the antioxidant on photo-quenching. One possibility is residual monomer, which is the largest contaminant even though present at under 0.3 % by weight.

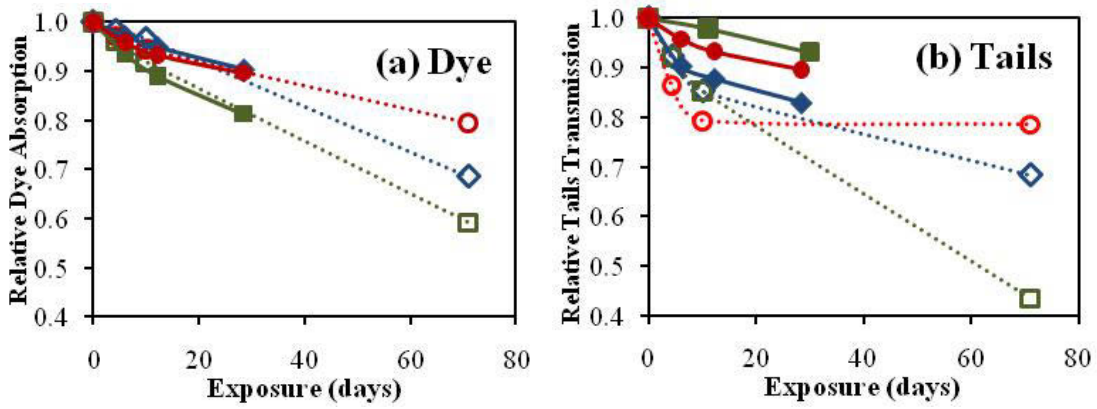

Figure 10.5 Photodegradation curves for (a) dye absorption and (b) tails transmission, for two batches of LSC's. Batch 1 (dotted lines, open shapes) contains no antioxidant while batch 2 (solid lines, closed shapes) contains 0.2 mM DABCO antioxidant. Three different *Lumogen*® dyes were used in PMMA: violet F570 (diamonds), green F083 (squares), pink F285 (circles).

As outlined above, LSC stability is known to be strongly sensitive to minor ingredients in the matrix including additives and residual monomer (Kinderman et al. 2007b). Thus further annealing of LSC samples prior to exposure may help reduce residual monomer levels and thus improve their stability. Further work is required to isolate the key mechanism responsible for dye breakdown and clearly identify the origins of the tails absorption. Nonetheless, the above results confirm that the growth of tails absorption is related to photo-oxidation, and that antioxidants can be effective in improving tails stability in PMMA LSC's.

10.3.3 Impact of UV Radiation

Another possible degradation mechanism is that a small amount of UV radiation transmitted by the UV blocking cover sheet may be contributing to dye breakdown. Three separate tests were carried out to assess the effect of UV radiation on the LSC stability. Firstly, the specular and total hemispherical transmission spectra of the UV blocking cover sheet were measured as described in section 10.2.2. For wavelengths below 330 nm, the specular transmission was $< 0.001\%$, while the diffuse transmission was approximately $0.035\% \pm 0.01\%$. Therefore, for every 10,000 incident UV photons with wavelength $\lambda \leq 330$ nm, less than four are transmitted into the LSC sheets. Hence UV radiation was not expected to have a significant impact on LSC stability.

Secondly, to confirm any impact of UV photons, the photodegradation rates of dye absorption and tails transmission were measured for a second series of LSC samples identical to those containing DABCO in Figure 10.5, by exposing the samples outdoors underneath two UV blocking cover sheets. If one cover sheet transmits one out of every 3,300 UV photons, two UV cover sheets will transmit only one photon out of 11 million. Such a small transmission may be considered negligible.

Figure 10.6 shows LSC degradation curves for (a) dye absorption and (b) tails transmission, in PMMA LSC's containing *Lumogen*® dyes - F570 violet (diamonds), F083 green (squares), and F285 pink (circles). The samples were exposed underneath either one UV cover (open shapes, solid line), or two UV covers (solid shapes). These measurements indicate that the use of a second UV cover sheet makes no significant difference to either the rate of fluorescence quenching (Figure 10.6(a)), or the build-up of tails absorbing byproducts (Figure 10.6(b)). The small differences observed are not statistically significant compared to the errors associated with the experimental method (approximatley ±2%). Accordingly, the impact of UV photons at wavelengths ≤ 330 nm was ruled out as a significant cause of LSC instability. This conclusion concurs with other observations that fluorescence quenching can occur for organic dyes under visible light exposure in the absence of UV light (Kinderman et al. 2007b; van Sark et al. 2008b), and that the photostability of PMMA LSC's is sensitive to minor impurities or additives in the matrix (Kinderman et al. 2007b). Hence the most likely explanation of the data is that the observed dye degradation is *not* primarily due to UV exposure, but is due to chemical interactions between the photoexcited dye molecules, the polymer matrix, and any additives or impurities present or generated in the matrix.

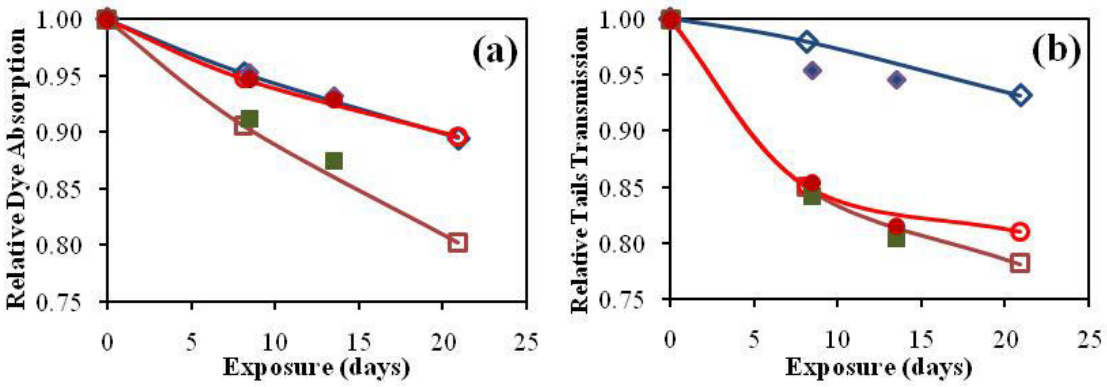

Figure 10.6 Degradation rates of various LSC performance parameters: (a) dye absorption, and (b) tails transmission. PMMA LSC's containing three different *Lumogen*® dyes: F570 violet (diamonds), F083 green (squares), and F285 pink (circles) were exposed underneath one UV cover (open shapes) or two UV covers (solid shapes).

10.3.4 The Impact of a UV Additive

Although UV radiation was ruled out as a significant contributor to dye degradation, this does not necessarily rule out the potential benefit of UV additives. In the second batch of collectors (containing DABCO), five samples were made with each dye: three at the standard concentrations listed in section 10.2.1, and two at half the standard concentrations. Each sample also contained a UV additive, the nature of which was not disclosed by the LSC manufacturer. A close inspection of the dye absorption spectra for the five different formulations reveals that the samples vary in their short wavelength UV attenuation between 250 – 300 nm. Given that the dyes have minimal absorption in this region, this variation in UV attenuation was attributed to additives that absorb at short-wavelength. Thus the magnitude of the UV absorption peak in this region was taken as an indicator of the relative concentration of the UV additive used in each sample. There was a large variation in the amount of the additive used throughout the batch, as the peak UV attenuation varied by a factor of 10, from 110 m^{-1} to 1100 m^{-1}.

To relate the concentration of the UV additive to stability, all samples were exposed simultaneously underneath a single UV cover sheet, and photodegradation curves for dye absorption and tails transmission were measured for each sample. The degradation curves initially drop sharply as the most volatile components of the dye react, and after a few days, the degradation stabilises to a slower rate. Similar behaviour has been observed for these dyes (Kinderman et al. 2007b) and other organic dyes (Batchelder, Zewail & Cole 1979b; Goetzberger & Wittwer 1981), and exponential functions have been used to fit the decay curves (El-Shaarawy et al. 2007). However, insufficient data were recorded for these fifteen LSC samples to justify exponential fits. Alternatively, empirical linear fits were made to the photodegradation curves in the stabilised degradation period between 5 days exposure and 30 days exposure. From each linear fit, the slope coefficient was used to represent the degradation rate during this time period in units of percent per day.

Figure 10.7 shows the rate of degradation of (a) dye absorption and (b) tails transmission in PMMA LSC's containing *Lumogen*® dyes violet F570 (diamonds), green F083 (squares) and pink F285 (circles), as a function of the relative concentration of the UV additive. Here the additive concentration has been quantified by recording for each sample the magnitude of the attenuation peak in the wavelength range 250 - 300 nm. From Figure 10.7(a), the rates of fluorescence quenching for all three dyes show good correlation with the relative concentration of the UV stabiliser ($0.67 < R^2 < 0.90$). This suggests that higher concentrations of the UV stabiliser are beneficial in slowing dye photodegradation. Combined with the null effect of reducing UV radiation levels (from the previous section), it is likely that the additives in the collectors are not simply UV absorbers, which only absorb UV radiation, but also free radical scavengers, which help to chemically stabilise the system.

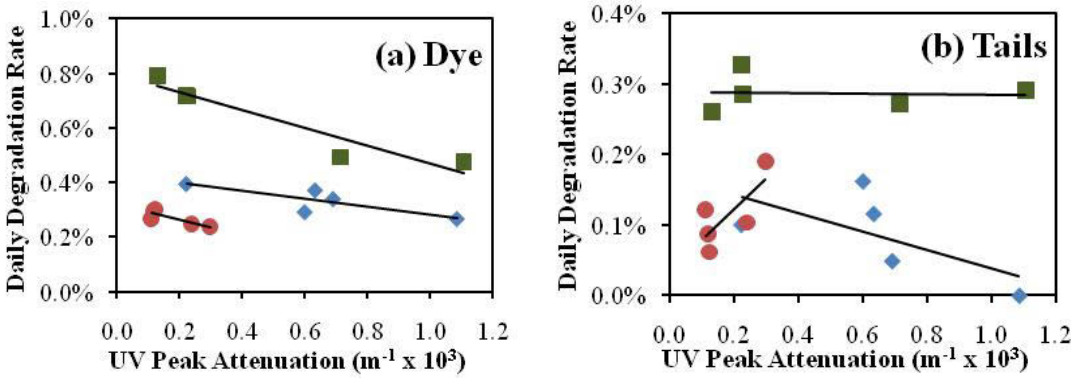

Figure 10.7 Photodegradation rates of (a) dye absorption and (b) tails transmission for PMMA LSC's containing *Lumogen*® dyes violet F570 (diamonds), green F083 (squares) and pink F285 (circles), as a function of relative concentration of a UV stabiliser. High UV peak attenuation relates to high concentration of the UV additive. Samples were exposed to sunlight under a UV cover sheet, and degradation rates were calculated from linear fits to the photodegradation curves between 5 days and 30 days exposure. Linear fits to the data are shown as solid lines to highlight any trends.

However, from Figure 10.7(b), the UV stabiliser showed no consistent effect on the tails transmission stability. For the violet dye, whose absorption region is primarily in the UV, the stabiliser appears to have a positive effect on tails transmission stability. For the green dye the effect is neutral, while for the pink dye, the degradation rates increase with increasing concentration of the UV stabiliser. However, linear fits to the data show poor correlation ($0.002 < R^2 < 0.56$), so there is not sufficient evidence to provide any reliable relationship between the UV stabiliser and the stability of tails transmission. Further to the results from section 10.3.2 above, this result also suggests that fluorescence quenching (associated with normal dye breakdown) and the formation of tails absorbing photoproducts are independent processes, requiring different catalysts. Further work in this field is required to isolate the two degradation mechanisms and determine how to reduce photodegradation rates for the two processes independently.

10.3.5 The Impact of Heat and Illumination

Another possibility is that heating the LSC's increases the mobility of the molecules within the LSC, making photodegradation more likely. Heating of organic dye-based PMMA LSC's to temperatures less than 100°C causes reductions in fluorescence (El-Shaarawy et al. 2007; Meseguer et al. 1981), which can be attributed to the formation of dimers and trimers due to increased dye mobility (Meseguer et al. 1981). If this was occurring in the current study, then the increase in dye tails absorption could be attributed to dye aggregates formed through heating, and photo-excitation would not be an important factor in the primary degradation mechanism.

This theory was tested systematically by subjecting 1200 x 150 x 2.0 mm LSC samples to four different conditions: i) light without heat – exposure with five fluorescent visible lamps and

two UV fluorescent lamps, but with the surrounding air cooled with a fan to keep the ambient temperature below 25 ^{o}C; ii) heat without light – heating samples in an oven at 100 ^{o}C for periods ranging from 24 – 72 hours (during heating, the LSC samples were suspended by holes drilled in the top corner, to maximise airflow around the LSC); iii) heat and light - sunlight exposure under a UV cover sheet; and iv) heat without light - outdoor exposure underneath an opaque cover sheet.

Any changes in the optical efficiency of the LSC's were identified by measuring the tails transmission of the LSC's before and after treatment. The results are summarised in Table 10-2 for the four different treatments, where the three right hand columns list the relative tails transmission of each sample compared to its initial value before treatment. When the LSC's were illuminated at temperatures <25 ^{o}C, the tails transmission steadily reduced with increasing duration of illumination. The violet LSC degraded much more slowly than the green and pink. This is attributed to the fact that the absorption band of the F570 dye lies mostly in the UV region, and the majority of the light from the UV fluorescent tubes was blocked by the UV cover, leaving minimal UV light at appropriate wavelengths for absorption by this dye. This suggests that photoexcitation is a key requirement for photodegradation in these samples, and that increased photoexcitation leads to faster photodegradation.

Table 10-2 Relative tails transmission (compared to initial values) of 1.2 m long LSC samples after exposure to either heat, light, or both. Dashes denote unavailable data.

LSC Treatment	Length of treatment (hrs)	Maximum Temperature (^{o}C)	Total illuminance (Mlux.h)	Relative Tails Transmission		
				Violet (F570)	Green (F083)	Pink (F285)
Light without heat (lamp)	60	25	1.0	-	0.854	0.889
	100	25	1.6	0.955	0.780	0.726
	390	25	6.3	0.953	0.603	0.605
Heat without light (oven)	24	100	0	0.946	0.986	0.984
	72	100	0	0.928	0.977	0.959
Heat and light (sun)	130	70	7.2	0.732	0.519	0.562
Heat without light (sun)	130	70	0	0.934	0.979	0.687

For the samples heated in a dark oven at 100^{o}C, the tails transmission showed only modest reductions with increased heating time. A large part of this degradation can be attributed

to the experimental method of suspending the samples during heating via a hole in their top corner. Heating of the PMMA under these conditions lead to slight warping of the LSC's, which will result in geometric light losses from the non-parallel LSC surfaces (Batchelder, Zewail & Cole 1979b). Nonetheless, one end of the LSC was unaffected, so the light source was fed into the sample through the unaffected end. As the small light losses observed for these samples are believed to be primarily geometrical losses, it was concluded that the ambient heat did not significantly increase the tails absorption in these LSC samples.

After 130 hours exposed to sunlight (11 days outdoors) with a total illuminance of 7.2 klux.h and maximum temperatures of up to 70 ^{o}C, the tails transmission had reduced to 52%, 56% and 73% for the green, pink and violet LSC's respectively. Both the violet and the green LSC showed significantly smaller reductions in tails transmission when subjected to similar temperatures, in the dark, underneath an opaque cover. Therefore, photoexcitation is believed to be a more important factor than heat in the observed degradation mechanism.

The pink sample that was heated by the sun underneath the opaque cover dropped to 69% of its initial tails transmission, showing much larger degradation than the violet and green LSC's with the same conditions. This anomaly can be explained by the fact that the pink LSC used for this test had a poor initial tails transmission of approximately 70%, with a substantial absorption peak at approximately 665 nm, while the violet and green LSC's had high tails transmission of approximately 95%. Hence it is likely that the dye was poorly dissolved in this pink sample, but well dissolved in the green and violet samples. Therefore, in this pink sample, the growth of tails absorption with heating is likely to be due to aggregation of dye molecules, as previously proposed (Meseguer et al. 1981), with a large contribution from undissolved dye.

Hence even without illumination, some tails transmission degradation is possible due to the increased mobility of heated dye molecules. However, the relative stability of the green and violet samples suggests that this is not a major problem if the dye is very well dissolved. Hence it is possible that a sub-set of dye molecules is involved, which are not fully dispersed but aggregated from the outset, as proposed by Wilson et al (Wilson et al. 2010a), and that the energy provided by illumination allows more such clusters to form. Given we have taken great care to monitor dye dispersion in solution prior to casting it is quite possible that some dye aggregates are forming during polymerisation with mobility provided by the heat involved during polymerisation and subsequent thermal annealing, and either mobility or dye aggregation could be aided by trace impurities, given the benefits of ultra high purity. Heat is also generated under solar illumination from both the dye Stokes shift and from various NIR absorption peaks in PMMA. If this is the case, then limiting dye molecule mobility should enhance stability, as previously demonstrated with an organic dye (Avnir, Levy & Reisfeld 1984). The influence of

details of the internal crystal structure of the PMMA, possibly including trace impurities and residual monomer, are worth investigating in this regard.

In summary, the data in Table 10-2 suggest that the photoexcitation of dye molecules during illumination of LSC's is the key underlying factor in the observed photodegradation mechanism, while uniform heating is not a significant factor unless undissolved dye is present. However, the details of the process initiated by photoexcitation is still to be resolved and LSC photodegradation rates are higher if heating and illumination occur simultaneously, due to the increased mobility of photoexcited dye molecules.

10.4 CONCLUSIONS

The photostability of dye peak absorption and long wavelength tails absorption were measured for a range of LSC's consisting of *Lumogen*® organic dyes in PMMA – F570 (violet), F083 (green) and F285 (pink). When these LSC's were exposed to sunlight under a UV cover, the rates of fluorescence quenching observed were approximately 3 – 4 times faster than a similar study. As the dye absorption decreased, the UV absorption and tails absorption both increased with exposure for all three dyes, leading to significant reductions in luminous output.

The use of an antioxidant (DABCO) in the LSC formulation lead to improved stability of tails absorption for all three dyes, although the fluorescence quenching rates were unaffected by the DABCO. This suggests that the formation of tails absorbing byproducts is related to an oxidative process, whereas the fluorescence quenching mechanism is not. Alternatively, the stabilising effect of the DABCO may have been inhibited by impurities in the matrix, such as residual monomer or dye aggregates. Further annealing of LSC samples may help improve stability by reducing monomer levels.

Ultraviolet radiation at wavelengths < 330 nm was ruled out as major contributing factor in the observed degradation. Decreasing the UV radiation levels by a factor of 3300 made no significant difference to either fluorescence quenching or to tails absorption photodegradation rates. However, results suggest that the use of a free radical scavenger that absorbs in the UV may still help improve photostability in PMMA LSC's. Heating of LSC's up to 100^{o}C did not cause significant photodegradation if the dye was well dissolved, although when the dye was not well-dissolved, faster growth of tails absorption occurred. Photoexcitation of dye molecules was identified as the key factor causing photodegradation in these PMMA LSC's.

The additional UV absorption and tails absorption may both be related to dye photodegradation products, although the exact mechanism linking them is unclear at this stage. Identification of the species responsible for this growth in tails absorption and their formation mechanism is a difficult task but would greatly aid in developing LSC's that are sufficiently stable for various long-term outdoors applications. The absence of these absorption tails in

as-prepared PMMA and their presence at significant, but much weaker levels in as-prepared dye doped samples indicates one strong possibility is dye molecule aggregation induced by the rise in temperature during polymerisation or under solar illumination. Given the enhanced stability found in some reported PMMA made from ultra pure monomer, this dye molecule aggregation may be aided by trace impurities with the heat from solar illumination by itself insufficient to form the problem photoproducts. If dye aggregation is not the main problem then either heat or visible light could be facilitating dye reactions with impurities by enhancing impurity mobility and dye-impurity reaction kinetics.

We have thus pinpointed the key drivers of degradation in this chapter. However, since these drivers are integral to the fluorescence processes they cannot easily be avoided entirely. However, it may be possible to reduce their impact on light transport in LSC sheets and so achieve the durable sheets required for practical daylighting with LSC's.

11 CONCLUSIONS

Creating a practical luminescent solar collector system for daylighting with high lumens-to-lumens efficiency must take account of each of three interrelated parts:

Optical design. This is a problem in geometric optics with a focus on avoiding reductions in étendue. Issues include the aspect ratio of the collector sheets, designs for high efficiency flat-to-round couplers, and high efficiency light extractors.

Mechanical design. This requires attention to strong and reliable optical joints, mass production of flat-to-round couplers, affordable flexible light guides, cover materials, roof and façade mounting, and total mass.

The optical properties of the collector sheets. Maximising fluorescence yield involves dye quantum efficiency, Stokes shift, long wavelength absorption "tails", dye dispersion, light transport inside a sheet and long term stability.

Solutions to key problems in each of these areas have been found, with the one key exception of increase in absorption tails over the long term. As-prepared complete units yielded total outdoor-to-indoor-space lumens-to-lumens efficiency with long flexible guides of around 5% as expected from quantitative studies of each of the above issues applied in simulation models.

11.1 OPTICAL AND MECHANICAL DESIGN

The key tool for sound optical design is the application of étendue to system design as outlined in section 3.1. A lack of understanding of the role of étendue was a major factor in the poor performance of prior work on LSC based daylighting. This may have been because the impact of étendue on system performance can be less in some LSC applications, such as PV and display, depending on their system geometry. The most important result from étendue analysis for LSC daylighting systems is that, to first order, the cross sectional area of the system cannot decrease along its length. Since the optical conduits are expensive, and that expense increases with their cross section, it follows that the collector sheets must have the smallest possible cross section measured perpendicular to the mean direction of light transport. This necessitates a high aspect ratio for the collector sheet if one is to achieve the collection area required for adequate output lumens.

A second, and equally important result from étendue analysis, is the absolute requirement for a solid optical system, with no air gaps anywhere along the optical path. A single air gap will block all trapped light and can halve system output. Prior daylighting studies neglected the

impact of trapped light, which is blocked by air gaps. The "offset-T-joints" of section 3.2.1 provide a method of making strong, high-efficiency optical joints from collector sheets while maintaining the essential optical isolation between stacked collector sheets.

Round optical fibres were found to have many advantages for LSC daylighting systems including good flexibility and low attenuation. Prior to this project there was no known practical method of efficiently coupling rectangular LSC sheets to round optical fibres. The "curled-sheet" designs of chapter 4 have a calculated efficiency of up to 99%. Production grade components made by injection moulding demonstrated a measured efficiency of 95% that agreed well with the modeled efficiency of 96% for the design used.

The light extractor designs of chapter 6 demonstrated a very high extraction efficiency that boosts system output by more than 60%, mainly from better use of trapped light. Our hollow-cone extractors gave close to 100% extraction and would be easy to make by injection moulding.

Full-sized pre-production units were made to the designs in this thesis and were assessed as commercial prototypes. They had sufficient light output and low enough cost to be commercially viable.

11.2 Optical Properties of the Collector Sheets

The key remaining problem is the durability of the collector sheets. A great deal of work has been done by many investigators to try to find suitable luminophores for LSC's (Debije & Verbunt 2012). The commonly agreed requirements are: i) a high quantum efficiency (most would regard 80% as a minimum), ii) a large Stokes shift to minimize losses from self-absorption, and iii) resistance to bleaching, as measured by fractional reduction in active luminophore. The BASF *Lumogen*® series of dyes were the best of class for all of these requirements when the UTS daylighting project was started and so formed the basis for this project. Recent progress with other luminophores such as quantum dots and doped inorganic nanoparticles appear as yet to not be competitive on output, although some though may have better durability and increased Stokes shift.

However, it turned out that there was a fourth requirement that ultimately overrode the other requirements. The key problem is stability of internal light transport efficiency due to the growth of the absorption tails. This ***far*** outweighs all other factors effecting cost and efficiency as a technical limiting factor. The presence and impact of these tails was almost unknown when we identified them. As chapters 9 and 10 showed, when PMMA sheets doped with *Lumogen*® dyes are exposed to ***only visible light***, a broadband though weak absorber is created that greatly reduces the light transport efficiency in the collector sheets. It is important to note that it was

shown in sections 9.2 and 9.3 that there is no measurable increase in scattering: the increased attenuation is purely through increased absorption.

The origin of this tails absorption is not understood, although chapter 10 has some hints. It may have more than one source including initial trace chemical impurities and intrinsic phenomena in the fluorescent process affecting matrix or dye molecules. However the experiments in chapter 10 showed clearly that ***UV is not the source of this problem, nor is heat by itself***. It is surprising that dyes with very different chemistries seem to give the same type of tails, and this hints at some kind of interaction of the excited dye with the matrix, or one of its components, rather than a breakdown product of the dye. It should also be noted that photoinduced loss of active dye molecules does not significantly impact directly on output.

Previous studies, and our own early work with smaller samples, equated lack of dye loss with overall optical stability. However, eliminating active dye loss has nothing to do with light transport: it just maintains net emission, while the existence of "tails" is ultimately a light transport problem.

The importance of tails in LSC sheets was not appreciated before this study because almost all previous experimental work used small samples. Unfortunately the tails are only apparent in samples that have a long optical path length. The minimum path length for good measurements is 250 mm, and 1000 mm is better. Making high quality 250 mm sheets requires a substantial laboratory and only full-sized commercial plants can produce 1000 mm sheets. An alternative technique is casting test samples in fluoropolymer tubes. A bench-top rig at UTS gave good as-prepared results for 250 mm samples and we routinely achieved high as-prepared optical quality in *Lumogen*® doped 2000 mm long rods using the facilities at Poly Optics Pty Ltd in the initial development stages of this project.

If progress is to be made in achieving a practical LSC for daylighting, future investigators will have to measure the long-term optical stability of large samples and rod casting offers a practical route for making such samples.

11.3 Areas of Future Work

Thinner collector sheets would be highly desirable for daylighting systems (but not necessarily for PV work) as for this application system cost is almost inversely proportional to LSC sheet thickness, as is the collector concentration factor. However, required luminophore concentration is inversely proportional to sheet thickness and luminophore solubility becomes an increasing problem as concentration increases. Excessive concentration can lead to very high light losses. Also, there might be some difficulties in joining very thin collector sheets to flexible guides with flat-to-round converters.

A great deal of work is being done to try to increase LSC efficiency by using luminophores that have higher quantum efficiencies, larger Stokes shifts, and less overlap between the emission and absorption spectra. Anything that could be done to reduce the long wavelength absorption tail would give a big boost to output lumens. Approaches include those noted by (de Boer et al. 2011) and by (Debije & Verbunt 2012).

However, it was argued in section 11.2 that the emphasis on efficiency is not the key problem for the short term, although the work may be useful for the long term. A dye that had a quantum efficiency of 70%, and a Stokes shift somewhat worse than the *Lumogen*® dyes, would typically be rejected as not meeting minimum criteria for either parameter. However, it would in fact be suitable for a commercially viable LSC daylighting system ***provided that it did not exhibit significant tails absorption upon photoexposure***. On the other hand, a luminophore with 99% quantum efficiency and a wide Stokes shift but similar tails losses to the *Lumogen*® dyes, would be not be of use for LSC daylighting.

The key steps to overcoming the problem of tails absorption are recognizing that it exists, finding ways to measure it, and identifying its origin. Chapters 9 and 10 have addressed two of these areas. A refocusing of current work to address this problem, which has only been recognised quite recently, is likely to yield good progress.

While the performance of current LSC systems would be acceptable if collector sheet durability was enhanced, the potential from a basic science perspective for marked improvement in the overall performance of LSC's is large. The most likely source of such gains will come from developments in the performance of luminophores. A long-term performance with around 10% lumens-to-lumens efficiency seems a practical goal. This would approximately halve the cost of each lumen of output and would lead to a many-fold increase in commercial potential. However, it cannot be over stressed that even this level of performance would not be viable without a long-term solution to the "tails" problem.

Future developments in alternative matrix and starting materials may also add to performance, or stability and to cost reductions. Possibilities include copolymers of PMMA that have been shown to improve the photostability of the matrix (Mansour 2004) and glassy polymers (Montarnal et al. 2011). These materials may also provide a route to solving the "tails" problem

APPENDIX 1: MASS PRODUCTION OF HIGH-PERFORMANCE LSC SHEETS

This appendix records some of the guidelines and production details developed during the UTS daylighting project that may be of interest to anyone attempting to mass-produce high performance LSC sheets. The core lessons and science from these studies are summarized in chapter 8.

1.1 EXTRUDED SHEET

A sheet extruder line is large, complex and very expensive. It is only suited to producing large quantities of identical sheet. However, it is the lowest cost way of producing sheet in high volumes. Changing dies and rollers is a very time consuming and expensive operation so a typical production run for a given thickness of sheet would be at least 20,000 kg. Changing the type of plastic extruded typically requires running about 500 kg of material through the machine to avoid cross-contamination, which adds to costs. This is a particular problem with fluorescent sheet as tiny amounts of fluorescent material can ruin many types of ordinary sheet. Thus the required purge volume can be much larger than standard, with details depending upon the machine. Purge volumes (and hence cost) can be reduced by making sheets in the order clear, violet, green and pink, for the reasons described in section 8.2. Purge volume will also be minimized if the next sheet to be extruded is heavily pigmented with a dark colour as a small amount of fluorescence is not apparent in these materials.

Another common problem is moisture in the pellets. The screw extruder quickly heats the material to about 223 ^{o}C (MatWeb-Extruded 2011) which causes any moisture to flash to steam with a rapid 1000-fold increase in volume. Even small amounts of moisture can lead to the formation of micro-bubbles that have a very adverse impact on the final sheet's half-length. The cure is to: (i) handle and store the pellets in a way that keeps them as dry as possible, (ii) to *thoroughly* dry the pellets before use (this takes many hours as moisture must diffuse from the centre of the pellet), (iii) pre-heat the pellets in the feed hopper to reduce thermal shock when they enter the barrel of the extruder, and (iv) to have good venting along the whole length of the extruder's barrel (some machines only vent near the feed section). In order to produce optical-grade LSC sheets, the pellet drying and venting arrangements need to be of a much higher performance standard than is required for making ordinary sheets, which has a significant cost

impact. Good venting and thorough drying also helps to remove residual monomer and other volatiles that can also lead to the formation of micro-bubbles.

Clear PMMA pellets are made by specialist manufactures via the batch polymerisation of MMA. The extrudability of the pellets depends upon their molecular weight with the optimum being about 1000 monomer units. This is less than a 10^{th} of the molecular weight of cell cast PMMA. The low molecular weight of extruded sheet means that it is relatively soft, which adversely affects its machinability and makes it more prone to edge chipping when diamond polished.

For various thermodynamic reasons, the batch polymerisation of MMA to form PMMA pellets never goes to completion: there is always a significant amount of residual monomer. Cheap pellets often have residual monomer levels as high as several percent while high-grade pellets with expensive post processing have residual monomer levels under one percent. During sheet production, the extruder heats and melts the pellets with an average barrel temperature of about 220 ^{o}C rising to a typical 233 ^{o}C at the nozzle (MatWeb-Extruded 2011). These elevated temperatures vaporise the residual monomer and on a good line this monomer gas is vented from the barrel, which reduces the concentration of residual monomer in the final sheet to a level significantly less than that of the pellets. However, the elevated temperatures also break down some of the PMMA back to MMA, which tends to increase monomer levels and sets a limit on the achievable residual monomer concentration in extruded sheet. The precise level depends on the pellets used, the designs of the extruder and extrusion die, and the skill of the operator. But it is inherently significantly higher than for best quality cast sheet. The relatively high residual monomer levels in extruded sheet reduce its hardness (particularly the surface hardness), which adversely affects its machinability.

Note that any “dead spots” or regions of poor melt flow in the extruder or extrusion die will cause some of the molten PMMA to experience an excessive period of high temperature. This will lead to thermal breakdown of the melt and the formation of excess residual monomer. In extreme cases this thermal breakdown leads to carbonised “black spots” in the final sheet. Most extrusion sets are designed so that the flow is uniform enough to not form “black spots”. However, minimising the formation of monomer is a much more stringent requirement and a production line suitable for ordinary sheets may not be suitable for making LSC sheets.

With careful pellet preparation, good barrel venting, a high-quality (million dollar plus) calendaring roller stack and the use of expensive low-tack polymer protective films, the sheet’s surface finish is good enough so that the sheet’s half-length is determined almost entirely by matrix losses. With a good extrusion line and skilled operators, matrix losses are determined primarily by the quality of the solid PMMA pellets fed into the extruder. With virgin optical-grade pellets, half-lengths of better than 5 m are readily achieved for clear sheets. “Virgin” is a

standard industry term meaning “having no admixture of recycled material”. “Virgin monomer” is MMA made by direct synthesis from basic feedstock in a $100 million plus integrated chemical plant, rather than by the destructive distillation of recycled PMMA. “Virgin pellets” are made purely from virgin monomer.

The key problem with extruded sheet is its light transport properties. Manufacturers often like to reduce costs by adding “re-grind” pellets made by grinding up waste sheets. This is standard practice for most sheet production as it recycles expensive materials and has no impact on quality for ordinary applications. However, even tiny amount of “re-grind” have a very adverse effect on half-length. The high temperatures and pressures experienced inside the extruder slightly change the polymer’s molecular weight and hence it’s refractive index. So if “re-grind” is mixed with virgin pellets and extruded, the resulting sheet has micro-regions of slightly different refractive indices. This is because although the extruder’s screw melts and stretches each “re-grind” pellet, the high viscosity of the melt means that the mixing is incomplete at a micro scale. Thus the final sheet has micro-regions that are “re-grind” and micro-regions that are “virgin pellet”. However, because of thermal processing, the “re-grind” has a slightly different refractive index to that of the virgin material. This means that the “re-grind” micro-regions scatter light via a process similar to that of the TRIMM particles described in chapter 5. The result is considerable light loss and it is not uncommon for the half-length to drop well under a meter. A quick test is the laser test procedure described in section 8.3 – sheet with even a few percent “re-grind” gives a bright laser beam unlike sheet made from virgin optical-grade pellets in which the laser beam is very faint. In sheet containing “re-grind” the scattering at right angles to the laser’s plane of polarization is highly polarized which indicates that the scale of the scattering regions is small compared to the wavelength of light (Hecht 2002, pp. 346-7).

It was mentioned in section 8.4.1 that the standard method of making dyed extruded sheet is to use a masterbatch of pellets that have a high dye concentration (typically x100). The masterbatch pellets are mixed with an appropriate fraction of clear pellets and the combination is extruded, relying on the screw in the extruder to homogenize the mixture. This method works well for ordinary sheets, but it will be shown below that this technique cannot be used to make LSC collector sheets.

The ordinary method of making masterbatch pellets is to mix the dye (usually as a powder, but sometimes dissolved in a suitable solvent) with clear pellets and to use a screw extruder to homogenize the mixture and continuously extrude 2 mm diameter rods. The molten rods are water cooled in a 5-metre long water bath, (which adds considerable moisture that must be removed at a later stage,) and chopped into pellets. (As an aside, the poor photostability of sheets made with one masterbatch was traced back to iron contamination from worn rod

cutters. PMMA rods are surprisingly abrasive and it is essential that the rod cutter blades are made from very hard materials and are properly maintained.)

It is also possible to make masterbatch pellets by the "poor man's method" of solvent casting a sheet with a high dye concentration and cutting up the sheet into pellets. Multiple attempts to do this in the early stages of the project by UTS and by one commercial masterbatcher all gave *very* bad results and the technique was abandoned.

Masterbatches made by the rod extrusion method were commissioned from three Australian and three German companies. Unfortunately, all gave sheets that had very high levels of scattering. The problem is the tendency of the *Lumogen*® dyes at high concentration to form scattering complexes. The only solution appears to be to incorporate the dyes into the polymer at the time of polymerization.

A more fundamental problem is that it is extraordinarily difficult to produce masterbatch pellets that have the same molecular weight distribution as the virgin clear pellets. If the molecular weights are slightly different then the refractive indices will also differ and the masterbatch pellets will cause the same scattering losses as "re-grind". Multiple attempts by various Australian and German companies to produce suitable dyed masterbatch were all unsuccessful. The only apparent solution is to dope the matrix pellets with the final dye concentration at the time of polymerisation. This is technically straightforward, but is relatively expensive. Unfortunately, it is not feasible on a small scale.

We did manage to arrange for a German company to produce some extruded sheets using custom manufactured pellets doped with the final dye concentration. Tests were disappointing with the sheets showing excessive scattering and very short half-lengths, consistent with a matrix half-length of approximately 0.5 m (i.e. about 10% of standard). Matrix problems were initially ruled out because clear control sheets made at the same time in the same polymerization unit had excellent half-lengths. However, further tests strongly indicated that the problem with the dyed sheets was due to excessive scattering, almost certainly due to a bad matrix, rather than any problem with dye dissolution. Lengthy investigation showed that the production staff had actually formulated a masterbatch at 10 times concentration and mixed it with clear pellets that had a closely matched molecular weight distribution. As for the clear control sheets, the technicians could not see the point of making a clear masterbatch, so they made the "control sheet" from highest quality 100% virgin optical-grade material, that is from a different batch to the pellets used for dyed sheet. This is why the sheet made from this material performed so well! Unfortunately its origin meant it was not in fact a "control sheet".

It is interesting that the dyed sheet's half-length was so poor, despite the best efforts of the production staff to match molecular weights between the masterbatch and the clear pellets. This failed experiment convinced us that there was no prospect of making good extruded LSC

sheets by masterbatching, and the only viable solution is adding the dye at time of polymerisation of the extrusion pellets.

Unfortunately we were not able to get further access to the polymerisation unit and extrusion line to conduct proper tests with fully formulated pellets. So the definitive test on whether one can make extruded dyed sheets with good light transfer properties still has to be conducted. If this approach eliminates the scattering arising from admixing slightly different materials and achieves the optical quality approaching that of its dye free counterparts, it could be attractive from a cost and mass production perspective. The main remaining drawback would be the need to make large quantities of final formulation rather than concentrated dyed masterbatch pellets, which would add to costs. While avoiding this non-standard step by our industry collaborators led to our one trial failing, production scale volumes of dyed pellets are possible and may not raise costs much for mass production.

1.2 CELL CASTING

In the cell casting process most shrinkage occurs in the thickness direction because the surfaces of the mould (tempered glass sheets) restrains the plastic sheet from shrinkage in the length-width direction. Hence, the final annealing, in which the sheet is heated to its softening point, allows it to relax or shrink and this removes residual stress (Graf 2000).

After the final heat treatment, the clamps are removed and the top glass sheet is manually detached by placing a wedge between the edges of the pair of mould sheets, and giving the wedge a sharp twist. The glass flexes in an alarming way and usually springs free of the cast sheet with a sharp cracking sound. There is a surprising amount of flexure of the glass sheet and this greatly contributes to the free release of the cast sheet. Manufacturers also usually add a small quantity of sheet release agent to the casting liquor to assist with the release of the glass mould sheets. The release agent's recipe is usually a closely held trade secret.

The goal for LSC sheets is to have the cast sheet's thickness vary by no more than ± 0.10 mm. As noted earlier a specified thickness variation of ± 0.20 mm is the industry standard but ± 0.10 mm is feasible. It is not possible to produce glass sheets that are planar to this tolerance over square metre areas. So the surface deviations of a large number of glass sheets are measured to an accuracy of < 0.01 mm. These measurements are then used to select *pairs* of mould sheets so that the surface deviations cancel out – where one glass sheet is slightly convex; the other has an exactly matching concavity and so on. The net result is a cast sheet with a good tolerance on thickness. The cast sheet's surface may still deviate from perfectly planar by up to 0.30 mm. However, this happens over a distance of perhaps 500 mm and so has no effect on light propagation inside the sheet. Note that the paired mould sheets

must always be used in the same orientation – if one sheet was rotated end-to-end it is most unlikely that the convexities and concavities would line up.

Sheet thickness also depends upon placing the sacrificial continuous PVC gasket in the correct position with straight sides and uniform corners. If this is not achieved, the mould volume will be incorrect and so the cast sheet will bulge out at the centre if the mould volume was too small, or inwards if the gasket sealed too large an area. It is also essential that the clamps are correctly placed and have the correct compressive force, although this is usually less important than the correct set up of the gasket. The gasket typically has a circumference of nine metres. Its accurate and rapid positioning requires a pair of highly trained operators that must work together as a team. Their skill and attention to detail has a major impact on the optical quality of the cast sheet.

It was pointed out in section 8.4.3 that a major problem with cell cast sheets is the variation in sheet thickness. The tight tolerances for assembly of the LSC stack mean that thick sheets can cause major problems with gluing the sheets to the flat-to-round converter. This means that it is essential that the factory have a quality control system that can reject over thickness sheets.

Other aspects of the production process can have a large impact on sheet quality, and these can sometime be challenging to diagnose.

At the start of this project, *Lumogen*® dyed green and violet sheets were available with a half-length of almost 1.0 m from Critesa SA and they were selected as the cell casting contractor. Red sheets, involving the largest dye molecules, were initially a major problem as extensive tests of multiple manufacturers showed that none of the commercially available red sheets had half-lengths of 0.50 m. However, experiments by UTS at Poly Optics Australia Pty Ltd showed that the half-length of all the *Lumogen*® dyes could be improved by using ultrasound to dissolve the dyes to a monomolecular level, with a particularly large improvement for the red dye. This lead to the procedures and test methods described in sections 8.2 and 8.3, and a patent (Franklin & Swift 1997). *Critesa* adopted our test methods and were soon producing sheets for all colours with a half-length of almost a metre.

Unfortunately the quality of the sheets then started to vary considerably from batch to batch. The problem seemed to be due to excessive scattering. A visit to the factory in Spain for several weeks and application of the techniques described in section 8.3 to test the raw MMA, "pre-pol" casting liquor and the as-produced sheets gave no anomalous results: all the starting materials and cast sheets had low scattering. However, laser testing of the factory's "sheet library" of clear sheets showed very large variations in the scattering of different batches of sheets produced over the previous two years. The available records were limited with no obvious correlation of sheet quality with any set of parameters. One factor that was suspicious

was that sometimes the factory used MMA made by destructive distillation of PMMA, rather than virgin MMA. Limited records made it impossible to test whether this was the key factor, but it was agreed that all future sheets made for the project would use virgin MMA.

Sheets made after our visit were initially of high quality. However, subsequent batches exhibited very variable quality with some half-lengths of less than 0.30 m. The inability to reliably procure good quality LSC sheets came close to shutting down the project.

Dr Günter Zimmer, the research director at that time for Resart GmbH (Critesa's parent company then) finally found the cause of the problem. He spent considerable time at the factory and used the laser testing techniques of section 8.3 to show that on occasion some of the "pre-pol" had excessive scattering. It turned out that sometimes one or more of the polymerisation vats for making "pre-pol" was not properly cleaned. Build up of small particles of PMMA gave TRIMM like scattering. He also showed that all the polymerisation vats had been carefully cleaned just before our visit. That was why our on-site laser tests of raw materials found no problems and why the sheets made at that time were good. Quality subsequently varied erratically over time as determined by the polymerisation vat's variable cleaning cycle.

It also turned out that no customer of clear or fluorescent sheets had ever complained about lack clarity or inferior optical quality. This emphasizes that production of high quality LSC sheets is much more demanding than producing standard fluorescent or clear sheets. All the cell cast manufacturers involved with this project learnt valuable lessons about weak points in their production procedures and how to fix them.

1.3 THE INDUSTRIAL CULTURE OF PLASTICS PRODUCERS

Up until now we have been concentrating on the physical and chemical aspects of sheet production while also accounting for financial parameters. However, the human element in production was also found to be critical and cannot be ignored: plastic is made by men, not by machines. (As an aside, production is literally "made by men". Over a long period working on this project at factories in Australia, Spain, Germany, Japan and China I met no women at all with line authority or working as operators on the production lines. Women were restricted to scientific staff (including 2 lab directors), logistics support, administrative support, etc.)

The biggest problem throughout the project was inertia in industrial practice and the force of Standard Operating Procedures (SOP's). Production teams usually have very good reasons for their SOP's and often feel that they know better than outsiders about the way things should be done. Most of the time they are justified in this attitude, as there is a *lot* of hard won experience and tacit knowledge in running a plastics production line. However, for an item, such as high-performance LSC sheets, new approaches are essential. One has to individually brief people so that they *understand* the value and importance of doing things differently. Even

after adhering to new protocols for one or two runs, production staff sometimes unconsciously reverted to standard procedures for later batches. It can be very frustrating to go to a foreign factory, explain things carefully to the management and the production staff, document the required procedures, and then find after a few months that the production staff have reverted to all their traditional methods and are producing junk material by the standards required for high-performance LSC sheets (it is high quality product for standard applications).

Another problem is that for some reason the plastics industry is very prone to takeovers and group reorganizations with many plants changing owners, or management teams, every few years. Indeed, ***every*** plastics plant that worked with this project had at least one such change during the project, except for one minor supplier in Indonesia that was only involved for less than one year. Each new set of managers rewrote the of Standard Operating Procedures to conform to their understanding of Standard Industry Practice, so it was usually necessary to go through the entire process of explaining why LSC sheets must be made and tested differently to normal sheets.

One area where this was very important was the provision of clear control sheets that are vital for determining whether a sheet's problems are caused by the dye dissolution process or by a bad matrix. It proved quite impossible to procure clear control sheets for every batch of test sheets, despite on-site visits, extensive correspondence, written agreements with the suppliers and a written order with every batch for clear control sheets. *Every* sheet supplier used for this project (Spanish, German, Japanese, Chinese, Indonesian and Australian) regularly failed in this respect, either supplying no clear sheet or a "clear control sheet" that was just a clear sheet from one of their standard production runs. The latter sometimes caused great difficulties. The root cause of the problem is the overriding influence of the Standard Operating Procedure, when significant though manageable new procedures are essential.

On the other hand, where people in the plastics industry saw a direct benefit to their everyday operations from our ideas, they quickly latched onto these innovations and permanently added them to their standard operating procedures. For example, the test methods of sections 8.2 and 8.3 enabled some factories to solve long-standing problems with making fluorescently dyed sheets (not just those using the *Lumogen*® dye series) and derivatives of these test methods have become standard techniques in at least three countries. Similarly, the advantages of ultrasonic agitation described in (Franklin & Swift 1997) lead to a multimillion euro BASF GmbH plant using this technology (Böhm 2000). (The plant was commissioned and initially operated by BASF GmbH but now has a new owner). We also believe that some other factories are now using this method to cope with various low solubility dyes and pigments. However, manufactures regard their techniques in this area as trade secrets, and we have not been able to positively confirm this broader flow on from our work.

One important aspect of industrial culture, that was remarkably consistent across all the different companies and countries, was the attitude of different production staff to non-standard product. Cell casters are very used to dealing with special requests. Indeed, with the increasing cost pressures from extruded sheet, making small quantities of many different specialised products has become most cell casters forte. Most extruders are also mentally flexible and are used to dealing with special requests. We found in one case that large plants dedicated to producing highly specialised PMMA products such as LED screen backlights were justifiably wary about problems with cross-contamination from fluorescent dyes. However, continuous casters have a quite different mind set. They tend to produce large quantities of standard products. For them "customisation" is usually limited to at most adjusting the concentration of one of their standard dyes or pigments. Production staff do ***not*** like working with new dyes, even though sales staff invariably state that it is not a problem, and adds little or no extra costs. Persuading a continuous caster to make LSC sheets will not be a trivial challenge, but it would be worth the effort once long-term outdoor stability is ensured.

1.4 MASS PRODUCTION OF OPTICAL-GRADE EDGES FOR LSC'S

After considerable experiment in the early parts of the project we found that the best method for producing low-loss side surfaces was diamond polishing. A number of machines were tested and the best results were obtained with a *C.R. Clarke 1550*® (CR Clarke & Co. (UK) Ltd). A contractor used the standard version, illustrated in, Figure 1.1 to perform the diamond polishing for the early stages of the project. In the commercialization phase, Fluorosolar Systems Ltd purchased a polisher with longer in-feed and out-feed tracks to simplify the edge polishing of long light guides.

With a *C.R. Clarke 1550*®*,* polishing is carried out by a vertical axis cutter hub fitted with diamond tooling (C. R. Clarke 1550 2011). The cutter hub is mounted on a variable speed precision spindle that rotates at 12,000 – 20,000 rpm. Feed tracks on either side of the cutter hub accurately guide the material over the cutter. A belt transport system feeds the material across the cutter at around 1 metre per minute, automatically compensating for different material thicknesses. Up to a twenty 2.0 mm light guides can be stacked up and processed simultaneously, or a single sheet with a thickness of up to 55 mm.

Figure 1.1 *Clarke 1550*® diamond polishing machine. Photo from (C. R. Clarke 1550 2011)

With a skilled operator the *C.R. Clarke 1550*® can give very high quality edges at a low cost. However, achieving this requires using high-grade sheet, careful sheet preparation and the use of selected sheet protection films. Cast sheet is the easiest to machine and gives the best edges while extruded sheet is prone to edge chipping. The latter can me minimised by employing high spindle speeds, medium feed rates, and sacrificial strips on each side of the sheet stack being polished.

It is essential that the sawn edges of the rough-cut sheets are as straight as possible. The cutter hub has two diamonds – a relatively cheap synthetic diamond tool on the outside that removes the saw marks, and a more central expensive gem-grade diamond that imparts the final polish. The outer diamond removes about 0.65 mm while the polishing stone removes only 0.10 mm, for a total removal of 0.75 mm per pass. This means that the sawn edge of each sheet *must* be flat to a tolerance of better than about 0.50 mm. This allows 0.15 mm for the saw marks and 0.10 mm for the honing action of the central diamond. If the dip in the sawn edge exceeds this amount then that part of the edge will not be polished. Even a small segment of as-sawn edge has a very adverse effect on a collector sheet's half-length.

The cutting process generates plastic swarf, which is removed by extraction unit shown at the bottom left hand corner of Figure 1.1. However, some types of protective film tend to become smeared across the sheet edges by the high-speed shearing motion of the cutter hub (the inner diamond has a tangential speed of over 200 km/hr). This contamination can have an adverse impact on the sheet's half-length. The best cure is to use a protective film that does not have this problem. Attempts to remove the residue from sheet edges caused more problems than they solve, while suitable films are readily available.

APPENDIX 2: CITING AND ACCESSING PATENTS

This thesis is unusual in that a substantial portion of the work was first published as patents. There are a number of problems in how to cite these publications, and how to list the inventors.

2.1 CITING PATENTS: PATENT FAMILY VS PATENT

A patent is a legal document that must be written to conform to the rules of specific country. However, different countries often have such different rules that there may be very significant differences in the applications lodged for each country. Then the examination process in each country can sometimes be very subjective, with some examiners requiring substantial changes to a section that other examiners find perfectly acceptable. Additionally, some jurisdictions are broad in what can be the subject of a single patent, while others are very narrow, requiring the original (usually Australian) application to be split into multiple independent applications, or into several "Continued in Part" applications or various Divisional applications. Accordingly, a single original patent application may morph into multiple different texts in different countries, or even into multiple patents in a given country. This means that it is better to talk of a *patent family*, rather than a single patent. This term can be understood to mean "a set of patents taken in various countries to protect a single invention (when a first application in a country - the priority - is then extended to other offices)" (OECD 2001). However, this thesis employs the broader definition used by INPADOC "all the documents which are directly or indirectly linked via a priority document belong to the same patent family". See the discussion at the European Patent Office website (EPO 2011).

The distinction between patent and patent family can be very important for anyone trying to practice a patent, but is not normally relevant to understanding the nature of the invention. Figure 2.1 shows the patent family for the first luminescent solar collector patent for the UTS daylighting project, US 5,548,490 (Smith & Franklin 1996). This family tree was created with (Patent Lens 2011), a free online patent data base that is discussed in section 2.3. The 5,548,490 patent family is relatively simple because only two jurisdictions are involved: multi-jurisdiction families can quickly become very complex.

US patents tend to be easier to access online compared to those issued in other countries and contain enough information for a skilled person to track down all the other patents in the family. Accordingly, usually only the US patent has been cited in this thesis when reference is made to a particular patent family, and the citation should be understood to refer to the entire family. Patents issued in other jurisdictions are usually only cited where they have important

features that are not in the corresponding US patent(s), or where there is no granted US patent for that family. Note that citing only the US member of a patent family is a bit like describing the position of an iceberg by only referring to the location of the portion visible above the water line. The distinction is unimportant for most purposes, but can lead to problems at an operational level, as the captain of the Titanic found out to his cost when his ship was sliced open by the invisible part of an iceberg whose visible position was well clear of his ship.

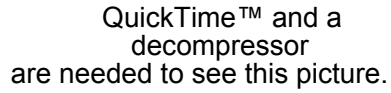

[Production Note: This figure is not included in this digital copy.
The print copy of the thesis is available for consultation at UTS Library.]

Figure 2.1 Patent family for US 5,548,490 generated with *Patent Lens*®

2.2 INVENTORS NAMES

A patent is a legal document. It must list all the inventors, and no one who was not an inventor. Indeed, finding someone who was an inventor, but is not listed on the patent application, is one of the surest ways to invalidate a patent. An "inventor" is defined as someone who makes an inventive step that contributes to the *concept* of the invention – carrying out or even designing experiments does not count. The inventor must be able to point to a specific *claim* (the legally enforceable part of the patent) and be able to say "that was *my* idea" or "that was x's and my joint idea".

Now when an invention is patented in multiple jurisdictions, differences in local law and the inclinations of particular examiners mean that there well may be very different claims for the various nations' patents that cover a single basic invention. If the claims differ then the inventors may also differ. Additionally, the order of the list of inventors has no legal force and patent attorneys often jumble the list when applications are filled in different countries. So different members of a patent family may list different inventors, or the same inventors in different order. An additional complication is that the different patents in a patent family may have different titles.

An example may help clarify things. Suppose that in country 1, *A* has an original idea with contributions from *B*. Colleague *C* then comes up with a commercially useful development to *B*'s innovation and *A* spent a lot of time in the lab seeing if it would work, including devising some really innovative experiments and profound advances in the theory. Everyone agrees that *A* will be the first author when the work is published in the scientific literature. A patent is filed in country 1 with *A*, *B* and *C* listed as the inventors in that order. In country 2, the inventors feel that *C*'s idea is the most commercially important part of the work for that market, so the patents' claims and the title are rewritten to emphasize this area and the inventors are listed as *C*, *A* and *B*. In country 3 the patent attorney lists the inventors as *B, A* and *C* for no obvious reason. In country 4, the local law is very narrow and the invention is split to patent 4a with inventors *A* and *B*, and invention 4b with inventors *C* and *B* (*A* did a lot of important lab work for this area, and will be the first author on scientific papers, but he was not an inventor for this subset of the original application). Under the INPADOC definition there is one patent family (patents 1, 2, 3, 4a and 4b). With the OECD definition, there are two patent families (family 1 with patents 1,2, 3 and 4a, and family 2 with patents 1,2, 3 and 4b). We also note that none of the five patents has an identical list of names, or publication dates and indeed, they may all have different titles. A conventional literature search will (correctly) show that there are five different documents. They have different authors, different dates, and may have different titles. So for scientific literature they would be counted as different papers – a scientific paper (Alfredo, Brown and Collins 2001) is usually quite different to (Collins and Brown 2005). However, the

five patents actually cover just the one basic invention. So it is more appropriate to give just one citation to the family, or perhaps 2 citations if the split to patents 4a and 4 b is genuinely important and not just an idiosyncratic legalism in country 4.

One final subtlety is the precise form of the name(s) used in the citations. For this thesis, the convention adopted is to use the full name of all inventors *exactly* as they appear on the relevant cited patent for the patent family. This may or may not differ from the name listed on some other members of the patent family, and is usually more complete than the name listed for the same person writing a scientific paper.

2.3 Online Access to Patents

An excellent website for accessing post 1976 US patents is the *(Patent Lens)* http://www.patentlens.net/. This excellent site also covers all world post 1978 PCT applications, post 1980 European granted patents and post 1998 granted Australian patents. *Patent Lens* gives free, searchable full-text access to nearly eleven million documents. It now also has an excellent tool to help visualize patent families with tree diagrams. Figure 2.1 was generated with this tool. In the original on-line map, the underlined patent numbers are clickable links to web pages for the patents and associated documents. However, only the links to US patents work properly: all the links for Australian documents are either missing or lead only to null pages. To examine these documents, one must turn to the Australian national website run by (IP Australia 2011) at http://www.ipaustralia.gov.au/patents/search_index.shtml.

The websites for national patent offices can be difficult to use with exceedingly obscure, idiosyncratic, counterintuitive and punctilious requirements for search terms combined with some very unhelpful error messages. (They are getting better, but off a very low base.) However, the national sites offer the most detailed records, particularly for older, pending, and abandoned patents. Basically, one uses sites like *Patent Lens* if one can, and the national sites if one must. Useful national sites include: the (US Patent and Trademark Office 2011) at http://patft.uspto.gov, the (UK portal to the European Patent Office 2011) http://gb.espacenet.com, which is much more user friendly than the direct link to the European Patent Office (European Patent Office 2011) http://www.epoline.org/portal/public/registerplus, and IP Australia (IP Australia 2011)http://www.ipaustralia.gov.au/patents/search_index.shtml.

BIBLIOGRAPHY

Abramowicz, M.A., Daecher, J.L. & Hallden-Abberton, M.P. 1997, *Flexible light pipe for side-lit applications,* Patent US 6091878.

Acrylics USA 2011, *Technical Advantages: Why Should You Choose Acrylics USA's Material?*, viewed 29/10/2011 <http://www.acrylicsusa.us/tech_advantages.htm>.

Acrylite 2012, *Fluorescent Acrylite® GP sheet*, viewed 6/6/2012 <http://www.acrylite-shop.com/CA/us/sheet/acrylite-fluorescent-8wgbpwrlk9e.html>.

Ahmad, M., Rahn, M.D. & King, T.A. 1999, 'Singlet oxygen and dye-triplet-state quenching in solid-state dye lasers consisting of Pyrromethene 567–doped poly-methyl methacrylate', *Applied Optics*, vol. 38, no. 30, pp. 6337 - 42.

Avnir, D., Levy, D. & Reisfeld, R. 1984, 'The nature of the silica cage as reflected by spectral changes and enhanced photostability of trapped Rhodamine 6G', *The Journal of Physical Chemistry*, vol. 88, no. 24, pp. 5956-9.

Balaras, C.A., Droutsa, K., Argiriou, A.A. et al. 2002, 'Assessment of energy and natural resources conservation in office buildings using TOBUS', *Energy and Buildings*, vol. 34, no. 2, pp. 135-53.

Batchelder, J.S., Zewail, A.H. & Cole, T. 1979a, 'Luminescent solar concentrators. 1: Theory of operation and techniques for performance evaluation', *Applied Optics*, vol. 18, no. 18, pp. 3090 - 110.

Batchelder, J.S., Zewail, A.H. & Cole, T. 1979b, 'Luminescent Solar concentrators. 1:Theory of operation and techniques for performance evaluation', *Applied Optics*, vol. 18, no. 18, pp. 3090 - 110.

Batchelder, J.S., Zewail, A.H. & Cole, T. 1981, 'Luminescent Solar Concentrators. 2: Experimental and theoretical analysis of their possible efficiencies', *Applied Optics*, vol. 20, no. 21, pp. 3733 - 54.

Bleasby, D. 1995, pers. comm.

Böhm, A. 1997, pers. comm.

Böhm, A. 2000, pers. comm.

Böhm, A. 2004, pers. comm.

Bonello, M. 2003, 'Sales resistance for mirror light pipes with 'hot spots'', pers. comm.

Bornstein, J.G. & Friedman, P.S. 1985, *Lighting system combining daylight concentrators and an artificial source,* Patent US 4539625.

C. R. Clarke 1550 2011, viewed 1/11/2011 <http://www.crclarke.co.uk/products/EP/1550.html>.

Cahill, P.A. 1993, 'Toward Red-Emitting, Radiation Tolerant Chromophores', *Radiation Physics and Chemistry*, vol. 41, no. 1-2, pp. 351-63.

Carrascosa, M., Unamuno, S. & Agullo-Lopez, F. 1983, 'Monte Carlo Simulation of the Performance of PMMA Luminescent Solar Collectors', *Applied Optics*, vol. 22, no. 20, pp. 3236 - 41.

Chirarattananon, S., Chedsiri, S. & Renshen, L. 2000, 'Daylighting through light pipes in the tropics', *Solar Energy*, vol. 69, no. 4, pp. 331-41.

Compagnon, R., Scartezzini, J.L. & Paule, B. 1993, 'Application of nonimaging optics to the development of new daylighting system', *ISES Solar World Congress, Budapest*, Budapest, Hungary.

DayRay 2009, *DayRay flexible lighting*, <www.dayray.com/index.cfm?page=technology>.

de Boer, D.K.G., Ronda, C.R., Keur, W. et al. 2011, 'New luminescent materials and filters for luminescent solar concentrators', *Proc. of SPIE Vol. 8108. High and Low Concentrator Systems for Solar Electric Applications VI*, vol. 8108, SPIE, pp. 81080E-E-8.

Debije, M.G. 2010, 'Solar Energy Collectors with Tunable Transmission', *Advanced Functional Materials*, vol. 20, no. 9, pp. 1498-502.

Debije, M.G. & Verbunt, P.P.C. 2012, 'Thirty Years of Luminescent Solar Concentrator Research: Solar Energy for the Built Environment', *Advanced Energy Materials*, vol. 2, no. 1, pp. 12-35.

Deller, C.A. 2005, 'LEDs and Doped Polymer Light Guides for Efficient Illumination and Colour Engineering', PhD thesis, University of Technology, Sydney, Sydney.

Deller, C.A., Franklin, J. & Smith, G.B. 2006a, 'Monte Carlo ray-tracing in particle-doped light guides', *Lighting Research and Technology*, vol. 38, no. 2, pp. 95-108.

Deller, C.A. & Franklin, J.B. 2005, 'Optimising the Length of Doped Polymer Light Mixers', *Proceedings of the Australian Institute of Physics 16th Biennial Congress*, ANU, pp. 85-8.

Deller, C.A., Franklin, J.B. & Smith, G.B. 2006b, 'Lighting simulations using smoothed LED profiles compared with measured profiles', *Proceedings of SPIE 6337. Sixth International Conference on Solid State Lighting)*, vol. 6337, San Diego.

Deller, C.A., Smith, G. & Franklin, J. 2004a, 'Colour mixing LEDs with short microsphere doped acrylic rods', *Optics Express*, vol. 12, no. 15, pp. 3327-33.

Deller, C.A., Smith, G.B. & Franklin, J.B. 2004b, 'Uniform white light distribution with low loss from colored LEDs using polymer-doped polymer mixing rods', *Proceedings of SPIE Vol 5530: Fourth International Conference on Solid State Lighting*, vol. 5530, pp. 231-40.

Deller, C.A., Smith, G.B., Franklin, J.B. et al. 2002, 'The integration of forward light transport and lateral illumination of polymer optical fibre', *Proceedings of the Australian Institute of Physics 15th Biennial Congress* pp. 307-9.

Deshpande, A.V. & Namdas, E.B. 2000, 'Correlation between lasing and photophysical performance of dyes in polymethylmethacrylate', *Journal of Luminescence*, vol. 91, no. 1-2, pp. 25-31.

Dwight, H.B. 1961, *Tables of Integrals and Other Mathmematical Data*, 4th edn, The Macmillan Company, New York.

Earp, A., Smith, G. & Franklin, J. 2007, 'Simplified BRDF of a Non-Lambertian Diffuse Surface', *Lighting Research and Technology*, vol. 39, no. 3, pp. 265-81.

Earp, A.A. 2001, 'Optical Properties of Microsphere-Doped Polymers', thesis, UTS, Sydney.

Earp, A.A. 2006, 'Luminescent Solar Concentrators for Fibre Optic Daylighting', thesis, UTS, Sydney.

Earp, A.A., Franklin, J.B. & Smith, G.B. 2005, 'Extraction of Trapped Light From Luminescent Solar Concentrators', *Proceedings of the Australian Institute of Physics 16th Biennial Congress*, AIP, ANU, pp. 104-7.

Earp, A.A., Rawling, T., Franklin, J. et al. 2009, 'Perylene Dye Degradation due to Ketones and singlet oxygen', *Dyes and Pigments*, vol. 84, pp. 59-61.

Earp, A.A., Rawling, T., Franklin, J.B. et al. 2010, 'Perylene dye photodegradation due to ketones and singlet oxygen', *Dyes and Pigments*, vol. 84, no. 1, pp. 59-61.

Earp, A.A., Smith, G.B. & Franklin, J. 2010, 'Absorption tails and exctinction in Luminescent Solar Concentrators', *Solar Energy Materials and Solar Cells*, vol. submitted 17 September 2010, in press.

Earp, A.A., Smith, G.B., Franklin, J. et al. 2004a, 'Optimisation of a three-colour luminescent solar concentrator daylighting system', *Solar Energy Materials and Solar Cells*, vol. 84, no. 1-4, pp. 411-26.

Earp, A.A., Smith, G.B., Franklin, J.B. et al. 2004b, 'Optimisation of a three-colour luminescent solar concentrator daylighting system', *Solar Energy Materials and Solar Cells*, vol. 84, no. 1-4, pp. 411-26.

Earp, A.A., Smith, G.B., Swift, P. et al. 2003, 'Optimisation of a three-colour luminescent solar concentrator daylighting system', paper presented to the *International Solar Energy Society World Congress 2003*, Gothenburg, Sweden.

Earp, A.A., Smith, G.B., Swift, P.D. et al. 2004c, 'Maximising the light output of a Luminescent Solar Concentrator', *Solar Energy*, vol. 76, no. 6, pp. 655-67.

Eddington, S.A.S. 1928, *The Nature of the Physical World*, 1st edn, Cambridge University Press, Cambridge.

Edmonds, I.R. 1993, 'Performance of laser cut light deflecting panels in daylighting applications', *Solar Energy Materials and Solar Cells*, vol. 29, no. 1, pp. 1-26.

El-Shaarawy, M.G., El-Bashir, S.M., Hammam, M. et al. 2007, 'Bent fluorescent solar concentrators (BFSCs): Spectroscopy, stability and outdoor performance', *Current Applied Physics*, vol. 7, no. 6, pp. 643-9.

Element Displays Dr Wiemer GmbH 2012, *Brilliant displays with solar energy*, viewed 6/6/2012 <http://element-displays.com/eng_startseite.html>.

EPO 2011, *Patent Families* viewed 1/11/2011 <http://www.espacenet.dk/dk/dk/help/161.htm>.

European Patent Office 2011, viewed 1/11/2011 <http://www.epoline.org/portal/public/registerplus>.

Fiber Optics Products Inc 2011, viewed 13/6/2011 <http://www.fiberopticproducts.com/>.

Franklin, J.B. 2001a, *Lighting system for transmitting and releasing luminescent radiation,* Patent US 6272265.

Franklin, J.B. 2001b, *Lighting system for transmitting and releasing luminescent radiation US 6,272,265 B1,* US 6,272,265 B1.

Franklin, J.B., Joseph, E.K. & Smith, G.B. 2004, *Improvements in side-scattering light guides,* Patent AU 2003/258363 B2.

Franklin, J.B. & Smith, G.B. 2004a, *A light collector,* Patent AU 2003/277982 B2.

Franklin, J.B. & Smith, G.B. 2004b, *A light transfer component,* Patent AU 2003/273627 B2.

Franklin, J.B. & Smith, G.B. 2007, *A Method of Coupling Light Collector sheets to a Light Transfer Component,* WO 2007/048181 A1.

Franklin, J.B., Smith, G.B. & Joseph, E.K. 2003, *Side scattering polymer light guide and method of manufacture,* Patent AU 2002/308415 B2.

Franklin, J.B., Smith, G.B. & Joseph, E.K. 2007, *Light emitting device,* Patent US 7218824 B2.

Franklin, J.B. & Swift, P.D. 1997, *Improvements in fluorescent materials,* Patent AU 717665 B2.

Goetzberger, A. & Wittwer, V. 1981, 'Fluorescent planar collector-concentrators: A review', *Solar Cells*, vol. 4, no. 1, pp. 3-23.

Goldschmidt, J.C., Peters, M., Hermle, M. et al. 2009, 'Characterizing the light guiding of fluorescent concentrators', *Journal of Applied Physics*, vol. 105, no. 11, pp. 114911--9.

Gordon, J.E. 1978, *Structures, or, Why things don't fall down*, Penguin, Harmondsworth

Graf, G. 2000, 'More on the Manufacture of Acrylic Sheet', *Plastics Distributor & Fabricator*, p. Article number 3053.

Hecht, E. 2002, *Optics*, 4th edn, Addison Wesley, San Francisco.

Henderson, M., Franklin, J.B. & Smith, G.B. 2005, *An Optically Traceable Transmission Cable for Transmitting Data or Electricity and a Traceable Conduit,* WO 2005/106899 A1.

Hermann, A.M. 1982, 'Luminescent solar concentrators--A review', *Solar Energy*, vol. 29, no. 4, pp. 323-9.

Hyldahl, M.G., Bailey, S.T. & Wittmershaus, B.P. 2009, 'Photo-stability and performance of CdSe/ZnS quantum dots in luminescent solar concentrators', *Solar Energy*, vol. 83, no. 4, pp. 566-73.

Inoue, T. 2003, 'Solar shading and daylighting by means of autonomous responsive dimming glass: practical application', *Energy and Buildings*, vol. 35, no. 5, pp. 463-71.

IP Australia 2011, viewed 1/11/2011 <http://www.ipaustralia.gov.au/patents/search_index.shtml>.

Jakhua, Z. 2011, *Knife Edge Grind Types*, viewed 4/7/2011 <http://zknives.com/knives/articles/knifeedgetypes.shtml>.

Jonsson, J.C., Smith, G.B., Deller, C. et al. 2005, ' Directional and angle-resolved optical scattering of high-performance translucent polymer sheets for energy-efficient lighting and skylights', *Applied Optics*, vol. 44, no. 14, pp. 2745-53.

Joseph, E.K. & Molitoris, R.J. 1999, *Method of manufacturing a light guide,* Patent AU_736582_B2.

Kinderman, R., Slooff, L.H., Burgers, A.R. et al. 2007a, 'I-V performance and stability study of dyes for luminescent plate concentrators', *Journal of Solar Energy Engineering-Transactions of the ASME*, vol. 129, no. 3, pp. 277 -82.

Kinderman, R., Slooff, L.H., Burgers, A.R. et al. 2007b, 'I-V performance and stability study of dyes for luminescent plate concentrators', *Journal of Solar Energy Engineering-Transactions of the ASME*, vol. 129, no. 3, pp. 277-82.

Klampaftis, E., Ross, D., McIntosh, K.R. et al. 2009, 'Enhancing the performance of solar cells via luminescent down-shifting of the incident spectrum: A review', *Solar Energy Materials and Solar Cells*, vol. 93, no. 8, pp. 1182-94.

Klein, M.V. 1970, *Optics*, John wiley & Sons, Inc, New York.

Lam, J.C. & Li, D.H.W. 1999, 'An analysis of daylighting and solar heat for cooling-dominated office buildings', *Solar Energy*, vol. 65, no. 4, pp. 251-62.

Li, D.H.W. & Lam, J.C. 2001, 'Evaluation of lighting performance in office buildings with daylighting controls', *Energy and Buildings*, vol. 38, no. 8, pp. 793-803.

Lumenyte Optical Fiber 2011, viewed 8/11/2011 <http://www.lumenytesecurity.com/index.php?option=com_content&view=article&id=104&Itemid=178>.

Lynch, S. 2000, 'Problems with 'hot spots' in mirror light guides', pers. comm., Sydney.

MacQueen, R.W., Cheng, Y.Y., Clady, R.G.C.R. et al. 2010, 'Towards an aligned luminophore solar concentrator', *OPTICS EXPRESS*, vol. 18, pp. A161-A6.

Mansour, A.F. 1998a, 'Optical efficiency and optical properties of luminescent solar concentrators", *Polymer Testing*, vol. 17, no. 5, pp. 333 - 43.

Mansour, A.F. 1998b, 'Outdoor testing of luminescent solar concentrators in a liquid polymer and bulk plate of PMMA', *Polymer Testing*, vol. 17, no. 3, pp. 153 - 62.

Mansour, A.F. 2004, 'Photostability and optical parameters of copolymer styrene/MMA as a matrix for the dyes used in fluorescent solar collectors', *Polymer Testing*, vol. 23, no. 3, pp. 247-52.

MatWeb-Cast 2011, *Overview of materials for Acrylic, Cast*, viewed 15/10/2011 <http://www.matweb.com/search/datasheet.aspx?MatGUID=a5e93a1f1fff43bcbac5b6ca51b8981f>.

MatWeb-Extruded 2011, *Overview of materials for Acrylic, Extruded*, viewed 29/11/2011 <http://www.matweb.com/search/DataSheet.aspx?MatGUID=632572aeef2a4224b5ac8fbd4f1b6f77>.

Meseguer, F.J., Cusso, F., Jaque, F. et al. 1981, 'Temperature effects on the efficiency of luminescent solar concentrators (LSC) for photovoltaic systems', *Journal of Luminescence*, vol. 24, no. 25, pp. 865 - 8.

Montarnal, D., Capelot, M., Tournilhac, F. et al. 2011, 'Silica-Like Malleable Materials from Permanent Organic Networks', *Science*, vol. 334, no. 6058, pp. 965-8.

Mulder, C.L., Reusswig, P.D., Vel·zquez, A.M. et al. 2010, 'Dye alignment in luminescent solar concentrators: I. Vertical alignment for improved waveguide coupling', *Opt. Express*, vol. 18, no. S1, pp. A79-A90.

Narendran, N. & Deng, L. 2002, 'Color Rendering Properties of LED Light Sources', *Proceedings of SPIE 4776 (Solid State Lighting II)*, Seattle, pp. 61-7.

Ne'eman, E. 1984, 'A comprehensive approach to the integration of daylight and electric light in buildings', *Energy and Buildings*, vol. 6, no. 2, pp. 97-108.

OECD 2001, *OECD science, technology and industry scoreboard: towards a knowledge-based economy*, no. ISBN 9264186484, OECD Publishing.

Orcutt, D.E. 1981, *Optical distribution system including light guide,* Patent US 4,422,719.

Page, J., Kaempf, J. & Scartezzini, J.L. 2003, 'Assessing daylighiting performances of electrochromic glazings coupled to an anidolic device,' *ISES Solar World Congress, Gothenburg*, Gothenburg. Sweden.

Parans 2011, *Parans Suntracker System*, viewed 9/11/2011 <http://www.parans.com/eng/products/>.

Patent Lens 2011, viewed 1/11/2011 <http://www.patentlens.net/>.

Patrick, D., Leger, J., McDowall, S. et al. 2011, *LUMINESCENT SOLAR CONCENTRATOR,* US 2011/0253198 A1.

Pedrotti, F.L. & Pedrotti, L.S. 1987, *Introduction to Optics*, Practice Hall International, New Jersey.

Pern, F.J. 1996a, 'Factors that affect the EVA encapsulant discoloration rate upon accelerated exposure', *Solar Energy Materials and Solar Cells*, vol. 41 - 42, no. 587 - 615.

Pern, F.J. 1996b, 'Factors that affect the EVA encapsulant discoloration rate upon accelerated exposure', *Solar Energy Materials and Solar Cells*, vol. 41-42, pp. 587-615.

Pohl, W. & Anslem, C. 2002, 'Natural Room Illumination Using Sunlight', *Proc. World Renewable Energy Congress VII (WREC 2002)*, Cologne, Germany.

Poly Optics Australia Pty, L. 2011, viewed 16/6/11 <http://www.fiberopticlight.com/home.html>.

Ratner, V.L. 1994, 'Calculation of the angular distribution and waveguide capture efficiency of the light emitted by a fluorophore situated at or adsorbed to the waveguide side wall', *Sensors and Actuators B: Chemical*, vol. 17, no. 2, pp. 113-9.

Reda, S.M. 2007, 'Stability and photodegradation of phthalocyanines and hematoporphyrin doped PMMA as solar concentrators', *Solar Energy*, vol. 81, no. 6, pp. 755-60.

Reisfeld, R., Brusilovsky, D., Eyal, M. et al. 1989, 'A new solid-state tunable laser in the visible', *Chemical Physics Letters*, vol. 160, no. 1, pp. 43 - 4.

Reisfeld, R. & Jorgensen, C.K. 1982, 'Luminescent solar concentrators for energy conversion', *Structure and Bonding*, vol. 49, no. 2, pp. 1-36.

Reisfeld, R., Yariv, E. & Minti, H. 1997, 'New developments in solid state lasers', *Optical Materials*, vol. 8, no. 1-2, pp. 31-6.

Robbins, C.L. 1986, *Daylight, Buildings and Design*, Van Nostrand Reinhold, New York.

Robbins, J.A., Zarian, J.J. & Willford, S.R. 1989, *Linear optical conduits* Patent US 5,067,831.

Rosemann, A. & Kaase, H. 2005, 'Lightpipe applications for daylighting systems', *Solar Energy*, vol. 78, no. 6, pp. 772-80.

Rustin, D. 2000, 'The Basics: Acrylic Sheet', *Plastics Distributor & Fabaricator*, p. Article number 2506.

Rutten, A.J.F. 1994, 'Sky luminance research imperative for adequate control of temporary supplementary artificial lighting installations', *Building and Environment*, vol. 29, no. 1, pp. 105-11.

Saleh, B.E.A. & Teich, M.C. 2007, *Fundamentals of Photonics*, 2nd edn, John Wiley & Sons, New Jersey.

Sanderson, K. 2009, 'Quantum dots go large', *Nature*, vol. 459, no. 7248, pp. 760-1.

Seybold, G. & Wagenblast, G. 1989, 'New perylene and violanthrone dyestuffs for fluorescent collectors', *Dyes and Pigments*, vol. 11, no. 4, pp. 303 - 17.

Slooff, L.H., Burgers, A.R. & Debije, M.G. 2008, 'Reduction of escape cone losses in luminescent solar concentrators with cholesteric mirrors', *SPIE Proceedings Vol. 7043 High and Low Concentration for Solar Electric Applications III*, ed. M. Symko-Davies, p. 704306.

Smith, G.B., Earp, A., Franklin, J. et al. 2001, 'Novel high-performance scattering materials for use in energy-saving light fittings and skylights based on polymer pigmented with polymer', *Proceedings of the SPIE 4458 (Solar Materials)*, vol. 4458, San Diego, pp. 8-18.

Smith, G.B., Earp, A.A., Stevens, J. et al. 2000, 'Materials Properties for Advanced Daylighting in Buildings', *World Renewable Energy Congress VI*, Elsevier, Brighton, pp. 201-6.

Smith, G.B. & Franklin, J. 2002, *Final NSW SERDF Project Report, January 2002. Adavanced Daylighting Collection and Transfer System*, UTS.

Smith, G.B. & Franklin, J.B. 1996, *Sunlight collecting and transmitting system,* Patent US 5548490.

Smith, G.B. & Franklin, J.B. 1998, *Sunlight collecting and transmitting system,* Patent US 5709456.

Smith, G.B. & Franklin, J.B. 2000, *Sunlight collecting and transmitting system,* Patent US 6059438.

Smith, G.B. & Franklin, J.B. 2004, *A hybrid lighting system,* Patent AU 2003/275796 B2.

Smith, G.B. & Franklin, J.B. 2007, *A lighting system,* AU 2006/101069 A4.

Smith, G.B., Jonsson, J.C. & Franklin, J. 2003, 'Spectral and Global Diffuse Properties of High-Performance Translucent Polymer Sheets for Energy Efficient Lighting and Skylights', *Applied Optics*, vol. 42, no. 19, pp. 3981-91.

Smith, T. 1971, 'Angular distribution of "trapped" light in rectangular scintillation counters', *Nuclear Instruments and Methods*, vol. 97, no. 2, pp. 409-11.

Solar Magazine 2002, *Controlling and Transporting Light - The German Museum of Technology in Berlin*, viewed 9/11/11 <http://www.solarserver.com/solarmagazin/anlagemaerz2002-e.html>.

Soti, R., Farkas, E., Hilbert, M. et al. 1996, 'Photon transport in luminescent solar concentrators', *Journal of Luminescence*, vol. 68, no. 2-4, pp. 105-14.

Swift, P.D. & Smith, G.B. 2003, 'Color considerations in fluorescent solar concentrator stacks', *Applied Optics*, vol. 42, no. 25, pp. 5112-7.

Swift, P.D., Smith, G.B. & Franklin, J. 1999a, 'Light to light efficiencies in Luminescent Solar Concentrators', *SPIE Conference on Solar Optical Materials*, vol. 2789, SPIE, Denver, Colorado, pp. 21-8.

Swift, P.D., Smith, G.B. & Franklin, J. 2006, 'Hotspots in cylindrical mirror light pipes: description and removal', *Lighting Research and Technology*, vol. 38, no. 1, pp. 19-31.

Swift, P.D., Smith, G.B. & Franklin, J.B. 1999b, 'Light-to-light efficiencies in luminescent solar concentrators', *SPIE 3789 Conference on Solar Optical Materials XVI*, vol. SPIE 3789, Denver, pp. 21-8.

Thomas, W.R.L., Drake, J.M. & Lesiecki, M.L. 1983a, 'Light transport in planar luminescent solar concentrators: the role of matrix losses', *Applied Optics*, vol. 22, no. 21, pp. 3440-50.

Thomas, W.R.L., Drake, J.M. & Lesiecki, M.L. 1983b, 'Light transport in planar luminsecent solar concentrators: the role of matrix losses', *Applied Optics*, vol. 22, no. 21, pp. 3440 - 50.

UK portal to the European Patent Office 2011, viewed 1/11/2011 <http://gb.espacenet.com>.

US Patent and Trademark Office 2011, viewed 1/11/2011 <http://patft.uspto.gov>.

van de Hulst, H.C. 1981, *Light scattering by small particles*, Dover publications Inc., New York.

van Sark, W.G.J.H.M., Barnham, K.W.J., Slooff, L.H. et al. 2008a, 'Luminescent Solar Concentrators - a Review of Recent Results', Optics Express, vol. 16, no. 26, pp. 21773 - 91.', *Optics Express*, vol. 16, no. 26, pp. 21773 - 91.

van Sark, W.G.J.H.M., Frederix, P.L.T.M., van den Heuvel, D.J. et al. 2002, 'Time-Resolved Fluorescence Spectroscopy Study on the Photophysical Behavior of Quantum Dots', *Journal of Fluorescence*, vol. 12, no. 1, pp. 69-76.

van Sark, W.G.J.H.M., Keith W.J. Barnham, Lenneke H. Slooff et al. 2008b, 'Luminescent Solar Concentrators - a Review of Recent Results', *Optics Express*, vol. 16, no. 26, pp. 21773 - 91.

Vargas, W.E. 1999, 'Diffuse radiation intensity propagating through a particulate slab', *Journal of the Optical Society of America A*, vol. 16, no. 6, pp. 1362-72.

Verbunt, P.P.C., Kaiser, A., Hermans, K. et al. 2009, 'Controlling Light Emission in Luminescent Solar Concentrators Through Use of Dye Molecules Aligned in a Planar Manner by Liquid Crystals', *Advanced Functional Materials*, vol. 19, no. 17, pp. 2714-9.

Weber , W.H. & Lambe, J. 1976, 'Luminescent greenhouse collector for solar radiation', *Applied Optics* vol. 15, no. 10, pp. 2299-300.

Welford, W.T. & Winston, R. 1989, *High Collection Nonimaging Optics*, Academic Press, San Diego.

Wilson, L.R., Rowan, B.C., Robertson, N. et al. 2010a, 'Characterization and reduction of reabsorption losses in luminescent solar concentrators', *Applied Optics*, vol. 49, no. 9, pp. 1651-61.

Wilson, L.R., Rowan, B.C., Robertson, N. et al. 2010b, 'Characterization and reduction of reabsorption losses in luminescent solar concentrators', *Applied Optics,*, vol. 49, no. 9, pp. 1651 - 61.

Wilson, R., Minano, J. & Benitez, P.G. 2005, *Nonimaging Optics*, Elsevier Academic Press, Amsterdam.

Wittwer, V., Goetzberger, A. & Heidler, K. 1982, 'Fluorescent Planar Concentrator (FPC) Monte Carlo computer model limit efficiency and latest experimental results', *4th E.C. Photovoltaic Solar Energy Conference*, D. Reidel Pub. Co., Stresa, Italy, pp. 682 - 6.

Wittwer, V., Stahl, W. & Goetzberger, A. 1984, 'Fluorescent planar concentrators', *Solar Energy Materials*, vol. 11, pp. 187 - 97.

Woan, G. 2000, *The Cambridge Handbook of Physics Formulas*, Cambridge University Press, Cambridge.

Yablonovitch, E. 1980, 'Thermodynamics of the fluorescent planar concentrator', *J. Opt. Soc. Am.*, vol. 70, no. 11, pp. 1362-3.

Zarian, J. & Robbins, J.A. 1989, *High temperature plastic light conduit and composition of matter therefor,* Patent US 5298327.

Zastrow, A. 1981, 'Physikalische Analyse der Energieverlustmechanismen im Fluoreszenzkollektor', thesis, Albert-Ludwigs-Universität Freiburg, Freiburg.

Zastrow, A. & Wittwer, V. 1986a, 'Daylight with mirror light pipes and with fluorescent planar concentrators. First results from the demonstration project Stuttgart-Hohenheim', *SPIE, 3rd International Technical Symposium on Optical and Electro-Optical Applied Science '86. Proceedings*, SPIE, pp. 227-34.

Zastrow, A. & Wittwer, V. 1986b, 'Daylighting with fluorescent planar concentrators and highly reflective silver coated plastic films - a new application for new materials', *SPIE: Optical materials technology for energy efficiency and solar energy V*, vol. SPIE Proceedings Series 653, SPIE, Bellingham / Washington, pp. 93-100.

Zemax, D.C. 2006, *Zemax® Optical Design Program User's Guide (2006)*, 2006 edn, Zemax Development Corporation.

Zhao, F., Narendran, N. & Van Derlofske, J.F. 2002, 'Optical elements for mixing colored LEDs to create white light', *Proceedings of SPIE 4776 (Solid State Lighting II)*, Seatle, p. 206.